ROOM TEMPERATURE SELF-ASSEMBLY OF METAL ORGANIC CAGES AND COORDINATION POLYMERS: STRUCTURAL DIVERSITY, MAGNETIC STUDY AND CATALYSIS

A thesis submitted for the partial fulfillment of the degree of Doctor of Philosophy

By

Biswajit Laha

PH12135

Under the supervision of

Professor Sanjay K Mandal

Department of Chemical Sciences

Indian Institute of Science Education and Research Mohali

Knowledge city, Sector 81, SAS Nagar, Manauli PO, Mohali 140306, Punjab, India.

March 2019

To

My Elder Brother

Late Suvankar Laha

Declaration

The work presented in this thesis has been carried out by me under the guidance of Prof. Sanjay K. Mandal at the Indian Institute of Science Education and Research Mohali. This work has not been submitted in part or in full for a degree, a diploma, or a fellowship to any other university or institute. Whenever contributions of others are involved, every effort is made to indicate this clearly, with due acknowledgement of collaborative research and discussions. This thesis is a bona fide record of original work done by me and all sources listed within have been detailed in the bibliography.

Biswajit Laha

In my capacity as the supervisor of the candidate's thesis work, I certify that the above statements by the candidate are true to the best of my knowledge.

Prof. Sanjay K. Mandal

Acknowledgements

First of all, I would like to convey my sincere gratitude to my advisor Prof. Sanjay K. Mandal for his constant support and guidance to make the path of my Ph.D. smooth. His immense knowledge, patience, hard-working nature, and his way of solving the problems kept me motivated all the time, and helped me to carry out the work and writing this thesis. Without his superior guidance, the path of my Ph.D. could not be the same. A heartfelt thanks goes out to him for giving me the opportunity to work with, and for sharing his knowledge and experiences.

Besides him, I would like to thank my thesis committee members, Dr. Ramesh Ramachandran and Dr. Ananth Venkatesan, for their valuable comments, inputs and constant encouragement all the time.

My seniors, Dr. Sadhika Khullar, and Dr. Navnita Kumar, have taught me the basics of research and trained me for smooth utilization of instruments, which has helped me during my Ph.D. tenure. They always guided me by clearing my doubts and strengthening my knowledge. Their suggestions and help made the path easy for me. They are truly the strongest pillars of our lab. Their contribution is heartily appreciated.

I want to thank all my labmates (Sandeep, Vijay, Prasenjit, Datta, Gouri, Shradha, Smriti, Sheeba, and Alisha) and project students for keeping the lab environment homely and for their constant help.

The help of all the lab assistants (particularly, Mr. Bahadur, Mr. Mangat and Mr. Pralhad) is appreciated from the bottom of my heart.

The use of X-ray facility (SCXRD and PXRD) has helped a lot to make this research possible. I appreciate the contribution of this facility. All other instrumentation facilities provided by the Central Analytical Facility, IISER Mohali (HRMS, NMR, and SQUID) and Department of Chemical Sciences, IISER Mohali (FTIR, UV-vis, TGA, and Elemental Analysis) are acknowledged rightly.

I am thankful to all the people (cleaners, security personnel, mess people and everyone) who made my stay comfortable at IISER Mohali.

Last but not the least, I would like to thank my family and friends for their unconditional support and sacrifices.

List of Figures

List of Schemes

Chapter III (Results and Discussion)

List of Tables

Chapter III (Results and discussion)

Appendix

Acronyms and Abbreviations

dicarb	Dicarboxylate
adc	Acetylene dicarboxylate
H_2adc	Acetylene dicarboxylic acid
H_2fum	Fumaric acid
fum	Fumarate
H_2suc	Succinic acid
suc	Succinate
H_2glu	Glutaric acid
glu	Glutarate
H_2adi	Adipic acid
adi	Adipate
H_2cdc	cyclohexane-1,4-dicarboxylic acid
cdc	cyclohexane-1,4-dicarboxylate
H_2tdc	thiophene-2,5-dicarboxylic acid
tdc	thiophene-2,5-dicarboxylate
H_3btc	Benzene-1,3,5-tricarboxylic acid
btc	Benzene-1,3,5-tricarboxylate
tpbn	N^1,N^1,N^4,N^4-tetrakis(pyridin-2-ylmethyl)butane-1,4-diamine
tphn	N^1,N^1,N^6,N^6-tetrakis(pyridin-2-ylmethyl)hexane-1,6-diamine
tphpn	N^1,N^1,N^7,N^7-tetrakis(pyridin-2-ylmethyl)heptane-1,7-diamine
tpon	N^1,N^1,N^8,N^8-tetrakis(pyridin-2-ylmethyl)octane-1,8-diamine
tpchn	N,N'-(cyclohexane-1,4-diylbis(methylene))bis(1-(pyridin-2-yl)-N-(pyridin-2-ylmethyl)methanamine)
tpxn	N,N'-(1,4-phenylenebis(methylene))bis(1-(pyridin-2-yl)-N-(pyridin-2-ylmethyl)methanamine)
CPs	Coordination Polymers
MOMs	Metal Organic Materials
MOFs	Metal Organic Frameworks
MOCs	Metal Organic Cages
SMMs	Single Molecule Magnets
M.p.	Melting Point
1D	one dimensional
2D	two dimensional
3D	three dimensional
BET	Brunauer–Emmett–Teller
RT	Room Temperature

SC	Single Crystal
Ads	adsorption
Des	desorption
2D	two dimensional
3D	three dimensional
FTIR	Fourier Transform Infrared
UV-Vis	Ultraviolet-Visible
Asym	Asymmetric
Sym	Symmetric
TGA	Thermogravimetric analysis
NMR	Nuclear magnetic resonance
PXRD	Powder X-ray Diffractometery
SCXRD	Single Crystal X-ray Diffractometery

Contents

Abstract

In the last two decades, self-assembled Metal Organic Materials (MOMs) with intriguing structures and properties have become a hot topic for scientists in various fields for their potential applications in gas sorption and storage, catalysis, magnetism, sensing, drug delivery, etc. Discrete Metal Organic Cages (MOCs) and Coordination Polymers (CPs) are the two major subclasses of MOMs. These materials are strategically designed for various applications based on the choice of ligands/linkers and diverse coordination chemistry offered by numerous metal ions. Although several synthetic methods have been reported in the literature, the room temperature self-assembly method is desired for its simplicity, cost-effectiveness and easy to scale-up.

The most important aspect of this research was to find the strategic combination of ligand and linker for the structural diversity (nuclearity and dimensionality) and hence the properties of MOCs and CPs. In combination with various di/tricarboxylic acids, several flexible and spanning bis(tridentate) polypyridyl ligands with variable spacer were used to explore their chemistry. A series of MOCs and CPs have been successfully synthesized under ambient conditions and in good yields. These have been extensively characterized by various analytical techniques including elemental analysis, FT-IR and UV-Vis spectroscopy, TGA, single crystal and powder X-ray diffraction. The first part of this work focuses on mostly MOCs (and few CPs) using various magnetically active cores, like $\{Mn_2(\mu\text{-}O)(\mu\text{-}O_2CR)_2\}^{2+}$, $\{Fe_2(\mu\text{-}O)(\mu\text{-}O_2CR)_2\}^{2+}$ and $\{Mn_2(\mu\text{-}O)_2(\mu\text{-}O_2CR)\}^{2+}$ for demonstrating their magnetic properties. Both tetranuclear and unprecedented octanuclear MOCs have been obtained, where both flexibility and methylene chain length of bis(tridentate) polypyridyl ligands and dicarboxylates play a huge role in the structural diversity and magnetic properties of these compounds. Their magnetic behaviour was according to expected ferro- and antiferro-interactions within as well as between the cages. In the second part, a rich and diverse chemistry of four different divalent metal ions (Mn^{2+}, Co^{2+}, Ni^{2+} and Cd^{2+}) was unveiled through a systematic combination of (a) rigid carboxylates and semirigid spanning ligands, (b) flexible carboxylates and semirigid spanning ligands, (c) a heterocyclic dicarboxylate and all spanning ligands, and (d) a semirigid dicarboxylate and semirigid spanning ligands. In addition to their spectroscopic and thermal properties, and structural elucidation, examples of heterogeneous catalysts for the Knoevenagel condensation reaction are demonstrated utilizing the open metal sites as Lewis acidic centers.

CHAPTER I

INTRODUCTION

The progress of science and technology highly depends on the design and development of new materials with targeted physiochemical properties and functionality required for their applications in various fields. For such materials, the synthesis methods under ambient conditions are always preferred for commercialization and cost benefits. Furthermore, any nature-inspired methodology can be thought of icing on the cake. In this regard, the following quotation can be appropriate:

"Self-assembly is the autonomous organization of components into patterns or structures without human intervention. Self-assembling processes are common throughout nature and technology. They involve components from the molecular (crystals) to the planetary (weather systems) scale and many different kinds of interaction. The concept of self-assembly is used increasingly in many disciplines, with a different flavor and emphasis in each."- George M. Whitesides and Bartosz Grzybowski.[1]

Materials with desirable shape and structure are of great importance for their particular uses in various field like host-guest chemistry.[2-6] Self-assembly is one of the best synthetic tools to prepare material with particular geometry and shape. Directional-bonding approach[7] and molecular library approach[8] are two methods for the self-assembly synthetic route. In this process, a carefully designed building unit can connect to form a material with desired structure. The interaction(s), hence the geometry, is controlled by the building unit. A slight change in the building unit can make huge changes in the structure and shape of self-assembled material. As an example, it is shown in Figure 1.1, how a little change in the ligand can affect the overall structure of the compounds. The properties of self-assembled material can also be encoded during the designing of building unit or post synthesis.

In the last few decades, researchers are showing enormous interest to prepare self-assembly of metal organic materials (MOMs) for their application in various fields like, gas storage/separation,[10-17] magnetism,[18-23] drug delivery,[24-33] NLO,[34, 35] luminescence and sensing,[36-44] catalysis[45-54] etc. MOMs are made up of metal center or metal cluster, organic ligand(s) and/or organic linker(s). According to the way these assemble, MOMs can form a material with different dimensionality, and can be classified as polygons, cages, chains, ladders, sheets, coordination polymers (CPs), metal organic frameworks (MOFs), etc. as shown in Figure 1.2. As compared to organic or inorganic materials, these classes of

compounds show different properties like, stability during guest exchange, high surface area, low density.[55, 56]

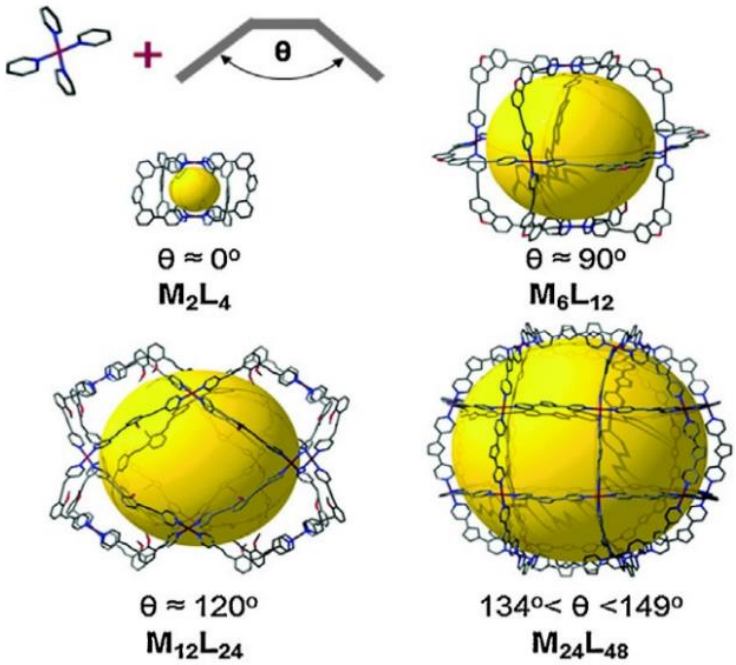

Figure 1.1. Iinfluence of the bent angle of the ligand on the geometry of the resulting Self-assembly.[9]

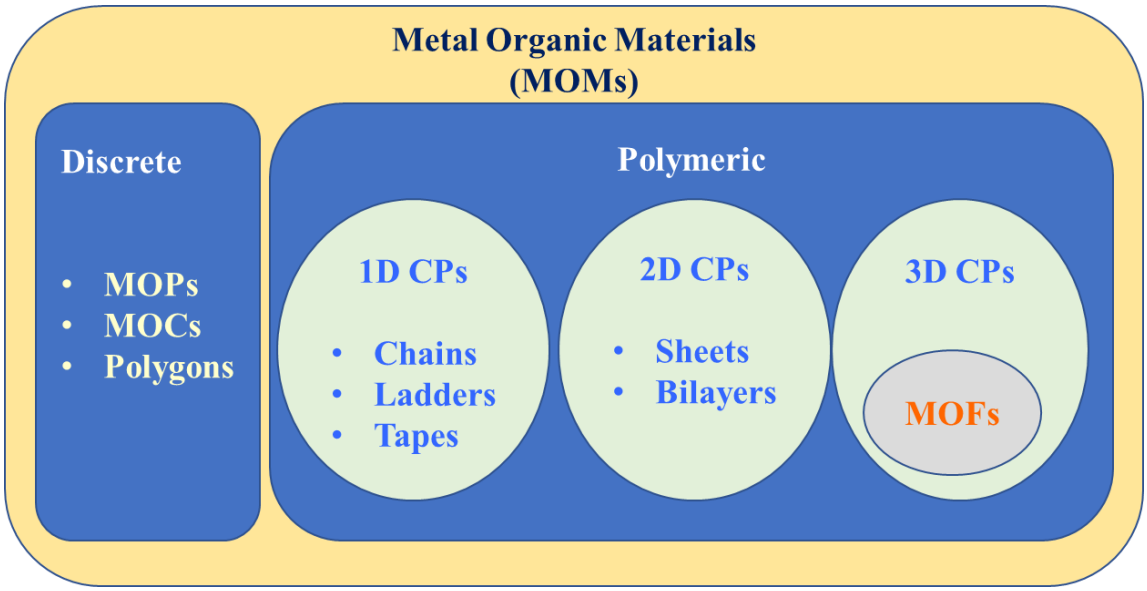

Figure 1.2. Classification of metal organic material (MOMs).

Metal Organic Cages (MOCs)

The class of 3D discrete molecule having an internal cavity of molecular dimensions, capable of trapping ions and neutral guest molecules is called molecular cages. The versatility in application makes these molecules an attractive and important class. According to the nature of molecules or

component, molecular cages are classified into three categories: Organic Cages (all the components are organic in nature, mostly prepared by the reaction of aldehyde, ketones or carboxylic acid with amine), Inorganic cages (components are inorganic in nature; phosphate, silicates or aluminates are mostly used components), and Metal Organic Cages (metal ions or clusters are connected by some organic ligand or linker or both). The high tunability of the structure/pore, high crystallinity, greater stability and breathing nature of the pores makes metal organic cages most desirable among these three. The presence of metal center in metal organic cages again provide some advantages over the other two. The first part of this thesis work is to explore the Metal Organic Cages comprised of some well-known dimetal cores.

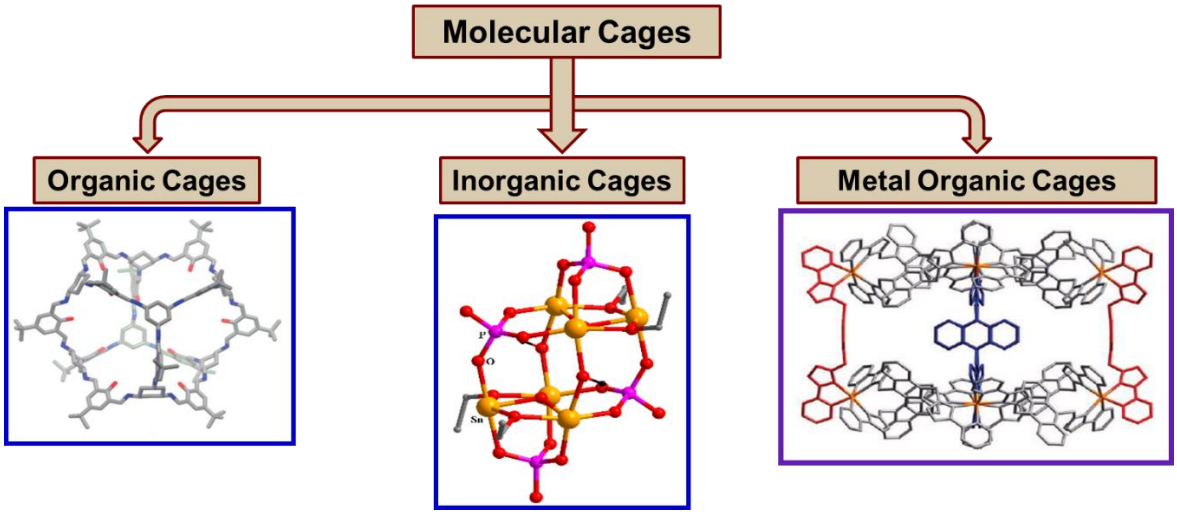

Figure 1.3. Classification of molecular cages.[57-59]

In recent years, the field of Metal organic cages (MOCs) has emerged and it has become one of the hot topics of research. The porosity in these compounds can be modulated by tuning the various components (metal center, ancillary ligand or/and linker) of these cages. The presence of pores and channels of different sizes in MOCs make them viable for many fascinating applications like catalysis, sensing, storage, transport, nano-vessel (flask for doing chemical reaction) and also for the encapsulation of unstable and non-crystalline materials and their isolation.[60-66] If such cages are comprised of transition metal subunits and multitopic organic linkers, the inherent property of the transition metal offering variable coordination number and their magnetic property provides some advantages over the organic cages. Fujita has used pyridyl and pyrimidyl ligands along with different metals to make metal-organic cages.[67-73]

The MOCs were generally synthesized by using a tetrahedral or square planar metal template by connecting these with a predesigned ligand in the early days of research in this field. The metals like Pd^{2+}, Pt^{2+} or Ni^{2+}, Co^{2+} favor square planar or tetrahedral geometry.

Thus, these metals are most commonly used as building units for MOCs formation[74-80]. Examples of Pd^{2+} based MOCs are shown in Figure 1.4a[81], where two square planar metal centers are connected by a pillar-like bidentate ligand through the vertices of the square plane. In Figure 3b, Pd^{2+} is cis-capped; only two sites of the vertices are open to bind with the ligand. These two sites are connected via a rigid tridentate ligand to form a MOC. The capping is done to avoid further connectivity; otherwise, the Pd^{2+} could accommodate another two similar ligands in a similar fashion to form a repeat of the same cage in all the possible directions, which would end up in the formation of a 3D MOF. Again, if the ligand used was bidentate instead of tridentate, it could form a rectangle. It clearly indicates that the synthesis of MOCs needs proper planning and design of the components.

(a)

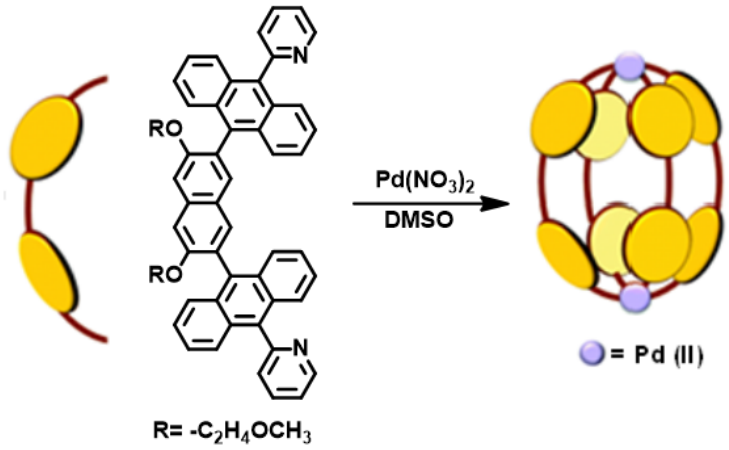

(b)

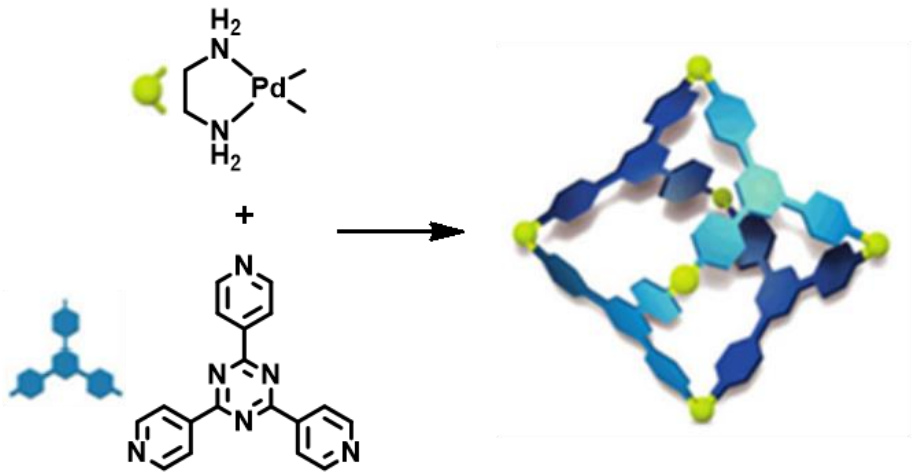

Figure 1.4. Schematic representation of the synthesis of MOCs.

Magnetism in Polymetallic Cages

One of the many applicative features of metal organic materials is magnetism. The requirements for a material to become magnetically active are: (i) presence of paramagnetic metals or radical organic ligands, or, both as they act as the magnetic moment carriers, (ii) there must be some exchange/interaction of spins between the magnetic moment carriers. Therefore, it is needed to connect the magnetic moment carriers at a desirable distance and geometry to achieve the exchange/interaction between them. Depending on the interactions, the material behaves as a paramagnet, ferromagnet, an antiferromagnet or, a ferrimagnet (see Figure 1.5).

A molecular magnet is a class of material that shows a non-vanishing magnetic moment, produced by the interaction of spins. This magnetic moment can be permanent or can be introduced by an external magnetic field. In the recent past, molecular magnets based on polymetallic cages have got enormous attention because of their application in the field of single-molecule magnets (SMMs),[82-91] molecular coolants,[92-98] spin phonon traps,[99] data storage,[100] quantum computing,[101-106] etc. It is well established that in polymetallic cages, the magnetic properties depend on the relative position of the metal ions.

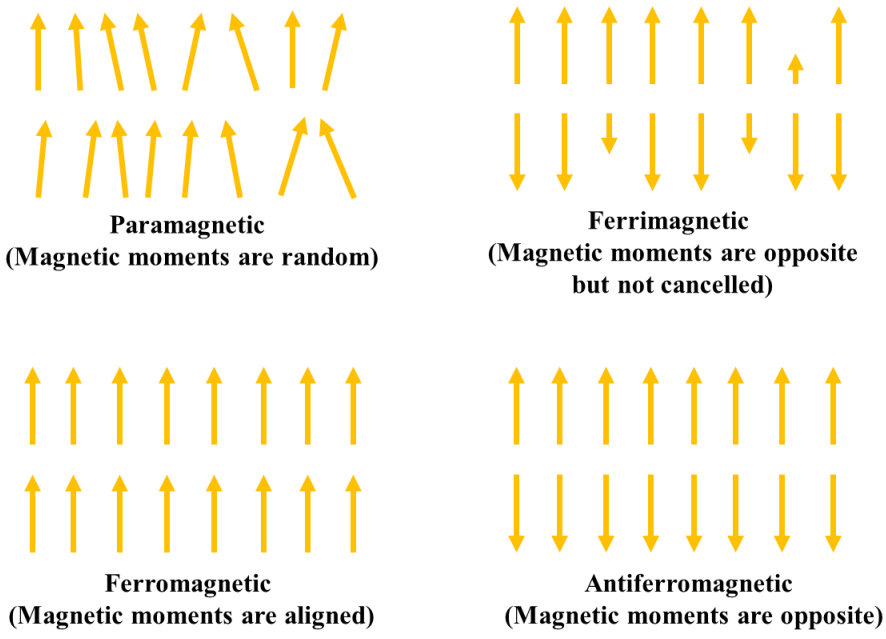

Figure 1.5. Types of magnetic interactions.

So, there must be a magneto-structural correlation and the study of magnetic properties is obvious to find this correlation. There are many instances where the structure predicted from the magnetic properties was solved later and was proven to be similar.[107-117] Many research group have studied systems like bis(μ-hydroxo)copper(II) dimers, bis(μ-

hydroxo)dichromium(III), (μ-oxo)diiron(III) species, etc., and tried to correlate the magnetic coupling constant J with the structural parameters. Over the last 25 years, after the synthesis of Mn_{12} cluster-based single molecule magnet,[118] many polymetallic cage molecules like Mn_6, Mn_{18}, Mn_{21}, Mn_{22}, Mn_{30}, Mn_{84}, Fe_8, and Ni_8, etc., have been synthesized, which behave as SMMs and their magneto-structural study has been done by various research groups.[119-128] The synthesis of new polymetallic cages through self-assembly method lies in the importance to correlate structure and magnetic property of the materials.

In the last few decades, the chemistry of compounds containing high valent $\{Mn_2(\mu\text{-}O)(\mu\text{-}O_2CR)_2\}^{2+}$ (**A**), $\{Fe_2(\mu\text{-}O)(\mu\text{-}O_2CR)_2\}^{2+}$ (**B**) and $\{Mn_2(\mu\text{-}O)_2(\mu\text{-}O_2CR)\}^{2+}$ (**C**) cores (see Figure 1.6), involved in water oxidation system of the plant, has been well established with various polypyridyl based ligands.[129, 130] These compounds show interesting magnetic behavior, and catalytic activity like C-H bond activation.[131-133]

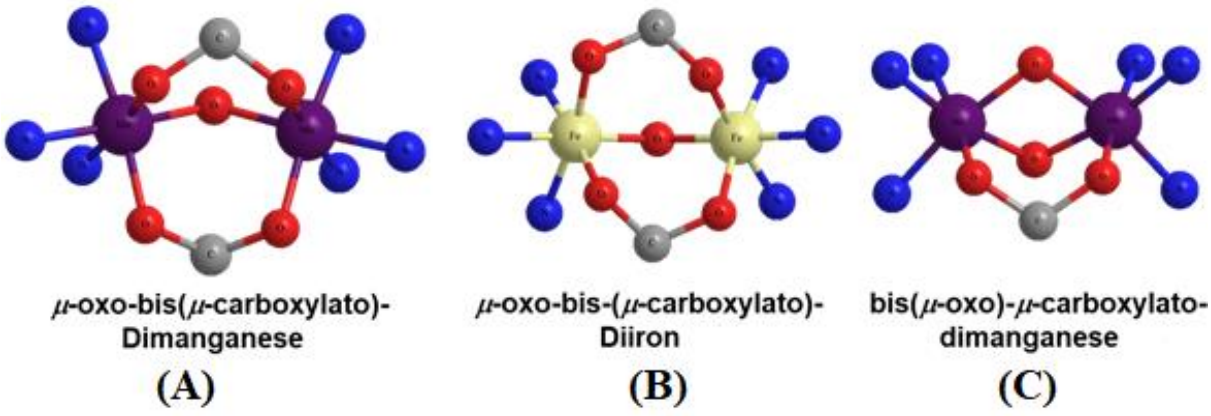

Figure 1.6. Representation of different cores used as a building unit of MOCs.

Mostly dinuclear and only a few tetranuclear complexes with core type **A**[134-159] have been reported (Figure 1.7). The oxidation states of Mn center in the core are III and III. In all cases, both the Mn-ions are hexacoordinated. A compound containing this core generally shows weak ferromagnetic or antiferromagnetic interaction with J values ~-40 cm^{-1} or 2-10 cm^{-1}, respectively. The Mn···Mn distance varies from 3.08 to 3.26 Å and Mn-O-Mn angle varies from 118 to 125°. This core is characterized by the presence of a peak at 730 cm^{-1} in the FTIR spectrum.

Core type **B**[160-170] is reported only in one tetranuclear compound (Figure 1.7) and some dinuclear compounds. Here, both the iron centers are in +3 oxidation state and hexacoordinated. The Fe···Fe distance is around 3.1 Å. Like core type **A**, the core **B** also shows a peak ~730 cm^{-1} in the FTIR spectrum.

This core however shows very strong antiferromagnetic coupling between the iron centers with the J values ~100-140 cm^{-1}.

Many dinuclear complexes with core type **C**[171-179] have been reported. The oxidation states of two Mn centers are III and IV, respectively, in the core. Almost in all cases, both the Mn centers are hexacoordinated, with an exception of a pentacoordinated Mn(III) center.[180] Compounds containing this core generally show strong antiferromagnetic interaction with J = -90 to -220 cm^{-1}. The Mn···Mn distance varies from 2.5-2.6 Å. The presence of this core can be confirmed by a FTIR peak at 690 cm^{-1}.

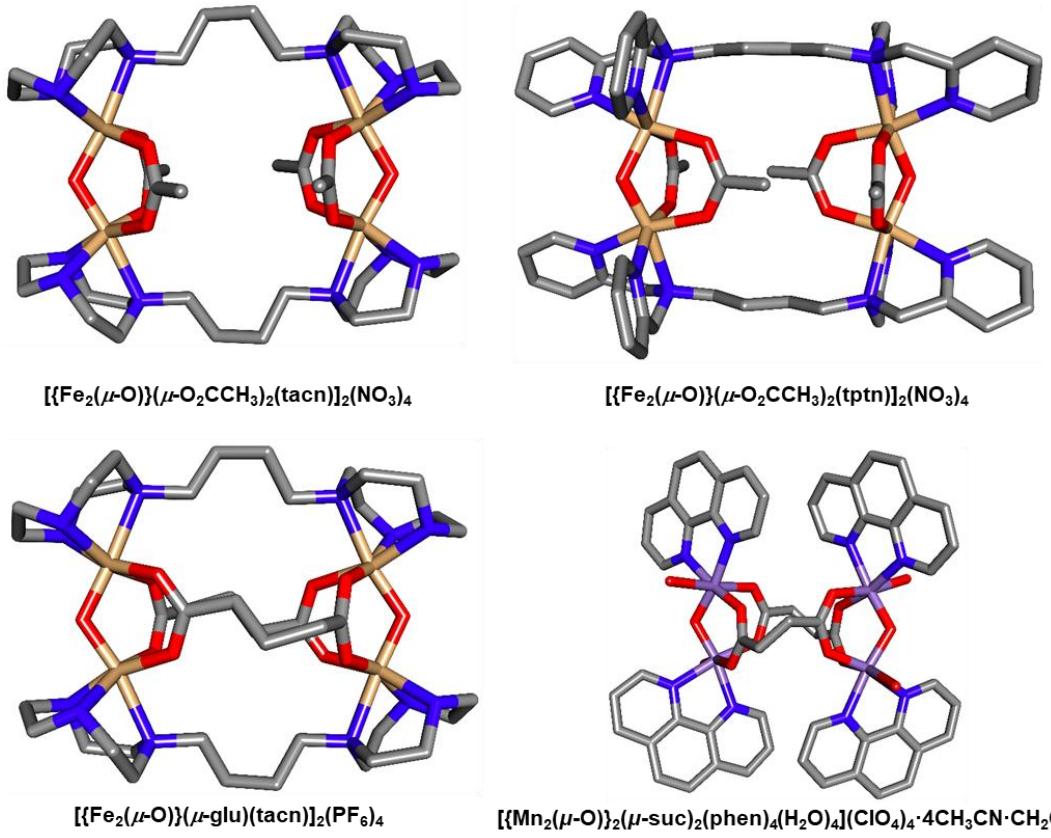

Figure 1.7. Few examples of compounds known with these cores.[164, 181-183]

In this work, we have explored the use of $\{Mn_2(\mu\text{-}O)(\mu\text{-}O_2CR)_2\}^{2+}$ or $\{Fe_2(\mu\text{-}O)(\mu\text{-}O_2CR)_2\}^{2+}$ or $\{Mn_2(\mu\text{-}O)_2(\mu\text{-}O_2CR)\}^{2+}$ core as the building units with bis(tridentate) polypyridyl ligands and dicarboxylates for the preparation of Metal Organic Cages (MOCs).

Coordination Polymers (CPs)

Though the first prototype of Coordination Polymers (CPs)[181] was present as Prussian blue in the 1700s, it was in the early 1990s when the strategic synthesis of CPs started to emerge. Nowadays, CPs are one of the richest areas of research for scientists. Coordination polymer

is an extended network formed by coordination bond between metal center (or cluster) and ligand/linkers. It can be 1D, 2D or 3D depending upon the binding sites on the metal center. These polymeric compounds may be connected with each other via some other weak interactions such as H-bonding, π-π interaction, etc., to form 2D or 3D supramolecular networks.

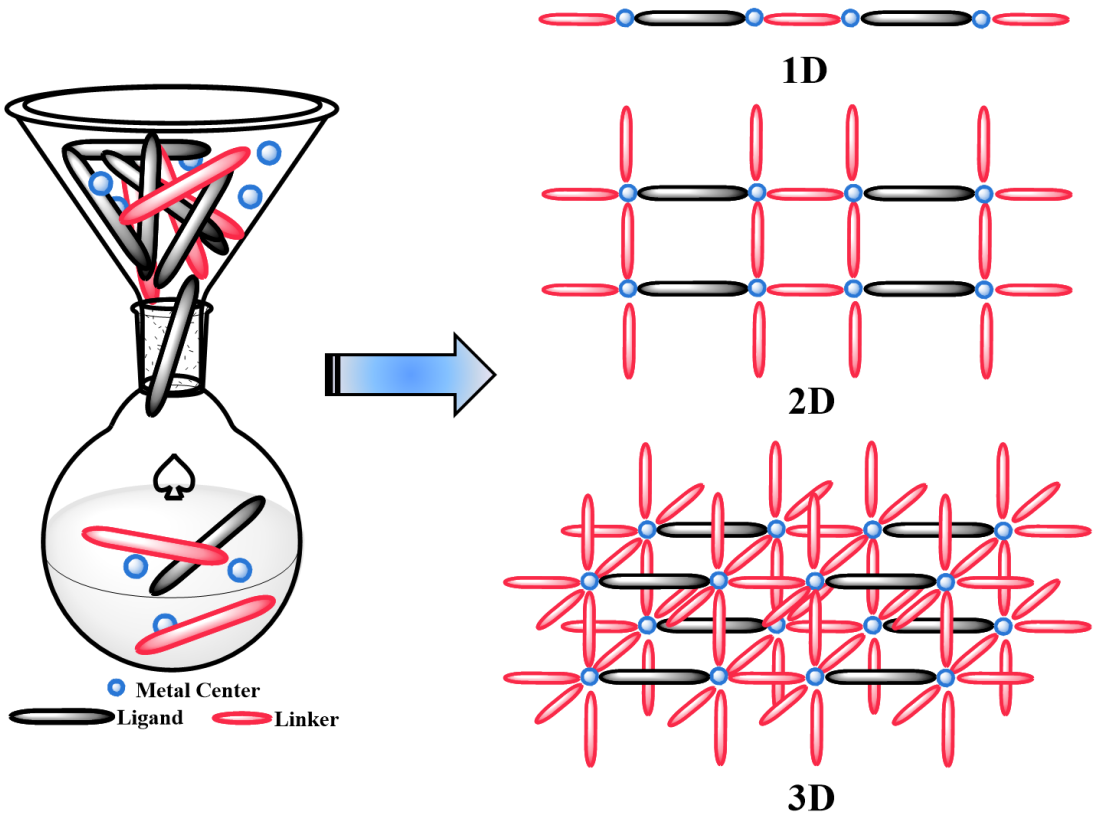

Figure 1.8. Formation of CPs with different dimensions.

This is another class of compounds which can be made through the similar self-assembly method. Generally, in self-assembly method, few coordination sites of the metal(s) are blocked by chelation of ancillary ligand(s), so that it can grow in one particular direction via some linker. In these molecules, metal centers are called the nodes which are connected with ligand/linker or both. Controlling the synthetic variable such as metal salt, ligand/linker, solvent, temperature, it is possible to control the dimensionality and structure of CPs. Higher dimensional CPs with complex structures can be generated by changing various factors, like increasing the coordination number of metal or coordinating sites of ligand, pH of the reaction medium; even the rigid or flexible nature, spacer length of ligand/linker, has high influence on the structure and dimensionality of CPs[185-193]. Because of the possibility of showing higher and variable coordination number, transition metals and lanthanides are generally used as the metal center. Ligands/linkers are organic

compounds with N, O or S donor atoms. Here metal acts as Lewis acid and ligands as Lewis bases. Thus, the synthesis of CPs largely depends on the Hard-Soft Acid-Base (HSAB) principle. Depending upon the number of open sites on the metal center, the CPs can be 1D, 2D or 3D as shown in Figure 1.8.

Similar to other MOMs, CPs are also used in various applications like anion exchange, crystal-to-crystal transformation, gas sorption, drug delivery, luminescence, sensing, magnetism, and catalysis.[194]

Supramolecular Assembly of MOCs and CPs

As discussed above, MOCs or CPs are formed via coordination linkage between metal and ligand. Although this bond is highly directional and strong, the role of weak interactions cannot be neglected in the formation and applications of MOCs or CPs. The considerable weak interactions are H-bonding, π–π stacking, C–H···π, cation–π, anion–π and lone pair–π, etc. The self–assembled MOCs or CPs (particularly CPs with lower dimension) form higher dimensional supramolecular network through H-bonding between the functional groups present in the ligand/linker molecules like -NH_2, -OH, -COOH, etc., non-bonded solvent molecules present as guest in the molecule (H_2O, CH_3OH, C_2H_5OH, DMF, etc.) and other similar molecules. It is also evident that the presence of the aromatic rings in the molecules help to increase the dimensionality of the framework through π-π interactions.

The dynamic nature of weak interactions helps ionic MOCs or CPs to be involved in the ion exchange process. During the process of exchange, the weak interactions break and form new interactions which may change the nature and dimensionality of supramolecular assembly. In the crystallization process, usually solvent molecules are trapped as guests within the crystal. Thermal treatment or exchange of solvent molecules can be introduced for SC-SC transformation and the overall supramolecular assembly can be changed.[195-197]

Scope and Significance of Present Work

i. Prior examples of metal organic cages show that Pd^{2+}, Pt^{2+}, Ni^{2+} and Co^{2+} are the most used metal ions to prepare MOCs. The use of Mn^{3+}, Mn^{4+} or Fe^{3+} in the synthesis of MOCs is very rare.

ii. The chemistry of high valent $\{Mn_2(\mu\text{-}O)(\mu\text{-}O_2CR)_2\}^{2+}$, $\{Fe_2(\mu\text{-}O)(\mu\text{-}O_2CR)_2\}^{2+}$ and $\{Mn_2(\mu\text{-}O)_2(\mu\text{-}O_2CR)\}^{2+}$ cores are well established but very few MOCs are known with

these cores. Moreover, the synthetic chemistry of these compounds is a highly challenging task because of the probable formation of metal oxides in such cases.

iii. All these cores are known for their interesting magnetic behavior.

iv. Connecting these cores through ligand and carboxylate, it is possible to form various metal organic cages (MOCs) with different nuclearity. The formation of compounds with these cores is facilitated by ancillary N-donor and O-donor ligands as these play a critical role in the formation and stabilization of oxo-manganese or oxo-iron clusters. By using spanning ligand, which can bind to the cores from both the ends, and dicarboxylates, many possible structural features can be attained as shown in Figure 1.9 and 1.10.

v. Though the study of CPs has been done to a large extent, still the effect of flexibility of ligand and linker on the structure has a lot to explore which can help to explain how the combination of flexible, rigid or semi-rigid ligands and linker affect the structure.

vi. Trapping of different water cluster is possible through the synthesis of supramolecular assemblies.

vii. Choosing a greener route for the synthesis of these MOCs and CPs using more environment friendly solvents and reactants is another aspect of this research.

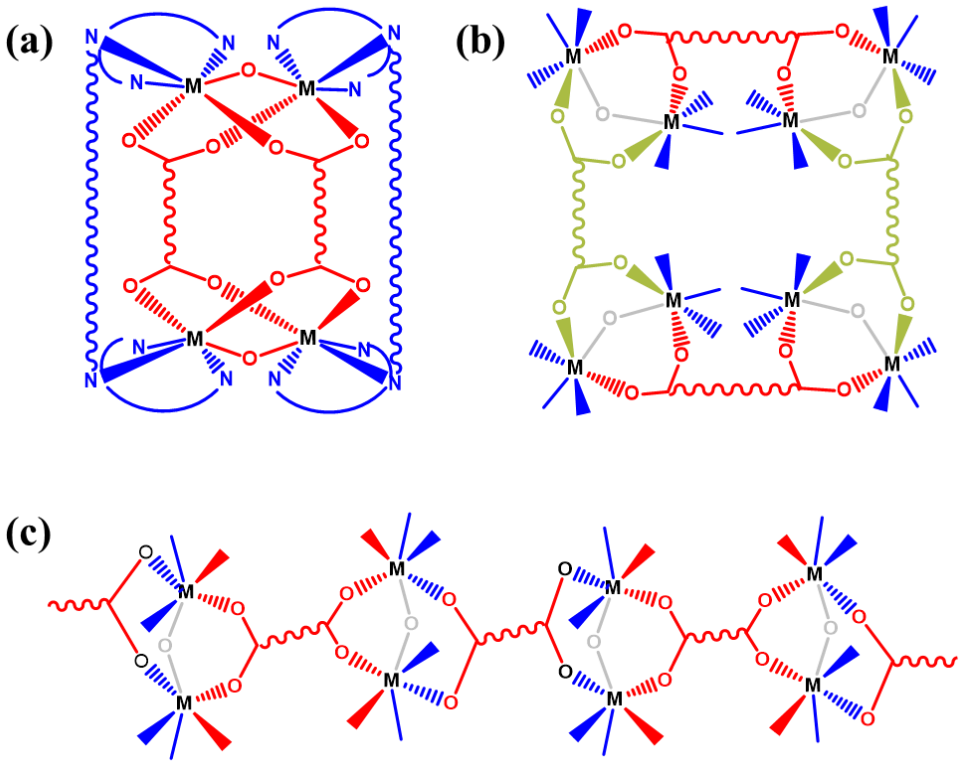

Figure 1.9. Structural possibilities after connecting the cores of **A** and **B** with bis(tridentate) ligand and aliphatic dicarboxylate: (a) tetranuclear, (b) octanuclear, (c) polymeric.

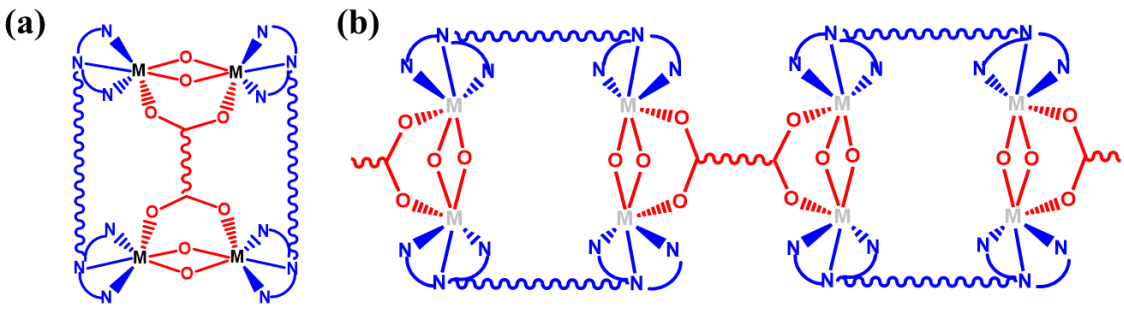

Figure 1.10. Structural possibilities after connecting the core **C** with bis(tridentate) ligand and aliphatic dicarboxylate: (a) tetranuclear, (b) polymeric.

After understanding the cause and importance of this work, two strategies for synthesis were adopted as shown in Figure 1.11 and 1.12. In the first part, i.e., metal organic cages, series of bis(tridentate) ligands and dicarboxylates are used to achieve higher nuclearity with the cores

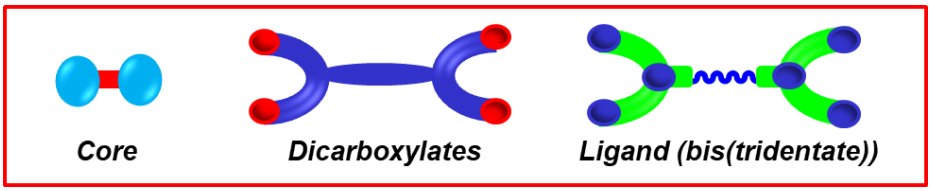

Figure 1.11. Strategic combination used for the synthesis of MOCs.

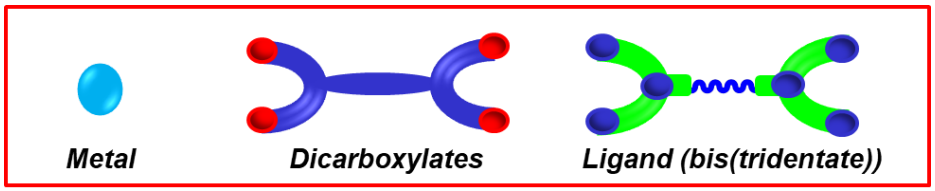

Figure 1.12. Strategic combination used for the synthesis of CPs.

mentioned above. To attain variation in nuclearity, the spacer length of ligands and linkers was varied. For the second part, i.e., coordination polymers, the flexibility of these ligands was varied by changing the spacer from the aliphatic chain to aliphatic ring to aromatic ring. The metal centers are chosen as Co(II), and Ni(II) in most of the cases, and in few cases Mn(II) is also used for comparision. The reason behind choosing these metal centers is that, the first-row transition metals are likely to be more abundant on earth, inexpensive and more environment friendly than the noble transition metals. Moreover, the chemistry of CPs with Co(II) and Ni(II) is less explored than the other first row transition metals. The Cd(II) metal center is used because of the possibility of high coordination number of cadmium, that can allow to prepare higher dimensional coordination polymers. The various linkers and dicarboxylates used throughout this work are shown in Figures 1.13 and 1.14.

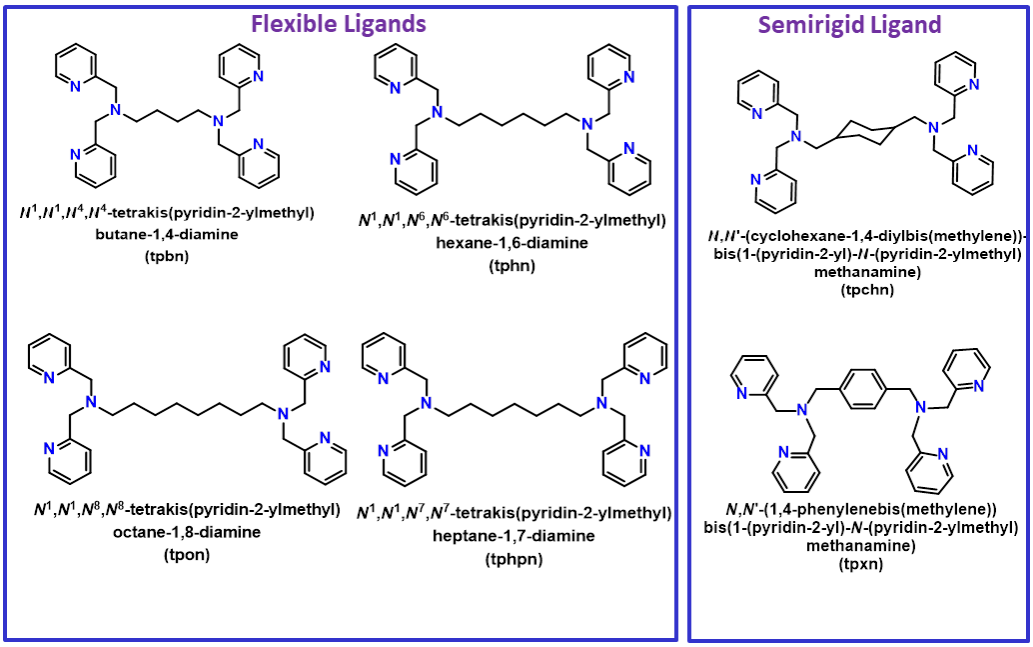

Figure 1.13. Organic ligands used in this study.

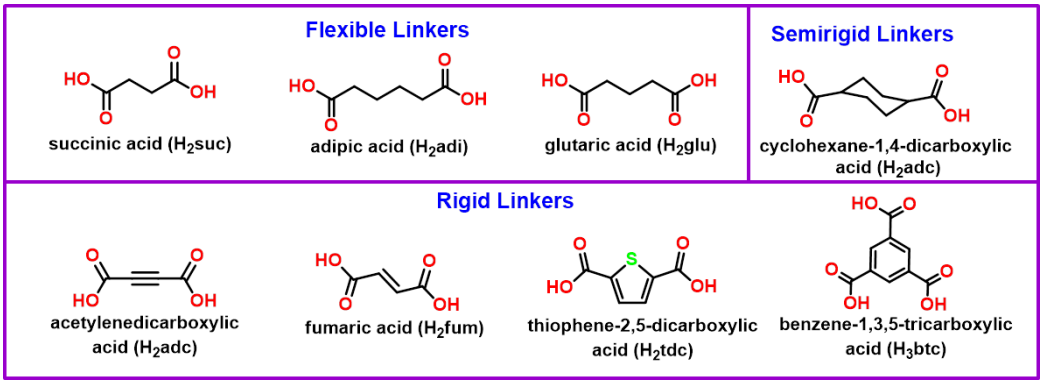

Figure 1.14. Organic linkers used in this study.

CHAPTER II

EXPERIMENTAL SECTION

2.1 Materials and Methods

In this research work, all chemicals and solvents used for synthesis were obtained from commercial sources and were used as received, without further purification. All reactions were carried out under aerobic conditions.

2.2 Physical Measurements

^{1}H NMR spectra of the synthesized ligands were obtained in deuterated solvents at 25 ℃ on a Bruker ARX-400 spectrometer; chemical shifts are reported relative to the residual solvent signals. Each sample was prepared by taking 5-10 mg of the compound in approx. 0.5 mL of the deuterated solvent. Each data obtained was analyzed and plotted using either TOPSPIN software by Bruker or Spinworks.

Melting points (M.pt.) were measured on a *Büchi Melting and Boiling Point Apparatus*. All melting points have been measured in open melting point capillaries.

FTIR spectra were measured in the range of 4000-400 cm^{-1} on a Perkin-Elmer Spectrum I spectrometer with samples prepared as KBr pellets.

Elemental analysis (C, H, N) was carried out using either a Leco-USA Tru Spec CHNS micro version 2.7x analyzer at IISER Mohali or Mettler CHNS analyzer at NIPER Mohali.

Thermogravimetric analysis was carried out from 25 to 500 ◦C (at a heating rate of 10 ◦C/min) under dinitrogen atmosphere on a Shimadzu DTG-60. The sample to be analyzed was weighed using an analytical balance, put in a pan and weighed again using the micro balance of the instrument to avoid any discrepancy. The data obtained were analyzed using TA 60 software.

UV-vis spectra of the compounds in different solvents were recorded in an Agilent Technologies Cary60 UV-vis spectrophotometer using a cuvette of path length 10 mm. solid state reflectance of solid samples were recorded in Cary 5000 UV-vis spectrophotometer using KBr medium.

Powder X-ray data were recorded on a Rigaku Ultima IV diffractometer equipped with a 3 kW sealed tube Cu Kα X-ray radiation (generator power settings: 40 kV and 40 mA) and a DTex Ultra detector using BB geometry (2.5° primary and secondary solar slits, 0.5°

divergence slit with 10 mm height limit slit). Each sample grounded into a fine powder using a mortar and a pestle was placed on a glass sample holder that was placed on the sample rotation stage (120 rpm) attachment. The data were collected over an angle range 5° to 50° with a scanning speed of 1° per minute with 0.02° step with XRF reduction for the metals.

Single crystal X-ray analysis were performed by initial crystal evaluation and data collection were performed on a Kappa APEX II diffractometer equipped with a CCD detector (with the crystal-to-detector distance fixed at 60 mm) and sealed-tube monochromatic MoKα radiation using the program APEX2.[198] By using the program SAINT[198] for the integration of the data, reflection profiles were fitted, and values of F^2 and $\sigma(F^2)$ for each reflection were obtained. In some cases, a lot of efforts were invested to recollect data sets with new crystals a few times but no better data sets that are used here could be obtained. Data were also corrected for Lorentz and polarization effects. The subroutine XPREP[198] was used for the processing of data that included determination of space group, application of an absorption correction (SADABS),[198] merging of data, and generation of files necessary for solution and refinement. Using Olex2,[199] the structure was solved with the ShelXT[200] structure solution program using Intrinsic Phasing and refined with the ShelXL[201] refinement package using least squares minimization. The space group was chosen based on systematic absences and confirmed by the successful refinement of the structure. Positions of most of the non-hydrogen atoms were obtained from a direct methods solution. Several full-matrix least-squares/difference Fourier cycles were performed, locating the remainder of the non-hydrogen atoms. Some cases the solvents molecules are highly disordered. Therefore, the Olex2[199] masking program was used to remove those peaks. In order to obtain reasonable thermal parameters compared to other atoms, the lowest residual factors and optimum goodness of fit with the convergence of refinement, occupancy factors of some of the atoms were adjusted accordingly. The occupancy factors of some of the atoms were adjusted to obtain favorable thermal parameters. All non-hydrogen atoms for all structures were refined with anisotropic displacement parameters except where mentioned. Crystallographic parameters and basic information pertaining to data collection and structure refinement for all compounds are summarized in the appendix. All figures were drawn using and MERCURY V 3.10.2[202] and hydrogen bonding parameters were generated using PLATON.[203, 204]

Solvent adsorption measurements were recorded for pressures in the range 0–1.2 bar by

the volumetric method using a BELSORP instrument. Each solid sample was transferred to pre-weighed analysis tubes, which were capped with transeals and evacuated by heating at a temperature between 110-150 °C (based on thermal profile obtained from TGA) under dynamic vacuum until an outgas rate of less than 2 mTorr min^{-1} (0.27 Pa min^{-1}) was achieved (ca. 12-24 h). The evacuated analysis tubes containing the degassed sample was then carefully transferred to an electronic balance and weighed again to determine the mass of the sample. The tube was then placed back on the analysis port of the gas adsorption instrument. The outgas rate was again confirmed to be less than 2 mTorr min^{-1} (0.27 Pa min^{-1}). For all isotherms, warm and cold free-space (dead volume) correction measurements were performed using ultra-high-purity He gas (UHP grade 5.0, 99.999% purity). The change of the pressure was monitored and the degree of adsorption was determined by the decrease in pressure at the equilibrium state via computer controlled automatic operations that are set up at the start of each measurement. Oil-free vacuum pumps and oil-free pressure regulators were used for all measurements to prevent contamination of the samples during the evacuation process or of the feed gases during the isotherm measurements.

2.3 Synthesis of Ligands

All these ligands were synthesized either by following or modifying the reported procedures in the literature.[205]

N^1,N^1,N^4,N^4-tetrakis(pyridin-2-ylmethyl)butane-1,4-diamine (tpbn). The ligand was prepared by following the literature procedure with slight modifications. In a 100 mL round bottom flask, 1 mL (10 mmol) of butane-1,4-diamine was taken. An aqueous solution of 6.56 g (40 mmol) picolyl chloride was added to it and stirred continuously. After few minutes, aqueous solution of 3.20 g (80 mmol) sodium hydroxide (10 M) was added drop wise over a period of 30 minutes. The solution became red; it was left for stirring for 24 h. A white solid was formed and filtered. The solid was washed thoroughly with water and air dried. Yield: 3.52 g (77%). ^{1}H NMR ($CDCl_3$): δ 1.458 (q, 4H), 2.099 (t, 4H), 3.725 (s, 8H), 7.062 (t, 4H), 7.449 (d, 4H), 7.557 (t, 4H), 8.430 (d, 4H).

N^1,N^1,N^6,N^6-tetrakis(pyridin-2-ylmethyl)hexane-1,6-diamine (tphn). It was prepared following the same procedure as for tpbn except using 1.16 g (10 mmol) hexane-1,6-diamine instead of butane-1,4-diamine. Yield: 3.840 g (80%). ^{1}H NMR ($CDCl_3$): δ = 1.18-1.22 (m, 2H), 1.51(s, 4H), 1.94 (s, 2H)2.48-2.52 (m, 4H), 3.80 (s, 8H), 7.13-7.16 (m, 4H), 7.53-7.55 (m, 4H), 7.63-7.67 (m, 4H), 8.52-8.53 (m, 4H).

N^1,N^1,N^7,N^7-tetrakis(pyridin-2-ylmethyl)heptane-1,7-diamine (tphpn). It was prepared following the same procedure as for tpbn except using 1.30 g (10 mmol) of heptane-1,7-diamine instead of butane-1,4-diamine. Yield: 4.94 g (66%). ^{1}H NMR ($CDCl_3$): δ = 1.13-1.24 (m, 6H), 1.48-1.56 (m, 4H), 2.54-2.58 (m, 4H), 3.86 (s, 8H), 7.13-7.16 (m, 4H), 7.56-7.58 (m, 4H),7.64-7.69 (m, 4H), 8.52-8.53 (m, 4H).

N^1,N^1,N^8,N^8-tetrakis(pyridin-2-ylmethyl)octane-1,8-diamine (tpon). It was prepared following the same procedure as for tpbn except that 1.42 g (10 mmol) of octane-1,8-diamine was used instead of butane-1,4-diamine. Yield: 3.45 g (68%). ^{1}H NMR ($CDCl_3$): δ = 1.18-1.88(m, 8H), 1.48-1.56 (m, 4H), 2.51-2.55 (m, 4H), 3.82 (s, 8H), 7.14–7.16 (m, 4H), 7.54-7.56 (m, 4H), 7.63-7.68 (m, 4H), 8.52–8.53 (m, 4H).

N,N'-(cyclohexane-1,4-diylbis(methylene))bis(1-(pyridin-2-yl)-N-(pyridin-2-ylmethyl)methanamine) (tpchn). It was prepared following the same procedure as for tpbn except using 1.42 g (10 mmol) of cyclohexane-1,4-diyldimethanamine instead of butane-1,4-diamine. Yield: 3.59 g (71%). ^{1}H NMR ($CDCl_3$): δ = 0.72 (m, 2H), 1.07-1.10 (m, 2H), 1.41-1.46 (m, 2H), 1.88-1.90 (m, 2H), 2.28-2.33 (m, 4H), 3.77 (s, 8H), 7.12-7.16 (m, 4H), 7.51-7.58 (m, 4H), 7.63-7.68 (m, 4H), 8.48-8.52 (m, 4H).

N,N'-(1,4-phenylenebis(methylene))bis(1-(pyridin-2-yl)-N-(pyridin-2-ylmethyl)methanamine) (tpxn). It was prepared following the same procedure as for tpbn exce[t using 1.36 g (10 mmol) of 1,4-phenylenedimethanamine instead of butane-1,4-diamine. Yield: 3.50 g (70%). ^{1}H NMR ($CDCl_3$, 400 MHz): δ = 2.17 (s, 4H), 3.66 (s, 4H), 3.80 (s, 8H), 7.12–7.15 (m, 4H), 7.36 (m, 4H), 7.58-7.60 (m, 4H), 7.64-7.68 (m, 4H).

2.4 Synthesis of Compounds

[{Mn_2(μ-O)}(μ-glu)(tpbn)]$_2$(ClO_4)$_4$ (1). In a 10 mL round bottom flask, 45.8 mg (0.1 mmol) of tpbn was dissolved in 1.5 mL methanol. To this solution, 53.6 mg (0.2 mmol) of $Mn(OAc)_3{\cdot}2H_2O$ was added. The solution was stirred for 5 minutes. To this reaction mixture, 13.2 mg (0.1 mmol) of glutaric acid (H_2glu) was added with stirring. The reaction mixture was further stirred for an hour. The red-brown solution was filtered and methanolic solution of excess $NaClO_4$ was added to the filtrate. The light red-brown solid obtained was filtered using a G4 crucible, washed with methanol and air dried. Yield: 72.6 mg (80%). Anal. Calc. (%) for **1**·3H_2O (MF $C_{66}H_{82}N_{12}O_{29}Cl_4Mn_4$, FW 1814.9386): C, 42.41; H, 4.42; N, 8.99. Found: C, 42.54; H, 4.28; N, 8.62. Selected FTIR peaks (KBr, cm^{-1}): 1607 (s),

1573 (w), 1560 (s), 1484 (s), 1442 (m), 1433(m), 1365 (s), 1089 (br), 768 (s), 731 (w), 625 (s).

[{Mn_2(μ-O)}(μ-adi)(tpbn)]$_2$(ClO_4)$_4$ (2). A procedure similar to that of **1** was followed except 14.6 mg (0.01 mmol) adipic acid (H_2adi) was used instead of glutaric acid. Yield: 68.7 mg (76%). Selected FTIR peaks (KBr, cm^{-1}): 1607 (s), 1573 (w), 1562 (s), 1483 (s), 1443 (m), 1435(m), 1417(w), 1310 (br), 1089 (br), 768 (s), 730(m), 624(s).

[{Mn_2(μ-O)}(μ-cdc)(tpbn)]$_2$(ClO_4)$_4$·9H_2O (3). A procedure similar to that of **1** was followed except 17.2 mg (0.01 mmol) cyclohexanedicarboxylic acid (H_2cdc) was used instead of glutaric acid. Yield: 76 mg (85%). Anal. Calc. (%) for **3**·1.5H_2O ($C_{64}H_{71}N_{12}O_{27.5}Cl_4Mn_4$, FW 1809.8766): . C, 42.04; H, 5.00; N, 8.17. Found: C, 41.95; H, 4.52; N, 7.86. Selected FTIR peaks (KBr, cm^{-1}): 1607 (v), 1573 (w), 1561 (s), 1482 (s), 1446 (m), 14344 (w), 1411 (m), 1347 (s), 1089 (br), 770 (s), 731 (w), 625 (s).

[{Mn_2(μ-O)}(μ-glu)(tphn)]$_2$(ClO_4)$_4$ (4). A procedure similar to that of **1** was followed except 48 mg (0.01 mmol) tphn was used instead of tpbn. Yield: 80 mg (86%). Anal. Calc. (%) for **4**·2H_2O (MF $C_{70}H_{96}N_{12}O_{28}Cl_4Mn_4$, FW 1915.1390): C, 44.09; H, 4.65; N, 8.81. Found: C, 44.11; H, 4.44; N, 8.84. Selected FTIR peaks (KBr, cm^{-1}): 1608 (s), 1573 (w), 1561 (s), 1484 (s), 1434 (br), 1410 (w), 1089 (br), 769 (s), 731(m), 624 (s).

[{Mn_2(μ-O)}(μ-adi)(tphn)]$_2$(ClO_4)$_4$ (5). A procedure similar to that of **1** was followed except 48 mg (0.01 mmol) tphn and 14.6 mg (0.01 mmol) adipic acid (H_2adi) was used instead of tpbn and glutaric acid. Yield: 74 mg (78%). Anal. Calc. (%) for **5** (MF $C_{72}H_{88}N_{12}O_{26}Cl_4Mn_4$, FW 1899.0981): C, 44.51; H, 4.59; N; 8.90. Found: C, 43.43; H, 4.48; N, 9.09. Selected FTIR peaks (KBr, cm^{-1}): 1607 (s), 1573 (w), 1562 (s), 1483 (s), 1442 (w), 1433 (w), 1415(w), 1310 (br), 1090 (br), 768 (s), 731 (w), 624 (s). Crystals suitable for single crystal X-ray diffraction study were obtained by slow diffusion of diisopropyl ether into acetonitrile solution of **5**.

[{Mn_2(μ-O)}(μ-cdc)(tphn)]$_2$(ClO_4)$_4$ (6). A procedure similar to that of **1** was followed except 48 mg (0.01 mmol) tphn and 17.2 mg (0.01 mmol) cyclohexanedicarboxylic acid (H_2cdc) was used instead of tpbn and glutaric acid. Yield: 77 mg (79%). Anal. Calc. (%) for **6** (MF $C_{76}H_{92}N_{12}O_{26}Cl_4Mn_4$, FW 1951.1727): C, 46.78; H, 4.75; N, 8.61. Found: C, 44.35; H, 4.62; N, 8.01. Selected FTIR peaks (KBr, cm^{-1}): 1607 (s), 1573 (w), 1564 (w), 1482 (s), 1448 (s), 1434 (w), 1402 (s), 1345 (s), 1090 (br), 769 (s), 624 (s). Crystals suitable

for single crystal X-ray diffraction study were obtained by slow diffusion of dibutyl ether into acetonitrile solution of **6**.

[{Mn_2(μ-O)}(μ-glu)(tphpn)]$_2$(ClO_4)$_4$ (7). A procedure similar to that of **1** was followed except 49.4 mg (0.01 mmol) tphpn was used instead of tpbn. Anal. Calc. (%) for **7**·3H_2O (MF $C_{64}H_{78}N_{12}O_{29}Cl_4Mn_4$, FW 1840.9313): C, 43.89; H, 4.44; N, 9.03. Found: C, 43.36; H, 4.35; N, 8.90. Selected FTIR peaks (KBr, cm^{-1}): 1607 (s), 1573 (w), 1562 (m), 1483 (s), 1443 (w), 1433 (w), 1412 (w), 1309 (m), 1091 (br), 768 (s), 730 (w), 624 (s).

[{Mn_2(μ-O)}(μ-adi)(tphpn)]$_2$(ClO_4)$_4$ (8). A procedure similar to that of **1** was followed except 49.4 mg (0.01 mmol) tphpn and 14.6 mg (0.01 mmol) adipic acid (H_2adi) was used instead of tpbn and glutaric acid. Yield: 76 mg (85%). Selected FTIR peaks (KBr, cm^{-1}): 1607 (s), 1573 (w), 1562 (s), 1483 (s), 1443 (m), 1376 (br), 1090 (br), 768 (s), 624 (s).

[{Mn_2(μ-O)}(μ-cdc)(tphpn)]$_2$(ClO_4)$_4$ (9). A procedure similar to that of **1** was followed except 49.4 mg (0.01 mmol) tphpn and 17.2 mg (0.01 mmol) cyclohexanedicarboxylic acid (H_2cdc) was used instead of tpbn and glutaric acid. Yield: 76 mg (78%). Selected FTIR peaks (KBr, cm^{-1}): 1607 (s), 1573 (w), 1558 (s), 1483 (s), 1445 (m), 1434 (w), 1411 (w), 1380 (w), 1094 (br), 769 (s), 730 (m), 624 (s).

[{Mn_2(μ-O)}(μ-glu)(tpon)]$_2$(ClO_4)$_4$ (10). A procedure similar to that of **1** was followed except 50.8 mg (0.01 mmol) tpon was used instead of tpbn. Selected FTIR peaks (KBr, cm^{-1}): 1607 (s), 1574 (br), 1563 (br), 1484 (s), 1443 (w), 1431 (w), 1411 (w), 1379 (s), 1092 (br), 768 (s), 730 (m), 623 (s).

[{Mn_2(μ-O)}(μ-adi)(tpon)]$_2$(ClO_4)$_4$ (11). A procedure similar to that of **1** was followed except 50.8 mg (0.01 mmol) tpon and 14.6 mg (0.01 mmol) adipic acid (H_2adi) was used instead of tpbn and glutaric acid. Yield: 76 mg (85%). Anal. Calc. (%) for **11**·1.5H_2O (MF $C_{64}H_{71}N_{12}O_{27.5}Cl_4Mn_4$, FW 1809.8766): C, 43.89; H, 4.44; N, 7.62. Found: C, 42.60; H, 4.4; N, 9.66. Selected FTIR peaks (KBr, cm^{-1}): 1607 (s), 1575 (w), 1560 (s), 1464(s), 1443 (m), 1376 (br), 1089 (br), 768 (s), 625 (s).

[{Mn_2(μ-O)}(μ-cdc)(tpon)]$_2$(ClO_4)$_4$ (12). A procedure similar to that of **1** was followed except 50.8 mg (0.01 mmol) tpon and 17.2 mg (0.01 mmol) cyclohexanedicarboxylic acid (H_2cdc) was used instead of tpbn and glutaric acid. Yield: 76 mg (76%). Selected FTIR peaks (KBr, cm^{-1}): 1607 (s), 1573 (w), 1557 (s), 1483 (s), 1443 (m), 1430 (w), 1410 (s), 1376 (br), 1092 (br), 769 (s), 730 (w), 624 (s).

[{Mn$_2$(μ-O)}(μ-suc)(tpbn)]$_2$(ClO$_4$)$_4$ (13). A procedure similar to that of **1** was followed except 11.8 mg (0.01 mmol) succinic acid (H_2suc) was used instead of glutaric acid. Yield: 72 mg (85%). Anal. Calc. (%) for **13**·3H_2O (MF $C_{64}H_{74}N_{12}O_{29}Cl_4Mn_4$, FW 1836.8995): C, 43.89; H, 4.44; N, 9.03. Found: C, 43.36; H, 4.35; N, 8.90. Crystals suitable for single crystal X-ray diffraction study were obtained by slow diffusion of dibutyl ether into acetonitrile solution of **13**. Selected FTIR peaks (KBr, cm^{-1}): 1607 (s), 1577 (m), 1565 (br), 1483 (s), 1440 (w), 1431 (m), 1411 (w), 1089 (br), 767 (s), 731 (m), 624 (s).

[{Mn$_2$(μ-O)}(μ-fum)(tpbn)]$_2$(ClO$_4$)$_4$ (14). A procedure similar to that of **1** was followed except 11.6 mg (0.01 mmol) fumaric acid (H_2fum) was used instead of glutaric acid. Yield: 76 mg (85%). Selected FTIR peaks (KBr, cm^{-1}): 1607 (s), 1574 (w), 1563 (m), 1484 (s), 1443 (m), 1377 (br), 1090 (br), 769 (s), 730 (m), 625 (s).

[{Mn$_2$(μ-O)}(μ-suc)(tphn)]$_2$(ClO$_4$)$_4$ (15). A procedure similar to that of **1** was followed except 48 mg (0.01 mmol) tphn and 11.8 mg (0.01 mmol) succinic acid (H_2suc) was used instead of tpbn and glutaric acid. Yield: 48 mg (52%). Anal. Calc. (%) for **15**·H_2O (MF $C_{136}H_{158}N_{24}O_{53}Cl_8Mn_8$, FW 3699.9671): C, 43.89; H, 4.44; N, 9.03. Found: C, 43.36; H, 4.35; N, 8.90. Crystals suitable for single crystal X-ray diffraction study were obtained by slow diffusion of dibutyl ether into acetonitrile solution of **15**. Selected FTIR peaks (KBr, cm^{-1}): 1607 (s), 1576 (br), 1564 (br), 1484 (s), 1434 (br), 1094 (br), 769 (s), 730 (m), 624 (s).

[{Mn$_2$(μ-O)}(μ-fum)(tphn)]$_2$(ClO$_4$)$_4$ (16). A procedure similar to that of **1** was followed except 48 mg (0.01 mmol) tphn and 11.8 mg (0.01 mmol) fumaric acid (H_2fum) was used instead of tpbn and glutaric acid. Yield: 60 mg (65%). Anal. Calc. (%) for **16** (MF $C_{136}H_{154}N_{24}O_{52}Cl_8Mn_8$, FW 3679.9359): C, 44.4; H, 4.17; N, 9.14. Found: C, 44.71; H, 4.23; N, 9.12. Selected FTIR peaks (KBr, cm^{-1}): 1607 (s), 1574 (w), 1563 (s), 1484 (s), 1443 (m), 1379 (br), 1092 (br), 768 (s), 730 (m), 624 (s). 487, 526, 710, 260.

[{Fe$_2$(μ-O)}(μ-adc)(tphn)]$_2$(ClO$_4$)$_4$ (17). In a 10 mL round bottom flask, 48 mg (0.1 mmol) of tphn was dissolved in 0.5 mL of methanol. 70.8 mg (0.2 mmol) of Fe(ClO_4)$_3$.xH_2O was added to it with stirring. To this, a solution of 11.4 mg (0.1 mmol) of acetylenedicarboxylic acid (H_2adc) and 8 mg (0.2 mmol) of NaOH in 0.5 mL of water was added. Another 1 mL of water and 1 mL of methanol was added to it. The mixture was stirred for another 1 h. A yellow-brown solid was obtained, filtered, washed with methanol and air dried. Yield: 70

mg (74%). Selected FTIR peaks (KBr, cm^{-1}): 1608 (s), 1576 (s), 1484 (s), 1437 (s), 1382 (br), 1091 (br), 768 (s), 733 (s), 624 (s). 487, 526, 710, 260.

[{Fe_2(μ-O)}(μ-fum)(tphn)]$_4$(ClO_4)$_8$·H_2O (18). A procedure similar to that of **17** was followed except 11.6 mg (0.01 mmol) fumaric acid (H_2fum) was used instead of acetylenedicarboxylic acid. Yield: 77 mg (81%). Selected FTIR peaks (KBr, cm^{-1}): 1608 (s), 1573 (w), 1558 (s), 1485 (s), 1438 (m), 1391 (s), 1094 (br), 768 (s), 730 (m), 624 (s). 487, 526, 710, 260.

[{Fe_2(μ-O)}(μ-suc)(tphn)]$_4$(ClO_4)$_8$ (19). A procedure similar to that of **17** was followed except 11.8 mg (0.01 mmol) succinic acid (H_2suc) was used instead of acetylenedicarboxylic acid. Yield: 67 mg (82%). Selected FTIR peaks (KBr, cm^{-1}): 1608 (s), 1573 (w), 1551 (s), 1484 (m), 1433 (s), 1093 (s), 768 (s), 730 (m), 624 (s). 487, 526, 710, 260. Crystals suitable for single crystal X-ray diffraction study were obtained by slow diffusion of dibutyl ether into acetonitrile solution of **19**.

[{Fe_2(μ-O)}(μ-glu)(tphn)]$_2$(ClO_4)$_4$ (20). A procedure similar to that of **17** was followed except 13.2 mg (0.01 mmol) glutaric acid (H_2glu) was used instead of acetylenedicarboxylic acid. Yield: 72 mg (70%). Selected FTIR peaks (KBr, cm^{-1}): 1608 (s), 1574 (w), 1545 (s), 1484 (s), 1435 (m), 1376 (s), 1090 (br), 768 (s), 733 (s), 624 (s). 487, 526, 710, 260.

[{Fe_2(μ-O)}(μ-adc)(tpon)]$_2$(ClO_4)$_4$ (21). A procedure similar to that of **17** was followed except 50.8 mg (0.01 mmol) tpon was used instead of tphn. Yield: 70 mg (74%). Selected FTIR peaks (KBr, cm^{-1}): 1608 (s), 1576 (s), 1484 (s), 1437 (s), 1382 (br), 1091 (br), 768 (s), 733 (s), 624 (s). 487, 526, 710, 260.

[{Fe_2(μ-O)}(μ-fum)(tpon)]$_4$(ClO_4)$_8$·H_2O (22). A procedure similar to that of **17** was followed except 50.8 mg (0.01 mmol) of tpon and 11.6 mg (0.01 mmol) fumaric acid (H_2fum) was used instead of tphn and acetylenedicarboxylic acid, respectively. Yield: 77 mg (81%). Selected FTIR peaks (KBr, cm^{-1}): 1608 (s), 1573 (w), 1558 (s), 1485 (s), 1438 (m), 1391 (s), 1094 (br), 768 (s), 730 (m), 624 (s). 487, 526, 710, 260.

[{Fe_2(μ-O)}(μ-suc)(tpon)]$_4$(ClO_4)$_8$ (23). A procedure similar to that of **17** was followed except 50.8 mg (0.01 mmol) of tpon and 11.8 mg (0.01 mmol) succinic acid (H_2suc) was used instead of tphn and acetylenedicarboxylic acid, respectively. Yield: 67 mg (82%).

Selected FTIR peaks (KBr, cm^{-1}): 1608 (s), 1573 (w), 1551 (s), 1484 (m), 1433 (s), 1093 (s), 768 (s), 730 (m), 624 (s). 487, 526, 710, 260.

[{Fe_2(μ-O)}(μ-glu)(tpon)]$_2$(ClO_4)$_4$ (24). A procedure similar to that of **17** was followed except 50.8 mg (0.01 mmol) of tpon and 13.2 mg (0.01 mmol) glutaric acid (H_2glu) was used instead of tphn and acetylenedicarboxylic acid, respectively. Yield: 72 mg (70%). Selected FTIR peaks (KBr, cm^{-1}): 1608 (s), 1574 (w), 1545 (s), 1484 (s), 1435 (m), 1376 (s), 1090 (br), 768 (s), 733 (s), 624 (s). 487, 526, 710, 260.

[{Mn_2(μ-O)$_2$}$_2$(μ-adc)(tpbn)$_2$](ClO_4)$_4$ (25). In a 10 mL round bottom flask, 16.9 mg (0.1 mmol) of $MnSO_4 \cdot H_2O$ was taken and dissolved in 1.5 mL of methanol. 32.3 mg (0.07 mmol) of tpbn and 1 mL of acetylenedicarboxylic acid-sodium acetylenedicarboxylate buffer (pH 4.5) was added to the above solution. An aqueous solution of 0.07 mmol Na_2adc (8.2 mg H_2adc + 5.7 mg of NaOH) and aqueous solution of 6.77 mg $KMnO_4$ was added drop wise to the solution over a period of 10 min and 20 min, respectively. The solution was kept for stirring for another hour and filtered. The green solid was precipitated out by the addition of an aqueous solution of $NaClO_4$ to the filtrate. The compound was filtered by using a G4 crucible, washed with methanol and air dried. Yield: 60 mg (65%). Anal. Calc. (%) for **25**$\cdot 2H_2O$ (MF $C_{66}H_{84}N_{12}O_{26}Cl_4Mn_4$, FW 1823.0021): C, 43.48; H, 4.64; N, 9.22. Found: C, 43.47; H, 4.66; N, 8.75. Selected FTIR peaks (KBr, cm^{-1}): 1607 (s), 1573 (w), 1563 (s), 1483 (s), 1443 (m), 1374 (br), 1090 (br), 769 (s), 624 (s).

[{Mn_2(μ-O)$_2$}$_2$(μ-fum)(tpbn)$_2$](ClO_4)$_4$ (26). A procedure similar to that of **25** was followed except 0.07 mmol of Na_2fum (8.3 mg of H_2fum + 5.7 mg of NaOH) was used instead of Na_2adc and fumaric acid-sodium fumarate was used as buffer (pH 4.5) was used. Yield: 62 mg (66%). Anal. Calc. (%) for **26** (MF $C_{60}H_{66}N_{12}O_{24}Cl_4Mn_4$, FW 1700.7962): C, 42.37; H, 3.91; N, 9.88. Found: C, 42.23 H, 4.1; N, 10.34. Selected FTIR peaks (KBr, cm^{-1}): 1606 (s), 1594 (w), 1573 (s), 1484 (s), 1443 (m), 1380 (br), 1090 (br), 768 (s), 687 (w), 624 (s).

[{Mn_2(μ-O)$_2$}$_2$(μ-suc)(tpbn)$_2$](ClO_4)$_4$ (27). A procedure similar to that of **25** was followed except 0.07 mmol of Na_2suc (8.5 mg of H_2suc + 5.7 mg of NaOH) of was used instead of Na_2adc and succinic acid-sodium succinate was used as buffer (pH 4.5) was used. Yield: 68 mg (70%). Anal. Calc. (%) for **27**$\cdot 3H_2O$ (MF $C_{60}H_{74}N_{12}O_{27}Cl_4Mn_4$, FW 1756.8579): C, 41.30; H, 4.80; N, 9.90. Found: C, 41.02; H, 4.25; N, 9.57. Selected FTIR peaks (KBr, cm^{-1}): 1607 (s), 1571 (w), 1560 (s), 1484 (s), 1437 (s), 1388 (br), 1090 (br), 769 (s), 623

(s). 487, 526, 710, 260. Crystals suitable for single crystal X-ray diffraction study were obtained by slow diffusion of dibutyl ether into acetonitrile solution of **27**.

[{Mn$_2$(μ-O)$_2$}$_2$(μ-glu)(tpbn)$_2$](ClO$_4$)$_4$ (28). A procedure similar to that of **25** was followed except 0.07 mmol of Na$_2$glu (9.5 mg of H$_2$glu + 5.7 mg of NaOH) of was used instead of Na$_2$adc and glutaric acid-sodium glutarate was used as buffer (pH 4.5) was used. Yield: 69 mg (66%). Anal. Calc. (%) for **28**·4H$_2$O (MF $C_{61}H_{78}N_{12}O_{24}Cl_4Mn_4$, MW 1724.9022): C, 40.92; H, 4.36; N, 9.39. Found: C, 40.47; H, 4.12; N, 8.88. Selected FTIR peaks (KBr, cm^{-1}): 1607 (s), 1570 (w), 1561 (s), 1483 (s), 1438 (m), 1383 (br), 1091 (br), 768 (s), 690 (m), 624 (s). 487, 526, 710, 260.

[{Mn$_2$(μ-O)$_2$}$_2$(μ-adi)(tpbn)$_2$](ClO$_4$)$_4$ (29). A procedure similar to that of **25** was followed except 0.07 mmol of Na$_2$adi (10.5 mg of H$_2$adi + 5.7 mg of NaOH) was used instead of Na$_2$adc and adipic acid-sodium adipate was used as buffer (pH 4.5). Yield: 72 mg (64%). Anal. Calc. (%) for **29**·2H$_2$O (MF $C_{62}H_{76}N_{12}O_{26}Cl_4Mn_4$, FW 1766.8958): C, 42.15; H, 4.34; N, 9.51. Found: C, 41.60; H, 4.15; N, 9.39. Selected FTIR peaks (KBr, cm^{-1}): 1608 (s), 1569 (s), 1485 (s), 1438 (s), 1389 (m), 1089 (br), 770 (s), 690 (m), 626 (s). 487, 526, 710, 260. Crystals suitable for single crystal X-ray diffraction study were obtained by slow diffusion of dibutyl ether into acetonitrile solution of **29**.

[{Mn$_2$(μ-O)$_2$}$_2$(μ-adc)(tphn)$_2$](ClO$_4$)$_4$ (30). A procedure similar to that of **25** was followed except 0.07 mmol of tphn was used instead of tpbn. Yield: 76 mg (65%). Selected FTIR peaks (KBr, cm^{-1}): 1607 (s), 1573 (w), 1562 (s), 1483 (s), 1443 (m), 1376 (br), 1090 (br), 768 (s), 624 (s). 487, 526, 710, 260.

[{Mn$_2$(μ-O)$_2$}$_2$(μ-fum)(tphn)$_2$](ClO$_4$)$_4$ (31). A procedure similar to that of **25** was followed except 34.5 mg (0.07 mmol) of tphn, 0.07 mmol of Na$_2$fum (8.3 mg of H$_2$fum + 5.7 mg of NaOH) of was used instead of tpbn and Na$_2$adc. Fumaric acid-sodium fumarate buffer (pH 4.5) was used replacing the acetylenedicarboxylic acid-sodium acetylenedicarboxylate buffer. Yield: 77 mg (69%). Anal. Calc. (%) for **31**·H$_2$O (MF $C_{64}H_{78}N_{12}O_{25}Cl_4Mn_4$, FW 1776.9337): C, 43.75; H, 4.33; N, 9.62. Found: C, 43.31 H, 4.32; N, 9.47. Selected FTIR peaks (KBr, cm^{-1}): 1607 (s), 1573 (w), 1562 (s), 1483 (s), 1443 (m), 1376 (br), 1090 (br), 768 (s), 624 (s). 487, 526, 710, 260.

[{Mn$_2$(μ-O)$_2$}$_2$(μ-suc)(tphn)$_2$](ClO$_4$)$_4$ (32). A procedure similar to that of **25** was followed except 34.5 mg (0.07 mmol) of tphn, 0.07 mmol of Na$_2$suc (8.5 mg of H$_2$suc + 5.7 mg of NaOH) of was used instead of tpbn and Na$_2$adc. Succinic acid-sodium succinate buffer (pH

4.5) was used replacing the acetylenedicarboxylic acid-sodium acetylenedicarboxylate buffer. Yield: 79 mg (66%). Anal. Calc. (%) for **32**·$2H_2O$·$2NaClO_4$ (MF $C_{60}H_{72}N_{12}O_{34}Cl_6Mn_4Na_2$, FW 1983.7234): C, 36.33; H, 3.66; N, 8.47. Found: C, 36.25; H, 3.71; N, 7.72. Selected FTIR peaks (KBr, cm^{-1}): 1608 (s), 1573 (w), 1564 (s), 1484 (s), 1436 (m), 1386 (br), 1088 (br), 768 (s), 691 (s), 624 (s). 487, 526, 710, 260.

[{$Mn_2(\mu$-O)$_2$}$_2(\mu$-glu)(tphn)$_2$](ClO$_4$)$_4$ (33). A procedure similar to that of **25** was followed except 34.5 mg (0.07 mmol) of tphn, 0.07 mmol of Na_2glu (9.5 mg of H_2glu + 5.7 mg of NaOH) of was used instead of tpbn and Na_2adc. Glutaric acid-sodium glutarate buffer (pH 4.5) was used replacing the acetylenedicarboxylic acid-sodium acetylenedicarboxylate buffer. Yield: 82 mg (68%). Anal. Calc. (%) for **33**·$2H_2O$ (MF $C_{65}H_{82}N_{12}O_{26}Cl_4Mn_4$, FW 1808.9756): C, 44.09; H, 4.65; N, 8.81. Found: C, 43.43; H, 4.48; N, 9.09. Selected FTIR peaks (KBr, cm^{-1}): 1608 (s), 1573 (w), 1563 (w), 1484 (s), 1436 (m), 1375 (br), 1090 (br), 771 (s), 692 (m), 623 (s). 487, 526, 710, 260.

[{$Mn_2(\mu$-O)$_2$}$_2(\mu$-adi)(tphn)$_2$](ClO$_4$)$_4$ (34). A procedure similar to that of **25** was followed except 0.07 mmol of Na_2adi (10.5 mg of H_2adi + 5.7 mg of NaOH) of was used instead of tpbn and Na_2adc. Adipic acid-sodium adipate buffer (pH 4.5) was used replacing the acetylenedicarboxylic acid-sodium acetylenedicarboxylate buffer. Yield: 82 mg (66%). Anal. Calc. (%) for **34**·$2H_2O$ (MF $C_{66}H_{84}N_{12}O_{26}Cl_4Mn_4$, FW 1823.0021): C, 43.48; H, 4.64; N, 9.22. Found: C, 43.47; H, 4.66; N, 8.75. Selected FTIR peaks (KBr, cm^{-1}): 1608 (s), 1573 (w), 1561 (w), 1485 (s), 1441 (s), 1386 (s), 1090 (br), 769 (s), 690 (s), 624 (s). Crystals suitable for single crystal X-ray diffraction study were obtained by slow diffusion of dibutyl ether into acetonitrile solution of **34**.

{[Mn_2(tpxn)(fum)(H_2O)$_4$](fum)}$_n$ (**35**). In a 10 mL round bottom flask, 25 mg of tpxn (0.05 mmol) was taken and dissolved in 1.5 mL of methanol. To this clear solution, 24.5 mg (0.1 mmol) of Mn(OAc)$_2$·$4H_2O$ was added and stirred for a few minutes. As soon as the metal salt got dissolved, 11.6 mg (0.1 mmol) of H_2fum was added. A precipitate started to appear after stirring for few minutes. The reaction mixture was stirred for another 24 h. The solid product was separated by filtration and washing with methanol. Yield: 40 mg (85%). Selected FTIR peaks (KBr, cm^{-1}): 3400 (br), 3255 (br), 1682 (m), 1607 (br), 1565 (br), 1443 (m), 1366 (br).

{[Co_2(fum)(tpchn)(H_2O)$_4$](fum)}$_n$ (36). A procedure similar to that of **35** was followed, only 24.9 mg (0.05 mmol) of Co(OAc)$_2$·$4H_2O$ and 25.3 mg (0.05 mmol) of tpchn ligand

was taken instead of $Mn(OAc)_2 \cdot 4H_2O$ and tpxn. Yield: 40 mg (86%). Selected FTIR peaks (KBr, cm^{-1}): 3400 (br), 3257 (br), 1607 (m), 1575 (br), 3172 (m), 769 (s).

$\{[Co_2(fum)(tpxn)(H_2O)_4](fum)\}_n$ (37). A procedure similar to that of **35** was followed, only 24.9 mg (0.05 mmol) of $Co(OAc)_2 \cdot 4H_2O$ was taken instead of $Mn(OAc)_2 \cdot 4H_2O$. Yield: 38 mg (78%). Anal. Calc. (%) for **37**$\cdot 3H_2O$ (MF $C_{40}H_{50}N_6O_{15}Co_2$, MW 972.1998): C, 49.39; H, 5.18; N, 8.64. Found: C, 49.99; H, 5.58; N, 8.62. Selected FTIR peaks (KBr, cm^{-1}): 3420 (br), 3247 (br), 1607 (m), 1590 (br), 1385 (br), 769 (s).

$\{[Ni_2(fum)(tpchn)(H_2O)_4(fum)]\}_n$ (38). A procedure similar to that of **35** was followed, only 24.8 mg (0.05 mmol) of $Ni(OAc)_2 \cdot 4H_2O$ and 25.3 mg (0.05 mmol) of tpchn ligand was taken instead of $Mn(OAc)_2 \cdot 4H_2O$ and tpxn. Yield: 30 mg (61%). Anal. Calc (%) for **38**$\cdot 3H_2O$ (MF $C_{40}H_{56}N_6O_{15}Ni_2$, MW 978.2906): C, 49.11; H, 5.77; N, 8.59. Found: C, 48.87; H, 5.80; N, 8.75. Selected FTIR peaks (KBr, cm^{-1}): 3392 (br), 3248 (br), 1607 (m), 1574 (m), 1374 (m), 765 (s).

$\{[Ni_2(fum)(tpxn)(H_2O)_3(CH_3OH)](fum)\}_n$ (39). A procedure similar to that of **35** was followed, only 24.8 mg (0.05 mmol) of $Ni(OAc)_2 \cdot 4H_2O$ was taken instead of $Mn(OAc)_2 \cdot 4H_2O$. Yield: 41 mg (83%). Selected FTIR peaks (KBr, cm^{-1}): 1715 (s), 1607 (s), 1578 (br), 1379 (br), 767 (s).

$[Ni_2(suc)_2(tpchn)(H_2O)_4]$ (40). In a 10 mL round bottom flask, 25.3 mg (0.05 mmol) of tpchn was taken and dissolved in 1.5 mL of methanol. To this clear solution, 24.8 mg (0.1 mmol) of $Ni(OAc)_2 \cdot 4H_2O$ was added and stirred for few minutes. As soon as the metal salt got dissolved, 11.8 mg (0.1 mmol) of H_2suc was added. The reaction mixture stirred for 24 h. The solid product was separated after concentrating the resultant solution and removing the byproduct acetic acid with acetonitrile-toluene treatment. Yield: 46 mg (95%). Anal. Calc. (%) for **40**$\cdot 2H_2O$ (MF $C_{40}H_{58}N_6O_{14}Ni_2$, MW 964.3071): C, 49.82; H, 6.06; N, 8.72. Found: C, 49.88; H, 5.86; N, 8.47. Selected FTIR peaks (KBr, cm^{-1}): 3410 (br), 3257 (br), 1718 (s), 1605 (s), 1577 (br), 1409 (br), 767 (s).

$\{[Ni_2(glu)_2(tpchn)(H_2O)_2]\}_n$ (41). A procedure similar to that of **40** was followed, 13.2 mg (0.1 mmol) of H_2glu was taken instead of H_2suc. Yield: 47 mg (96%). Selected FTIR peaks (KBr, cm^{-1}): 1710 (m), 1607 (s), 1577 (br), 1406 (m), 766 (s).

$\{[Ni_2(adi)_2(tpchn)(H_2O)_2]\}_n$ (42). A procedure similar to that of **40** was followed, 14.6 mg (0.1 mmol) of H_2adi was taken instead of H_2suc. Yield: 41 mg (81%). Anal. Calc (%) for **42**$\cdot 3H_2O$ (MF $C_{44}H_{64}N_6O_{13}Ni_2$, MW 1002.3982): C, 52.72; H, 6.44; N, 8.38. Found: C,

53.04; H, 6.57; N, 8.46. Selected FTIR peaks (KBr, cm^{-1}): 1716 (m), 1605 (s), 1575 (br), 1405 (m), 767 (s).

[$Co_2(suc)_2(tpchn)(H_2O)_4$] (43). A procedure similar to that of **40** was followed, 24.9 mg (0.1 mmol) of $Co(OAc)_2 \cdot 4H_2O$ was added instead of $Ni(OAc)_2 \cdot 4H_2O$.Yield: 45 mg (90%). Anal. Calc. (%) for **4**·$4H_2O$ (MF $C_{40}H_{60}N_6O_{15}Co_2$, MW 1000.8173): C, 48.88; H, 6.15; N, 8.55. Found: C, 48.57; H, 5.43; N, 7.86. Selected FTIR peaks (KBr, cm^{-1}): 1717 (br), 1605 (m), 1577 (br), 1400 (br), 768 (s).

{[$Co_2(glu)_2(tpchn)(H_2O)_2$]}$_n$ (44). A procedure similar to that of **40** was followed, only 24.9 mg (0.1 mmol) of $Co(OAc)_2 \cdot 4H_2O$ and 13.2 mg (0.1 mmol) of H_2glu was added instead of $Ni(OAc)_2 \cdot 4H_2O$ and H_2suc. Yield: 34 mg (72%). Anal. Calc (%) for **44**·H_2O (MF $C_{42}H_{56}N_6O_{11}Co_2$, MW 938.7940): C, 53.73; H, 6.01; N, 8.95. Found: C, 53.69; H, 5.82; N, 8.29. Selected FTIR peaks (KBr, cm^{-1}): 1717 (m), 1607 (s), 1574 (m), 1404 (m), 767 (s).

{[$Co_2(adi)_2(tpchn)(H_2O)_2$]}$_n$ (45). A procedure similar to that of **40** was followed, only 24.9 mg (0.1 mmol) of $Co(OAc)_2 \cdot 4H_2O$ and 14.6 mg (0.1 mmol) of H_2adi was added instead of $Ni(OAc)_2 \cdot 4H_2O$ and H_2suc. Yield: 40 mg (83%). Anal. Calc. (%) for **45**·H_2O (MF $C_{44}H_{60}N_6O_{11}Co_2$, MW 966.8472): C, 54.66; H, 6.26; N, 8.69. Found: C, 54.84; H, 6.00; N, 8.00. Selected FTIR peaks (KBr, cm^{-1}): 1717(m), 1608 (s), 1573 (br), 1405 (m), 769 (s).

[$Ni_2(suc)_2(tpxn)(H_2O)_4$] (46). A procedure similar to that of **40** was followed, 25 mg (0.05 mmol) of tpxn was used instead of tpchn. Yield: 30 mg (65%). Anal. Selected FTIR peaks (KBr, cm^{-1}): 3213 (br), 1714 (s), 1607 (s), 1568 (br), 1417 (br), 766 (s). Crystals suitable for single crystal X-ray diffraction study were obtained from direct layering of the three components in 1:1 methanol and water mixture.

{[$Ni_2(glu)_2(tpxn)(H_2O)_2$]}$_n$ (47). A procedure similar to that of **40** was followed, 25 mg (0.05 mmol) of tpxn and 13.2 mg (0.1 mmol) of H_2glu was added instead of tpchn and H_2suc. Yield: 42 mg (88%). Selected FTIR peaks (KBr, cm^{-1}): 3393 (br), 3226 (br), 1710 (s), 1605 (m), 1567 (br), 1408 (br), 766 (s). Crystals suitable for single crystal X-ray diffraction study were obtained from direct layering of the three components in methanol and water solvent.

{[$Ni_2(adi)_2(tpxn)(H_2O)_2$]}$_n$ (48). A procedure similar to that of **40** was followed, 25 mg (0.05 mmol) of tpxn and 14.6 mg (0.1 mmol) of H_2adi was added instead of tpchn and

H_2suc. Yield: 36 mg (75%). Anal. Calc. (%) for **48**·H_2O $C_{44}H_{54}N_6O_{11}Ni_2$ (MW 960.3200): C, 55.03; H, 5.67; N, 8.75. Found: C, 55.27; H, 5.68; N, 8.44. Selected FTIR peaks (KBr, cm^{-1}): 3204 (br), 1605 (s), 1573 (s), 1416 (s), 767 (s). Crystals suitable for single crystal X-ray diffraction study were obtained from direct layering of the three components in 1:1 methanol and water mixture.

[Co_2(suc)$_2$(tpxn)(H_2O)$_4$] (49). A procedure similar to that of **40** was followed, 25 mg (0.05 mmol) of tpxn and 24.9 mg (0.1 mmol) of $Co(OAc)_2·4H_2O$ was used instead of tpchn and $Ni(OAc)_2·4H_2O$. Yield: 42 mg (91%). Selected FTIR peaks (KBr, cm^{-1}): 3401 (br), 3250 (br), 1714 (s), 1605 (m), 1573 (br), 1421 (br), 764 (s).

[Co_2(glu)$_2$(tpxn)(H_2O)$_2$] (50). A procedure similar to that of **40** was followed, 25 mg (0.05 mmol) of tpxn, 24.9 mg (0.1 mmol) of $Co(OAc)_2·4H_2O$ and 13.2 mg (0.1 mmol) of H_2glu was used instead of tpchn, $Ni(OAc)_2·4H_2O$ and H_2suc. Yield: 29 mg (66%). Selected FTIR peaks (KBr, cm^{-1}): 3407 (br), 3248 (br), 1713 (s), 1605 (m), 1575 (br), 1434 (br), 768 (s).

{[Co_2(adi)$_2$(tpxn)(H_2O)$_2$]}$_n$ (51). A procedure similar to that of **40** was followed, 25 mg (0.05 mmol) of tpxn, 24.9 mg (0.1 mmol) of $Co(OAc)_2·4H_2O$ and 14.6 mg (0.1 mmol) of H_2adi was used instead of tpchn, $Ni(OAc)_2·4H_2O$ and H_2suc. Yield: 30 mg (68%). Selected FTIR peaks (KBr, cm^{-1}): 3410 (br), 3245 (br), 1712 (s), 1605 (m), 1573 (br), 1434 (br), 769 (s).

{[Co_2(tdc)$_2$(tpbn)(H_2O)$_2$]}$_n$ (52). In a 10 mL round bottom flask, 22.5 mg (0.05 mmol) of tpbn was taken and dissolved in 1.5 mL of methanol. To this clear solution, 24.9 mg (0.1 mmol) of $Co(OAc)_2·4H_2O$ was added and stirred for few minutes. As soon as the metal salt got dissolved, 17.2 mg (0.1 mmol) of H_2tdc was added. A precipitate started to appear after 10 minutes. The reaction mixture stirred for 6 h. The solid product was separated by filtration and washed with methanol. Yield: 44 mg (89%). Anal. Calc. (%) for **52**·$2H_2O$ (MF $C_{40}H_{44}N_6O_{12}S_2Co_2$, MW 982.1767): C, 48.88; H, 4.51; N, 8.55. Found: C, 48.498; H, 3.954; N, 8.319. Selected FTIR peaks (KBr, cm^{-1}): 3399 (br), 3235 (br), 1607 (m), 1585 (br), 1572 (br), 1361 (br), 1338 (br), 772(s). Crystals suitable for single crystal X-ray diffraction study were obtained from direct layering of the three components in 1:1 methanol and water mixture.

[Co_2(tdc)$_2$(tphn)]$_n$ (53). A procedure similar to that of **52** was followed except that 24 mg (0.05 mmol) of tphn was used instead of tpbn. Yield: 48 mg (96%). Anal. Calc. (%) for **53**·H2O (MF $C_{42}H_{46}N_6O_{11}S_2Co_2$, MW 992.8446): C, 50.81; H, 4.67; N, 8.46. Found: C,

51.00; H, 4.54; N, 8.43. Selected FTIR peaks (KBr, cm^{-1}): 1606 (s), 1574 (m), 1545 (m), 1402 (s), 1343 (s), 771 (s). Crystals suitable for single crystal X-ray diffraction study were also obtained using similar method.

[Co_2(tdc)$_2$(tpchn)(H_2O)$_2$] (54). A procedure similar to that of **52** was followed, 25.3 mg (0.05 mmol) of tpchn was used instead of tpbn. Yield: 35 mg (65%). Anal. Calc. (%) for **54**·H_2O (MF $C_{44}H_{56}N_6O_{15}S_2Co_2$, MW 1090.9430): C, 48.44; H, 5.17; N, 7.70. Found: C, 48.30; H, 5.11; N, 7.70. Selected FTIR peaks (KBr, cm^{-1}): 3400 (br), 3221 (br), 1712 (s), 1605 (s), 1573 (br), 1361 (m), 773 (s). Crystals suitable for single crystal X-ray diffraction study were also obtained using similar method.

[Co_2(tdc)$_2$(tpxn)(H_2O)$_4$] (55). A procedure similar to that of **52** was followed, 24 mg (0.05 mmol) of tpxn was used instead of tpbn. Yield: 48 mg (90%). Anal. Calc. (%) for **55**·$2H_2O$ (MF $C_{44}H_{48}N_6O_{14}S_2Co_2$, MW 1066.8801): C, 49.53; H, 4.53; N, 7.88. Found: C, 49.89; H, 3.70; N, 7.72. Selected FTIR peaks (KBr, cm^{-1}): 1603 (m), 1570 (m), 1366 (br), 770 (s). Crystals suitable for single crystal X-ray diffraction study were also obtained using similar method.

{[Ni_2(tdc)$_2$(tpbn)(H_2O)$_2$]}$_n$ (56). A procedure similar to that of **52** was followed, 24.9 mg (0.1 mmol) of $Ni(OAc)_2·4H_2O$ was used instead of $Co(OAc)_2·4H_2O$. Yield: 45 mg (91%). Anal. Calc. (%) for **56**·$2H_2O$ (MF $C_{40}H_{44}N_6O_{12}S_2Ni_2$, MW 982.3272): C, 48.91; H, 4.51; N, 8.56. Found: C, 48.15; H, 4.87; N, 8.05. Selected FTIR peaks (KBr, cm^{-1}): 3239 (br), 1607 (s), 1586 (m), 1573 (m), 1361 (m), 776 (s). Crystals suitable for single crystal X-ray diffraction study were obtained from direct layering of the three components in 1:1 methanol and water mixture.

{[Ni_2(tdc)$_2$(tphn)]}$_n$ (57). A procedure similar to that of **52** was followed, 24.9 mg (0.1 mmol) of $Ni(OAc)_2·4H_2O$ and 24 mg (0.05 mmol) of tphn was used instead of $Co(OAc)_2·4H_2O$ and tpbn. Anal. Calc. (%) for **57** (MF $C_{42}H_{44}N_6O_{10}S_2Ni_2$, MW 974.3498): C, 51.77; H, 4.55; N, 8.63. Found: C, 51.11; H, 4.86; N, 8.92. Selected FTIR peaks (KBr, cm^{-1}): 1607 (s), 1575 (m), 1349 (s), 772 (s). Crystals suitable for single crystal X-ray diffraction study were also obtained using similar method.

[Ni_2(tdc)$_2$(tpchn)(H_2O)$_4$] (58). A procedure similar to that of **52** was followed, 24.9 mg (0.1 mmol) of $Ni(OAc)_2·4H_2O$ and 25.3 mg (0.05 mmol) of tpchn was used instead of $Co(OAc)_2·4H_2O$ and tpbn. Yield: 30 mg (57%). Anal. Calc. (%) for **58**·H_2O (MF $C_{44}H_{52}N_6O_{13}S_2Ni_2$, MW 1054.4329): C, 50.12; H, 4.97; N, 7.97. Found: C, 49.86; H, 4.99;

N, 8.03. Selected FTIR peaks (KBr, cm^{-1}): 1607 (s), 1575 (m), 1357 (m), 776 (s). Crystals suitable for single crystal X-ray diffraction study were also obtained using similar method.

[{$Ni_2(tdc)_2(tpxn)$] (59). A procedure similar to that of **52** was followed, 24.9 mg (0.1 mmol) of $Ni(OAc)_2 \cdot 4H_2O$ and 25 mg (0.05 mmol) of tpxn was used instead of $Co(OAc)_2 \cdot 4H_2O$ and tpbn. Yield: 50 mg (93%). Anal. Calc. (%) for **59**$\cdot 6H_2O$ (MF $C_{44}H_{48}N_6O_{14}S_2Ni_2$, MW 1066.4005): C, 49.53; H, 4.53; N, 7.88. Found: C, 49.51; H, 4.75; N, 7.59. Selected FTIR peaks (KBr, cm^{-1}): 1607 (s), 1578 (br), 1357 (br), 774 (s). Crystals suitable for single crystal X-ray diffraction study were also obtained using similar method.

{$[Cd_2(tdc)_2(tphn)_2]$}$_n$ (60). A procedure similar to that of **52** was followed, 26.6 mg (0.1 mmol) of $Cd(OAc)_2 \cdot 2H_2O$ and 24 mg (0.05 mmol) of tphn was used instead of $Co(OAc)_2 \cdot 4H_2O$ and tpbn. Yield 52 mg (91%). Selected FTIR peaks (KBr, cm^{-1}): 1605 (s), 1582 (br), 1364 (br), 771 (s). Crystals suitable for single crystal X-ray diffraction study were obtained from direct layering of the three components in 1:1 methanol and water mixture.

{$[Cd_2(tdc)_2(tpchn)_2$}$_n$ (61). A procedure similar to that of **52** was followed, 26.6 mg (0.1 mmol) of $Cd(OAc)_2 \cdot 2H_2O$ and 25.3 mg (0.05 mmol) of tpchn was used instead of $Co(OAc)_2 \cdot 4H_2O$ and tpbn. Yield 48 mg (81%). Selected FTIR peaks (KBr, cm^{-1}): 1606 (br), 1581 (br), 1351 (br), 769 (s). Crystals suitable for single crystal X-ray diffraction study were obtained from direct layering of the three components in 1:1 methanol and water mixture.

{$[Cd_2(tdc)_2(tpxn)]$}$_n$ (62). A procedure similar to that of **52** was followed, 26.6 mg (0.1 mmol) of $Cd(OAc)_2 \cdot 2H_2O$ and 25 mg (0.05 mmol) of tpxn was used instead of $Co(OAc)_2 \cdot 4H_2O$ and tpbn. Yield 45 mg (76%). Selected FTIR peaks (KBr, cm^{-1}): 1601 (s), 1576 (br), 1362 (br), 773 (s). Crystals suitable for single crystal X-ray diffraction study were obtained from direct layering of the three components in 1:1 methanol and water mixture.

{$[Co_2(cdc)_2(tpchn)(H_2O)_2]$}$_n$ (63). A procedure similar to that of **40** was followed, 24.9 mg (0.1 mmol) of $Co(OAc)_2 \cdot 4H_2O$, 25.3 mg (0.05 mmol) of tpchn and 13.2 mg (0.1 mmol) of H_2cdc was added instead of $Ni(OAc)_2 \cdot 4H_2O$, tpbn and H_2suc Yield: 44 mg (86%). Anal. Calc (%) for **63**$\cdot H_2O$ (MF $C_{48}H_{64}N_6O_{11}Co_2$, MW 1018.9218): C, 56.58; H, 6.33; N, 8.25. Found: C, 56.98; H, 6.25; N, 8.05. Selected FTIR peaks (KBr, cm^{-1}): 1606 (s), 1567 (br), 1406 (m), 768 (s).

[$Co_2(cdc)_2(tpxn)(H_2O)$] (64). A procedure similar to that of **40** was followed, 24.9 mg (0.1 mmol) of $Co(OAc)_2 \cdot 4H_2O$, 25 mg (0.05 mmol) of tpxn and 17.2 mg (0.1 mmol) of H_2cdc was added instead of $Ni(OAc)_2 \cdot 4H_2O$, tpbn and H_2suc. Yield: 40 mg (80%). Selected FTIR peaks (KBr, cm^{-1}): 1606 (s), 1573 (br), 1564 (br), 1447 (s), 1407 (m), 770 (s). Crystals suitable for single crystal X-ray diffraction study were obtained from direct layering of the three components in 1:1 methanol and water mixture.

[$Ni_2(cdc)_2(tpchn)$] (65). A procedure similar to that of **40** was followed, 25 mg (0.05 mmol) of tpchn and 17.2 mg (0.1 mmol) of H_2cdc was added instead of $Ni(OAc)_2 \cdot 4H_2O$, tpbn and H_2suc. Yield: 42 mg (84%). Anal. Calc. (%) for **65**$\cdot 2H_2O$ (MF $C_{48}H_{62}N_6O_{10}Ni_2$, MW 1000.4269): C, 57.63; H, 6.25; N, 8.40. Found: C, 57.33; H, 6.51; N, 8.34. Selected FTIR peaks (KBr, cm^{-1}): 3421 (br), 3217 (br), 1607 (s), 1564 (m), 1407 (s), 768 (s).

{[$Ni_2(cdc)_2(tpxn)(H_2O)_2$]}$_n$ (66). A procedure similar to that of **40** was followed, 25 mg (0.05 mmol) of tpchn and 17.2 mg (0.1 mmol) of H_2cdc was added instead of $Ni(OAc)_2 \cdot 4H_2O$, tpbn and H_2suc. Yield: 42 mg (76%). Anal. Calc. (%) for **66**$\cdot 6H_2O$ (MF $C_{48}H_{68}N_6O_{16}Ni_2$, MW 1102.4709): C, 52.29; H, 6.22; N, 7.62. Found: C, 52.64; H, 5.30; N, 7.40. Selected FTIR peaks (KBr, cm^{-1}): 1606 (s), 1577 (m), 1560 (m), 1406 (m), 770 (s). Crystals suitable for single crystal X-ray diffraction study were obtained from direct layering of the three components in 1:1 methanol and water mixture.

{[$Co_3(btc)_2(tpxn)_{1.5}(H_2O)_4$]}$_n$ (67). In a 10 mL round bottom flask, 30 mg (0.06 mmol) of tpxn ligand was taken and dissolved in 1.5 mL of methanol. To this clear solution, 29.8 mg (0.12 mmol) of $Co(OAc)_2 \cdot 4H_2O$ was added and stirred for few minutes. As soon as the metal salt got dissolved, 16.8 mg (0.079 mmol) of H_2tdc was added. The reaction mixture stirred for 24 h. A solid product was isolated via filtration and air dried. Yield: 42 mg (78%). Selected FTIR peaks (KBr, cm^{-1}): 1606 (s), 1573 (br), 1564 (br), 1447 (s), 1407 (m), 770 (s). Crystals suitable for single crystal X-ray diffraction study were obtained from direct layering of the three components in 1:1 methanol and water mixture.

CHAPTER III

RESULTS AND DISCUSSION

This chapter is divided into two major sections: metal organic cages (MOCs) and coordination polymers (CPs). The first section is divided into three subsections based on the dimetal core types while the second section is comprised of five subsections based on the possible combination flexibility/rigidity of carboxylate linkers and bis(tridentate) ligands. All new metal complexes reported in this thesis were synthesized using six different bis(tridentate) polypyridyl ligands shown in Figure 1.13. These differ by the spacer between the alkyl nitrogen atoms and thus have varied flexibility and length. In order to increase the rigidity and length of ligand, spacers were changed from aliphatic chain to 1,4-dimethylenecyclohexane to 1,4-phenylenedimethylene. However, a general procedure has been followed for their synthesis as shown in Scheme 3.1. Four equivalents of picolylchloride hydrochloride were added with the corresponding diamine in an aqueous medium. The chloride ion of picolylchloride reacted with amine to form HCl. Total eight equivalents of aqueous NaOH was needed for this reaction to neutralize HCl formed and already present as hydrochloride salt in picolylchloride. A solid was obtained as a product in all cases, which was filtered, washed with an excess amount of water and air-dried.

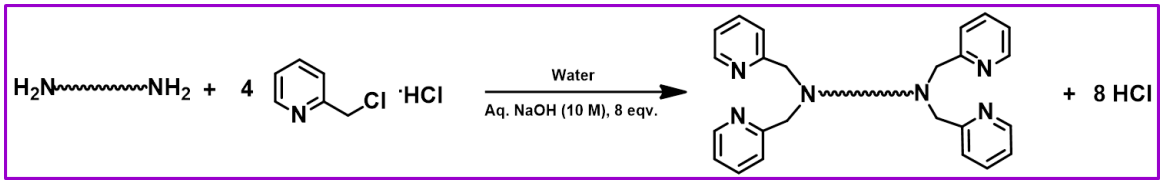

Scheme 3.1. General Synthesis of Ligands.

3.1 METAL ORGANIC CAGES (MOCs)

3.1.1 With $\{Mn_2(\mu\text{-}O)(\mu\text{-}O_2CR)_2\}^{2+}$ Core

Synthesis. These compounds were synthesized by following a procedure reported in literature.[141,147] In each case, the reaction was done at room temperature under aerobic conditions as shown in Scheme 3.2. Three components ligand, $Mn(OAc)_3 \cdot 2H_2O$, and the corresponding dicarboxylic acid in a 1:2:1 ratio were reacted in methanol followed by precipitation with excess $NaClO_4$ to get a reddish brown solid. The solid product was filtered, washed with methanol and air dried.

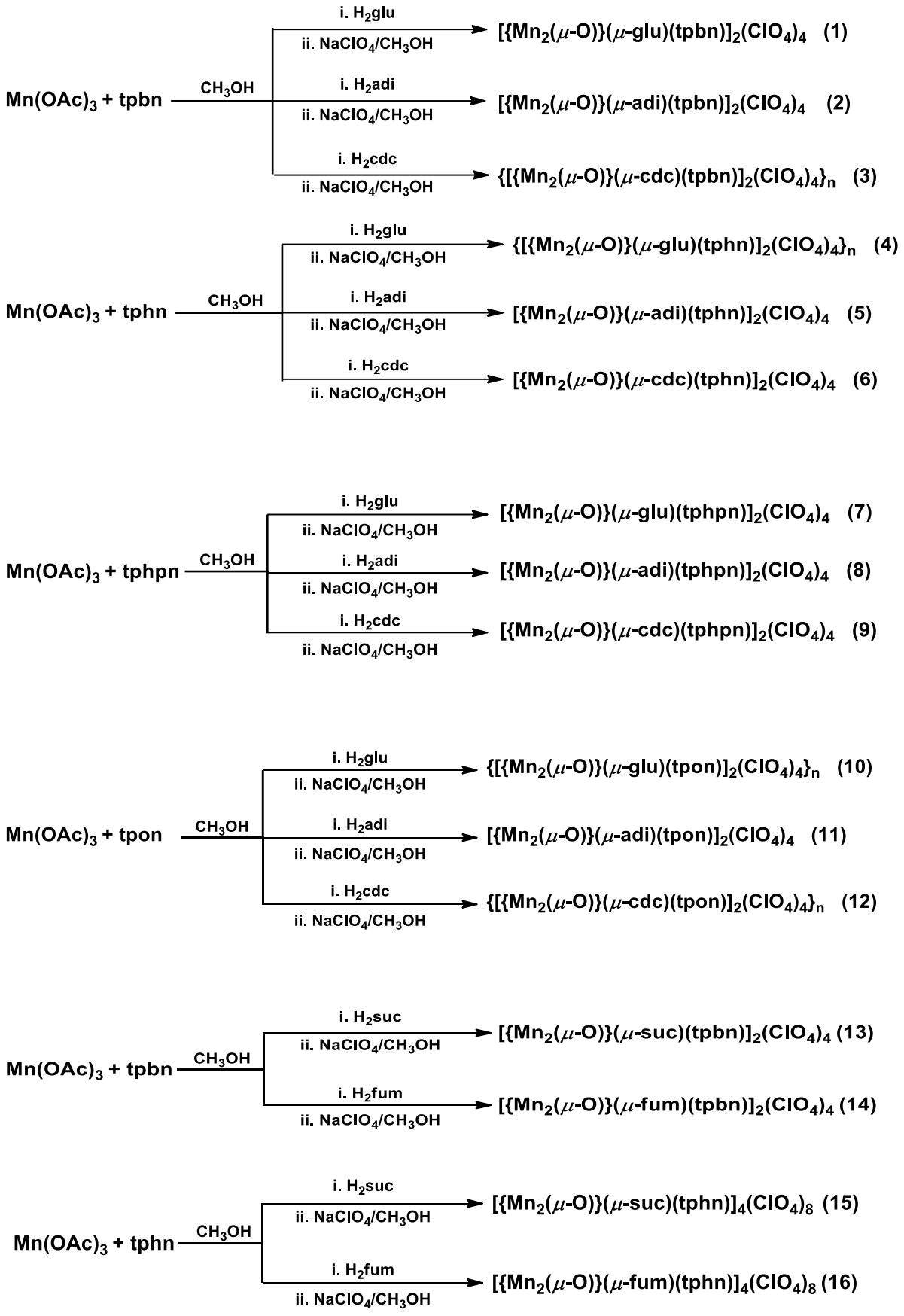

Scheme 3.2. Synthesis of **1-16**.

A total of sixteen new compounds (**1-16**) were prepared. The as-synthesized solids were used for characterization without any purification. Crystals suitable for single crystal study were obtained (wherever possible) by layering of an acetonitrile solution of the compound with either di-isopropyl ether or with di-tertiary-butyl ether.

FTIR Spectroscopy. As indicated in Chapter I, the $\{Mn_2(\mu\text{-}O)(\mu\text{-}O_2CR)_2\}^{2+}$ core has signature spectroscopic features. FTIR spectroscopy is a very helpful tool to determine the binding mode of the ligands/linkers for elucidating the structure of MOCs. For example, the difference in the asymmetric and symmetric stretching frequencies of carboxylates ($\Delta\nu = \nu_{asym}\text{-}\nu_{sym}$) confirms the binding modes of carboxylates in these compounds; a value less than 150 cm^{-1} is indicative of bridging mode to the dimetal core. Similarly, the presence of Mn-O-Mn bond in these compounds as well as the counter anion such as perchlorate can also be proven by their FTIR spectra. The FTIR data for compounds **1**-**16** has been tabulated in Table 3.1.

Table 3.1. Selected FTIR peaks for **1**-1**6.**

Compounds	$\nu_{asym}(COO^-)$, cm^{-1}	$\nu_{asym}(COO^-)$, cm^{-1}	$\nu(ClO_4^-)$, cm^{-1}	ν(Mn-O-Mn), cm^{-1}
1	1559	1434	1089, 625	732
2	1564	1440	1090, 624	732
3	1560	1438	1088, 625	728
4	1562	1434	1088, 625	733
5	1560	1436	1089, 624	730
6	1560	1432	1088, 625	734
7	1562	1433	1089, 625	730
8	1561	1433	1089, 624	734
9	1562	1431	1089, 624	730
10	1562	1434	1090, 625	733
11	1564	1430	1091, 624	731
12	1563	1433	1092, 625	735
13	1559	1423	1088, 625	730
14	1562	1431	1089, 624	733
15	1563	1430	1089, 624	730
16	1563	1431	1090, 625	734

The carboxylate stretching frequencies varies from 1559 to 1564 cm^{-1} for the asymmetric mode and 1423 to 1440 cm^{-1} for the symmetric mode. For the Mn-O-Mn bond, a peak

appears in the range of 728-734 cm^{-1} for these compounds. These data confirm that compounds **1-16** have similar core type and the carboxylate groups bind in an identical fashion. This is further established by their magnetic behaviour and single crystal structures for few compounds.

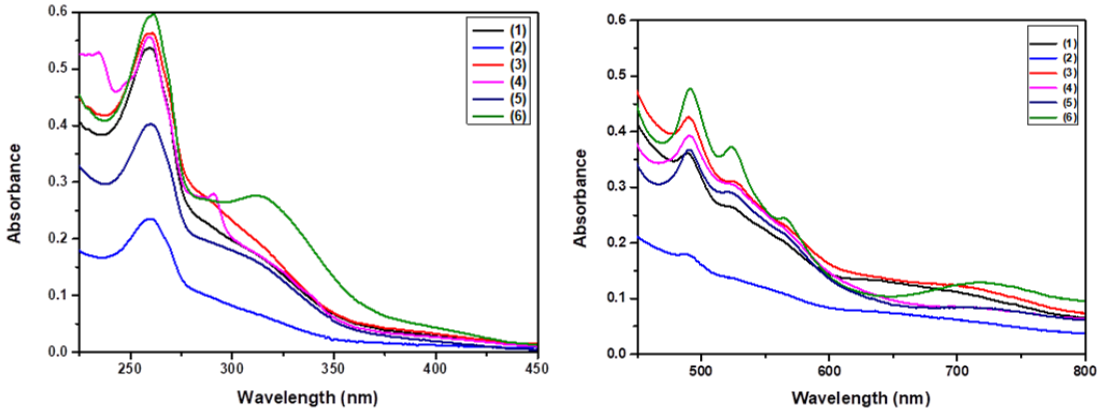

Figure 3.1. UV-vis spectra of **1- 6.**

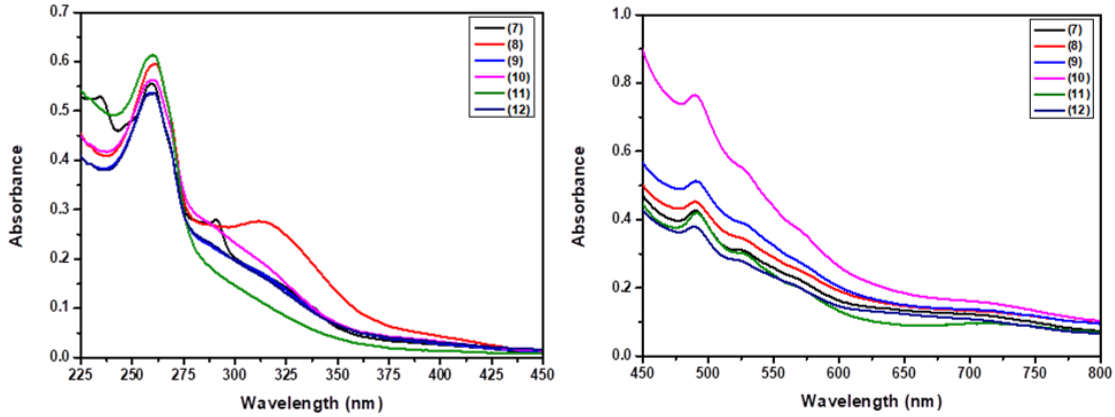

Figure 3.2.UV-vis spectra of **7-12.**

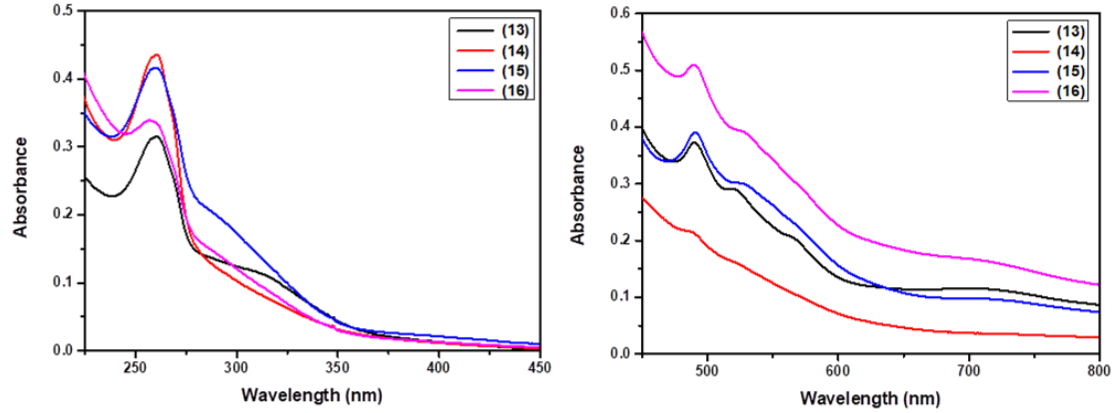

Figure 3.3. UV-vis spectra of **13-16.**

UV-Vis Spectroscopy. UV-Vis spectra of **1**-1**6** were recorded in acetonitrile solution: 0.1 mM (for the visible region) and 0.0035 mM (for UV region) (Figures 3.1, 3.2 and 3.3). All

these compounds show similar features, thereby proving the formation of compounds with an identical core. For explanation of the observed bands, one such set (**1**-**6**) is described below. In case of compounds **1**-**6**, intense bands at 490 nm, 520 nm, 570 nm and 720 nm are observed in the visible region. These bands correspond to the oxo-to-metal charge transfer and d-d transitions in the metal. For **2**, **11** and **14**, the peaks at around 720 nm and 570 nm are not resolved properly. These compounds show peaks at 270 nm and 320 nm in the ultraviolet region.

Single Crystal Structure Analysis. Based on the characteristic spectroscopic features described above for **1**-**16**, it is clear that all of these compounds have the $\{Mn_2(\mu\text{-}O)(\mu\text{-}O_2CR)_2\}^{2+}$ core. However, their nuclearity can only be ascertianed by determining their crystal structures. Thus, efforts were made to get their suitable crystals but only those of compounds **5**, **6**, **13** and **15** were good enough. In view of this, magnetic studies (vide infra) has also been coupled with the selected X-ray structures to make conclusive about their nuclearity. Interestingly, these compounds were found to be existing in all three possible structures proposed in Chapter I.

Structural Description of 5. It crystallizes in the monoclinic *C*2/*m* space group. The crystallographic information pertaining to data collection and structure refinement has been provided in Table A1. Both Mn atoms are distorted octahedrally and surrounded by three N-atoms from each end of the bis(tridentate) ligand, two carboxylate O-atoms and one oxo O-atom. Thus, a N_3O_3 coordination environment is present around each manganese center. All these N or O-atoms are bound to the metal in a facial manner. The Mn···Mn distance (within the core) is 3.129(3) Å and Mn-O_{oxo} distances are 1.774(8) Å and 1.797(8) Å, which commensurates with the value reported for similar type of compounds.[134-159] Selected bond distances and bond angles are listed in Table A14 and Table A40, respectively. The ligands as well as the carboxylates bridge between two Mn-atoms of two Mn_2O-dimetalic unit forming an overall tetranuclear (dimer-of-dimer) compound as shown in Figure 3.4. Each molecule further connected to form a 1D supramolecular assembly through strong π-π interaction (3.549 Å) between the pyridyl groups of the bis(tridentate) ligand tphn, present in compound **5**.

Structural Description of 6. It crystallizes in the triclinic *P*-1 space group. The crystallographic information pertaining to data collection and structure refinement has been provided in Table A1. Like compound **5**, it contains distorted octahedral Mn atoms with a N3O3 coordination environment, provided by one end of the tphn ligand, one oxo O-atom

and two carboxylate O-atoms from two cyclohexane dicarboxylic acid (Figure 3.5). The Mn···Mn distance (within the core) is 3.131(2) Å and Mn-O_{oxo} distances are 1.785(4) Å and 1.777(4) Å; these values are similar to those observed for **5**. Selected bond distances and bond angles are listed in Table A15 and Table A41, respectively. The Mn···Mn distance between two cores is 8.656 Å

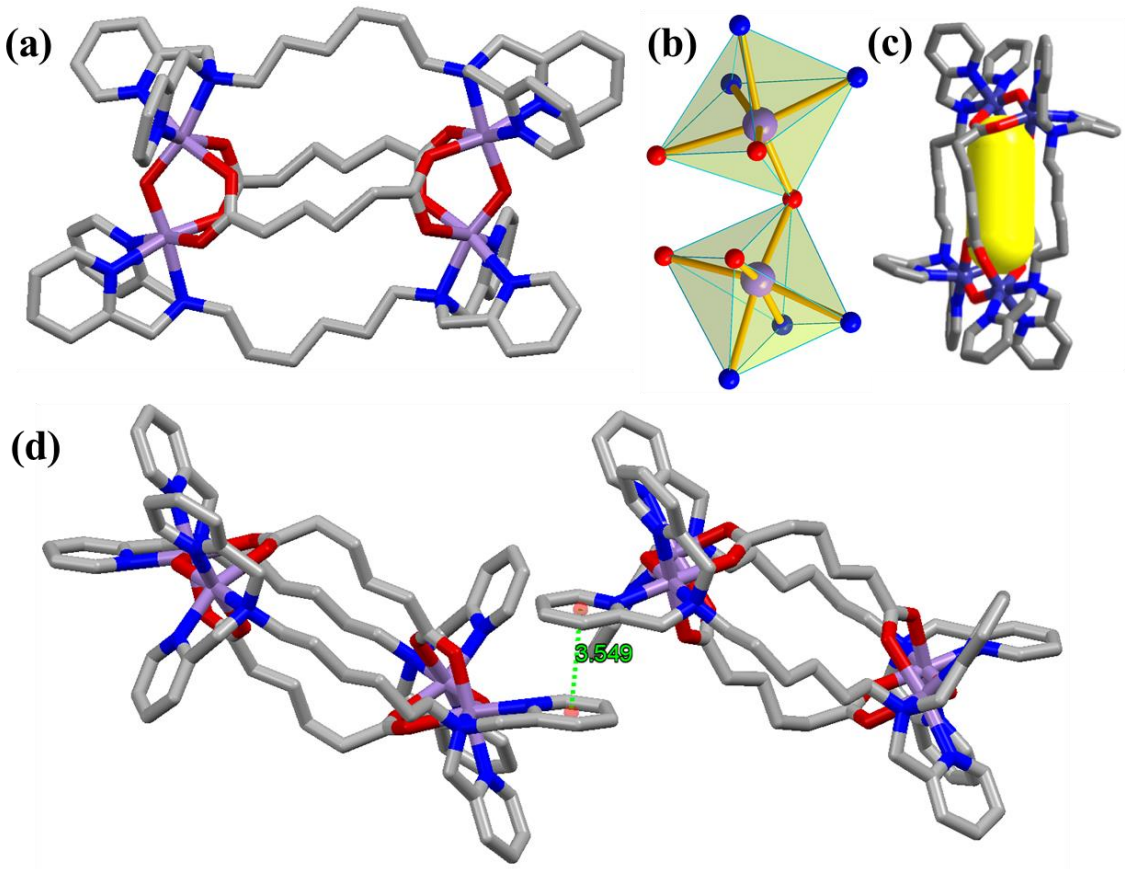

Figure 3.4. Crystal structure of **5**. (a) tetranuclear MOC, (b) coordination environment around Mn atoms, (c) pore inside **5**, and (d) π-π stacking between the molecules (color code used for different atoms are like, pink: Mn; red: O, blue: N, grey: C). H-atoms are removed for clarity.

Structural Description of 13·2CH₃CN. It crystallizes in triclinic *P*-1 space group. The crystallographic information pertaining to data collection and structure refinement has been provided in Table A2. The compound is isostructural with **5** and **6** (Figure 3.6). Each Mn center is in N3O3 type distorted octahedral environment occupied by three nitrogen atoms from one end of the tpbn ligand, two carboxylate oxygen atoms, and one oxygen atom bridged between two Mn centers. The Mn···Mn distance (within the core) is 3.182(1) Å and Mn-O_{oxo} distances are 1.799(3) Å and 1.791(3) Å. The Mn···Mn distance between two cores is 6.798 Å. Selected bond distances and bond angles are listed in Table A16 and Table A42, respectively.

Structural Description of 15·2CH₃CN. This compound crystallizes in triclinic system with *P*-1 space group. The crystallographic information pertaining to data collection and structure refinement has been provided in Table A2. Although each Mn atom has similar N3O3 coordination environment like compounds **5**, **6** and **13,** the overall structure of this compound

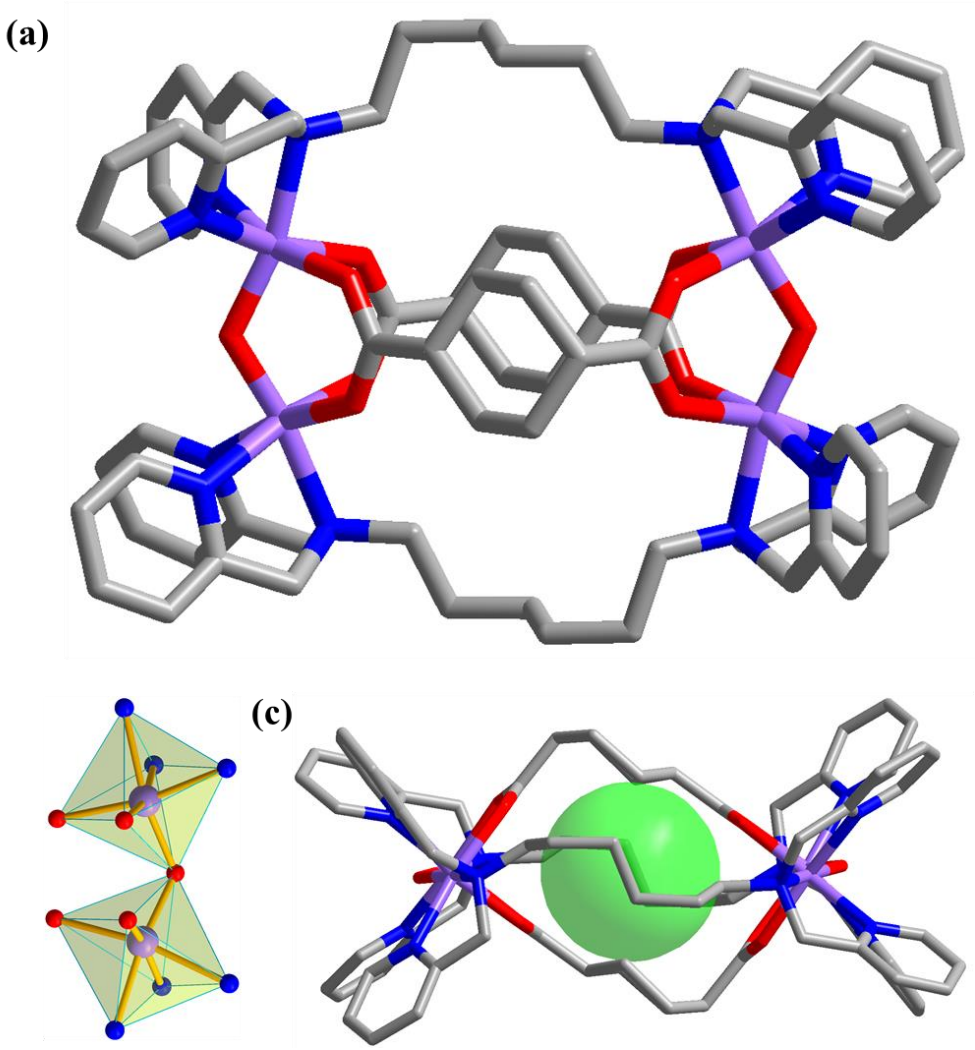

Figure 3.5. Crystal structure of **6**. (a) tetranuclear MOC. (b) coordination environment around Mn-atoms and (c) pore inside of **6** (color code used for different atoms are like, pink: Mn; red: O, blue: N, grey: C). H-atoms are removed for clarity.

is different from the earlier discussed structures. The Mn···Mn distances (within the core) are 3.154(3) Å and 3.159(3) Å, and the Mn-O_{oxo} distances are 1.804(9) Å, 1.792(9) Å, 1.787(9) Å and 1.834(8) Å. Selected bond distances and bond angles are listed in Table A17 and Table A43, respectively. Two tphn ligands and one succinate are bridged between two Mn_2O-dimetalic unit, forming a tetranuclear (dimer-of-dimer) unit as shown in Figure 3.7. Two of these similar tetranuclear units again are connected through two other succinates to form an overall octanuclear compound. Whereas in **5**, **6**and **13**, two tphn

ligands and two succinate are bridged between two Mn_2O-dimetalic unit. The Mn···Mn distances between two cores are 8.765 Å, 8.644 Å, 8.654 Å and 8.637 Å. The aromatic pyrydyl rings of next molecule are involved in forming a 2D supramolecular assembly through two types of strong π-π interactions (3.568 and 3.626 Å).

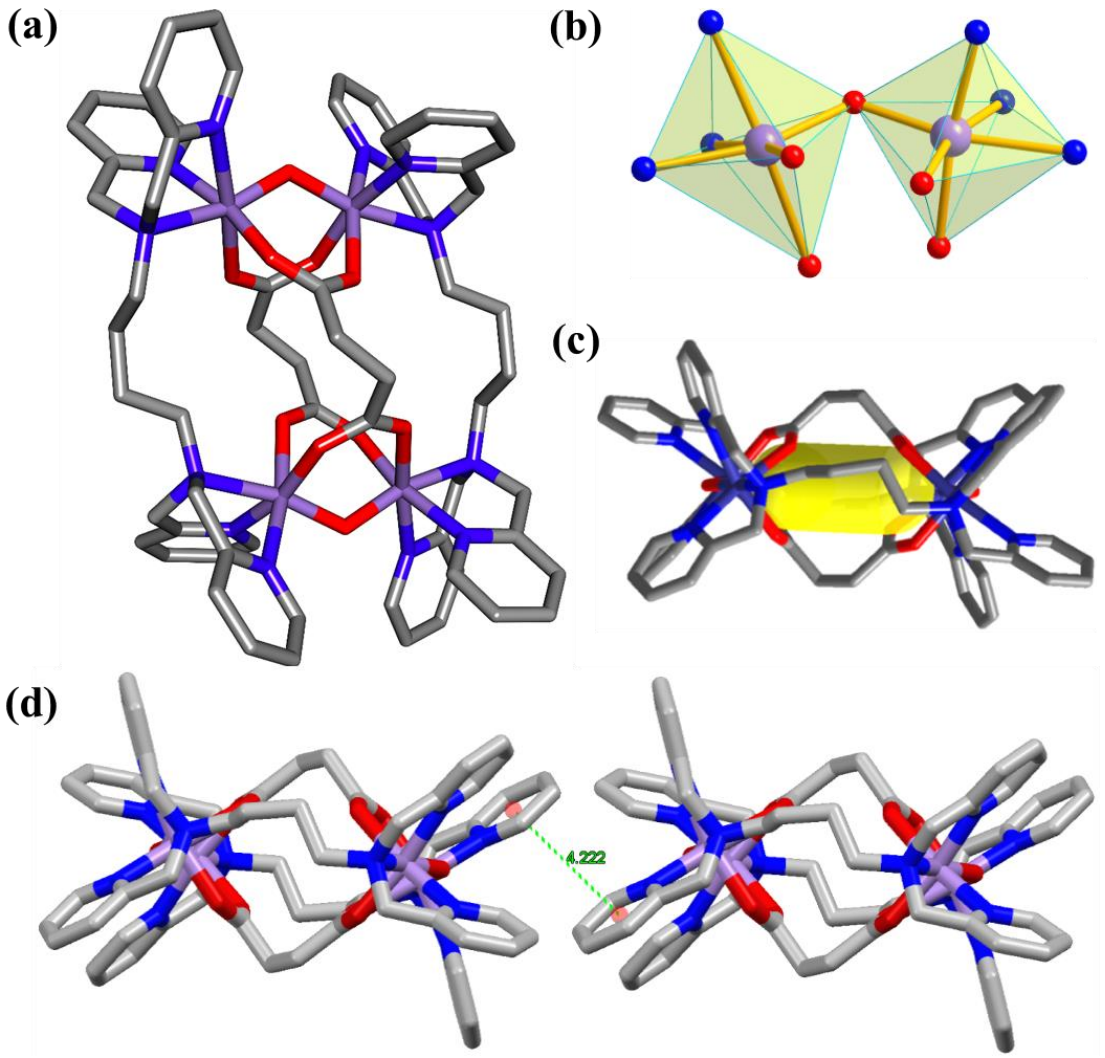

Figure 3.6. Crystal structure of **13**. (a) tetranuclear MOC, (b) coordination environment around Mn atoms, and (c) pore inside **13** (color code used for different atoms are like, pink: Mn; red: O, blue: N, grey: C). H-atoms are removed for clarity.

Effect of Bis(tridentate) Ligand and Dicarboxylate Combination

From the structural study of MOCs it is evident that the combination of bis(tridentate) ligand, tphn, and dicarboxylates, succinate and fumarate, forms an unprecedented octanuclear MOCs. Whereas, with the same dicarboxylate, tpbn forms a tetranuclear MOC. Comparing parameters like bond angles and lengths, it is clear that these are very similar in both octanuclear and tetranuclear cases, except the angle between two carboxylate

oxygens and manganese, and the angle between two manganese centers and oxo center, in $\{Mn_2(\mu\text{-}O)(\mu\text{-}O_2CR)_2\}^{2+}$ core (Figure 3.8) are different.

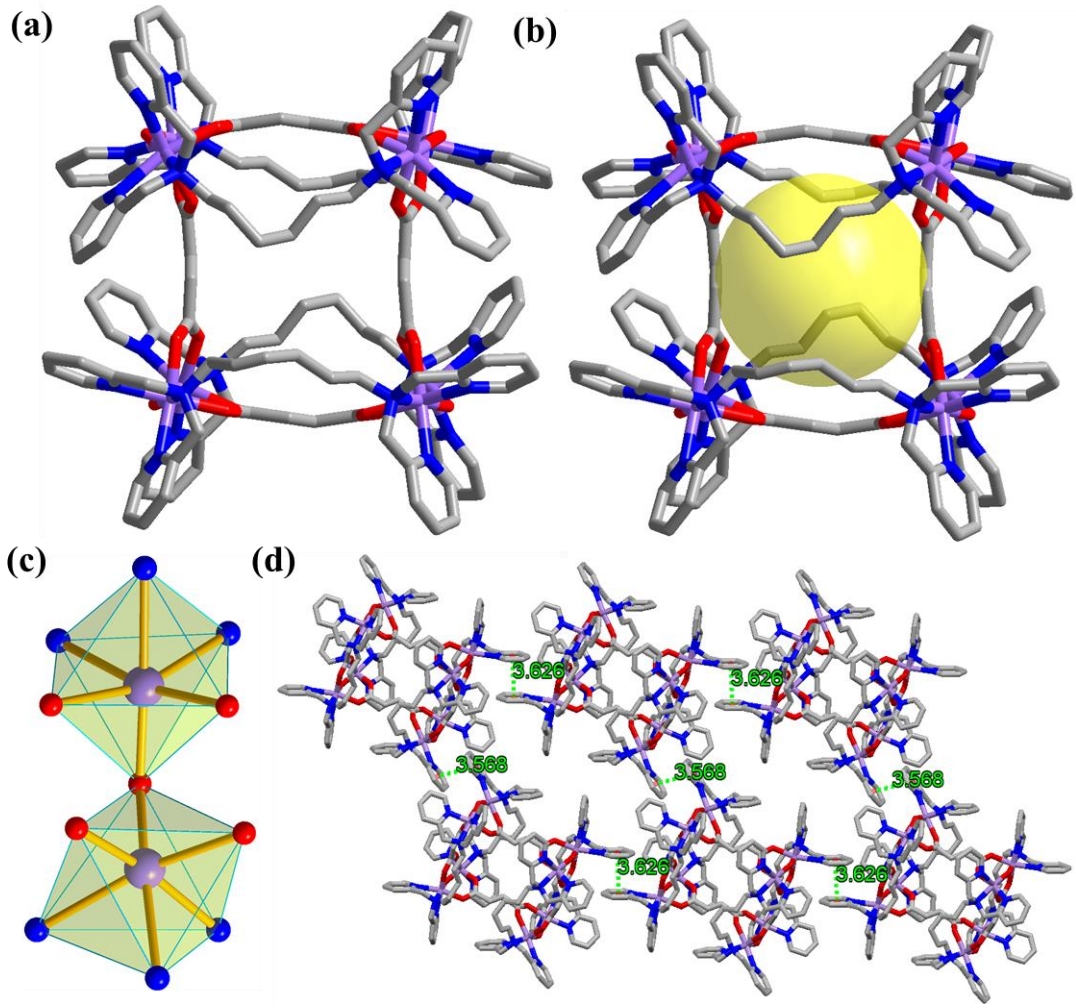

Figure 3.7. Crystal Structure **15**. (a) octanuclear MOC, (b) pore inside **15**, (c) coordination environment around the Mn, and (d) The π-π interaction between the molecules (color code used for different atoms are like, pink: Mn; red: O, blue: N, grey: C). H-atoms are removed for clarity.

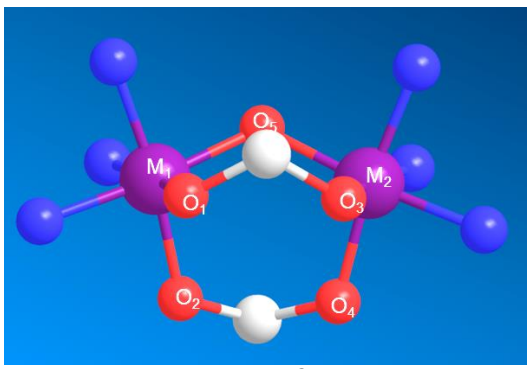

Figure 3.8. Representation of the $\{Mn_2(\mu\text{-}O)(\mu\text{-}O_2CR)_2\}^{2+}$ core.

In case of octanuclear complexes, the $\angle O_1\text{-}M_1\text{-}O_2$ angles are 86.47° and 89.18º, and $\angle O_3\text{-}M_2\text{-}O_4$ angles are 95.80° and 96.84°, while in case of tetranuclear complexes, these are

85.20° and 91.10°, respectively. The higher values of the angles forced the dicarboxylates to bind with two different Mn_2O groups in case of octanuclear MOCs but in case of tetranuclear MOCs, the lower values allow both the dicarboxylates to bind with the same Mn_2O group (Table 3.2).

Table 3.2. Various structural parameters for tetra and octanuclear MOCs.

Parameter	**Tetranuclear**	**Octanuclear**
$\angle O_1$-M_1-O_2 (^{o})	85.20	86.47 and 89.18
$\angle O_3$-M_2-O_4 (^{o})	91.10	95.80 and 96.84
$\angle M_1$-O-M_2 (^{o})	124.91	120.17 and 121.22
M_1-O_5 (Å)	1.799	1.815, 1.815
M_2-O_5 (Å)	1.790	1.822, 1.825
$M_1 \cdots M_2$ (Å)	3.182	3.163, 3.156

Gas Sorption Study. The N_2 sorption study with the PF_6^- analogues of **15** and **16** was done. As shown in Figure 3.9. both **15** and **16** exhibit very less N_2 gas uptake (11 cm^3g^{-1} in the case of **16**, and 6.2 cm^3g^{-1} in the case of **15**). The comparitively lesser uptake in **15** with respect to **16** is because of the two extra H-atoms present in succinate, which fills the pore partially. The BET surface area calculated for these two compounds are 7.82 m^2g^{-1} and 13.17 m^2g^{-1}.

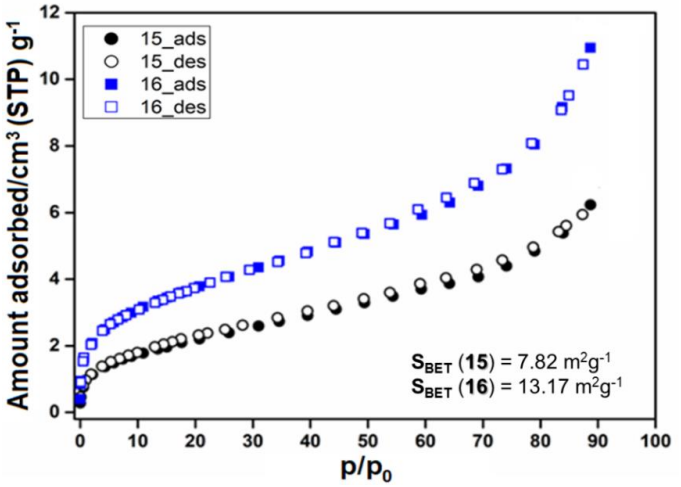

Figure 3.9. N_2 sorption isotherms of **15** and **16** at 77K**.**

Magnetic Properties. In addition to studying the magnetic property of compounds **1-16**, their magneto-structural correlation provides a definite proof to the three possibilities for their structures. The magnetic susceptibility data were measured for all but compound **11** from 300 K to 2 K. Based on these data, plots of $\chi_M T$ vs T were generated (Figures 3.10,

3.11 and 3.12). The room temperature $\chi_M T$ values are in between 11.6-13.5 cm^3Kmol^{-1} for **1**, **2**, **5** and **6**. These are close to that of four uncoupled Mn(III) ions (12 cm^3 K mol^{-1}). These values are also similar to those reported for other similar tetranuclear compounds reported in the literature. For **3** and **4**, this value is 5.5-5.9 cm^3Kmol^{-1}, which is close to the value of 6 cm^3Kmol^{-1} corresponding to two uncoupled Mn(III) ions. In case of compounds **1**, **2** and **5**, as the temperature decreases the $\chi_M T$ values goes slightly higher than 12 cm^3Kmol^{-1}, reaches a maximum and then decrease rapidly to a minimum at 2 K. This trend of $\chi_M T$ values indicates weak ferromagnetic coupling within the metal centers. In case of **2**, the value remains almost constant (just below 12 cm^3Kmol^{-1}) with a decrease of temperature indicating no substantial ferromagnetic interactions within metal centers. For compounds **3** and **4**, the room temperature $\chi_M T$ value is nearly 6 cm^3Kmol^{-1}, indicating the molecule is polymeric in nature and the value represents the repeat dimeric Mn_2O unit. This value for **3** and **4** is close to those observed for dinuclear compounds containing the $\{Mn_2(\mu\text{-}O)(\mu\text{-}O_2CR)_2\}^{2+}$ core. From the point of magneto-structural correlation in compounds **1**-**6**, it is

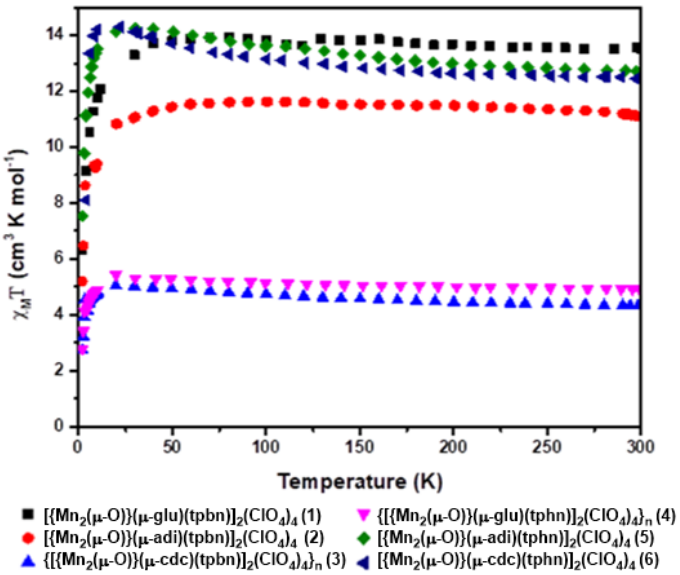

Figure 3.10. $\chi_M T$ s T plot of **1**-**6**.

clear that an increase in the methylene spacer length from tpbn to tphn ligands causes the formation of polynuclear compound (**3** and **4**) compared to **1** and **6** where the respective carboxylate is the same. On the other hand, a carboxylate with longer methylene chain length, such as adipate, dictates over this change, making both **2** and **5** tetranuclear complexes.

For **7**-**10** and **12**, the $\chi_M T$ values at room temperature show **7**, **8** and **9** behaving similar to

compounds **1**, **2**, and **5**. The $\chi_M T$ values increase as the temperature decreases, attain the highest value around 30 K and then decrease abruptly to a minimum at 2 K. The behavior of **7**, **8** and **9** indicates weak ferromagnetic coupling behavior in these compounds. In compounds **10** and 1**2** the value is nearly 6 cm^3Kmol^{-1}, which is closer to the value of two uncoupled Mn(III). This again indicates that these two compounds are also polymeric in nature and the dimeric unit is acting as the repeat unit. Once again, it appears that the longer chain length in the tpon ligand forces the formation of a polynuclear species such as **10** and **12**. Unfortunately, the data for **11** was not available to find the effect of adipate vs tpon in deciding the structure (tetranuclear vs polynuclear).

Similarly, compounds **13** and **14** showing a value near 12 cm^3 K mol^{-1} at room temperature are tetranuclear in nature. This is consistent with the observation for compounds with tpbn ligand as long as the dicarboxylate has a C3 or less spacer (succ, fum and glu). On the other hand, for compound **15** and **16** the $\chi_M T$ values are nearly 24 cm^3 $Kmol^{-1}$, which corresponds to eight uncoupled Mn(III) ions. The values increase as the temperature decreases and attain a maximum around 25 K and then a minimum at 2 K. This behavior evident weak ferromagnetic interaction between the metal ions within the cores. Thus, the magnetic data for **15** and **16** corroborates well with the octanuclear structure determined for **15**. In this case, an increase in the methylene chain length from tetra to hexa (tpbn vs tphn) provides an opportunity to have unprecedented octanuclear compounds **15** and **16** for the C2 dicarboxylates (succ or fum).

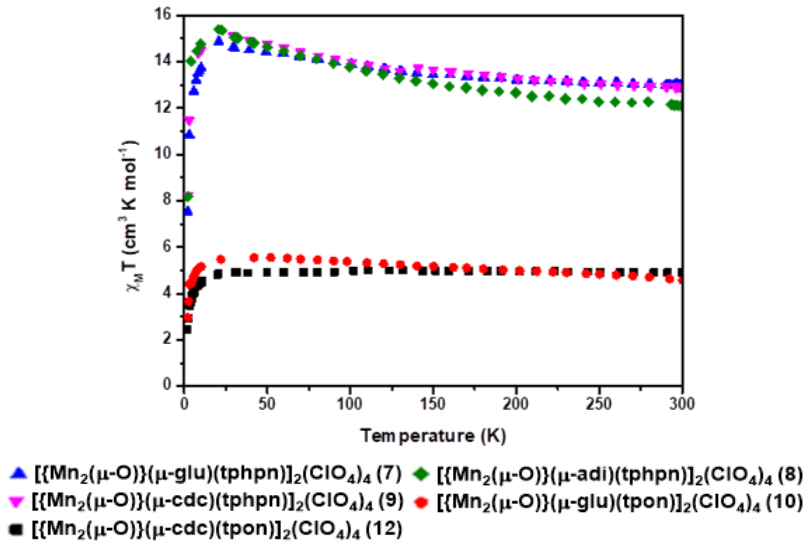

Figure 3.11. $\chi_M T$ vs T plot of **7**-**12**.

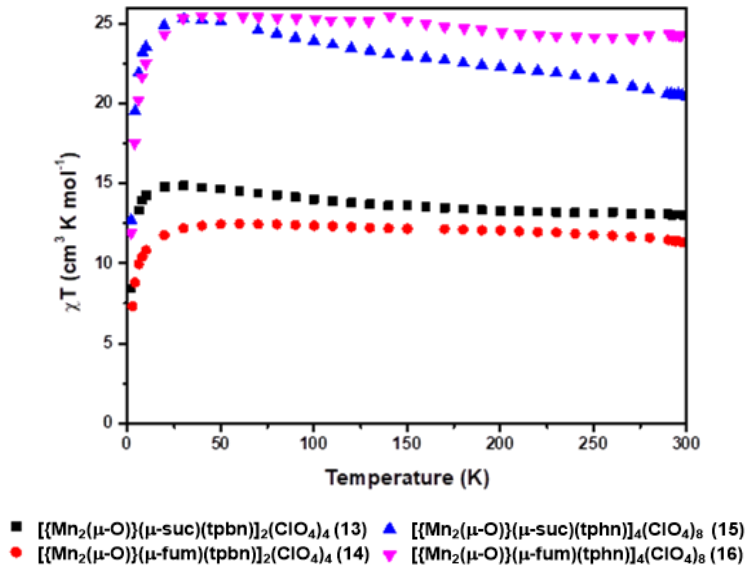

Figure 3.12. χ_MT vs T plot of compounds **13-16**.

3.1.2 With $\{Fe_2(\mu\text{-}O)(\mu\text{-}OOCR)_2\}^{2+}$ Core

Synthesis. These compounds were synthesized following a general procedure as shown in Scheme 3.3 where the three components ligand, $Fe(ClO_4)_3.xH_2O$, and the sodium salt of the corresponding dicarboxylic acid were reacted in a 1:2:1 ratio in methanol/water at room temperature. In each case, a yellowish-brown solid was obtained and air dried. The same solid was used for characterization. Crystals suitable for SCXRD study was obtained (wherever possible) by layering of acetonitrile solution of compounds with either di-isopropyl ether or di-tertiarybutyl ether.

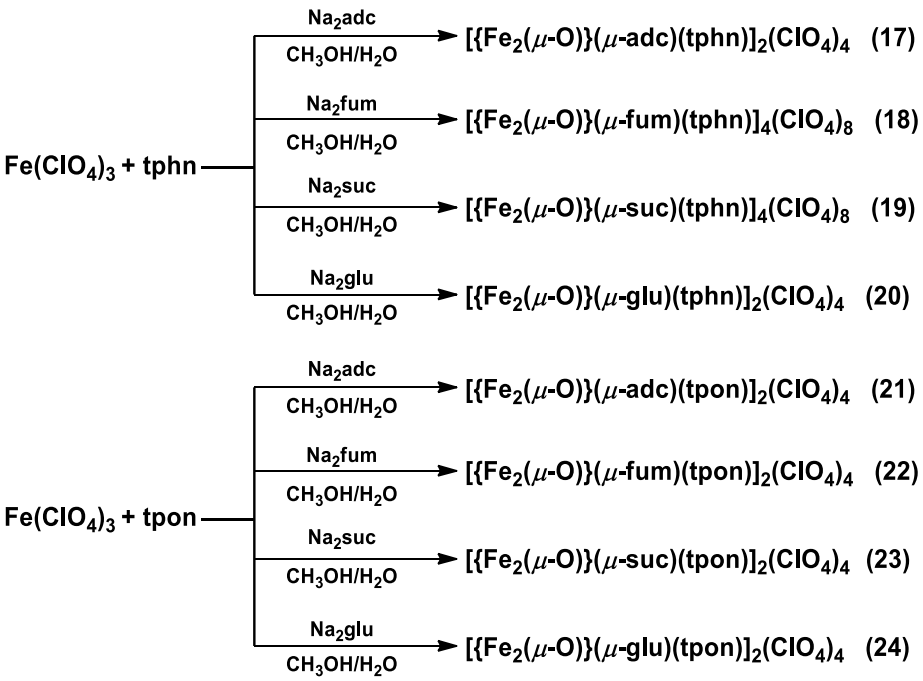

Scheme 3.3. Synthesis of **17-24**.

FTIR Spectroscopy. As indicated in Chapter I, the $\{Fe_2(\mu\text{-}O)(\mu\text{-}OOCR)_2\}^{2+}$ core has signature spectroscopic features. The FTIR spectra of Compound **17**-**24** were recorded and

Table 3.3 Selected FTIR peaks of **17**-**24**.

Compounds	$\nu_{asym}(COO^-)$, cm^{-1}	$\nu_{sym}(COO^-)$, cm^{-1}	$\nu(ClO_4^-)$,cm^{-1}	ν(Fe-O-Fe), cm^{-1}
17	1543	1433	1089, 625	731
18	1545	1433	1090, 625	735
19	1543	1435	1088, 624	732
20	1541	1430	1089, 625	731
21	1542	1433	1089, 624	732
22	1544	1433	1090, 625	730
23	1544	1436	1089, 625	732
24	1542	1432	1088,	734

compared. Similar to Mn-O-Mn bond stretching observed in **1**-**16**, the peak at around 730 cm^{-1} can be assigned to the Fe-O-Fe stretching frequency of **17**-**24**. The symmetric and asymmetric stretching frequencies of carboxylate appear at ~ 1540 and 1430 cm^{-1}. Moreover, the presence of perchlorate anions is proven by the peaks appearing around 1089 and 625 cm^{-1}, respectively.

UV-Vis Spectroscopy. UV-vis spectra of 1**7**-**24** were recorded in acetonitrile solution: 0.1 mM (for the visible region) and 0.0035 mM (for UV region) (Figure 3.13). All the compounds show similar features, thereby proving the formation of compounds with an identical core. For explanation of the observed bands, one such set (**17**-**20**) is described below. Intense bands at around 490 nm, 520 nm, 540 nm and 730 nm in the visible region correspond to the oxo-metal charge transfer and metal d-d transitions. These compounds show peaks at 270 nm and 340 nm in the ultraviolet region which can be ascribed to the π-π transition in the ligands.

Single Crystal Structure Analyses. On the basis of the characteristic spectroscopic features described above for **17**-**24**, it is clear that all of these compounds have the $\{Fe_2(\mu\text{-}O)(\mu\text{-}OOCR)_2\}^{2+}$ core. However, their nuclearity can only be ascertianed by determining their crystal structures. Thus, efforts were made to get their suitable crystals. However, even after multiple tries, we were successful in obtaining suitable single crystals for the structure determination only for compound **19.** In view of this, magnetic studies (vide infra)

has also been coupled with the its X-ray structure to make conclusive statements about their nuclearity.

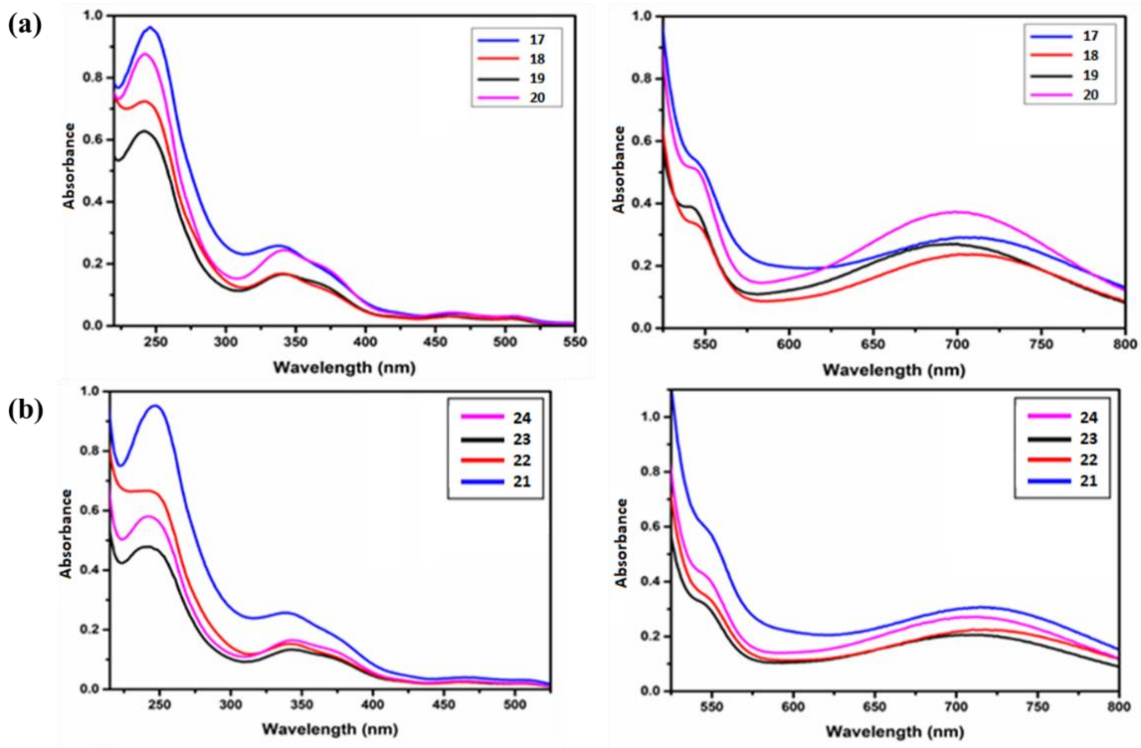

Figure 3.13. UV-vis spectra of (a) **17-20,** (b) **21-24.**

Structural Description of 19·2CH₃CN. This compound crystallizes in the triclinic *P*-1 space group. The crystallographic information pertaining to data collection and structure refinement has been provided in Table A3. All the Fe-atoms have distorted octahedron where each Fe center is surrounded by three N-atoms from each end of the bis(tridentate) ligand, two carboxylate O-atom and one oxo O-atom forming N_3O_3 atmosphere. All these N, or O-atoms are bound to the metal in a facial fashion.

The Fe···Fe distance (within the core) is 3.092(2) Å and 3.087(2) Å and Fe-O_{oxo} distances are 1.797(7) Å, 1.801(6) Å, and 1.799(7) Å, 1.790(8) Å which commensurates with the values reported for similar type of compounds.[160-170] Selected bond distances and bond angles are listed in Table A18 and Table A44, respectively. Two tphn ligands and one succinate are bridged between two Fe_2O-dimetalic unit forming a tetranuclear (dimer of dimer) unit. Two of this similar tetranuclear unit again is connected through succinate to form an overall octanuclear compound (shown in Figure 3.14.) as that of its Mn-analogue **15**. The Fe···Fe distance between two cores are 8.722 Å, 8.753 Å, and 8.628 Å, 8.873 Å.

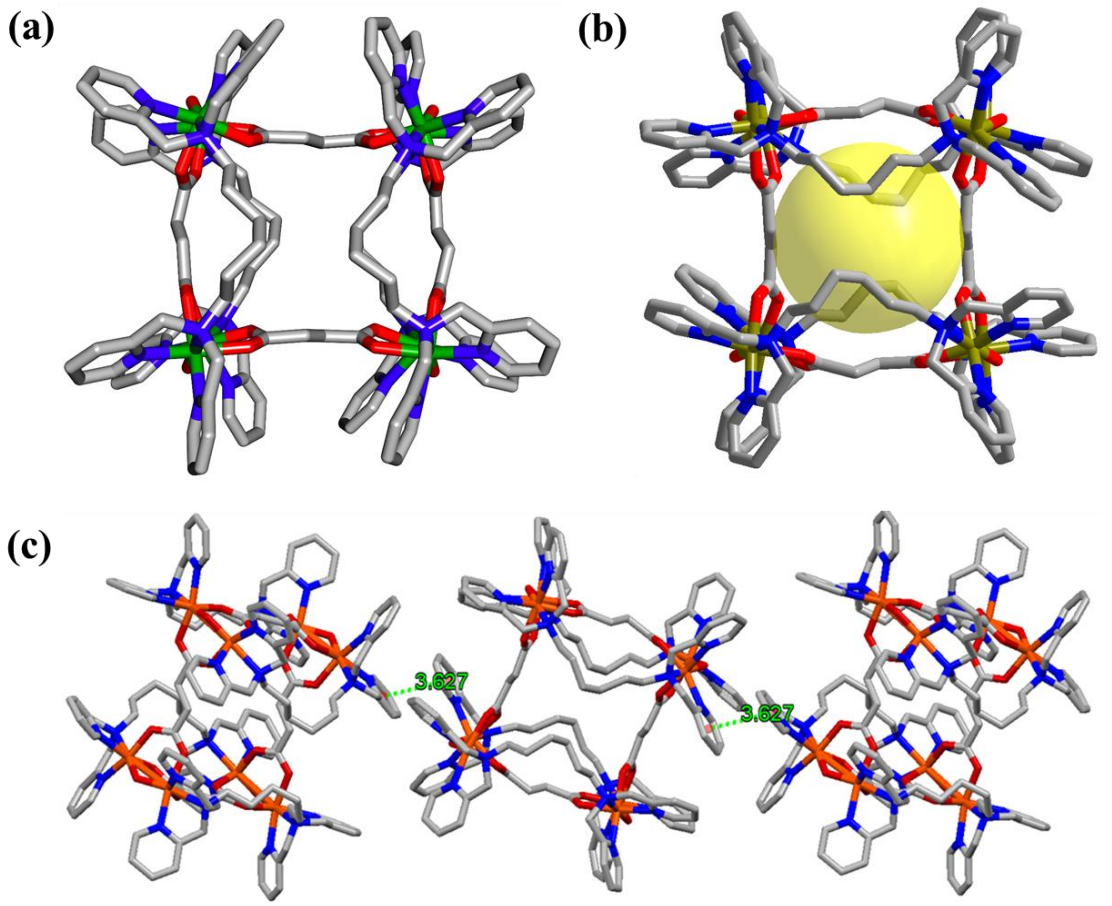

Figure 3.14. Crystal Structure of **19**. (a) octanuclear MOC, (b) showing the pore inside, and (c) the π-π interaction between two molecule (color code used for different atoms are like, pink: Mn; red: O, blue: N, grey: C). H-atoms are removed for clarity.

Magnetic Property. The magnetic susceptibility for compound **19** was measured from 2 K to 300 K. A plot $\chi_M T$ vs T shown in Figure 3.15 indicate a strong ferromagnetic interaction between the metal centers. Its magnetic behavior is similar to other tetranuclear compounds possessing the same dinuclear $\{Fe_2(\mu\text{-}O)(\mu\text{-}O_2CR)_2\}^{2+}$ core. In terms of magneto-structural correlation for the iron analogs, a similar (to manganese) trend is observed for the combination of bis(tridentate) polypyridyl ligands and dicarboxylates.

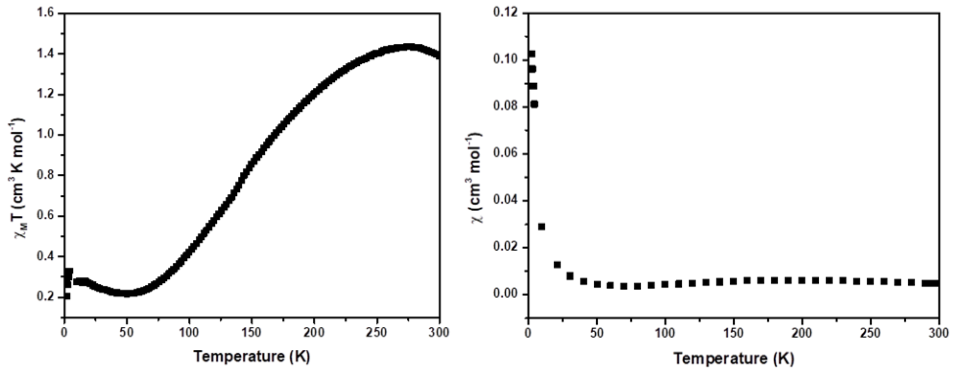

Figure 3.15. $\chi_M T$ vs T (top) and χ_M vs T (bottom) plot for **19**.

3.1.3 With $\{Mn_2(\mu\text{-}O)_2(\mu\text{-}OOCR)\}^{2+}$Core

Synthesis. The synthesis of compounds with $\{Mn_2(\mu\text{-}O)_2(\mu\text{-}OOCR)\}^{2+}$core is summarized in Scheme 3.4. The comproportionation reaction of Mn(II) and Mn(VII) with a 7:3 ratio was carried out to get Mn_2(III/IV) compounds as shown below.

$$7\ Mn^{2+} + 3\ Mn^{7+} \longrightarrow 5\ Mn^{3+} + 5\ Mn^{4+}$$

A mixture of $MnSO_4 \cdot H_2O$, the ligand was taken in methanol. The pH of the solution was maintained by the use of dicarboxylic acid/sodium dicarboxylate buffer (pH 4.5). Upon slow addition of an aqueous solution of sodium salt of the corresponding dicarboxylic acid and aqueous $KMnO_4$ a green solution was obtained, that was reacted with a methanolic solution of $NaClO_4$ to obtain a green-brown colored solid.

In this context it is important to convey that, $MnSO_4 \cdot H_2O$ is partially soluble in methanol, but, the moisture present in methanol and the bis(tridentate) ligands help $MnSO_4 \cdot H_2O$ to go inside the solution. Moreover, the water from other sources (buffer and aq. KMnO4 solution) also favours the course of the reaction.

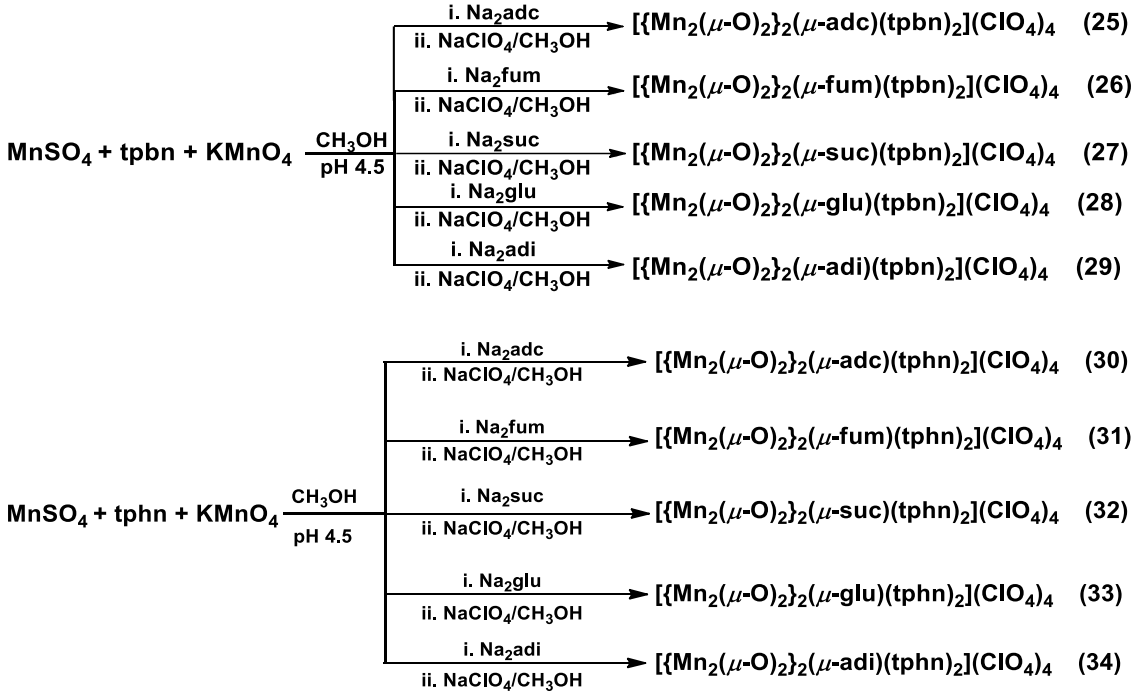

Scheme 3.4. Synthesis of **25**-**34**.

FTIR Spectrocopy. Similar to the above two cases, the Mn_2O_2-dimetalic unit exhibits signature spectroscopic features. Thus, a quick evaluation for their formation was conducted by FTIR spectroscopy. The presence of a peak around 690 cm^{-1} in all cases can be ascribed to the Mn-O-Mn bond stretching frequency in this type of core. The carboxylate

peaks at ~1575 and 1380 cm^{-1} correspond to the asymmetric and symmetric stretching frequencies, respectively. The difference in the asymmetric and symmetric stretching frequencies of carboxylates ($\Delta\nu = \nu_{asym}-\nu_{sym}$) confirms the binding modes of carboxylates in these compounds; a value less than 195 cm^{-1} is indicative of the bidentate bridging mode to the dimetal core. The peaks due to the perchlorate anion appears at around 1090 and 625 cm^{-1} and a ligand signature peak can be seen at ~769 cm^{-1}. The absence of peaks around 1750 cm^{-1} proves that all the carboxylic acids are fully deprotonated. Selected FTIR peaks for all these compounds are listed in Table 3.4.

Table 3.4. Selected FTIR peaks of **25-34**.

Compounds	$\nu_{asym}(COO^-)$, cm^{-1}	$\nu_{sym}(COO^-)$, cm^{-1}	$\nu(ClO_4^-)$, cm^{-1}	$\nu(Mn_2(\mu\text{-}O)_2)$, cm^{-1}
25	1573	1381	1089, 624	691
26	1572	1381	1088, 625	690
27	1572	1380	1089, 625	691
28	1577	1383	1090, 624	691
29	1570	1381	1089, 626	692
30	1576	1386	1089, 624	690
31	1573	1382	1090, 625	692
32	1575	1383	1089, 625	690
33	1576	1380	1088, 626	690
34	1570	1384	1089, 625	689

UV-Vis Spectroscopy. UV-vis spectra of **25-34** were measured in acetonitrile solution: 0.1 mM (for visible region) and 0.0035 mM (for UV region). All these compounds show similar types of spectra (Figure 3.16. and 3.17.), thereby proving the formation of compounds with an identical core. All these compounds show intense bands at around 565 nm and 650 nm, corresponding to the oxo-metal charge transfer transition and d-d transitions in the metal These observed peaks are similar in the reported compounds. These compounds show a peak at 270 nm which can be ascribed to the π-π transition in the ligand.

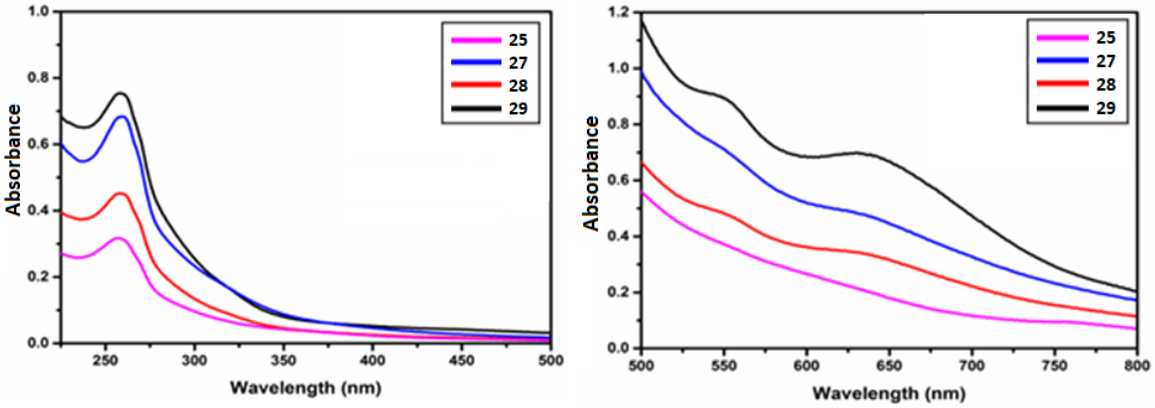

Figure 3.16. UV-vis spectra of **25-29.**

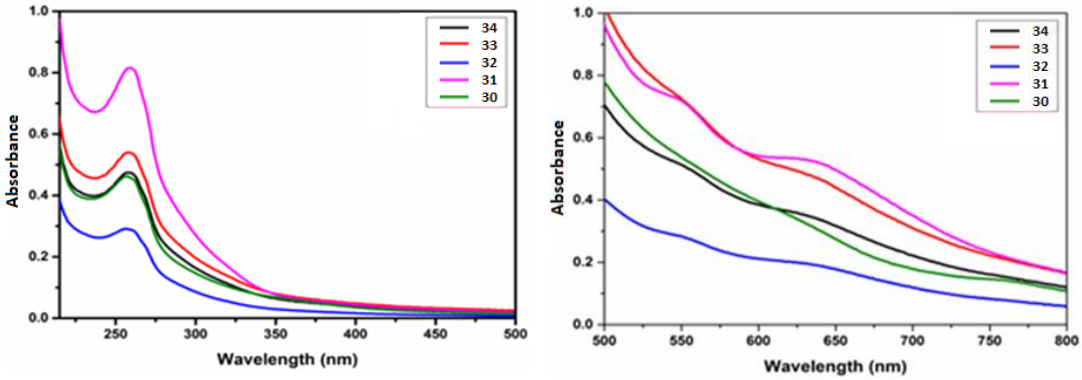

Figure 3.17. UV-vis spectra of **30-34.**

Thermogravimetric Analyses. These compounds are thermally less stable as shown in Figure 3.18 and 3.19. All these compounds lose lattice solvent molecules upto 100 ºC followed by decomposition.

Structural Description of 27·3CH₃CN·H₂O. This compound crystallizes in the triclinic *P*-1 space group. The crystallographic information pertaining to data collection and structure refinement has been provided in Table A3. The Mn centers have distorted octahedron coordination environment where each Mn-center is surrounded by three N-atoms from each end of the bis(tridentate) ligand, one carboxylate O-atom and two oxo O-atom forming a N_3O_3 atmosphere (Figure 3.20). The Mn···Mn distance (within core) are 2.615(1) Å, and Mn-O_{oxo} distances are 1.777(4) Å, 1.816(3) Å, and 1.769(3) Å, 1.836(4) Å ; for the other core this Mn-O_{oxo} distances are 1.769(3) Å, 1.848(3) Å, and 1.769(3) Å, 1.819(3) Å, which commensurates with the values reported for similar type of compounds.[171-179] Selected bond distances and bond angles are listed in Table A19 and Table A45, respectively. The tpbn ligand forms a bridge between two Mn-atom of two Mn_2O_2-dimetalic unit and the succinate dicarboxylate is also bridged between those two Mn_2O_2-dimetalic unit, forming an overall tetranuclear (dimer of dimer) compound. The Mn···Mn distance between two

cores are 6.798 Å. This molecule is further forming 2D supramolecular assembly through π-π interaction (3.741 Å).

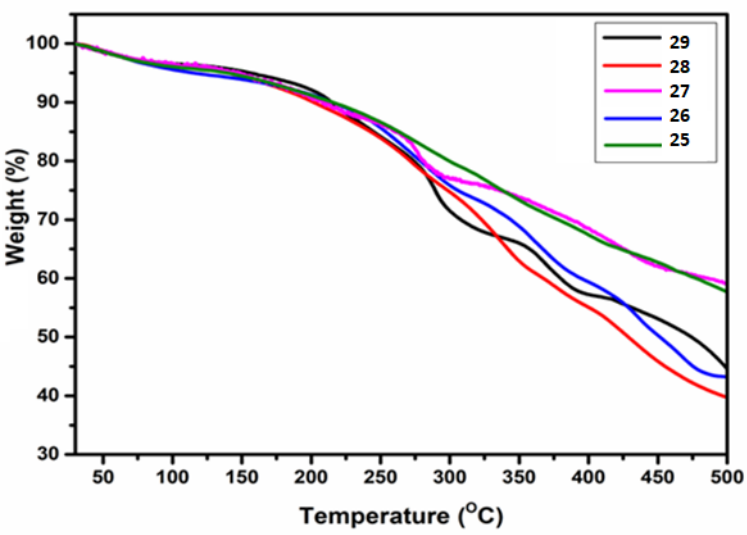

Figure 3.18. TGA scans of **25**-**29**.

Single Crystal Structure Analyses

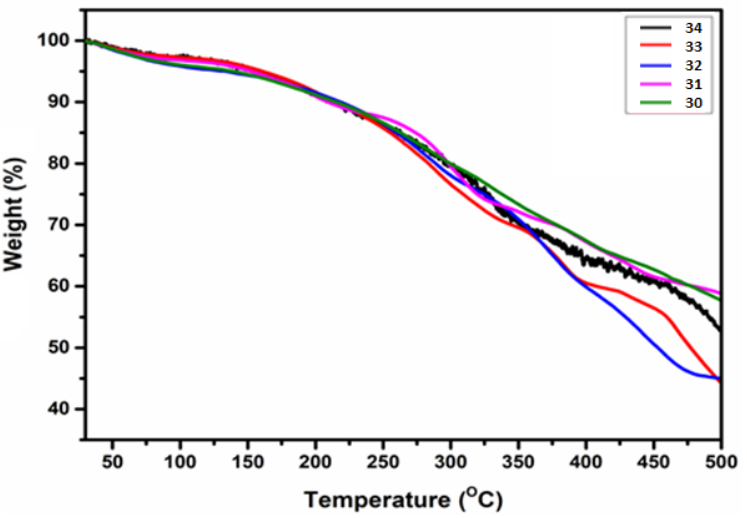

Figure 3.19. TGA scans of **30**-**34**.

Structural Description of 29·2CH₃CN. It crystallizes in the monoclinic *C*2/*c* space group. The crystallographic information pertaining to data collection and structure refinement has been provided in Table A4. Similar to **27**, the Mn centers in **29**, have distorted octahedron coordination environment where each Mn center is surrounded by three N-atoms from each end of the bis(tridentate) ligand, one carboxylate O-atom and two oxo O-atom forming a N_3O_3 atmosphere. The Mn···Mn distance (within the core) is 2.613(1) Å and Mn-O_{oxo}

distances are 1.776(4), 1.847(4) and 1.776(4) Å, 1.821(4) Å, which commensurates with

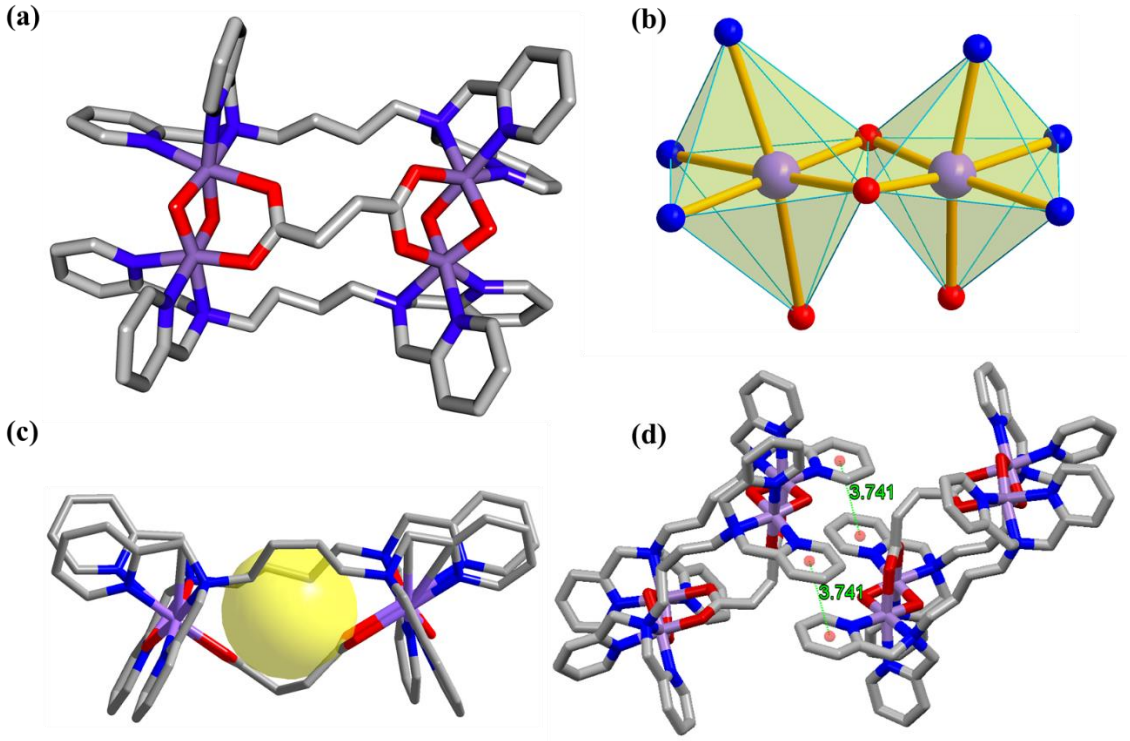

Figure 3.20. (a) Crystal Structure of **27**. (a) the tetranuclear MOC, (b) the coordination environment around the metal center, (c) pore inside **27**, and (d) π-π interactions between two molecules (color code used for different atoms are like, pink: Mn; red: O, blue: N, grey: C). H-atoms are removed for clarity.

the values of reported with similar type compounds.[171-179] Selected bond distances and bond angles are listed in Table A20 and Table A46, respectively. The tpbn ligand forms a bridge between two Mn atoms of two Mn_2O_2-dimetalic unit and the adipate dicarboxylate also bridges between two Mn_2O_2-dimetalic unit, forming an over all tetranuclear (dimer-of-dimer) compound, as shown in Figure 3.21. The Mn···Mn distance between the two cores is 8.576 Å. This molecule further forms a supramolecular assembly through very strong π-π interaction (3.816 Å).

Structural Description of 34·H₂O. This compound crystallizes in the triclinic *P*-1 space group. The crystallographic information pertaining to data collection and structure refinement has been provided in Table A4. All the Mn atoms are in distorted octahedral geometry and are surrounded by three N-atoms from each end of the bis(tridentate) ligand, one carboxylate O-atom and two oxo O-atoms. The Mn···Mn distance (within core) is 2.619(5) Å and Mn-O_{oxo} distances are 1.804(18) Å, 1.809(14) Å, and 1.844(12)Å, 1.775(16) Å. For the second Mn_2O_2-dimetallic unit, The Mn···Mn distance (within core) is 2.619(5) Å and Mn-O_{oxo} distances are 1.779(16) Å, 1.831(13) Å, and 1.812(14)Å,

1.878(15), which are commensurates with the value of already reported with similar type compounds. [171-179] Selected bond distances and bond angles are listed in Table A21 and Table A47, respectively. The tpbn ligand forms a bridge between two Mn-atom of two Mn_2O_2-dimetalic unit and the adipate dicarboxylate is also bridged between two Mn_2O_2-dimetalic unit, forming an over all tetranuclear (dimer-of-dimer) compound as that of **27** and **29**, as shown in Figure 3.22. The Mn···Mn distances between two cores are 9.121 Å and 9.113 Å. This molecule further forms a 2D supramolecular assembly through very strong π-π interaction (3.891 and 3.746 Å).

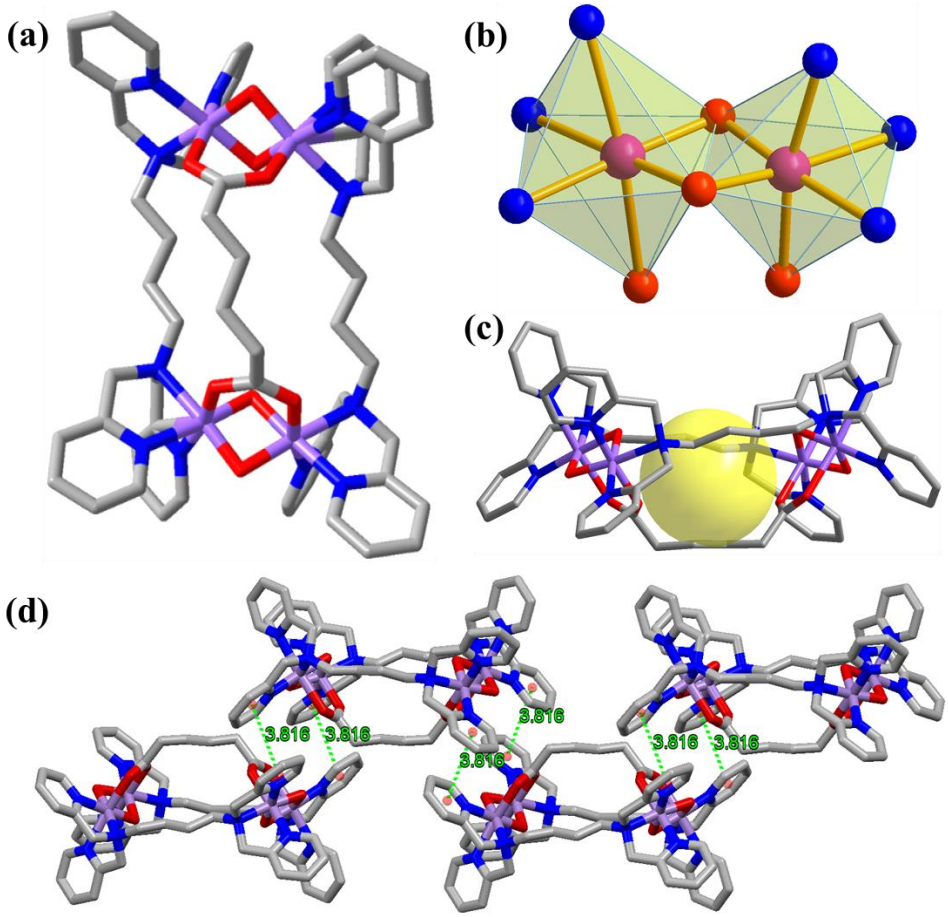

Figure 3.21. Crystal Structure of **29**. (a) the tetranuclear MOC, (b) the coordination environment around the metal center, (c) pore inside **29**, and (d) π-π interactions between two molecules (color code used for different atoms are like, pink: Mn; red: O, blue: N, grey: C). H-atoms are removed for clarity.

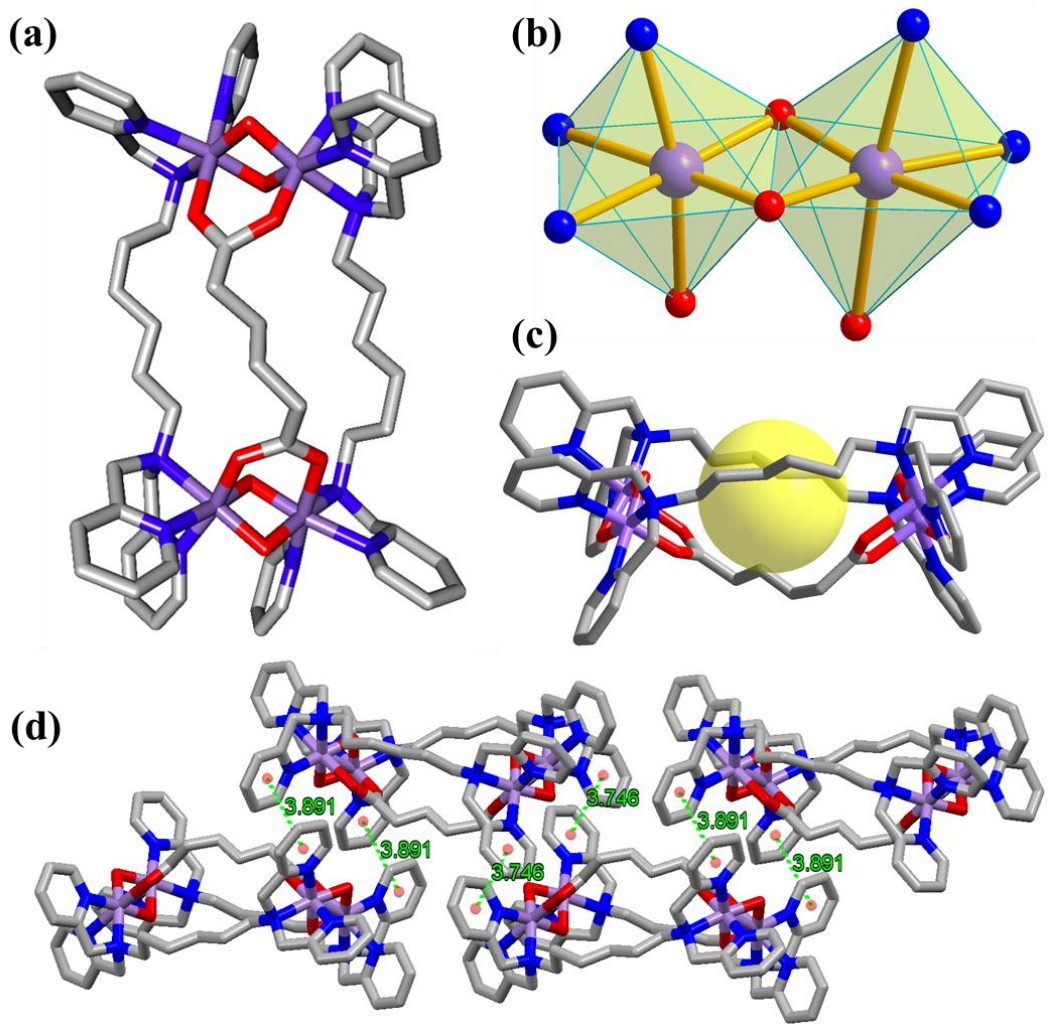

Figure 3.22. Crystal Structure of **34**. (a) the tetranuclear MOC, (b) the coordination environment around the metal center, (c) pore inside **34**, and (d) π-π interactions between two molecules (color code used for different atoms are like, pink: Mn; red: O, blue: N, grey: C). H-atoms are removed for clarity.

Magnetic Property. The magnetic susceptibility measurement for **34** is recorded from 300 K to 2 K. A plot of $\chi_M T$ vs T is shown in Figure 3.23. The $\chi_M T$ value of the compound decreases from 6.5 cm^3Kmol^{-1} as the temperature goes down from room temperature and attains a minimum of 0.4 cm^3Kmol^{-1} at 2 K. The room temperature $\chi_M T$ or the effective magnetic moment value suggests a ground state S = 1/2 per $Mn_2(\mu\text{-}O)_2$ core, i.e., Mn(III) and Mn(IV) centers in **34** are coupled antiferromagnetically. This trend is similar to other dinuclear compounds containing $\{Mn_2(\mu\text{-}O)_2(\mu\text{-}O_2CR)\}^{2+}$ core reported in the literature except the $\chi_M T$ values for **34** at room temperature is twice as large.

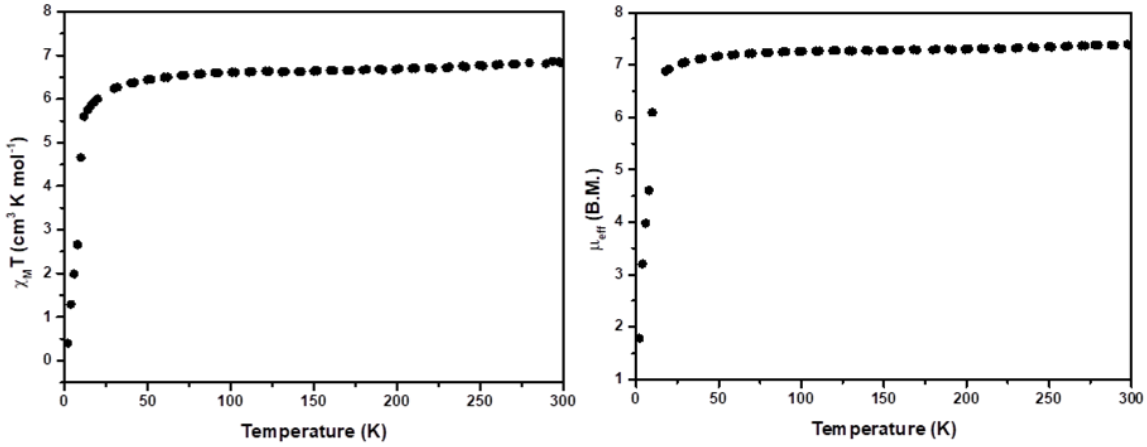

Figure 3.23. χ_MT vs T and μ_{eff} vs T plot of **34**.

3.2 COORDINATION POLYMERS (CPs)

3.2.1 Rigid Carboxylates and Semirigid Spanning Ligands

Synthesis. All these compounds were synthesized through the one pot self-assembly method. The compounds are listed in Scheme 3.5. The metal center used for the synthesis are Mn(II), Co(II) and Ni(II). Keeping the dicarboxylates fixed, two different bis(tridentate) ligands were used. For the synthesis, a 2:2:1 ratio of M(II):dicarboxylate:bis(tridentate) ligand has been used and stirred for 24 h at room temperature in methanol. In each case solid formed was filtered and air dried. The solid was used for characterization without any further purification. The single crystals were obtained (wherever possible) by the direct layering of the components in methanol and water mixture (1:1).

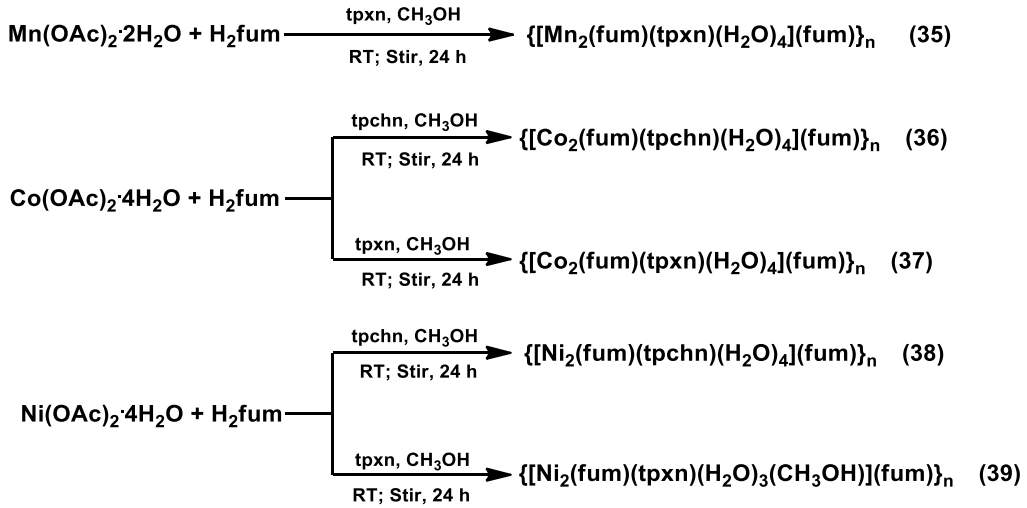

Scheme 3.5. Synthesis of **35-39**.

FTIR Spectroscopy. FTIR spectra of **35-39** was recorded in the solid stae as KBr pellets (see Figure 3.24). A broad band at ~3400 cm^{-1} indicates the presence of -OH stretching from the water of crystallization, whereas a broad band around 3200-3250 cm^{-1} is because of the presence of coordinated water. The carboxylate peaks for asymmetric and symmetric stretching frequencies appear at ~ 1575 and 1370 cm^{-1}, respectively. The difference of the stretching frequencies ($\Delta\nu > \sim 200\ cm^{-1}$) indicates the monodentate binding mode of fumarate. These observations are consistent with their single crystal X-ray structures. A characteristic peak of the ligand appears around 670 cm^{-1}. Selected FTIR peaks are listed in Table 3.5.

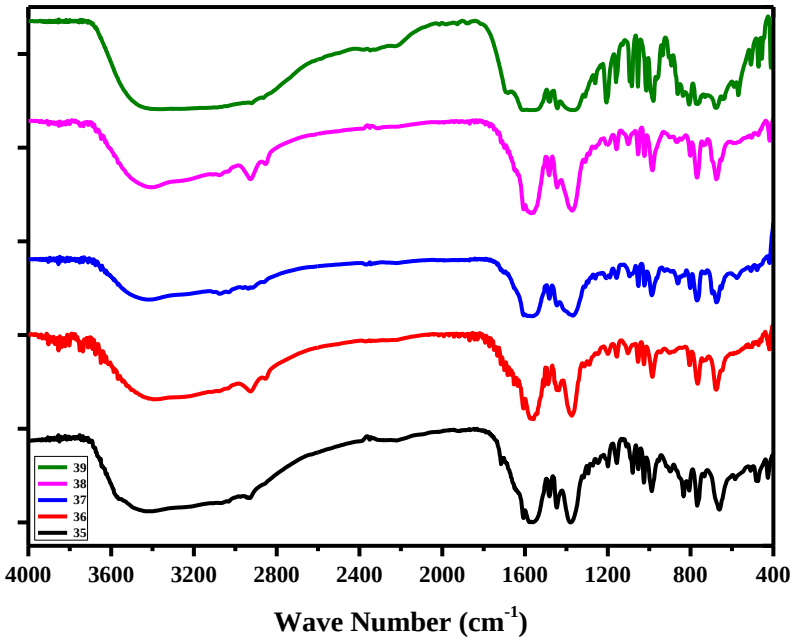

Figure 3.24. FTIR spectra of compound **35-39**.

Table 3.5. Selected FTIR peaks and binding modes of carboxylates of **35-39**.

Compounds	$\nu_{asym}(COO^-)$ cm^{-1}	$\nu_{sym}(COO^-)$ cm^{-1}	$\Delta\nu$ cm^{-1}	Binding mode
35	1577	1366	211	monodentate
36	1590	1369	221	monodentate
37	1582	1372	210	monodentate
38	1575	1374	201	monodentate
39	1579	1379	200	monodentate

Thermogravimetric Analysis. The thermal stability of these compounds is verified by thermogravimetric analysis (TGA). The TGA scans for **35-39** are shown in Figure 3.25 and step wise calculations for **35-39** are shown in Table 3.6. All these compounds are thermally stable up to 300 ºC. At the initial stage of heating, each compound loses only solvent molecules. In case of **35**, it loses 8.98% (ca. 9.00%) of its weight corresponding to removal of four lattice water molecules and a coordinated water molecule up to 85 °C. In the second step, the compound loses another three coordinated water molecules, a fumarate dicarboxylate anion and a tpxn ligand, corresponding to 67.39% (ca. 66.82%) at 390 °C after that it undergoes decomposition. In case of **36**, the first loss is due to four water molecules, one fumarate dicarboxylate anion and a ligand tpxn upto 306 °C, which corresponds to a 39.74% (ca. 39.05%) weight loss. Whereas, in **39** five water, two methanol molecules and two fumarate dicarboxylate anion, which corresponds to 38.79% of its total weight, are lost up to temperature 316 °C. In the next step, both the compounds **36** and **39**

lose part of the ligand upto 357 °C and 386 °C, respectively, followed by decomposition. In case of **37**, first it loses five water molecules and a fumarate dicarboxylate anion, which corresponds to 22.72% (ca. 21.79%) weight loss up to temperature 328 °C, and in the next step it loses the ligand, which results 52.10% (ca. 53.44%) weight loss up to 385 °C. After that, the compound undergoes decomposition. Compound **38** shows a 7.90% (ca. 7.79%) loss corresponding to four water molecules up to 72 °C temperature and then losses weight continuously.

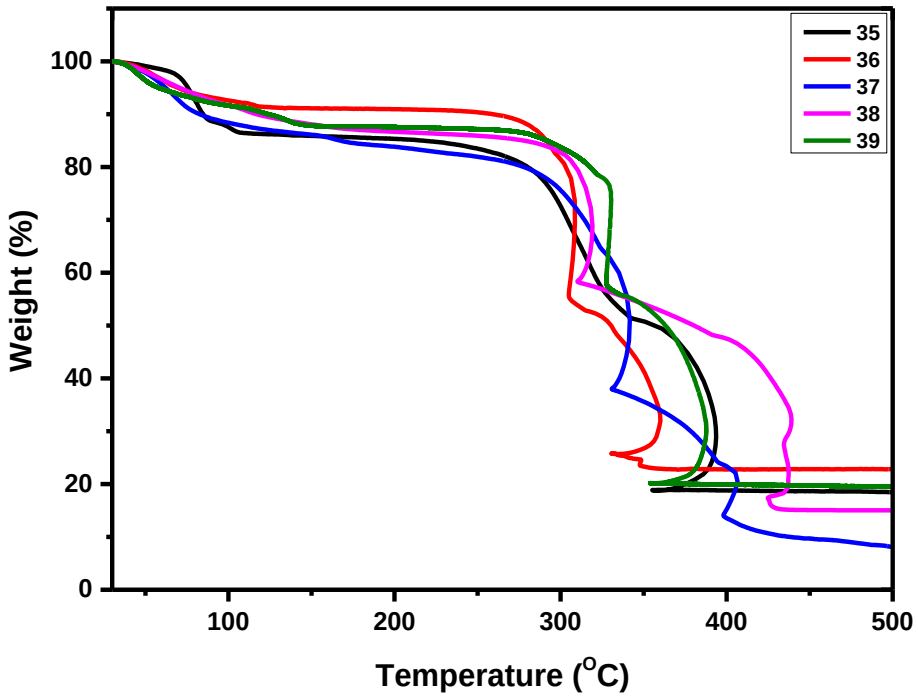

Figure 3.25. TGA scans of **35-39**.

Table 3.6 Calculation of weight loss of **35-39**.

Comp	Weight Loss											
	Step I				Step II				Step III			
	Ca.	Obs.	Loss	°C	Ca.	Obs.	Loss	°C	Ca.	Obs.	Loss	°C
35	9.00	8.98	$5H_2O$	85	66.82	67.39	$3H_2O$ + fum + tpxn	390	4.40	4.77	CO_2	500
36	39.05	39.74	$3H_2O$ + fum + tpxn	306	---	31.92	Part of ligand	357	---	---	decomposition	---
37	21.79	22.72	$5H_2O$ + fum	328	53.44	52.10	tpxn	385	7.04	7.25	1.5 CO_2	500
38	7.79	7.90	$4H_2O$	72								
39	38.21	38.79	$5H_2O$ + $2CH_3OH$ + 2fum	316	30.16	30.60	Part of ligand	386	---	---	decomposition	--

Single Crystal Structure Analysis.

Structural Description of 35·2H₂O. It crystallizes in the triclinic *P*-1 space group. The crystallographic information pertaining to data collection and structure refinement has been provided in Table A5. The asymmetric unit consists of one metal center, one-half of the ligand, one-half of the fumarate which is bound to the metal ion and one-half of the fumarate as a counter anion. The Mn(II) ion is octahedrally surrounded by N3O3 coordination enviornment. All three N-atoms belongs to one end of the bis(tridentate) tpxn ligand and O-atoms are from two coordinated water molecules and the other O-atom is from one end of the fumarate, bound to the metal ion in a monodentate fashion. The other end of the ligand is bound to another Mn(II) ion, which is further bridged by a fumarate in a similar fashion to another Mn(II) ion, forming a 1D polymeric chain with alternate fumarate and tpxn (see Figure 3.26). The bond distances are: Mn-N_{pyr} 2.302(2) Å, 2.337(2) Å; Mn-N_{CH2} 2.376(2) Å, Mn-O_{aq} 2.1902(19) Å, and 2.2381(19) Å; Mn-O_{oxo} 2.1207(18) Å. Selected bond distances and bond angles are listed in Table A22 and Table A48, respectively.

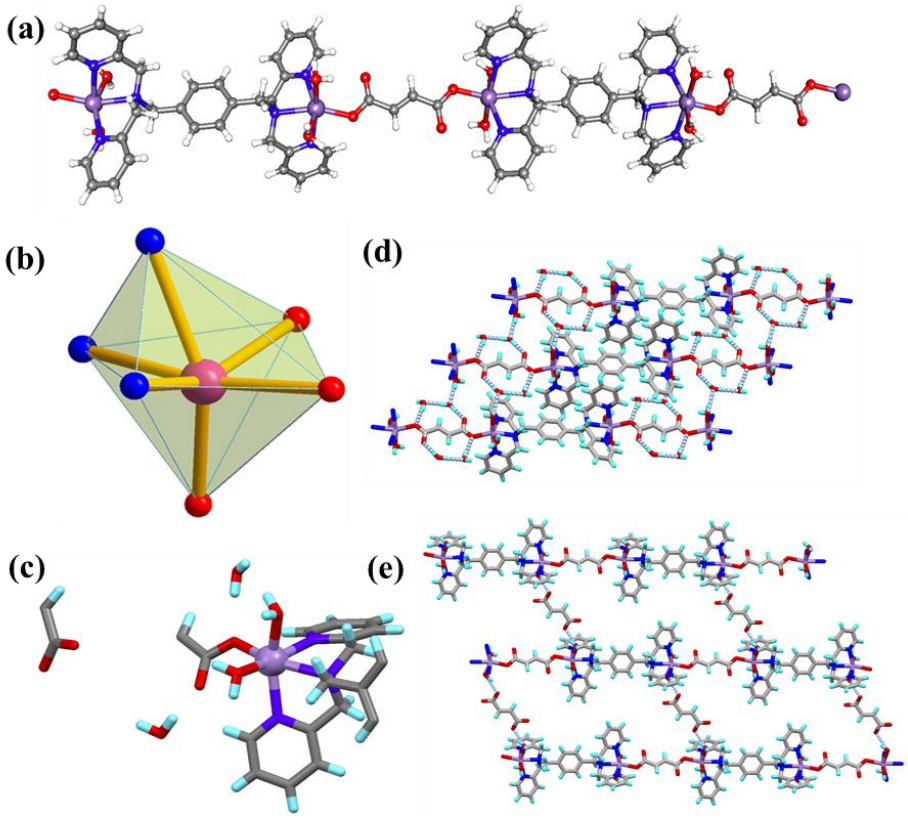

Figure 3.26. Crystal Structure of **35**. (a) 1D coordination polymer, (b) the coordination environment around metal center, (c) the asymmertic unit, (d) and (e) formation of supramolecular assembly through H-bonds (color code used for different atoms are like, pink: Mn; red: O, blue: N, grey: C, cyano: H).

The free fumarate forms H-bonds with one of the two bound water of two different polymeric chains resulting in a 2D sheet. The H-bond length in this case is 1.874 Å. Further, H-bonds are developed through the other coordinated water, two lattice water molecules and coordinated fumarate which increases the dimensionality of the framework. Through these H-bonds, the compound forms an overall 3D supramolecular assembly (Figure 3.26.).

Structural Description of 38·2CH$_3$OH. It crystallizes in the triclinic *P*-1 space group. The crystallographic information pertaining to data collection and structure refinement has been provided in Table A5. The asymmetric unit consist of one metal center, one-half of the ligand, one-half of the fumarate which is bound to the metal ion and one-half of the fumarate as counter anion and a methanol molecule. The Ni(II) ion is octahedrally surrounded by N3O3 atmosphere. All three N-atoms belongs to one end of the bis(tridentate) tpxn ligand and O-atoms are coming from two coordinated water and other is from one end of the fumarate bound to the metal ion in monodentate fashion. Other end of the ligand is bound to another Ni(II)-ion, which is further bridged by fumarate to another Ni(II)-ion, as a result forming a 1D polymeric chain. The distances are Mn-N_{pyr} 2.052(2) Å, 2.074(2) Å; Mn-N_{CH2} 2.159(2) Å, Mn-O_{aq} 2.091(2) Å, 2.099(2) Å; Mn-O 2.035(2) Å. Selected bond distances and bond angles are listed in Table A23 and Table A49, respectively.

The free fumarate present in the molecules forms two kind of H-bonding in two different directions. The free fumarate anion forms H-bond through the methanol -OH and coordinated water, thus connected two different 1D chains to form a 2D supramolecular sheet. This 2D supramolecular sheet is again connected to another similar 2D sheet via H-bond through the second coordinated water molecule and a fumarate molecule in other directions forming an overall 3D supramolecular assembly (see Figure 3.27).

Structural Description of 39·2CH$_3$OH·H$_2$O. It crystallizes in the triclinic *P*-1 space group. The crystallographic information pertaining to data collection and structure refinement has been provided in Table A6. The asymmetric unit contains two Ni(II) metal center, one ligand, one fumarate which is bound to the metal ion, three bound water, one bound methanol, two half of the fumarate as counter anions, and two each of methanol and water molecules as the solvent of crystallization. Both the Ni(II) ions are octahedrally surrounded by N3O3 coordination environment. In both cases, all three N-atoms belong to one end of the bis(tridentate) tpxn ligand and the O-atoms are come from two coordinated water and

another from the one end of the fumarate bound to Ni(II) in monodentate fashion. In the second Ni(II) ion, it is methanol instead of second water.

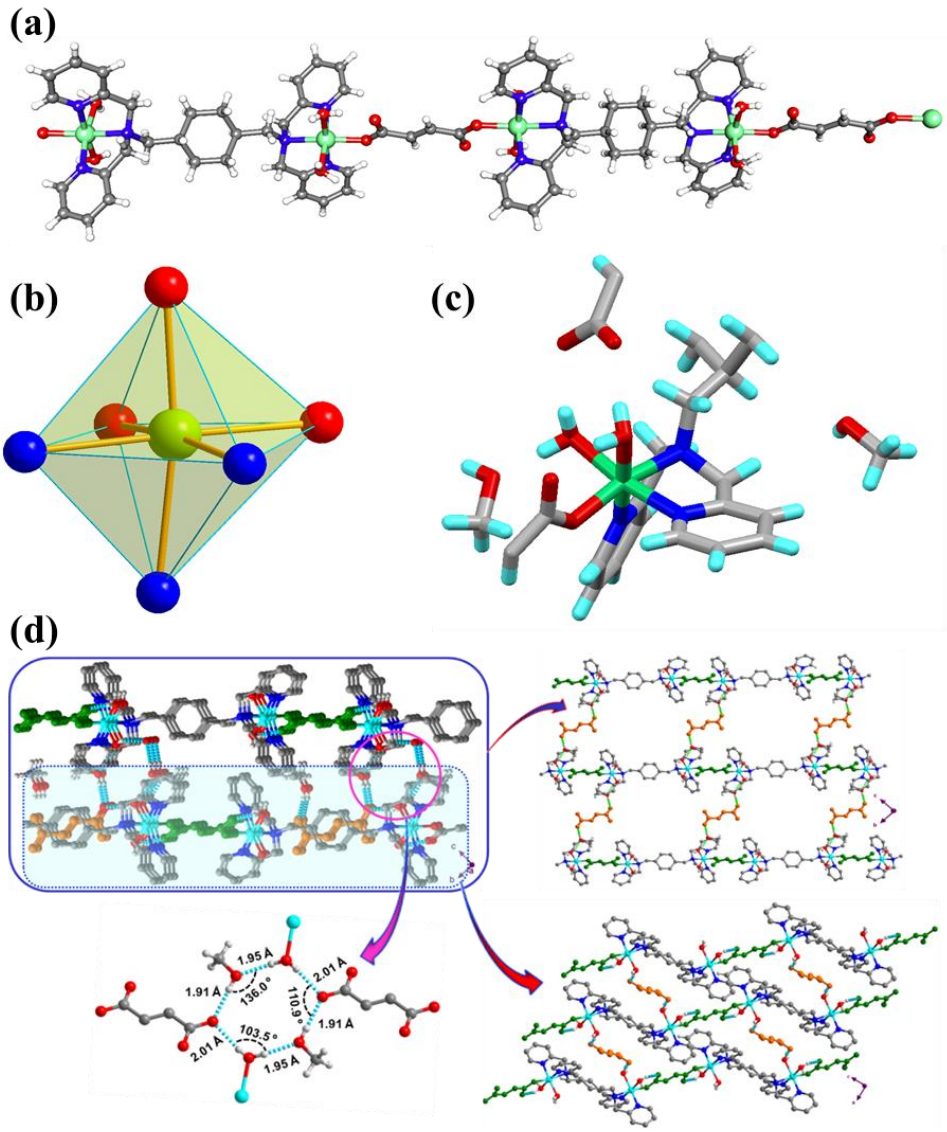

Figure 3.27. Crystal Structure of **38.** (a) 1D chain of **38**, (b) coordination environment around the metal center, (c) asymmetric unit, and (d) formation of supramolecular assembly through H-bonds (color code used for different atoms are like, green: Ni; red: O, blue: N, grey: C, cyano: H).

All Ni(II)-ions are alternatively bridged by tpxn ligand and fumarate, as a result forming a 1D polymeric chain. The bond distances are Ni-N_{pyr} 2.061(7) Å, 2.118(7) Å; Ni-N_{CH2} 2.176(7) Å, Ni-O_{aq} 2.066(5) Å, 2.078(6) Å; Ni-O 2.051(7) Å. The distances are Ni-N_{pyr} 2.081(7) Å, 2.051(7) Å; Ni-N_{CH2} 2.156(7) Å, Ni-O_{aq} 2.066(5) Å, Ni-$O_{methanol}$ 2.081(6)Å; Ni-O 2.043(6) Å. Selected bond distances and bond angles are listed in Table A24 and Table A50, respectively. The free fumarate present forms two kinds of H-bonding in two different directions through the methanol -OH and coordinated water, thus connecting two different 1D chains to form a 2D supramolecular sheet. This supramolecular sheet again is

connected to another 2D sheet via H-bond through second coordinated water and fumarate in other directions forming an overall 3D supramolecular assembly (see Figure 3.28).

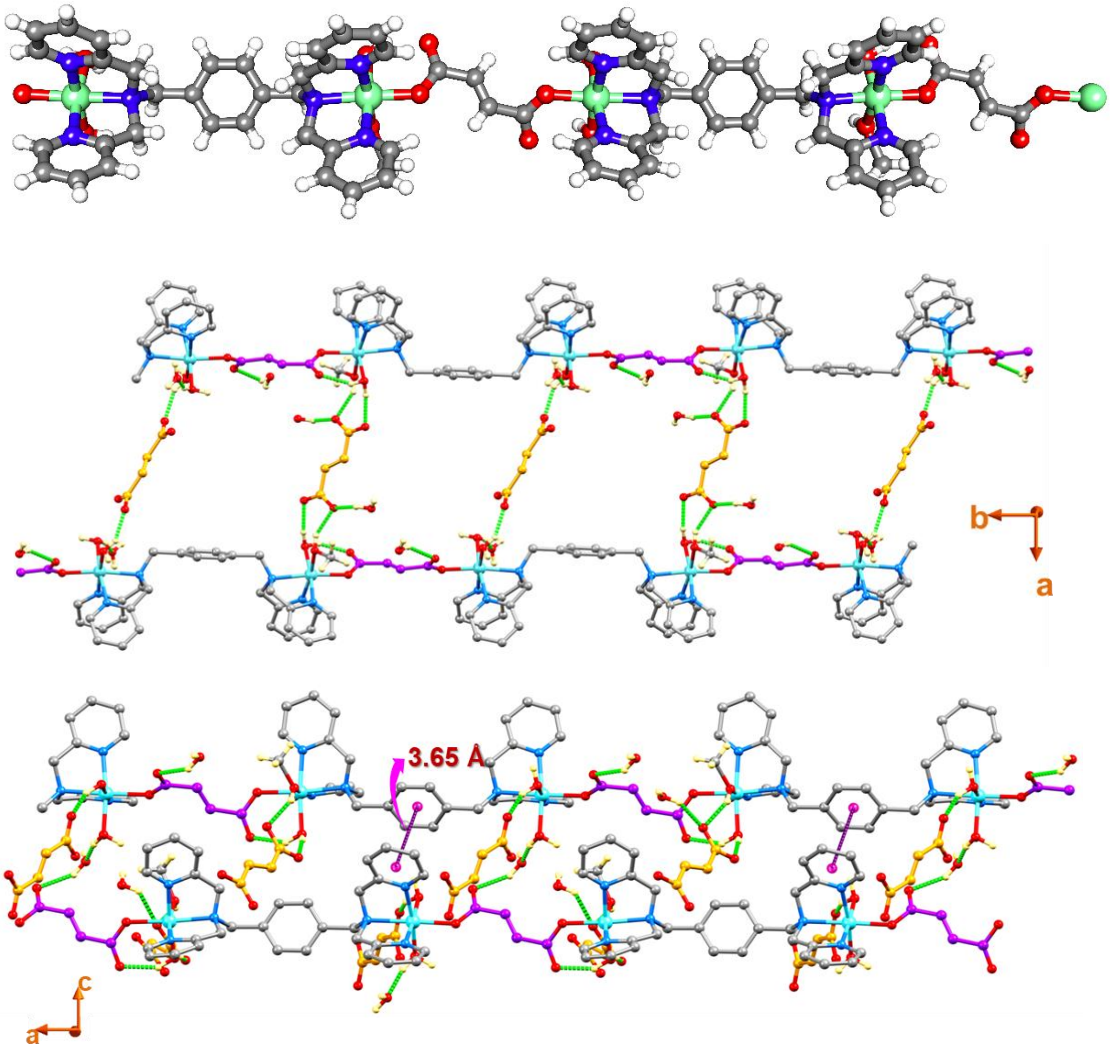

Figure 3.28. Crystal Structure and Supramolecular assembly of **39.** (a) the coordination environment around the metal center, (b) the asymmetric unit, (c) the 1D chain, (d) formation of supramolecular assembly through H-bonds (color code used for different atoms are like, green: Ni; red: O, blue: N, grey: C, cyano: H).

Compounds **35**, **38** and **39** have similar 1D polymeric chain structure with one of the fumarates present as a counter anion. In compound **35**, Mn(II) is present as the metal center and tpxn as semirigid ligand while in case of **38** and **39** both have Ni(II) as the metal center, and, tpchn and tpxn, are present as a semirigid ligands, respectively. From the structural viewpoint, it can be concluded that there is no effect of the ligand and metal center on the structure of these compounds, the dicarboxylate fum^{2-} is the directing factor. All these 1D CPs have distinguished supramolecular structures because of the presence of different solvent molecules in a different number. For compounds **36** and **37**, a similar 1D polymeric structure is expected where the metal center is Co(II).

3.2.2. Flexible Carboxylates and Semirigid Spanning Ligands Synthesis

Synthesis. All these compounds were synthesized through a one-pot self-assembly method as shown in Scheme 3.6. The metal center used for the synthesis of these compounds are Co(II) and Ni(II). Keeping the bis(tridentate) ligands fixed as tpchn or tpxn, three different dicarboxylates, succinate (suc^{2-}), glutarate (glu^{2-}) and adipate (adi^{2-}) were used.

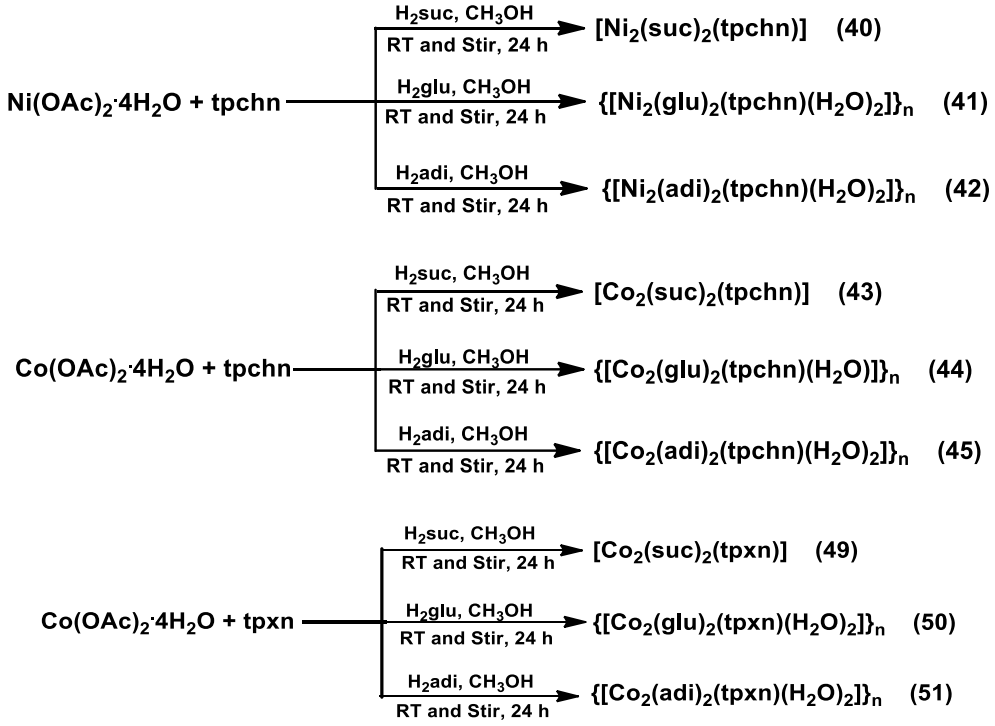

Scheme 3.6. Synthesis of **40**-**51**.

For the synthesis, a ratio of M(II):dicarboxylate:ligand (2:2:1) was taken and stirred for 24 h at room temperature in methanol. after concentrating the resultant solid was collected and used for further characterization. The crystals were obtained (wherever possible) by the direct layering of the components in methanol and water mixture (1:1).

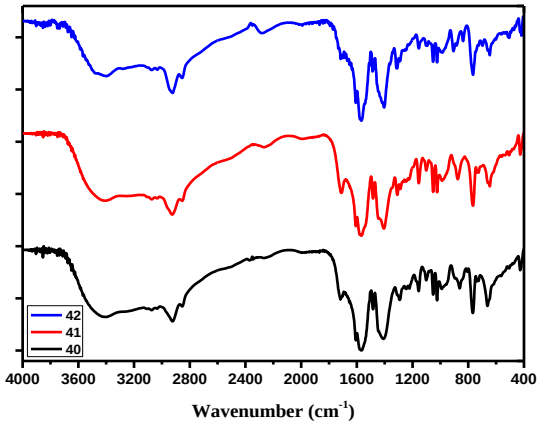

Figure 3.29. FTIR spectra of **40**-**42**.

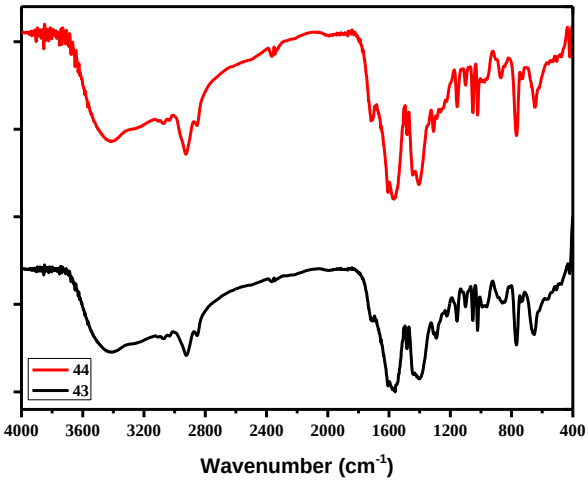

Figure 3.30. FTIR spectra of **43-44**.

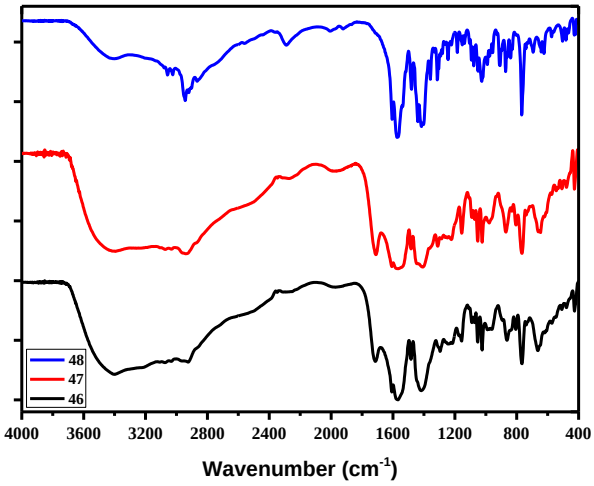

Figure 3. 31. FTIR spectra of **46-48**.

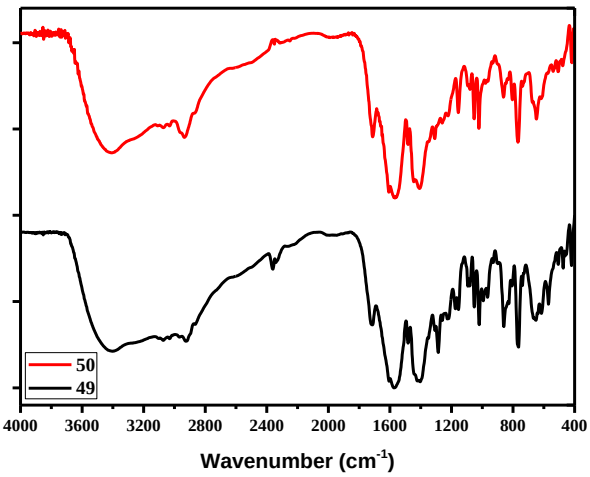

Figure 3.32. FTIR spectra of **49-51**.

Thermogravimetric Analysis.

In order to check the thermal stability of **40**-**51**, thermogravimetric analysis was carried out for the as-synthesized samples. The thermogravimetric profiles of **40**-**42** is shown in Figure. 3.33. All these compounds exhibit initial weight loss in the temperature range of 60-80 ℃ which can be assigned to be the lattice solvent molecules.

Table 3.7 Selected FTIR peaks and binding modes of carboxylates of **40**-**51.**

Compounds	$\nu_{asym}(COO^-)$ cm^{-1}	$\nu_{sym}(COO^-)$ cm^{-1}	$\Delta\nu$ cm^{-1}	Binding Mode
40	1608, 1576	1443, 1406	165, 170	monodentate, monodentate
41	1608, 1574	1445, 1405	163, 169	monodentate, monodentate
42	1604, 1575	1444, 1405	160, 170	monodentate, monodentate
43	1607, 1577	1445, 1405	162, 172	monodentate, monodentate
44	1605, 1574	1445, 1406	160, 168	monodentate, monodentate
45	1605, 1574	1445, 1404	160, 170	monodentate, monodentate
46	1605, 1574	1445, 1409	160, 165	monodentate, monodentate
47	1607, 1577	1445, 1405	162, 172	monodentate, monodentate
48	1605, 1574	1445, 1406	160, 168	monodentate, monodentate
49	1605, 1574	1445, 1404	160, 170	monodentate, monodentate
50	1605, 1576	1443, 1405	162, 171	monodentate, monodentate
51	1607, 1576	1445, 1404	162, 172	monodentate, monodentate

In case of **40**, the observed weight loss of 3.8% in the temperature range of 65- 75 ℃ can be attributed to the loss of two water molecules (ca. 3.73 %), followed by the weight loss due to four coordinated water molecules. Compounds **41** and **42** exhibit weight losses of about 3.7% (ca. 3.63%) and 5.4% (ca. 3.94%) due to two and three lattice water molecules, respectively. In the next step, both compounds undergo a weight loss corresponding to four and two water molecules coordinated to the metal centers, respectively, followed by one molecule of the corresponding carboxylate in each case which leads to the framework decomposition. A summary for the weight loss is shown in Table 3.8.

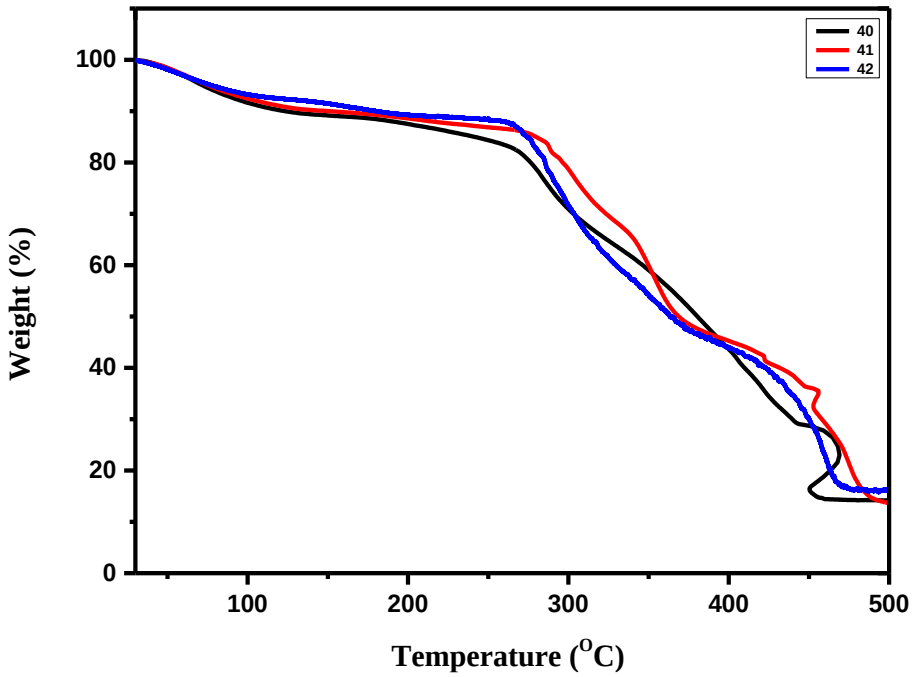

Figure 3.33. TGA scan of **40**-**42**.

Table 3.8. TGA calculations for **40**-**42**.

Compounds	Weight Loss											
	Step I				Step II				Step III			
	Ca.	Obs.	Loss	°C	Ca.	Obs.	Loss	°C	Ca.	Obs.	Loss	°C
40	3.73	3.82	$2H_2O$	64	7.47	7.62	$4H_2O$	187	15.77	12.21	suc	287
41	3.63	3.77	$2H_2O$	62	20.41	19.51	$4H_2O$ + glu	306	---	---	---	---
42	3.94	5.40	$3H_2O$	80	17.97	17.85	$2H_2O$ + adi	291	---	---	---	---

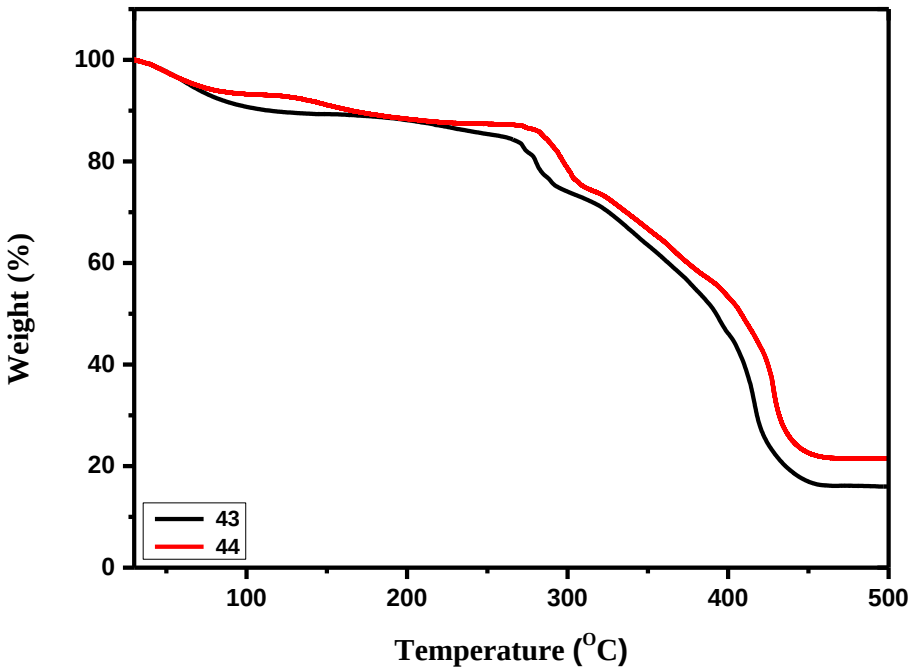

Figure 3.34. TGA profile of **43**-**44**.

TGA scans for **43**-**44** are shown in Figure 3.34. These compounds are moderately stable upon heating where the lose due to lattice water molecule occurs between 50-80 ℃. In case of **43** and **44**, four molecules and one molecule of lattice water are lost at 78 °C and 50 ℃, corresponding to 7.12% (ca. 7.20%) and 2.41% (ca. 1.91%) weight loss, respectively. In the next step, both compounds lose the bound water molecules and one molecule of the corresponding dicarboxylates at 303 °C and 299 ℃, respectively. A summary for weight loss is shown in Table 3.12.

Table 3.9. TGA calculation for **43**-**44.**

Compounds	Weight Loss											
	Step I				Step II				Step III			
	Ca.	Obs.	Loss	^{O}C	Ca.	Obs.	Loss	^{O}C	Ca.	Obs.	Loss	^{O}C
43	7.20	7.12	$4H_2O$	78	18.79	19.10	$4H_2O$ + suc	303		12.21	suc	287
44	1.91	2.41	H_2O	50	17.69	18.40	$2H_2O$ + glu	299	---	---	---	---

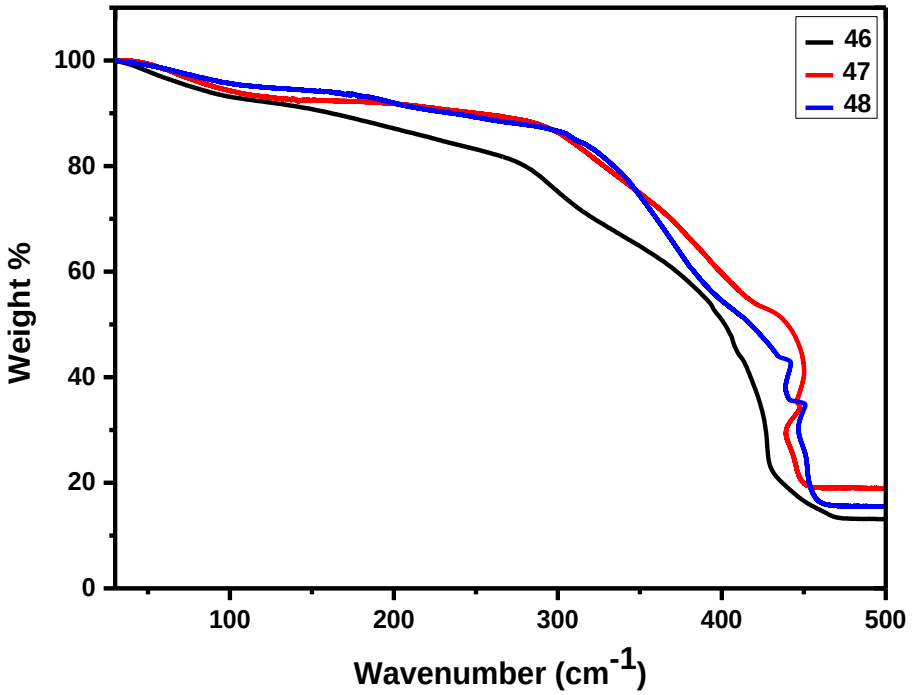

Figure 3.35. TGA profile of **46**-**48**.

TGA scans for **46**-**48** are shown in Figure 3.35. These compounds are moderately stable upon heating. All these compounds lose lattice water molecule between 48-80 °C. Compound **46**, **47** and **48** lose two, one and one lattice water molecules corresponding to 3.76% (ca. 3.91%), 3.91% (ca. 3.79%), and 2.52% (1.87%) at 65 °C, 79 °C and 48 °C, respectively. After losing the lattice water molecules, all these compounds undergo weight loss corresponding to all the bound water molecules and one of the corresponding carboxylates at 295 °C, 336 ℃, and 333 ℃. The weight loses are 19.81% (ca. 20.44%),

18.21% (ca. 17.48%) and 18.72% (ca. 18.75%). In the third step all these compounds undergo decomposition.

Table 3.10. TGA calculation of **46-48**.

Compounds	Weight Loss											
	Step I				Step II				Step III			
	Ca.	Obs.	Loss	^{O}C	Ca.	Obs.	Loss	^{O}C	Ca.	Obs.	Loss	^{O}C
46	3.91	3.76	$2H_2O$	65	20.44	19.81	$4H_2O$ + suc	295	---	---	---	---
47	3.79	3.91	$2H_2O$	79	17.48	18.21	$2H_2O$ + glu	336	---	---	---	---
48	1.87	2.52	H_2O	48	18.75	18.72	$2H_2O$ + adi	333	---	---	---	---

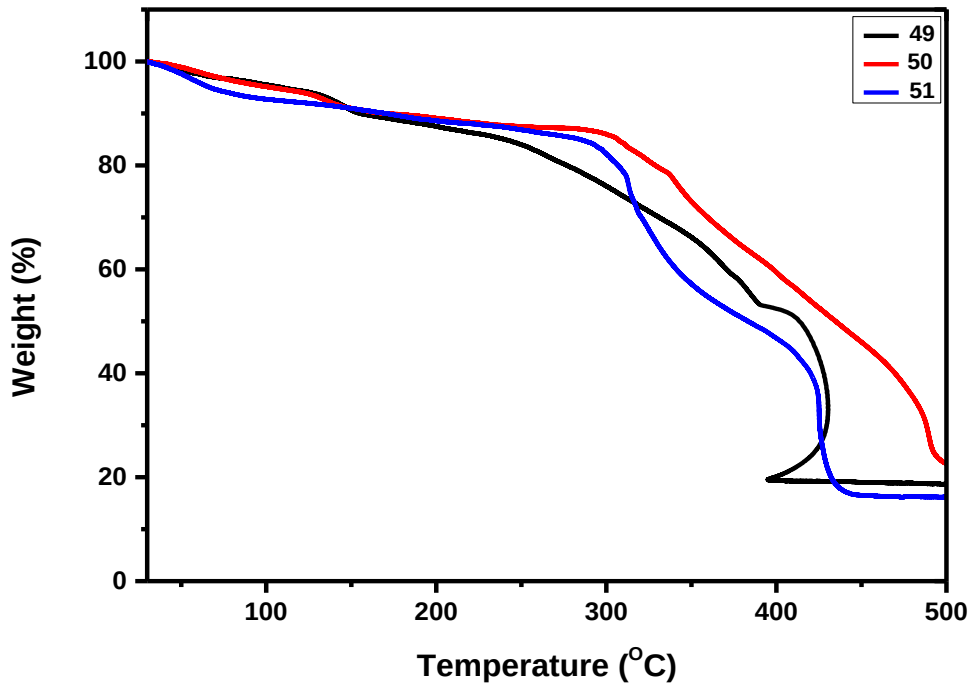

Figure 3.36. TGA profile of **49-51**.

TGA scans for **49-51** are shown in Figure 3.36. These compounds are moderately stable upon heating. All these compounds lose lattice water molecules initially at more or less 48-80 ℃. In the case of **49**, four bound water molecules are lost up to 145 ℃, corresponding to 8.26% (ca. 7.80%) weight loss. After that, the compound shows a weight loss of 12.41% (ca. 12.57%) up to 282 ℃, corresponding to a succinate molecule and then it undergoes decomposition. Compound **50** also initially lose two lattice water molecules and two bound water molecules up to 137 ℃, corresponding to 7.77% (ca. 7.57%) weight loss. Then it loses 14.51% (ca. 13.68%) of its weight at temperature up to 339 ℃, corresponding to the loss of one glutarate molecule followed by decomposition. On the other hand, **51** shows a continuous weight loss of 21.69% (ca. 21.24%) up to temperature 311 ℃; corresponding to one lattice water molecule, two bound water molecule and an adipate dicarboxylate.

Table 3.11. TGA calculation of **49**-**51**.

Compounds	Weight Loss											
	Step I				Step II				Step III			
	Ca.	Obs.	Loss	^{O}C	Ca.	Obs.	Loss	^{O}C	Ca.	Obs.	Loss	^{O}C
49	7.80	8.26	$4H_2O$	145	12.57	12.41	suc	282	---	---	---	---
50	7.57	7.77	$2H_2O$+ $2H_2O$	137	13.68	14.51	glu	339	---	---	---	---
51	21.24	21.69	H_2O + $2H_2O$ + adi	311	---	---	---	---	---	---	---	---

Single Crystal Structure Analysis

Structural Description of 46-48. Compound **46** crystallizes in the monoclinic $P2_1/n$ space group. The crystallographic information pertaining to data collection and structure refinement has been provided in Table A6. The asymmetric unit of **46** contains a Ni(II) metal center, one suc^{2-}, half of the bis(tridentate) ligand, and one water, two methanol as a solvent of crystallization. It is a dinuclear compound of nickel (Figure 3.37). Each Ni(II) is surrounded by N3O3 coordination environment. The bis(tridentate) ligand tpchn bridges between two nickel centers; each nickel is again coordinated to two water molecules and a dicarboxylate O-atom. Two suc^{2-} molecules are bound to two metal centers in a monodentate fashion from one end. The other end of the dicarboxylates is uncoordinated and as a result the molecule is not expanding in any direction to form a polymer, rather gives rise to a dinuclear compound. The bond distances are: Ni-N_{pyr} 2.048(4) Å, 2.075(4) Å; Ni-N_{CH2} 2.172(4) Å, Ni-O_{aquo} 2.083(3) Å, 2.055(3) Å, and Ni-O_{dicarb} 2.053(3) Å. Selected bond distances and bond angles are listed in Table A25 and Table A51, respectively.

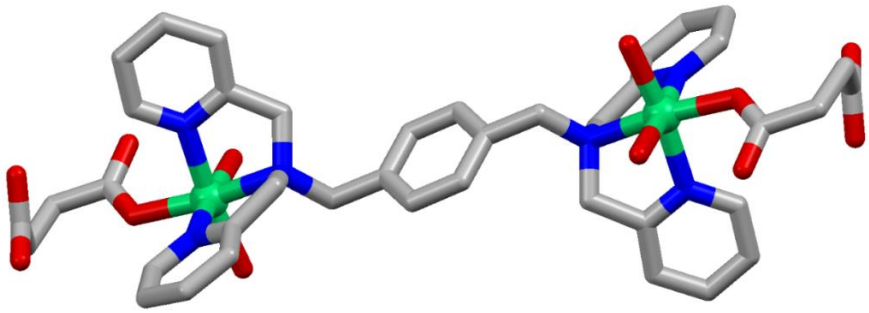

Figure 3.37. Crystal Structure of **46** (color code used for different atoms are like, green: Ni; red: O, blue: N, grey: C, cyano: H).

The uncoordinated ends of the dicarboxylate forms H-bonds with two coordinated water bound with one metal center of another dinuclear molecule and this kind of H-bonding continues with the next molecule. As a result, the molecule expands in all three directions through H- bonds and overall forms a 3D supramolecular assembly.

Both the compounds **47** (Figure 3.38) and **48** (Figure 3.39) form a 1D polymeric structure. In case **47**, the Ni(II) centers are octahedrally surrounded by N3O3 coordination environment. The ligand provides three N-atoms for binding from one end to each metal center. The remaining opening sites on the metals are occupied by one coordinated water molecule and two glutarate (glu^{2-}) molecules, which are bound in monodentate fashion with the metal. The flexibility of the dicarboxylate glu^{2-} allows it to bind and form a polymeric chain keeping the Ni(II) centers on a line. The bis(tridentate) ligand binds two of such polymeric chains vertically and results an one dimesional ladder kind of polymer. The polymeric chain behaves as the long arms of the ladder and the ligand as shorter arms between two long arms.

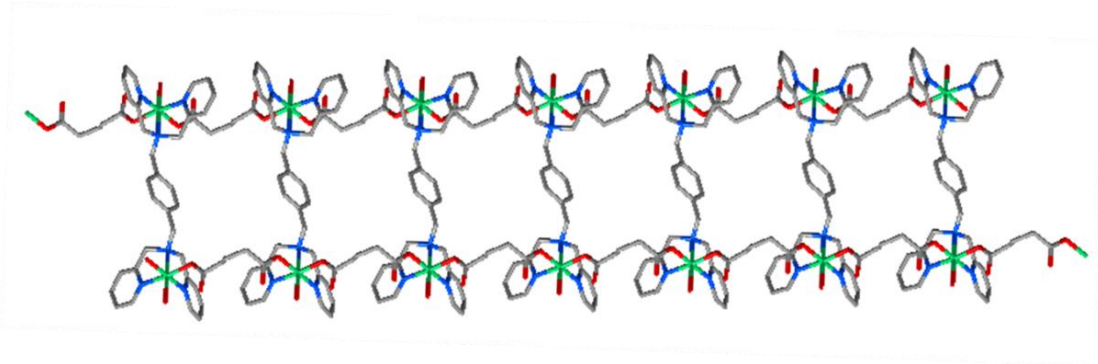

Figure 3.38. Crystal Structure of **47** (color code used for different atoms are like, green: Ni; red: O, blue: N, grey: C, cyano: H).

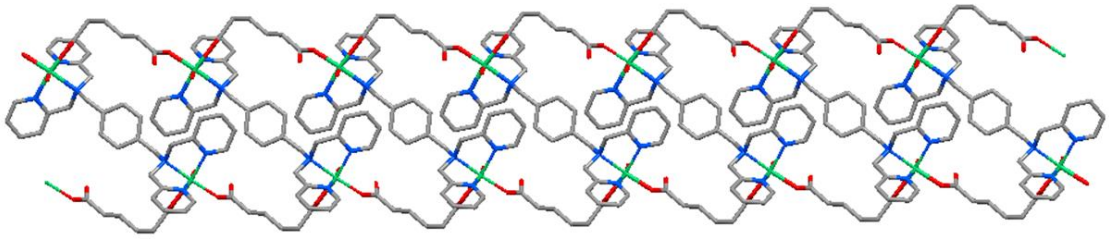

Figure 3.39. Crystal Structure of **48** (color code used for different atoms are like, green: Ni; red: O, blue: N, grey: C, cyano: H)**.**

On the other hand, **48** also shows a similar N3O3 coordination environment around the Ni(II) metal center. The bis(tridentate) ligand tpxn provides three N-atoms to binds with each metal center. The remaining sites are bound with one coordinated water and two adipate (adi^{2-}) dicarboxylates which bind to the metal center in a monodentate fashion. The higher flexibility of the dicarboxylates adipate allows it to form a polymeric chain keeping the Ni(II) center on a line. Two of such chains are diagonally connected by the ligands and form an overall 1D coordination polymer. Unlike the glutarate case, i.e. **47**, the carbon

chain is projected outwards of the main structure because of the higher flexibility of adipate dicarboxylate in **48**.

3.2.3 Heterocyclic Dicarboxylate with a Variation in Spanning Ligand

Synthesis. All these compounds were synthesized through one pot self-assembly method with the metal center (Co(II), Ni(II) and Cd(II)), 2,5-thiophene dicarboxylate (tdc^{2-}) and four different bis(tridentate) ligands at ambient conditions. For the synthesis, a ratio of M(II):dicarboxylate:bis(tridentate) ligand (2:2:1) was used and stirred for 24 h at room temperature in methanol. The solid formed was filtered and air dried. The same resultant solid was used for further characterizations. The single crystal suitable for X-ray diffraction analysis was obtained (where ever possible) by the direct layering of the components in methanol and water mixture (1:1).

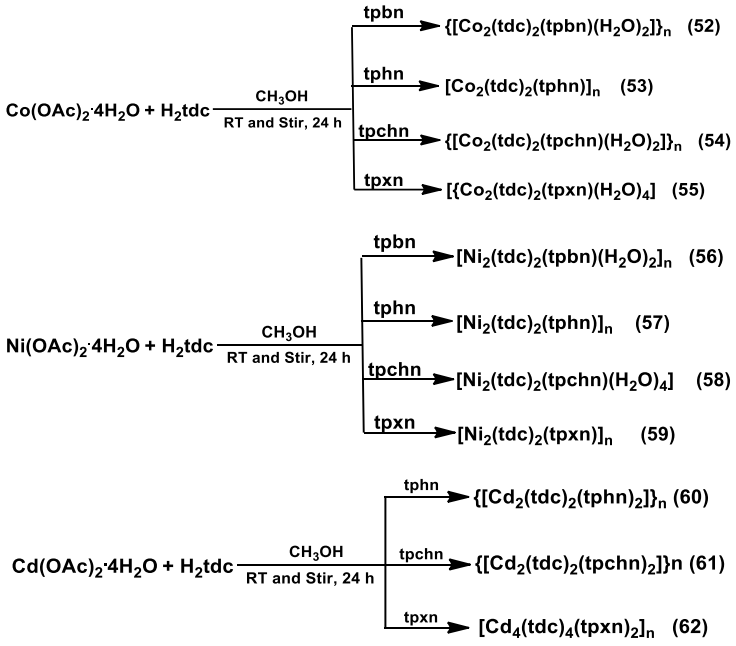

Scheme 3.7. Synthesis of **52-62**.

FTIR Spectroscopy. As the primary characterization technique, the FTIR spectra of **52-62** was recorded in the solid state as KBr pellets at room temperature. The FTIR data corrobortaes well with the structural finding from the single crystal X-ray diffraction analyses. The FTIR spectra for **52-55** are shown in Figure 3.40. The peaks observed at 3235, 3221 and 3230 cm^{-1} for **52**, **54** and **55,** respectively, can be assigned to the coordinated water molecules in each case. Two kinds of carboxylate bindings (monodentate and chelating bidentate) are evident from the two symmetric and asymmetric stretch of the carboxylate. Selected FTIR peaks for **52-55** are listed in Table 3.12.

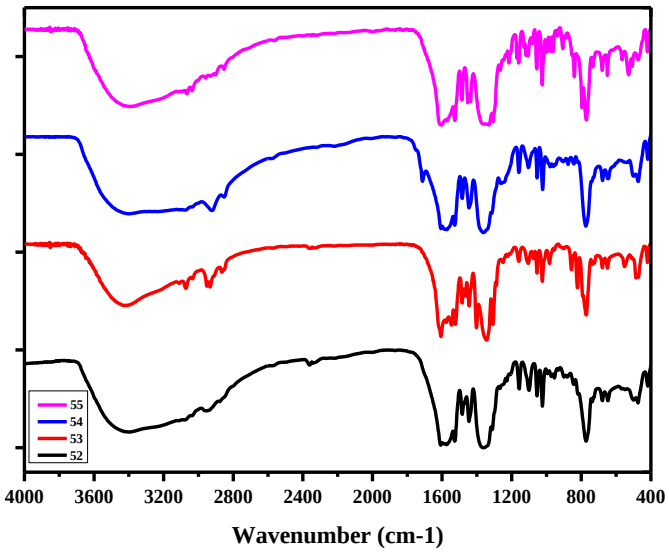

Figure 3.40. FTIR spectra of **52-55**.

Table 3.12. Selected FTIR peaks and binding modes of carboxylates for **52-55**.

Compounds	$\nu_{asym}(COO^-)$ cm^{-1}	$\nu_{sym}(COO^-)$ cm^{-1}	$\Delta\nu$ cm^{-1}	Binding Mode
52	1586	1361	225	monodentate
53	1575, 1545	1402, 1344	173, 201	chelating bidentate, monodentate
54	1583	1362	221	monodentate
55	1570	1367	203	monodentate

The FTIR spectra (Figure 3.41) indicates monodentate carboxylate binding in case of **56**, **58** and **59**, which is evident from the $\Delta\nu$ values in the range of 210-230 cm^{-1}. The two different symmetirc and asymmetric stretching frequencies with $\Delta\nu$ values of 171 and 198 cm^{-1}, indicates monodentate and chelating bidentate binding modes of the carboxylates, in

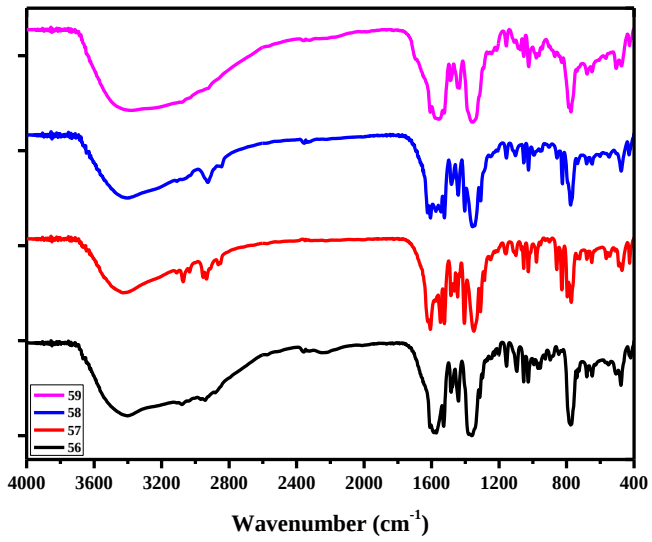

Figure 3.41. FTIR spectra of **56-59**.

case of **57**. The peaks at 3239 and 3225 cm^{-1} in case of **56** and **57** are because of the presence of the coordinated water molecule(s). The FTIR spectra for **56-59** are shown in Figure 3.41 and the selected FTIR peaks for **56-59** are listed in Table 3.13.**Table 3.13**. Selected FTIR peaks and binding modes of carboxylates for **56-59**.

Compounds	**$\nu_{asym}(COO^-)$ cm^{-1}**	**$\nu_{sym}(COO^-)$ cm^{-1}**	**$\Delta\nu$ cm^{-1}**	**Binding Mode**
56	1586	1361	225	monodentate
57	1576, 1547	1405, 1349	171, 198	chelating bidentate, monodentate
58	1574	1365	209	monodentate
59	1575	1360	215	monodentate

In compounds **60**, **61** and **62**, there are no coordinated water molecules present as there are no peaks found around 3230 cm^{-1} in the FTIR spectrum of the individual compounds (Figure 3.42). From the $\Delta\nu$ values coming as 221 cm^{-1}; 229 and 209 cm^{-1}; 214 and 226 cm^{-1}, respectively, the different binding modes of carboxylates can be interpreted in these CPs. In **60**, the carboxylate is bound to the metal in a chelating bidentate fashion. In **61** and **62**, both monodentate and chelating bidentate binding modes are observed. Selected FTIR peaks for **60-62** are listed in Table 3.13.

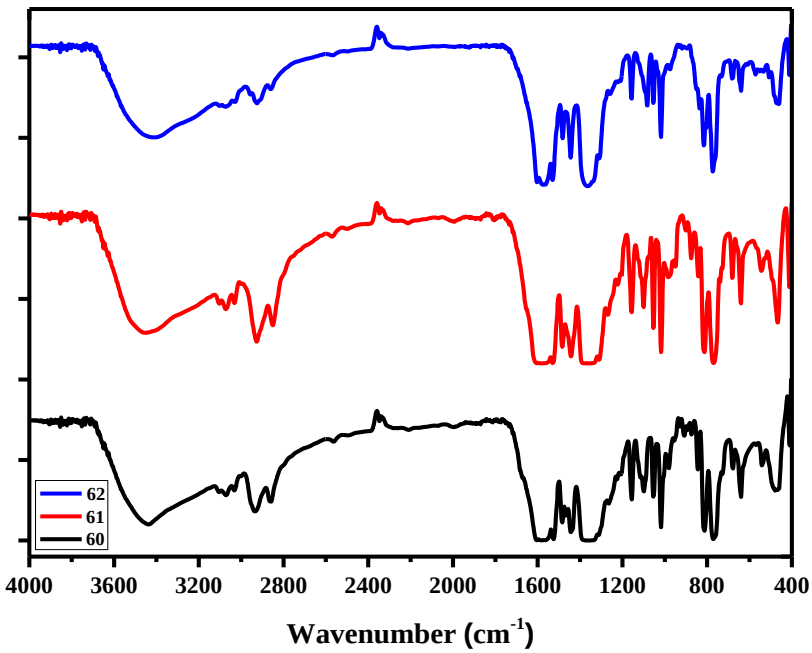

Figure 3.42. FTIR spectra of **60-62.**

Table 3.14. Selected FTIR peaks for **60-62**.

Compounds	$\nu_{asym}(COO^-)$ cm^{-1}	$\nu_{sym}(COO^-)$ cm^{-1}	$\Delta\nu$ cm^{-1}	Binding Mode
60	1586	1365	221	chelating bidentate
61	1590, 1560	1361, 1351	229, 209	monodentate, chelating bidentate
62	1576, 1564	1362, 1338	214, 226	chelating bidentate, monodentate

Thermogravimetric Analysis. Compounds **52, 53** and **55** are stable up to 300 ˚C while compound **54** is stable up to 280 ˚C. With the initial loss of solvent molecules, all these molecules show a three-step weight loss profile. In the first step, compound **52-55** lose lattice water molecule(s) followed by losing of coordinated water molecule(s) and dicarboxylate(s). Then the molecules undergo decomposition. The compounds **52, 53** and **54** lose lattice water molecule(s) up to 54, 53 and 44 ˚C, respectively. While for **55**, it is at around 70 ˚C. In the second step, **54** loses two bound water molecules and a tdc^{2-} dicarboxylate within 54-322 ˚C. While **53** loses two tdc^{2-} dicarboxylates within 53-314 ˚C, **54** loses two tdc^{2-} dicarboxylates within 44-294 ˚C along with two water molecules, **55** loses four water molecules and two tdc^{2-} dicarboxylate within 70-411 ˚C. After the second step, all these molecules undergo decomposition. The calculations are tabulated below (Table 3.15)

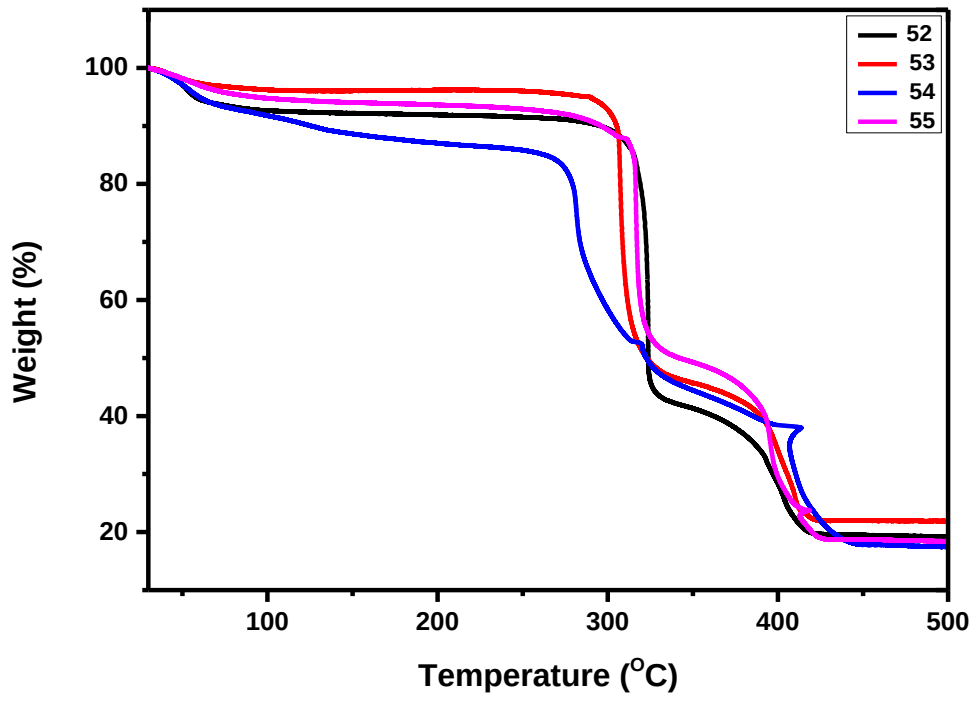

Figure 3.43. TGA plot of **52-55**.

Table 3.15. TGA calculation of **52-55**.

Compounds	Weight Loss											
	Step I				Step II				Step III			
	Ca.	Obs.	Loss	^{O}C	Ca.	Obs.	Loss	^{O}C	Ca.	Obs.	Loss	^{O}C
52	3.66	4.067	$2H_2O$	54	20.87	23.66	$2H_2O$ + tdc	322	---	---	---	---
53	1.88	2.08	H_2O	53	35.56	34.11	2 tdc	314	---	---	---	---
54	1.76	1.64	H_2O	44	36.93	34.68	$2H_2O$ + 2 tdc	294	---	---	---	---
55	3.37	3.93	2 H_2O	70	38.64	40.91	$4H_2O$ + 2 tdc	411	---	---	---	---

TGA profiles of **56**-**59** show the high stability of the molecules under the exposure of heat from 30 ℃ to 500 ℃. Compound **59** is stable up to 290 ℃, except the loss of solvent molecules. After that, the compound starts losing weight rapidly showing an overall three-steps weight loss profile. While all other molecules are stable up to 350 ℃ and after that lose weight rapidly and undergo decomposition. Except for **57** which shows a three-step profile of weight loss is evident in these molecules also. Compound **56**, **58** and **59** lose two, one and six lattice water molecules up to 53, 46 and 96 ˚C, respectively. In the second step, these three molecules (**52**, **53** and **54**) lose the bis(tridentate) ligand or the dicarboxylates along with the coordinated water molecules and then undergo decomposition. While compound **57**, having no lattice or coordinated water, shows the first weight loss within 30 to 359 ˚C for bis(tridentate) ligand tphn. Then these molecules undergo decomposition. The calculations are tabulated below (Table 3.16).

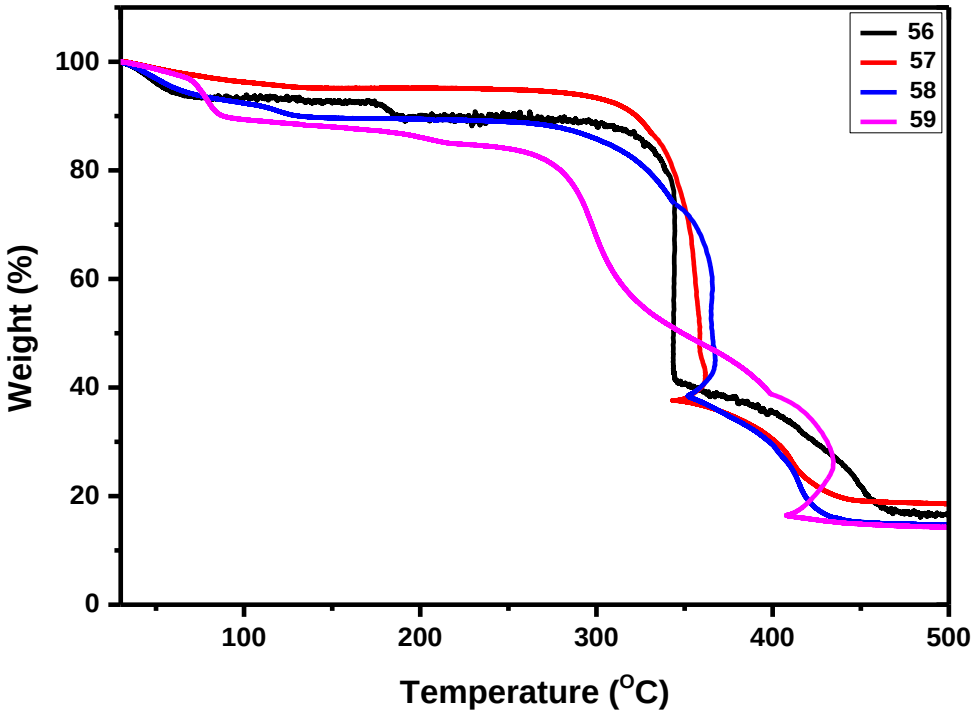

Figure 3.44. TGA scans of **56**-**59**.

Table 3.16. TGA calculationsfor **56-59**.

Compounds	Weight Loss											
	Step I				Step II				Step III			
	Ca.	Obs.	Loss	^{O}C	Ca.	Obs.	Loss	^{O}C	Ca.	Obs.	Loss	^{O}C
56	3.66	4.50	$2H_2O$	53	49.74	51.18	$2H_2O$ + tpbn	344	---	---	---	---
57	51.22	50.96	tphn	362	---	---	---	---	---	---	---	---
58	3.35	2.01	H_2O	46	38.44	41.09	4 H_2O + 2 tdc	301	---	48.21	---	439
59	10.13	10.47	6 H_2O	96	31.90	32.97	2 tdc	321	--	--	---	--

The Cd(II) analogue, **60-62** also show good thermal stability. As shown in Figure 3.45, the thermogravimetric profile of **60-62** doesn't show any weight loss till 290 ˚C, which indicate excellent thermal stability up to this temperature, after which the sudden weight loss in each case corresponds to the framework decomposition.

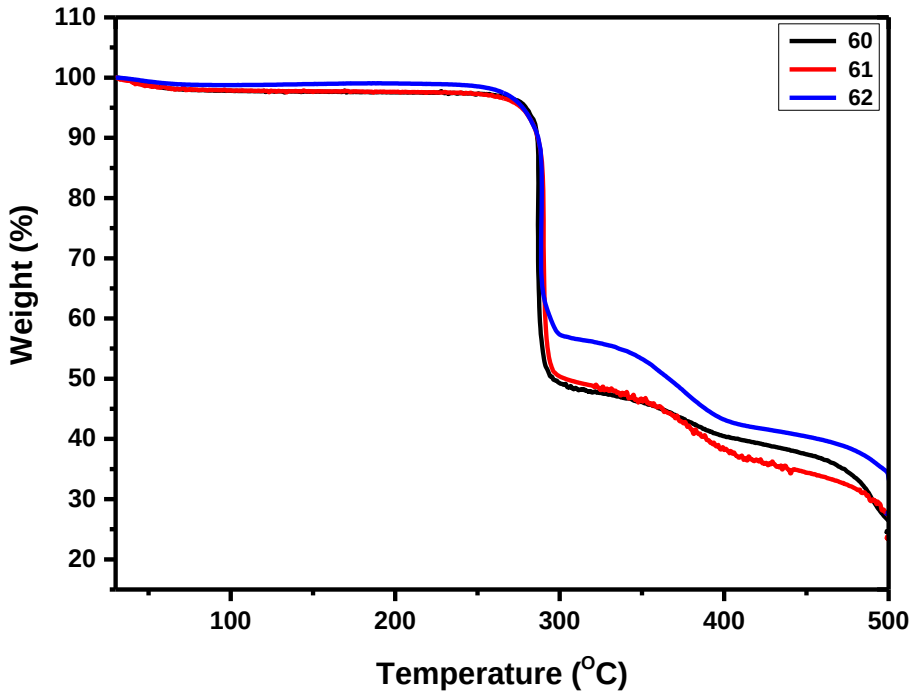

Figure 3.45. TGA scans of **60-62**.

Table 3.17. TGA calculation of **60-62**.

Compounds	**Weight Loss**											
	Step I				Step II				Step III			
	Ca.	Obs.	Loss	^{O}C	Ca.	Obs.	Loss	^{O}C	Ca.	Obs.	Loss	^{O}C
60	3.66	4.50	$2H_2O$	53	49.74	51.18	$2H_2O$ + tpbn	344	---	---	---	---
61	51.22	50.96	tphn	362	---	---	---	---	---	---	---	---
62	3.35	2.01	H_2O	46	38.44	41.09	4 H_2O + 2 tdc	301	---	---	---	---

Single Crystal Structure Analysis

***Structural Description of* 52.** It crystallizes in the monoclinic $P2_1/c$ space group. The crystallographic information pertaining to data collection and structure refinement has been

provided in Table A7. The asymmetric unit consists of one Co(II) metal center, one-half of the ligand, one tcd^{2-} which is bound to the metal ion in monodentate fashion and one bound water. which makes the Co(II) ion octahedrally surrounded by N3O3 coordiantion environment. All three N-atoms are coming from one end of the bis(tridentate) tpxn ligand, O-atoms are coming from one coordinated water and other two from the two fumarate bound to the metal ion in monodentate fashion. The distances are Co-N_{pyr} 2.106(4) Å, 2.114(4) Å; Co-N_{alkyl} 2.213(4) Å, Co-O_{aq} 2.160(3) Å, 2.092(3) Å; Co-O 2.050(3) Å. Selected bond distances and bond angles are listed in Table A26 and Table A52, respectively. Two Co(II) ions are bridged by one tpxn ligands and each of the Co(II) ions are further connected to two other Co(II) ions via tdc^{2-} and forming a 2D coordination polymer (Figure 3.46).

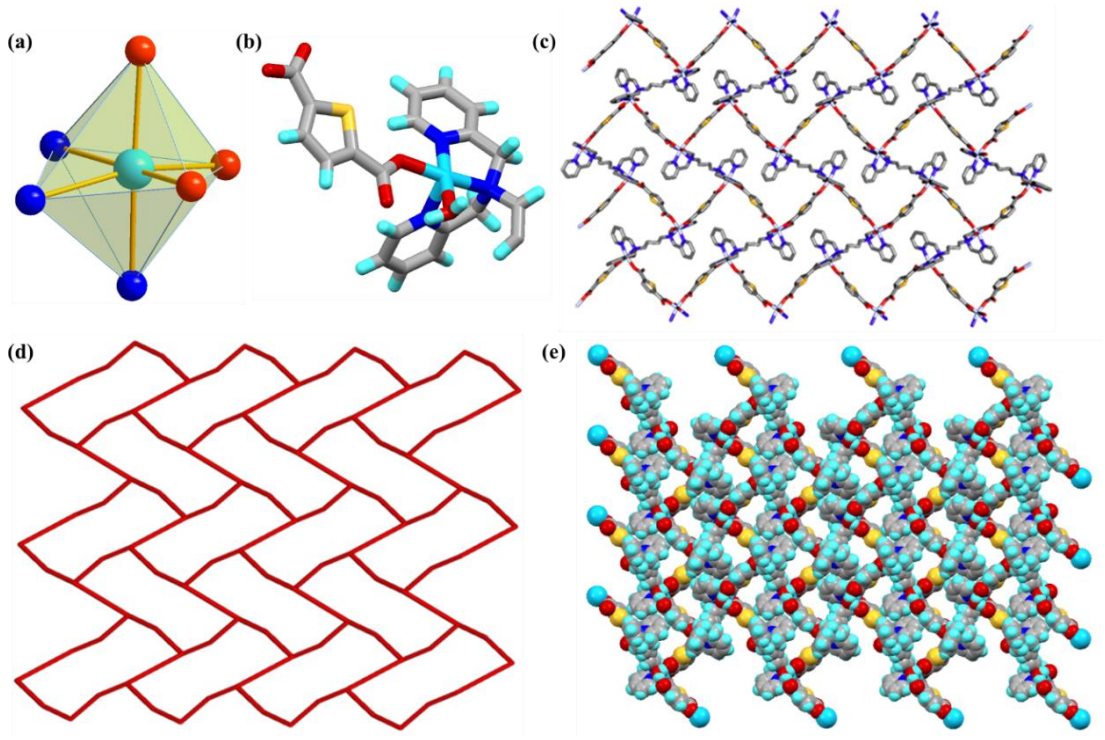

Figure 3.46. Crystal Structure of **52**. (a) the coordination environment around the metal center, (b) the asymmetric unit, (c) the 2D coordination polymer, (d) topological view, and (e) spacefill representation (color code used for different atoms are like, light purple: Co; red: O, yellow: S, blue: N, grey: C, cyano: H).

***Structural Description of* 53·CH_3OH·$2H_2O$.** It crystallizes in a triclinic *P*-1 space group. The crystallographic information pertaining to data collection and structure refinement has been provided in Table A7. The unit cell contains two independent molecules, two water molecules and a methanol molecule as a solvent of crystallization. The Co(II) is surrounded by N3O3 coordination atmosphere. One end of the ligand provides three N-binding centers and three O-atoms are coming from two tdc^{2-}, one binds in chelating bidentate fashion and

the other in monodentate fashion. The distances are Co-N_{pyr} 2.075(8) Å, 2.095(8) Å; Co-N_{CH2} 2.191(7) Å, Co-O 2.228(7) Å, 2.117(6) Å, 2.053(6) Å in one molecule and Co-N_{pyr} 2.102(8) Å, 2.110(8) Å; Co-N_{CH2} 2.208(7) Å, Co-O 2.121(6) Å, 2.239(6) Å, 2.052(6) Å in other molecule. Selected bond distances and bond angles are listed in Table A27 and Table A53, respectively. The two ends of ligand tphn connect two Co(II) ion and these Co_2 units are connected by $tdc^{2-,}$ almost in the perpendicular direction of tphn. The overall molecule looks like a ladder with Co(II), tdc^{2-} forming the long arms of the ladder and tphn forming the short arms in between the two long arms as shown in Figure 3.47.

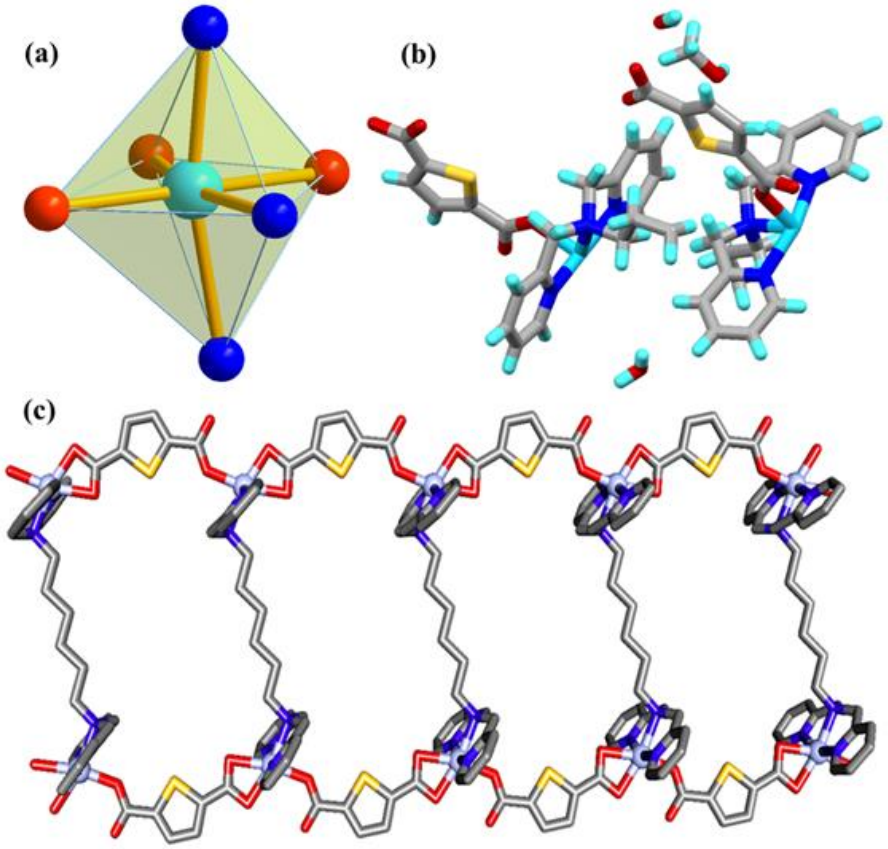

Figure 3.47. Crystal Structure of **53**. (a) the coordination environment around the metal center, (b) the asymmetric unit showing the presence of two individual molecules, (c) the 1D coordination polymer (ladder) (color code used for different atoms are like, light purple: Co; red: O, yellow: S, blue: N, grey: C, cyano: H).

***Structural Description of* 54·H_2O.** It crystallizes in the monoclinic $P2_1/c$ space group. The crystallographic information pertaining to data collection and structure refinement has been provided in Table A8. The asymmetric unit of the compound consists of a metal center, half of the ligand, a 2, 5- thiophene dicarboxylate (tdc^{2-}) linker, one coordinated water and one water of crystallization. The cobalt metal center is octahedrally surrounded by N3O3 coordiantion environment. The bond distances are 2.092(3) Å, 2.092(3) Å (between metal and two pyridyl N-atoms); 2.226(3) Å (between metal and alkyl N-atom); 2.133(3) Å

(between metal and coordinated water) and 2.089(3) Å, 2.065(3) Å (between metal and two carboxylate O-atoms), respectively. Selected bond distances and bond angles are listed in Table A28 and Table A54, respectively All the three N-atoms are coming from one end of the ligand and O-atoms are from coordinated water and from two monodentate carboxylate end. The spanning hexadentate ligand is bound to two metal centers leaving three sites vacant for binding on each metal center. Among these open sites, one is blocked by one coordinated water and other two opening are occupied by two bridging tdc^{2-} linkers in zigzg fashion, giving rise to a 2D net (Figure 3.48). This molecule is further connected through H-bonding. Two types of H-bonding, inter-molecular and intra-molecular H-bonding, is present in this molecule. The intermolecular H-bonding is formed between the coordinated water H-atoms and two free carboxylate O-atoms from two bound tdc^{2-} (2.049 Å and 1.816 Å). The uncoordinated water forms H-bonds with another uncoordinated water of another molecule and the same free O-atom of tdc^{2-}which is already formed H-bond with coordinated water (here O-atom of tdc^{2-} acts as a donor for two H-atoms). The H-bond between these two uncoordinated water forms a doubly H-bonded cyclic dimer of water, which again connects one 2D layer with another similar layer and yields an overall 3D-supramolecular assembly.

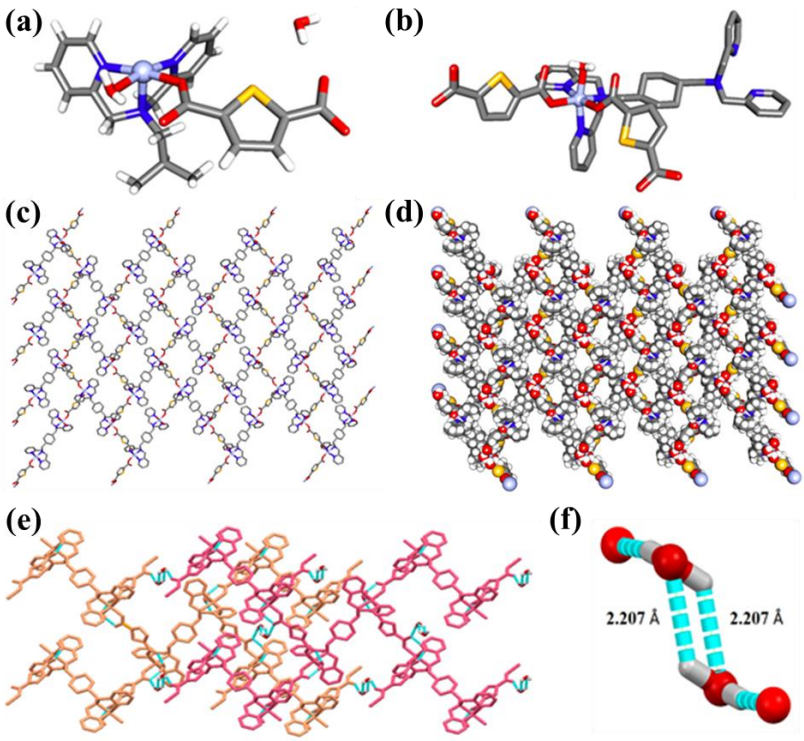

Figure 3.48. X-ray Single Crystal Structure of **54**. (a) asymmetric unit, (b) repeat unit, (c) 2D coordination polymer, (d) spacefill representation, (e) formation of supramolecular assembly through H-bonds, (f) dimer of water (color code used for different atoms are like, light purple: Co; red: O, yellow: S, blue: N, grey: C, cyano: H).

***Structural Description of* 55·8H$_2$O**. The compound crystallizes in the monoclinic $P2_1/n$ space group. The crystallographic information pertaining to data collection and structure refinement has been provided in Table A8. The asymmetric unit contains one cobalt, half of the ligand, two bound water and eight water of crystallization. It is a dimeric cobalt compound where both the cobalts are surrounded octahedrally by N3O3 coordiantion environment. Three N-atom binding sites is provided by one end of the bis(tridentate) ligand. The three O-atoms are provided by the two bound water and the rest is coming from one of each monodentate end of tdc^{2-} carboxylate. The other end of the ligand is connected to another metal center. Each of the tdc^{2-} is bound with the metal center in monodentate fashion. Though the carboxylates are at a favorable position to polymerize, the molecule does not extend further and exists as a dinuclear compound (Figure 3.49). The bond lengths are Co-N_{pyr} 2.075(4) Å, 2.072(4) Å; Cd-N_{alkyl} 2.144(4) Å and Co-$O_{carboxylate}$ 2.047(3) Å and Co-O_{aquo} 2.081(4) Å, 2.100(4) Å. Selected bond distances and bond angles are listed in Table A29 and Table A55, respectively

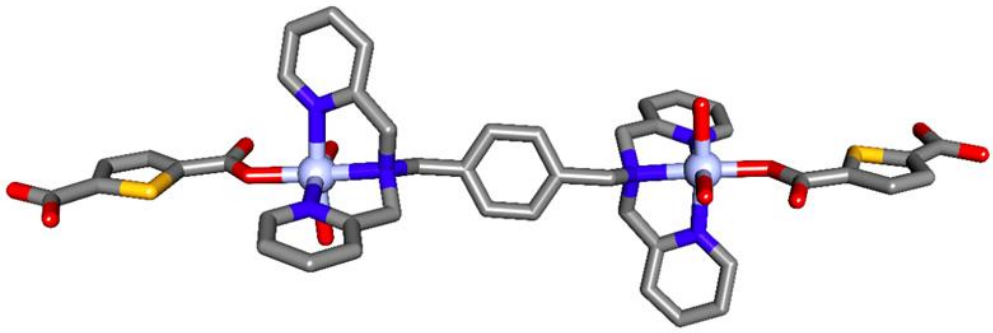

Figure 3.49. X-ray Single Crystal Structure of **55** (color code used for different atoms are like, light purple: Co; red: O, yellow: S, blue: N, grey: C, cyano: H).

Effect of Flexibility of the Bis(tridentate) Ligand. In this series of compounds, **52**-**54**, the metal center and dicarboxylates are fixed as Co(II) and tdc^{2-}, the flexibility of bis(tridentate) ligand is changed by changing the spacer in between. The comparison of these structure shows that compound **52** and **54**, where the ligands are tpbn (flexible) and tpchn (semirigid), forms an overall 2D polymeric structure. The binding and coordination environment is similar in both the case. In these two molecules, the metal center is coordinated with one water molecule and rest of the coordinating sites are occupied by ligands and dicarboxylate linkers. The carboxylate linkers binds in monodentate fashion from both ends. Each metal center is coordinated with two dicarboxylate linkers. Both the carboxylates bind to the metal center at a right angle, in the plane parallel to the plane of bis(tridentate) ligand, allowing to form 2D coordination polymers.

While in case of **53**, where the bis(tridentate) ligand is highly flexible tphn (flexibility is higher than tpbn or tpchn), two carboxylates binds in a monodentate and bidentate chelating fashion from two different ends and no coordinated water is present within this molecule. As the bis(tridentate) ligand in highly flexible, it allows the carboxylates to bind with the metal center almost at 180° in the plane of bis(tridentate) ligand and forms a 1D ladder kind of coordination polymer.

Again in case of **55**, where the bis(tridentate) ligand is semirigid tpxn, because of less flexibility of the ligand it allows to connect the metal center with two water molecule. The carboxylates binds in a monodentate fashion to the metal center keeping other end of the carboxylate free thus formation of a dinuclear compound is evident.

Structural Description of 56. It crystallizes in a triclinic *P*-1 space group. The crystallographic information pertaining to data collection and structure refinement has been provided in Table A9. The asymmetric unit of the compound consists of two metal center, two half of the ligand, two 2, 5-thiophene dicarboxylate (tdc^{2-}) linker, one coordinated water on each Ni(II) and seven water of crystallization. Both the nickel metal centers of repeat unit is octahedrally surrounded by N3O3 coordiantion environment and coordinated in similar fashion by half of the ligand, two monodentate tdc^{2-} molecules and one water molecule. Although the binding situation is the same for both the nickel centers but the bond distances are different. The bond distances are 2.057(5) Å, 2.033(5) Å (between metal and two pyridyl N-atom); 2.142(5) Å (between metal and alkyl N-atom); 2.125(4) (between metal and coordinated water) and 2.047(4) Å, 2.048(4) Å (between metal and two carboxylate O-atoms) and for other Ni(II), these bond distances are 2.077(5) Å, 2.054(6) Å (between metal and two pyridyl N-atom); 2.143(5) Å (between metal and alkyl N-atom); 2.096(4) (between metal and coordinated water) and 2.038(4) Å, 2.052(4) Å (between metal and two carboxylates O-atoms), respectively. Selected bond distances and bond angles are listed in Table A30 and Table A56, respectively.

Like **54**, here also, the ligand binds with two metal centers from two ends keeping three opening sites on the metal. One of the opening sites is blocked by one bound water molecule and other two are filled by two tdc^{2-}, connected in monodentate fashion, almost at a right angle. Alternatively it can be said that the carboxylates and metal centers are connected to form zigzag chains which are linked by the bis(tridentate) ligands for form a 2D coordination polymer. Six of these metal centers, two ligands and four tdc^{2-} within the

molecule form a chair formed cyclohexane-type chennel which is repeated throughout the molecule and clearly shown in the topological view of the molecule (Figure 3.50).

The H-bond is formed by the coordinated water and free O-atoms of the dicarboxylate tdc^{2-} from one 2D coordination polymer with two uncoordinated water molecule. These two water molecules are again connected through H-bonding with another similar 2D coordination polymer in identical manner and forms a hexagonal ring between these 2D coordination polymer. This six membered rings help to connect these 2D coordination polymers and form a 3D supramolecular structure.

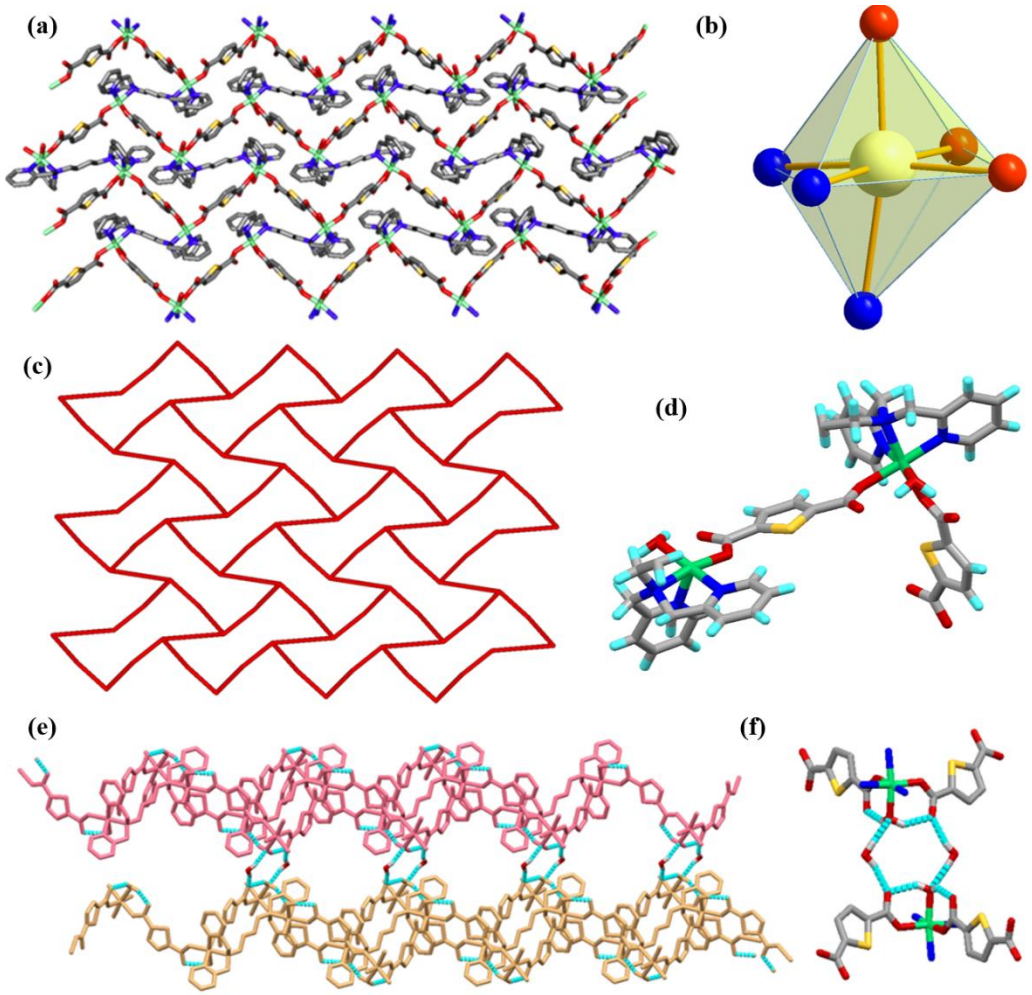

Figure 3.50. Crystal structure of **56**. (a) the 2D coordination polymer. (b) the coordination environment around metal center. (c) topological view. (d) the asymmetric unit. (e) formation of supramolecular assembly. (f) formation of hexagonal ring through H-bonding (color code used for different atoms are like, green: Ni; red: O, yellow: S, blue: N, grey: C, cyano: H).

Structural Description of 57. It crystallizes in a triclinic *P*-1 space group. The crystallographic information pertaining to data collection and structure refinement has been provided in Table A9. The unit cell consists of two individual molecules, along with two

water and two methanol molecules. In both the molecules, the Co(II) is surrounded by N3O3 coordination environment. One end of the bis(tridentate) ligand provides three N-binding centers and three O-atoms are coming from two tdc^{2-}, one binding in chelating bidentate fashion and the other in monodentate fashion. The distances are Ni-N_{pyr} 2.060(11) Å, 2.033(11) Å; Ni-N_{CH2} 2.108(9) Å, Ni-O 2.190(8) Å, 2.091(8) Å, 2.031(9) Å in one molecule and Ni-N_{pyr} 2.047(11) Å, 2.043(11) Å; Ni-N_{CH2} 2.123(9) Å, Ni-O 2.170(8) Å, 2.035(8) Å, 2.095(8) Å for another molecule. Selected bond distances and bond angles are listed in Table A31 and Table A57, respectively

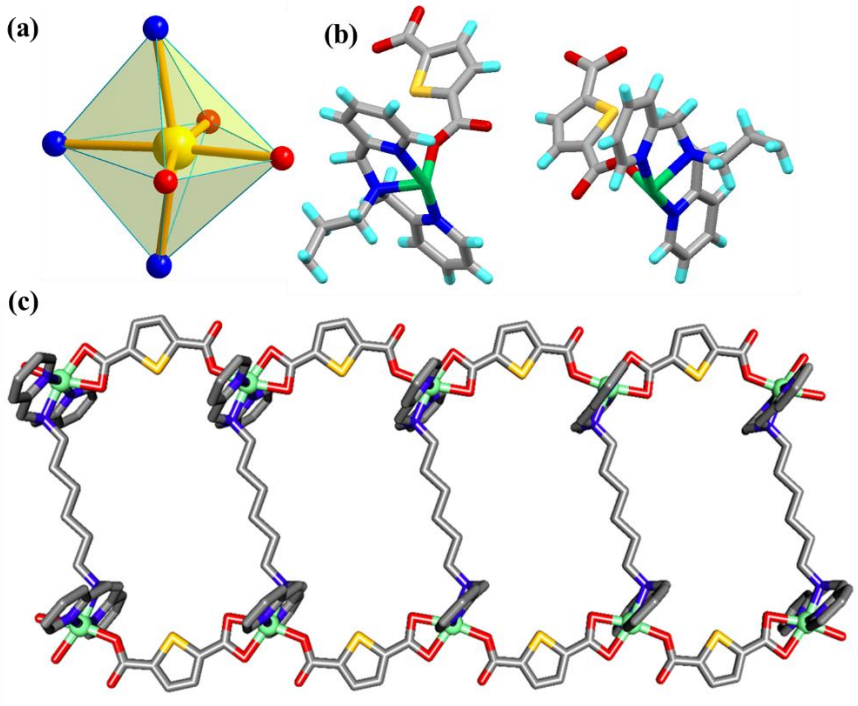

Figure 3.51. Crystal structure of **57**. (a) the coordination environment around metal center, (b) the asymmetric unit showing the presence of two individual molecules, (c) the 1D coordination polymer (ladder) (color code used for different atoms are like, green: Ni; red: O, yellow: S, blue: N, grey: C, cyano: H).

The two ends of ligand tphn connect two Ni(II) ion, keeping three more opening sites on each metal centers, forming a Ni_2 unit. Each of the Ni(II) center of these Ni_2 units are then connected by two tdc^{2-} in chelating bidentate and monodentate fashion, almost in the perpendicular direction of tphn. The overall molecule looks like a ladder where the linear chain with Ni(II), tdc^{2-} forming the long arms of the ladder and tphn forms the short arms in between two long arms (Figure 3.51).

***Structural Description of* 58·CH_3OH·$2H_2O$.** It crystallizes in the monoclinic $P2_1/n$ space group. The crystallographic information pertaining to data collection and structure refinement has been provided in Table A10. The asymmetric unit of this compound contains a Ni(II) metal center, one tdc^{2-}, half of the bis(tridentate) ligand, and two water, a

methanol as a solvent of crystallization. It is a dinuclear compound of nickel. Both the Ni^{2+} is surrounded by N3O3 coordiantion environment. The bis(tridentate) ligand tpchn is bridged between two nickel, each nickel is again bonded to two water molecules and a dicarboxylate O-atom. Two tdc^{2-} molecules are bound to two metal centers in a monodentate fashion from one end. The other end of the dicarboxylates is uncoordinated and as a result the molecule is not expanding in any direction to form polymer, rather, gives rise to a dinuclear compound (Figure 3.52). The bond distances are Ni-N_{pyr} 2.050(3) Å, 2.070(3) Å; Ni-N_{CH2} 2.157(3) Å, Ni-O_{aquo} 2.092(2) Å, 2.075(2) Å, and Ni-O_{dicarb} 2.036(2) Å. Selected bond length, bond angles are included in Table A32, and A58, respectively.

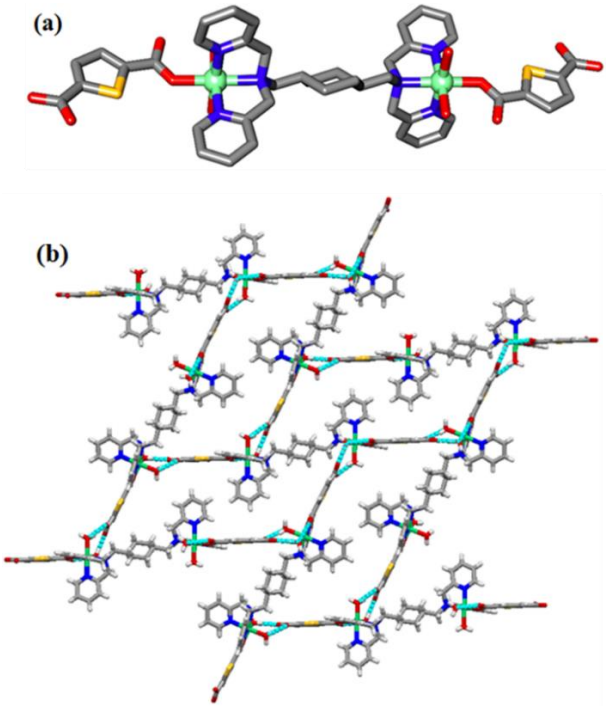

Figure 3.52. Crystal Structure of **58**. (a) dinuclear compound, (b) formation of supramolecular assembly through H-bonds (color code used for different atoms are like, green: Ni; red: O, yellow: S, blue: N, grey: C, cyano: H).

The uncoordinated ends of the dicarboxylate forms H-bonds with two coordinated water bound with one metal center of another dinuclear molecule and this kind of H-bonding continues with the next molecule. As a result, the molecule expands in all three directions through H-bonds and overall forms a 3D supramolecular assembly.

Structural Description of 59·2CH₃OH·5H₂O. It crystallizes in the monoclinic $P2_1/n$ space group. The crystallographic information pertaining to data collection and structure refinement has been provided in Table A10. The asymmetric unit contains one Ni(II) metal center, half of the bis(tridentate) ligand and a carboxylates. the repeat unit is a dimeric unit of Ni(II), where both the Ni(II) center is pentacoordinate with N3O2 coordiantion

environment. Each end of the bis(tridentate) ligand provides three N-atoms and the O-atoms are coming from two tdc^{2-}, act as monodentate from each end. The bond distances are Ni-N_{pyr} 2.089(5) Å, 2.058(5) Å; Ni-N_{CH2} 2.296(5) Å, and Ni-O_{dicarb} 2.978(4) Å, 2.991(4) Å. The τ value is 0.94, which proves that the Ni(II) is surrounded by a trigonal bipyramidal geometry, keeping the three N-atoms in one face. Two O-atom from tdc^{2-} are bound to the Ni(II) metal center nearly at right angle and the other end of the tdc^{2-}dicarboxylate further connected to another two similar Ni(II)-ions. The tdc^{2-} carboxylates and Ni(II) metal centers form zigzag chains, and these chains are lying on two different planes. These chains of different planes are connected via the bis(tridentate) ligands tpxn and result an overall 2D network (Figure 3.53). Selected bond length, bond angles are included in Table A33, and A59, respectively.

Effect of Flexibility of the Ligand. In this series of compound **56**-**59**, the metal center and dicarboxylates are fixed as Ni(II) and tdc^{2-}; the flexibility of bis(tridentate) ligand is changed by changing the spacer in between the dimetal subunit. The comparison of these structure shows that compounds **56** and **57**, where the ligands are tpbn (flexible) and tphn (flexible), form an overall 2D network and 1D ladder type of polymer, respectively. These two structures are comparable with the Co(II) analogue i.e. **52** and **53**. The binding and coordination environment is similar in both Co(II) and Ni(II) analogues. In **56**, the metal centers are coordinated to one water molecule and rest of the coordinating sites are occupied by ligands and dicarboxylate linkers. The carboxylate linkers are acting as monodentate from both ends. Each metal center is coordinated with two dicarboxylate linkers. Both the carboxylates bind to the metal center at right angle, in the plane parallel to the plane of bis(tridentate) ligand, allows to form 2D coordination polymers. While, in case of **57**, where the bis(tridentate) ligand is highly flexible tphn (flexibility is higher than tpbn or tpchn), two carboxylates bind in monodentate and bidentate chelating fashion at two different ends and no coordinated water is present within this molecule. As the bis(tridentate) ligand in highly flexible, it allows the carboxylates to bind with the metal center almost at 180˚ to the plane of bis(tridentate) ligand and forms a 1D ladder kind of coordination polymer.

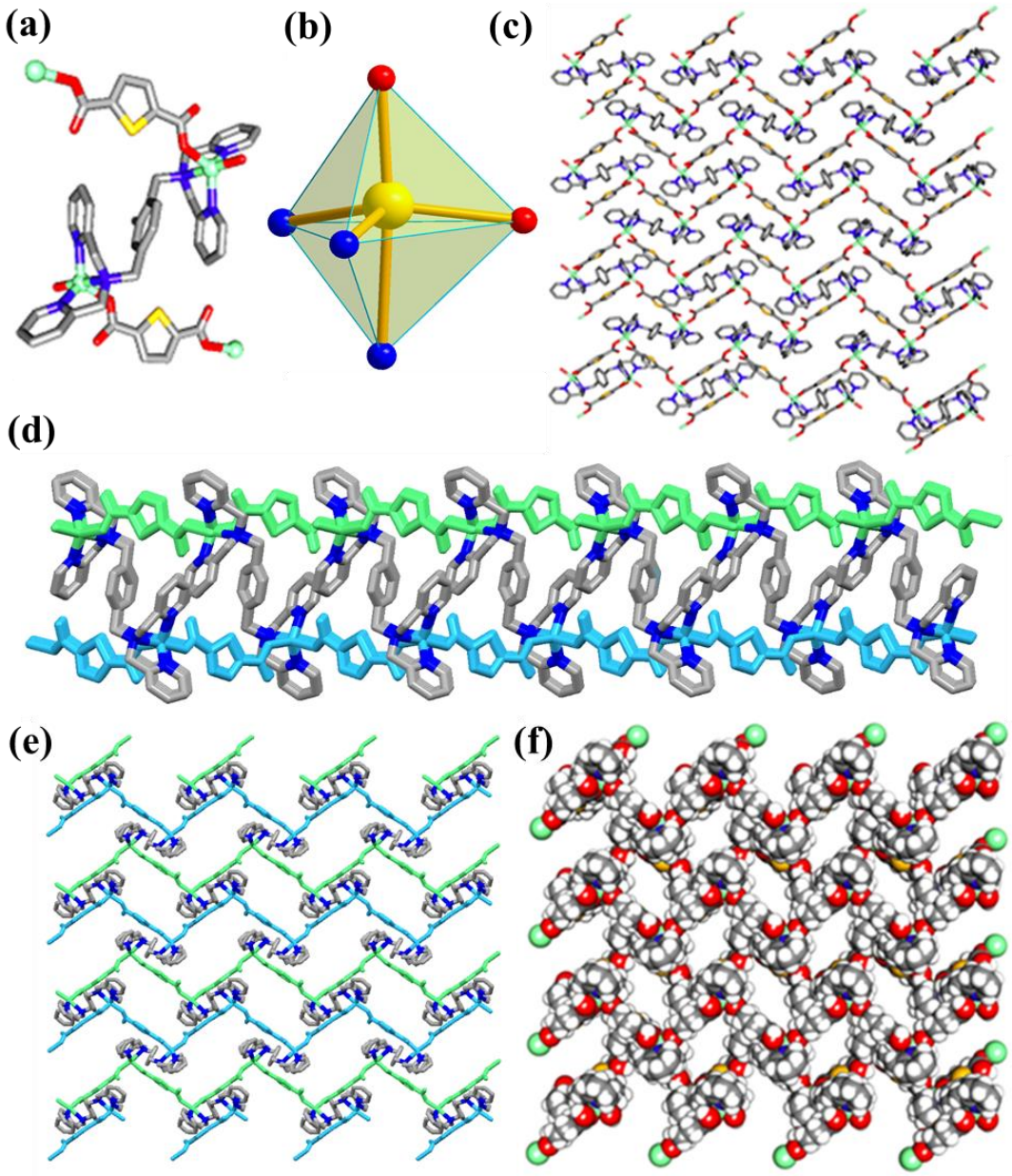

Figure 3.53. Crystal structure of **59**. (a) the repeat unit, (b) the coordination environment around metal center, (c) 2D coordination polymer, (d) and (e) zigzag chain formed by cadmium and tdc^{2-} in two different planes (shown in two different color), and (f) spacefill representation (color code used for different atoms are like, green: Ni; red: O, yellow: S, blue: N, grey: C, cyano: H).

Again in case of **58**, where the bis(tridentate) ligand is semirigid tpchn, and the metal is Ni(II), because of less flexibility of the ligand it allows to connect the metal center with two water molecules. The carboxylates bind in monodentate fashion to the metal center keeping another end of the carboxylate free resulting in a dinuclear compound. While in the case of **59**, where the bis(tridentate) ligand is tpxn and metal is Ni(II), a 2D coordination polymer is evident. A very rare pentacoordinated Ni(II) is present in this molecule. In this case, two monodentate carboxylates are bonded to the metal center and form zigzag chains

which are further connected with ligand and overall gives rise to a 2D CP. Here the coordination number and number bound water plays the role behind the formation of higher dimensional CP.

Table 3.18. Summary of structural types of **52-59**.

Metal Ion	Ligands			
	tpbn	**tphn**	**tpchn**	**tpxn**
Co(II)	2D	1D	2D	Dinuclear
Ni(II)	2D	1D	Dinuclear	2D

Structural Description of 60·CH₃OH·2H₂O. The compound crystallizes in the monoclinic $P2_1/c$ space group. The crystallographic information pertaining to data collection and structure refinement has been provided in Table A11. The asymmetric unit contains two Cd^{2+} metal center, a bis(tridentate) ligand tphn, two tdc^{2-}, methanol and two water of crystallization. Both the Cd^{2+} are hepta-coordinated with N3O4 coordiantion environment. Each end of bis(tridentate) ligand provides three N-atom to bind and tdc^{2-} binds as chelating bidentate fashion from each end, provides four O-atom. The bond distances are Cd-N_{pyr} 2.328(4) Å, 2.362(4) Å; Cd-N_{alkyl} 2.455(4) Å and Cd-$O_{carboxylate}$ 2.458(3) Å, 2.385(3) Å, 2.390(3) Å, 2.412(3) Å, respectively. For the second Cd^{2+}, these lengths are Cd-N_{pyr} 2.330(4) Å, 2.329(4) Å; Cd-N_{alkyl} 2.535(4) Å and Cd-$O_{carboxylate}$ 2.451(3) Å, 2.387(3) Å, 2.370(3) Å, 2.447(3) Å, respectively. Selected bond length, bond angles are included in Table A34, and A60, respectively. Two tdc^{2-} linkers bind to the metal center almost at an angle 90°and forms zig-zag chains. These chains are connected together by the bis(tridentate) ligands horizontally and form a 2D coordination polymer as shown in the Figure 3.54. From the space-fill diagram, although it is very low, the presence of small channels is evident.

Structural Description of 61·CH₃OH. It crystallizes in the monoclinic $P2_1$ space group. The crystallographic information pertaining to data collection and structure refinement has been provided in Table A11. The asymmetric unit consists of two Cd^{2+} metal center, a bis(tridentate) ligand tpchn, two tdc^{2-}, two methanol molecules as the solvent of crystallization. Two kinds of $Cd^{2+}$are present in the molecule. One Cd^{2+} is heptacoordinated with N3O4 coordiantion environment. Three N-atoms are provided by one end of the bis (tridentate) ligand and tdc^{2-} binds in chelating bidentate fashion from each end, provides

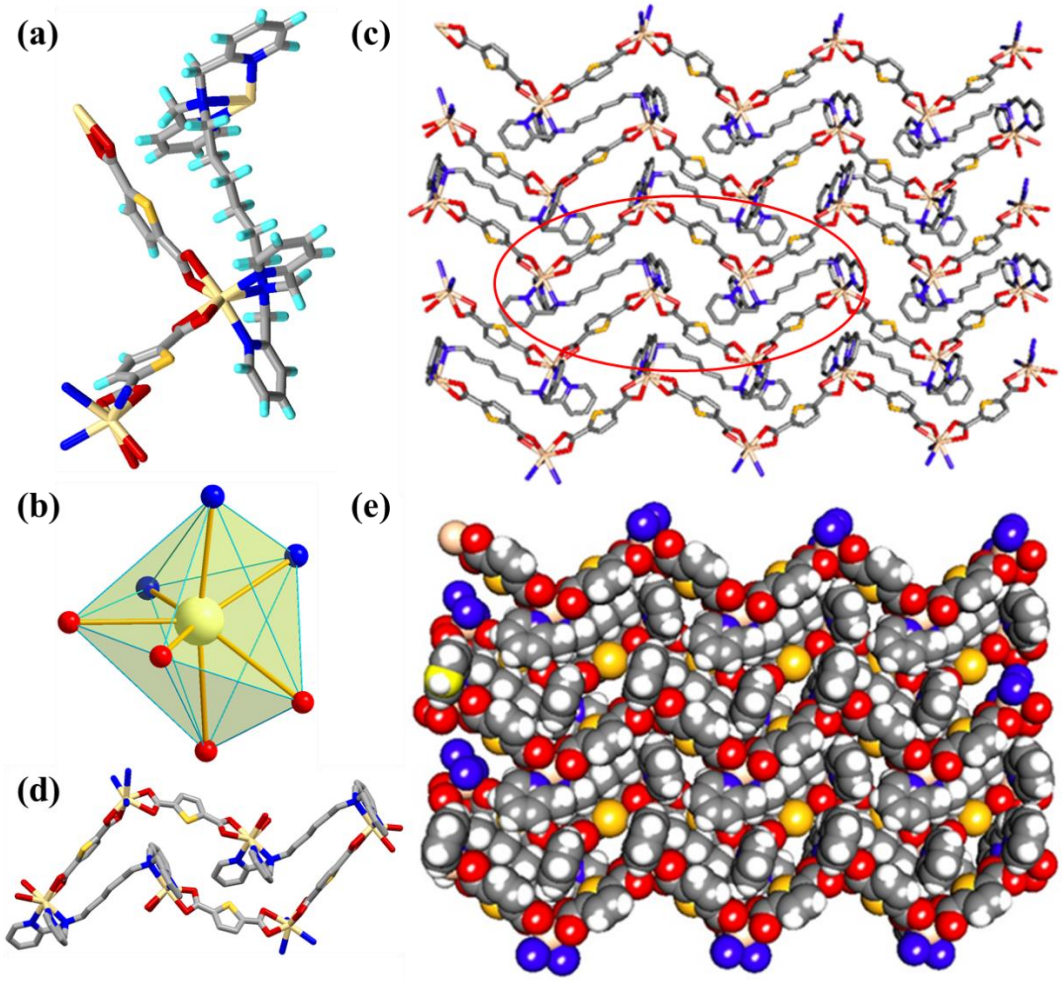

Figure 3.54. Crystal structure of **60**. (a) the repeat unit, (b) the coordination environment around the metal center, (c) 2D coordination polymer, (d) hexagon formation (marked in (c)), and (e) spacefill representation (color code used for different atoms are like, light yellow: Cd; red: O, blue: N, grey: C, yellow: S, cyano: H).

Four O-atoms. The bond lengths are like Cd-N_{pyr} 2.362(15) Å, 2.350(20) Å; Cd-N_{alkyl} 2.514(15) Å and Cd-$O_{carboxylate}$ 2.677 Å, 2.300(20) Å, 2.318(13) Å, 2.453(14) Å, respectively. The second Cd^{2+} is hexacoordinated with N3O3 coordiantion environment. Three N-atoms are provided by one end of the bis(tridentate) ligand, and two tdc^{2-} carboxylates provide the three O-atoms, binds as chelating from one end and monodentate from another end. The bond distances are Cd-N_{pyr} 2.336(18) Å, 2.297(19) Å; Cd-N_{alkyl} 2.478(19) Å and Cd-$O_{carboxylate}$ 2.237(16) Å, 2.284(14) Å, 2.571(17) Å, respectively. Selected bond length, bond angles are included in Table A35, and A61, respectively. These two types of Cd^{2+} individually form a zigzag chain via connection with tdc^{2-}. These chains are connected together by the bis(tridentate) ligands through the alternate Cd^{2+} of two different chains and forms a 2D coordination polymer. From the space filling diagram, although it is very low, the presence of small channels are evident (Figure 3.55).

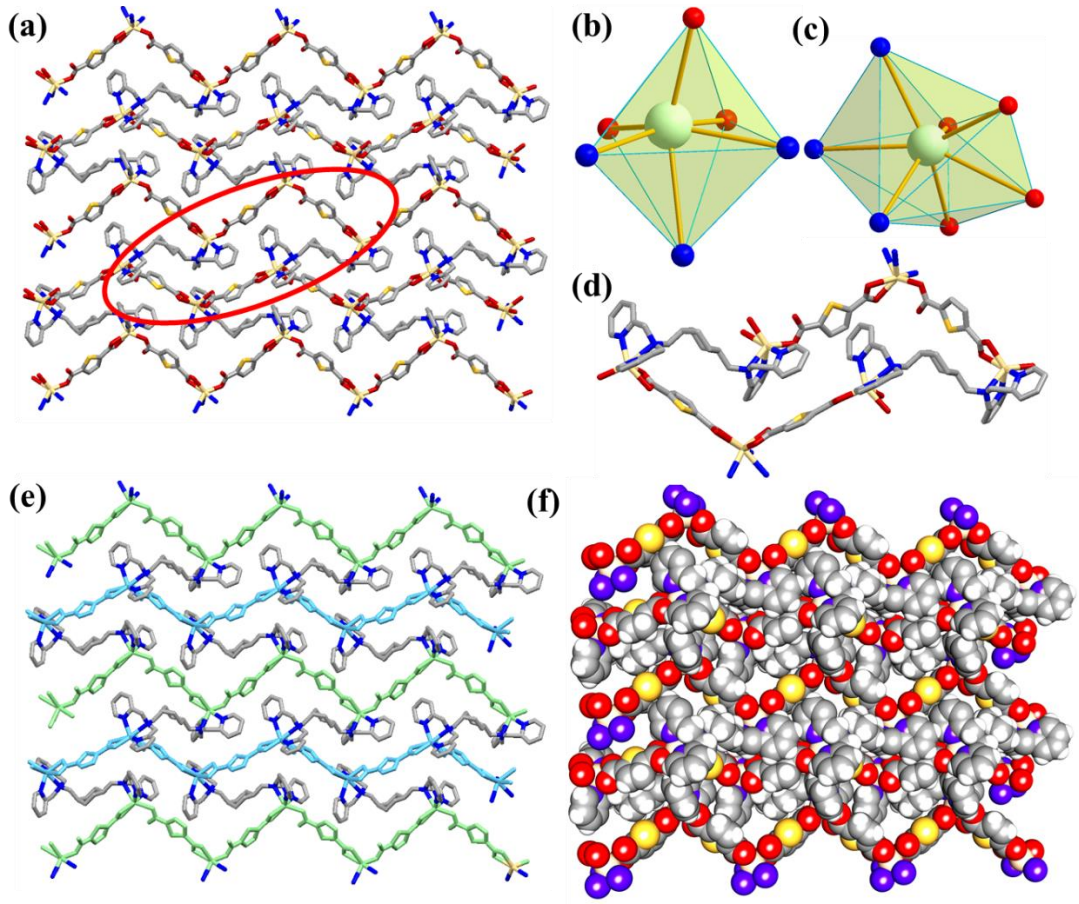

Figure 3.55. Crystal structure of **61**. (a) 2D coordination polymer, (b) and (c) the coordination environment around the hexacoordinated and heptacoordinated metal center. (d) hexagon formation (marked in (c)), (e) formation of zigzag chain by hexa and hepta coordinated cadmium with tdc^{2-} (shown in two different color), (f) spacefill representation (color code used for different atoms are like, light yellow: Cd; red: O, blue: N, grey: C, yellow: S, cyano: H).

Structural Description of 62. The compound crystallizes in the monoclinic *P*2/*n* space group. The crystallographic information pertaining to data collection and structure refinement has been provided in Table A12. The asymmetric unit contains two Cd^{2+} metal center, a bis(tridentate) ligand tpxn, two tdc^{2-} and seven water molecules of crystallization. Both the metal centers are distorted octahedrally surrounded by N3O3 coordiantion environment. Three N-atoms are provided by one end of the bis (tridentate) ligand and O-atoms are coming from two carboxylates tdc^{2-}. One of the tdc^{2-} acts as bidentate chelating ligand and the other as a monodentate ligand from both the ends. These two tdc^{2-} bind in an alternative manner with Cd^{2+} and form a polymeric zigzag chains in the two different planes keeping the remaining three coordination sites open. These two planes are connected through the uncoordinated site by the bis(tridentate) ligand and overall forms a 2D coordination polymer. The bond lengths are like Cd-N_{pyr} 2.311(9) Å, 2.282(10) Å; Cd-N_{alkyl} 2.416(9) Å and Cd-$O_{carboxylate}$ 2.487(7) Å, 2.327(9) Å, 2.258(8) Å, , respectively. For the

other Cd(II) center, the following are the bond lengths: Cd-N_{pyr} 2.292(9) Å, 2.317(9) Å; Cd-N_{alkyl} 2.516(9) Å and Cd-$O_{carboxylate}$ 2.218(7) Å, 2.260(7) Å. Selected bond length, bond angles are included in Table A36, and A62, respectively.

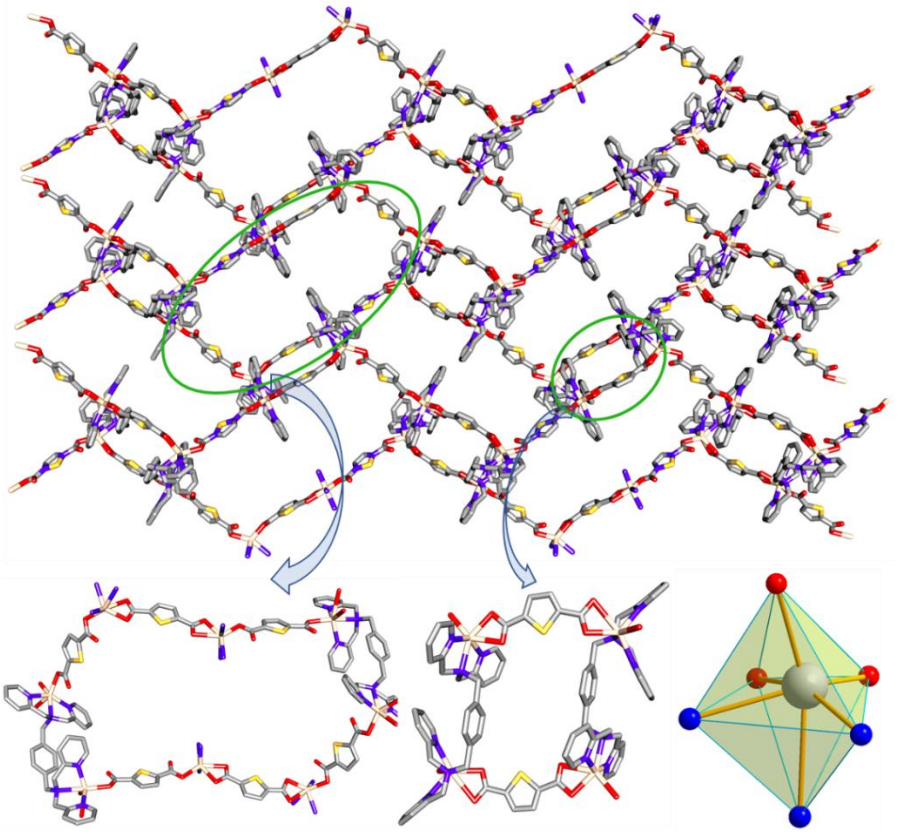

Figure 3.56. Crystal structure of **62** and coordination atmosphere around Cd (color code used for different atoms are like, light yellow: Cd; red: O, blue: N, grey: C, yellow: S, cyano: H).

*Structural Comparison of **60-62***. All three compounds **60-62** form 2D networks but the binding modes of the dicarboxylates and the coordination environments of the metal centers is different in each case. In the case of **60**, where the bis(tridentate) ligand is a highly flexible tphn ligand, the metal center Cd^{2+} is heptacoordinated. Each metal centers are connected with two carboxylates along with the bis(tridentate) ligand. The carboxylates bind with Cd^{2+} in bidentate chelating fashion from both the ends and form zigzag chains in two parallel planes. These chains in two different planes are again diagonally connected with the bis(tridentate) ligands and prompt a 2D coordination polymer.

In **61**, the bis(tridentate) ligand is semirigid tpchn, and gives an overall 2D coordination polymer. The comparison with **60** shows that the coordination environment of **61** is different from **60**. The Cd^{2+} metal centers are hexacoordinated and heptacoordinated with two carboxylates and bis(tridentate) ligand. All these heptacoordinated Cd^{2+} centers form zigzag chains in the same plane with dicarboxylates (bound in a chelating bidentate fashion

from both the ends) and are diagonally connected with other zigzag chains in another plane formed by hexacoordinated Cd^{2+} and dicarboxylates (bound in a monodentate and chelating bidentate fashion from two ends, respectively). As a result, this molecule ends up forming an overall 2D CP.

Again, in the case of tpxn, least flexible among these three bis(tridentate) ligand, tphn, tpchn, and tpxn, is present in 2D coordination polymer **62**. Like the case of **61**, here the Cd^{2+} metal centers are hexacoordinated with two carboxylates and a bis(tridentate) ligand but two carboxylate binds with metal in a different way than in **61**. One of the carboxylates binds in bidentate chelating fashion and other in monodentate fashion from both the ends. These alternative chelating bidentate and monodentate dicarboxylates form zigzag chains in two different planes which are vertically connected by the ligand and form a 2D coordination polymer. The result shows how the flexibility of the bis(tridentate) ligands control the coordination environment around the metal center and binding modes of the carboxyltes of the CPs, hence the structure.

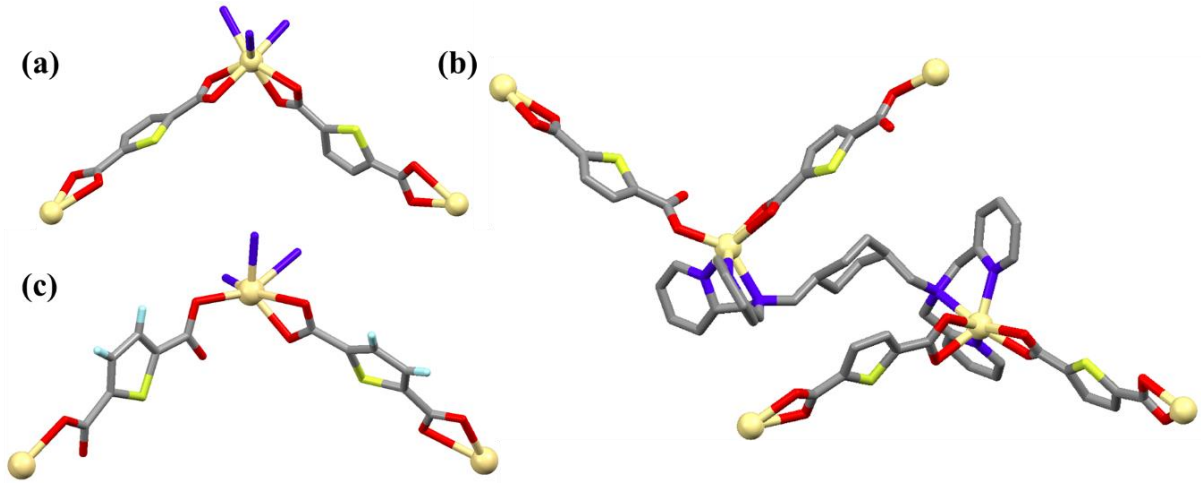

Figure 3.57. Different binding modes of tdc^{2-} in (a) **60,** (b) **61, and** (c) **62** (color code used for different atoms are like, light yellow: Cd; red: O, blue: N, grey: C, yellow: S, cyano: H).

PXRD Analysis. In order to check the phase purity of the bulk material, PXRD patterns of the as-synthesized samples of **52-55** was recorded at room temperature and compared with the simulated PXRD patterns obtained from single crystal structure. The simulated and experimental PXRD pattern of **53**, **54** and **55** are shown as an example (Figure 3.58). In all cases, the experimental result corroborates quite well with the simulated one.

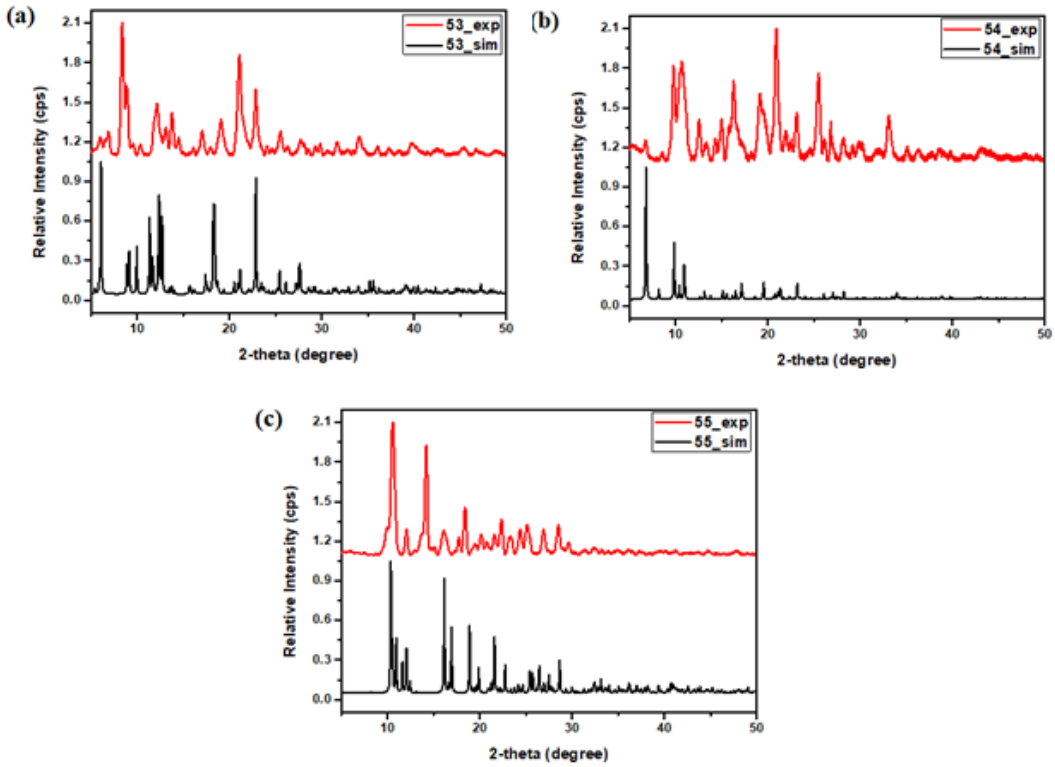

Figure 3.58. Simulated and experimental PXRD pattern of **53**-**55**.

To prove the purity of the bulk material, PXRD patterns of the bulk material of **56**-**59** was matched with the simulated PXRD patterns obtained from single crystal structure. The simulated and experimental PXRD pattern of **56** and **57** are shown as an example (Figure 3.59). In all cases, the experimental result corroborates quite well with the simulated one indicating the bulk phase purity of the as-synthesized samples of **56**-**59**.

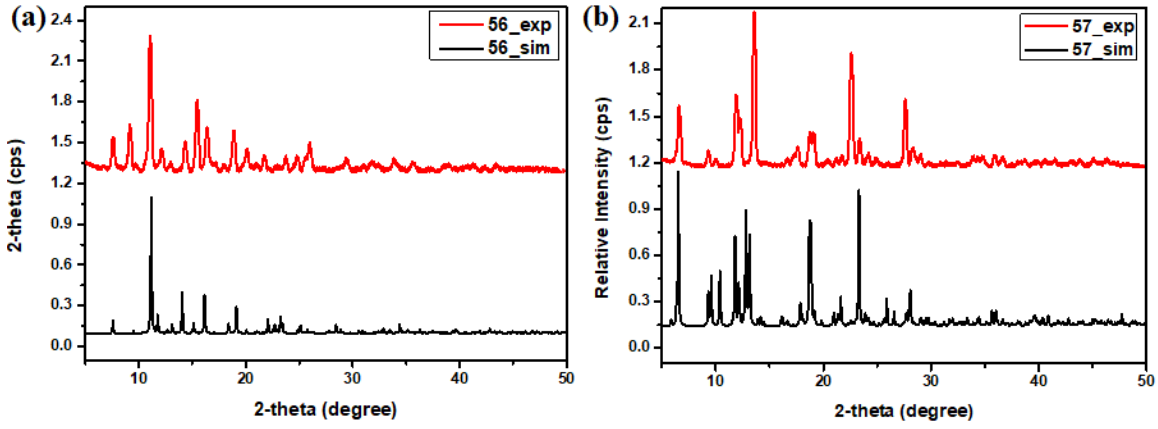

Figure 3.59. Simulated and experimental PXRD patterns of **56** and **57**.

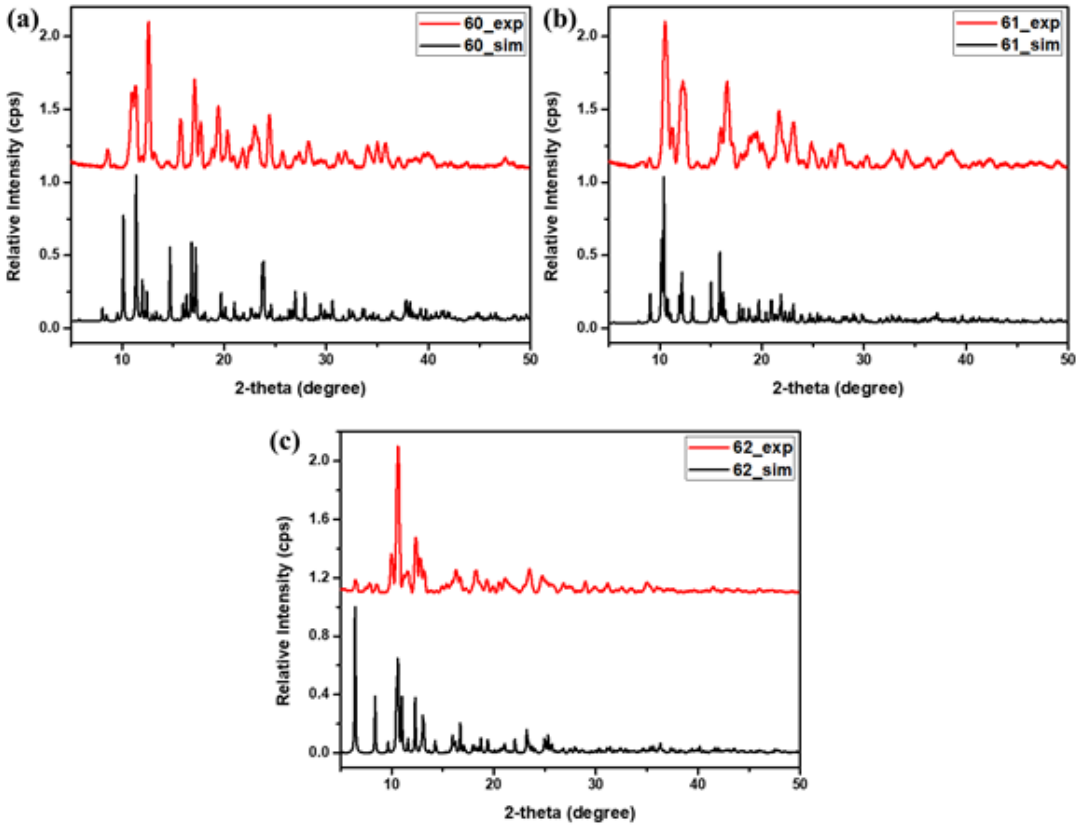

Figure 3.60. Simulated and experimental PXRD pattern of **60**-**62**.

Similarly, the PXRD patterns of the bulk material of **60**-**63** was recorded and compared with the simulated PXRD patten to check the bulk phase purity. The simulated and experimental PXRD pattern of **60**, **61** and **62** are shown as an example (Figure 3.60). In all cases, the experimental result corroborates quite well with the simulated one.

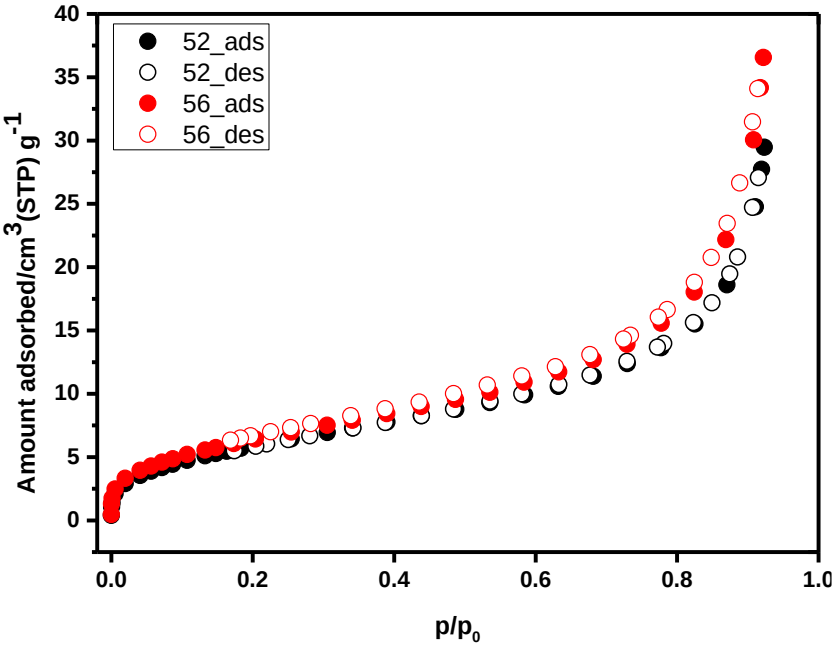

Figure 3.61. N_2 sorption isotherm of **52** and **56 at 77K.**

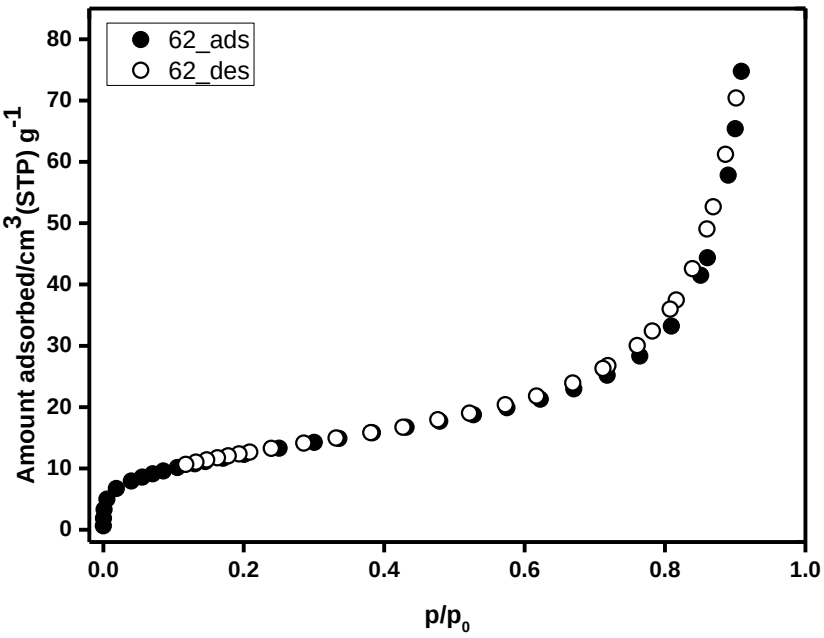

Figure 3.62. N_2 sorption isotherm of **62 at 77K.**

Gas Sorption Analyses. In order to check the porosity into the frameworks of **52**, **56** and **60**, gas adsorption analysis was carried out. Prior to adsorption measurements, the samples (~60-80 mg) were activated by degassing at temperature of 393 K under vacuum conditions (20 mTorr) for 24 hours to generate the desolvated compounds. N_2 sorption study of **52**, **56** and **60** was performed at 77 K. The p/p_0 vs gas uptake plot shows a classical type-II adsorption isotherms, indicates the mesoporous nature of the materials. Although the gas uptake values are not very high, 30, 37, and 74 cm^3g^{-1} for **52**, **56** and **60**, respectively.

Catalysis with 55. Form the structural analysis of **55**, it is clear that each of the Co(II) metal center are bind with two water molecule, this fact trigger us to use the material as catalyst. The possible to achieve an unsaturted Lewis acid metal center make this material a good candidate to screen to catalysea reaction, like Knovenagel Reaction. The reaction between aromatic aldehyde (with different substituents) with malononitrile was catalysed by **55**. Prior to use as catalyst, **55**, was activated at 120 °C within a vaccum oven to remove the water molecule bound to the metal center, which make the material to act as a Lewis acid catalyst. Optimization of the reaction benzaldehyde and malononitrile was done first by changing one parameter at a time. Taking 2 mol % of the catalyst and different solvent the reaction was carried out for 60 mins and methanol was found the best to use for this reaction. Then the reaction was screened with variour mol % of catalyst and for different

times. Afetr all these experiments it was found that in methanol with 2 mol % of catalyst and gives the best result in 60 mins (entry 2, Table 3.19).

Table 3.19. Optimization of reaction conditions for the Knovenagel Reaction catalyzed by **55**.

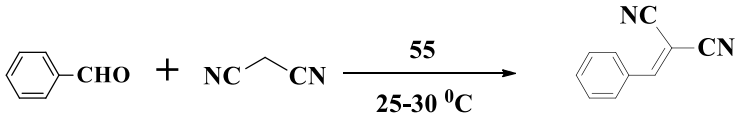

Entry	catalyst amount (mol %)	solvent	Reaction time (minutes)	% conversion[a]
1	2	water	60	89
2	**2**	**MeOH**	**60**	**96**
3	2	EtOH	60	92
4	2	CH_3CN	60	82
5	2	CH_3Cl	60	80
6	2	CH_2Cl_2	60	76
7	2	$PhCH_3$	60	52
8	--	MeOH	60	35
9	1	MeOH	60	81
10	3	MeOH	60	96
11	4	MeOH	60	98
12	5	MeOH	60	>99
13	2	MeOH	10	40
14	2	MeOH	20	55
15	2	MeOH	30	62
16	2	MeOH	40	78
17	2	MeOH	50	86
18	2	MeOH	70	>99
19	2	MeOH	80	>99
20	$Co(OAc)_2{\cdot}4H_2O$	MeOH	60	38

To check further posibilities of catalysis of different substrate, reaction between variour substituted benzaldehyde and malononitrile was performed under same optimized conditions. In all cases very high conversion 85 %-100% is observed (Table 3.20).

Table 3.20. Substrate scope in Knovenagel Reaction catalyzed by **55**.

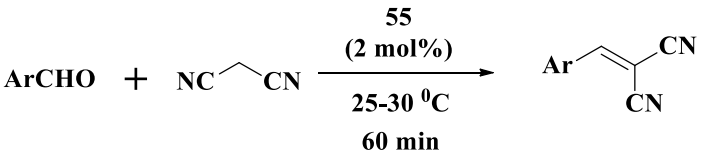

Entry	Aldehyde	% conversion[a]	TON[b]
1	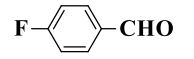	85	42.5
2	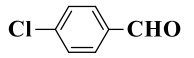	100	50
3	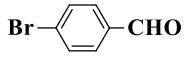	100	50
4	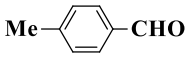	96	48
5	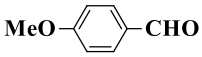	92	46
6	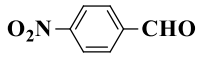	100	50
7	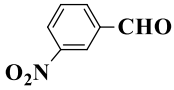	100	50

[a] Calculated by ^{1}H NMR. [b] Number of moles of product per mole of catalyst at 26-28 ^{o}C.

3.2.4 Semirigid Carboxylate and Semirigid Spanning Ligands

Synthesis. All compounds were synthesized through one pot self-assembly method. The metal center used for the synthesis of these compounds are Co(II) and Ni(II). Keeping the dicarboxylates fixed as 1,4-cyclohexane dicarboxylate (cdc^{2-}), two different bis(tridentate) ligands were used. For the synthesis, a 2:2:1 ratio of M(II):dicarboxylate:ligand was taken and stirred for 24 h at room temperature in methanol. The solvent was removed under vacuum and treated many times with acetonitrile and toluene to get rid of the acetic acid formed as a by-product. The resultant solid was collected and used for characterizations. The single crystal suitable for X-ray diffraction analysis was obtained (where ever possible) by the direct layering of the components in methanol and water mixture (1:1).

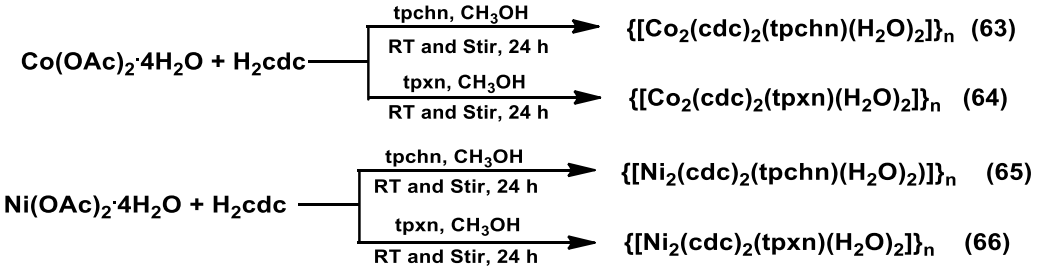

Scheme 3.8. Synthesis of **63-66**.

FTIR Spectroscopy. FTIR spectra of **63-66** was recorded and $\Delta\nu = \nu_{asym}-\nu_{sym}$ value was calculated to justify the carboxylate binding mode. The peaks around ~3225 cm^{-1} for all these compound confirms the presence of coordinated water molecule. The difference of the asymmetric and symmetric stretching frequency of carboxylates in all these compounds are in similar range and indicates a monodentate binding mode of the carboxylate with the metal centers. The similar binding situation of cdc^{2-} in case of **63** and **65** is also proved structurally.

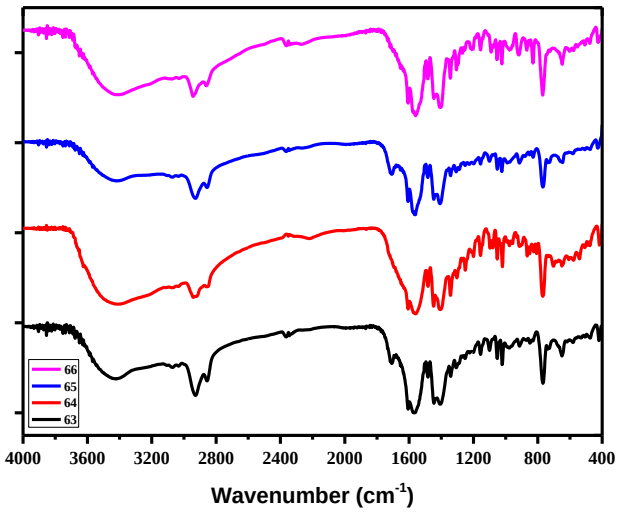

Figure 3.63. FTIR spectra of **63-66**.

Table 3.21. Selected FTIR peaks for **63-66**.

Compounds	$\nu_{asym}(COO^-)$ cm^{-1}	$\nu_{sym}(COO^-)$ cm^{-1}	$\Delta\nu$ cm^{-1}	Binding Mode
63	1576	1342	234	monodentate
64	1573	1343	230	monodentate
65	1577	1342	235	monodentate
66	1577	1344	233	monodentate

Thermogravimetric Analysis. The thermal stability of **63-66** was studied by thermogravimetric analysis. The as-synthesized sample of **63-66** were heated in the temperature range of 30 °C to 500 °C under dinitrogen atmosphere. All these compounds, **63-66**, show more or less similar thermal stability up to 280 °C. The initial weight loss can be ascribed due to the lattice water molecule. The compounds **63** and **66** exhibits weight loss of 3.90% (ca. 3.47%) and 3.63% (ca. 3.49%) in the temperature range of 60-80 °C, due to loss of two water molecules in each case. In the next step, both the compounds exhibit weight loss due to coordinated water molecules and the respective ligand, tpchn and

tpxn, up to 410 °C. The weight loses in this step is 52.62% (ca. 52.38%) and 51.73% (ca. 52.08%). Then these undergo decomposition. Compound **64**, losses six molecules of lattice water corresponding to 10.73% (ca. 10.13%) weight loss up to 90 °C temperature. Then, two bound water and the bis(tridented) ligand tpxn comes out from the compound, and gives a loss of 43.70% (ca. 46.94%) of its weight up to 407 °C. In case of **65**, a lattice water molecule is removed in the first step, corresponds to 2.40% (ca. 1.76%) weight loss and followed by removal of two bound water molecules and bis(tridentate) ligand, corresponds to 54.71% (ca. 53.28%) weight loss up to 432 °C. A summary of weight loss is tabulated in Table 3.20.

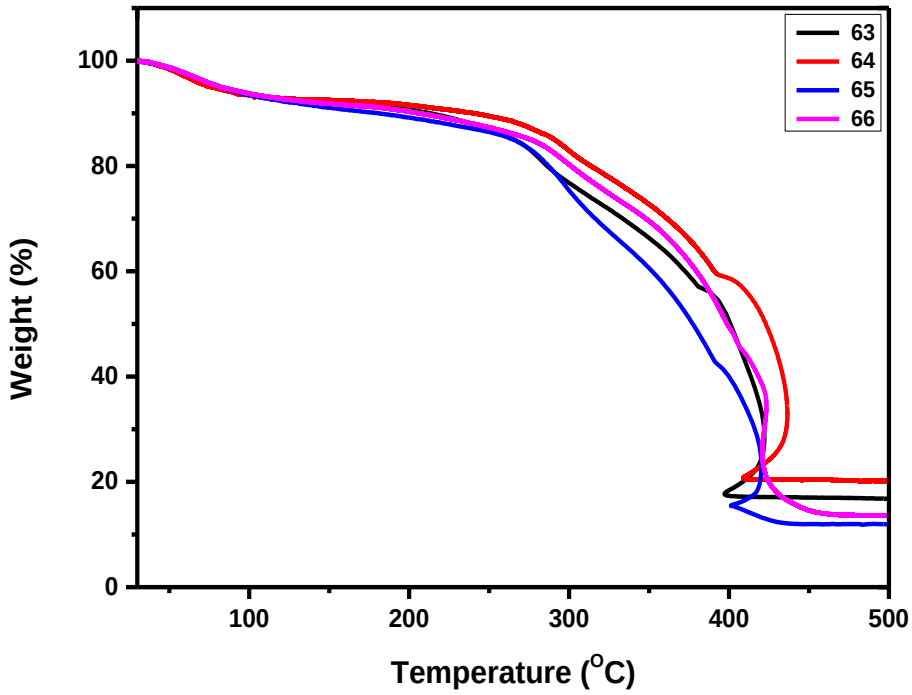

Figure 3.64. TGA profile of **63-66**.

Table 3.22. TGA calculation of **63-66**.

Compounds	Weight Loss											
	Step I				Step II				Step III			
	Ca.	Obs.	Loss	°C	Ca.	Obs.	Loss	°C	Ca.	Obs.	Loss	°C
63	3.47	3.90	2H2O	68	52.38	52.62	2H2O+ tpchn	410	---	---	---	---
64	10.13	10.73	6 H_2O	90	46.94	43.70	2H2O + tpxn	407	---	---	---	---
65	1.76	2.40	H_2O	56	53.28	54.71	2 H_2O + tpchn	432	---	--	---	--
66	3.49	3.63	2H2O	70	52.08	51.73	2H2O + tpxn	409	--	--	---	--

***Structural Description of* 64.** This compound crystallizes in the monoclinic $P2_1/n$ space group. The crystallographic informations pertaining to data collection and structure refinement are included in Table A12. The asymmetric unit contains a Co(II) metal center, half of the ligand tpxn, a cdc^{2-}, a bound water molecule. The Co^{2+} metal center is

octahedrally surrounded by N3O3 coordiantion environment. Three N-atoms are coming from one end of the ligand and two carboxylates, cdc^{2-} provides two O-atoms, bound in monodentate fashion, and one coordinated water gives the other O-atom. The bond distances are Co-N_{pyr} 2.127(4) Å, 2.156(4) Å; Co-N_{CH2} 2.171(4) Å, Co-O 2.057(3) Å, 2.093(3) Å and Ni-O_{aq} 2.125(3) Å. Selected bond length, bond angles are included in Table A37, and A63, respectively. The semirigid bis(tridentate) ligand binds with two Ni^{2+} and forms a Ni_2- unit which further extended through two cdc^{2-} carboxylates forms a 2D net. The two carboxylates end of the cdc^{2-} are binding from the equatorial site.

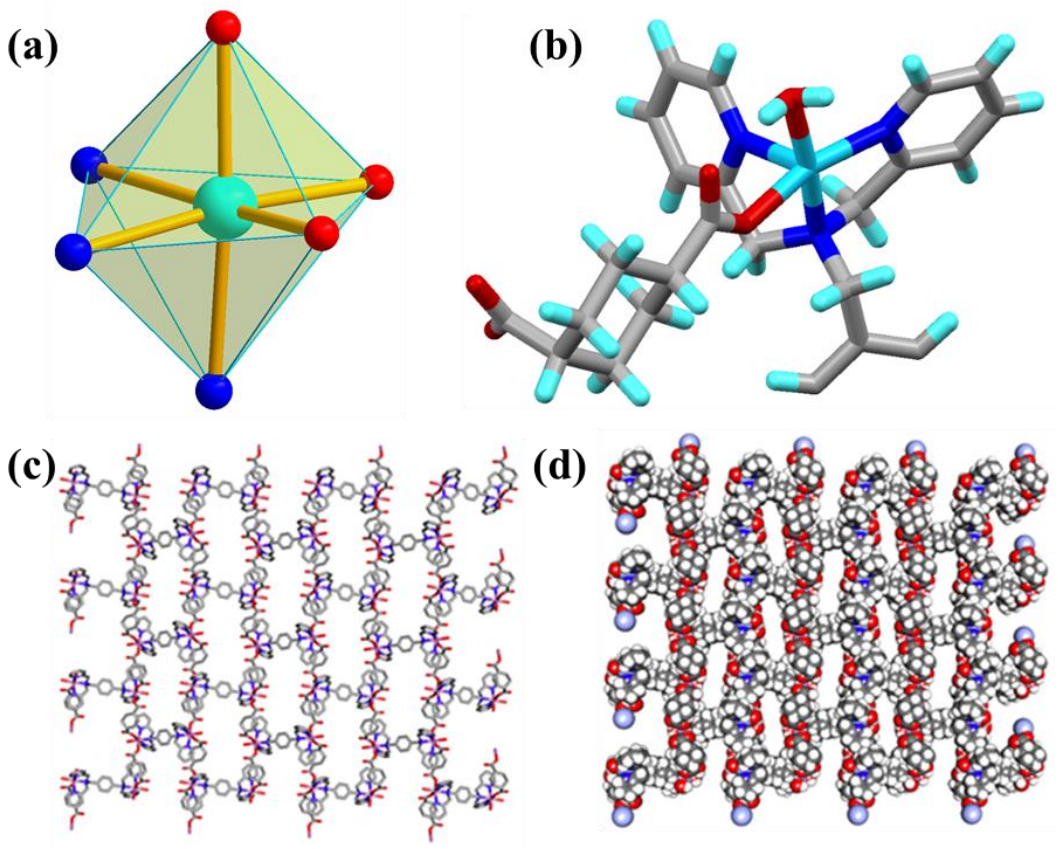

Figure 3.65. X-ray Single Crystal Structure of **64**. (a) the coordination environment around the metal center, (b) the asymmetric unit, (c) 2D coordination polymer, (d) spacefill representation (color code used for different atoms are like, light purple: Co; red: O, blue: N, grey: C, cyano: H).

***Structural Description of* 66·CH_3OH·$5H_2O$.** This compound crystallizes in the monoclinic $P2_1/n$ space group. The crystallographic informations pertaining to data collection and structure refinement are included in Table A13. The asymmetric unit contains one Ni(II) atom, half of the bis(tridentate) ligand tpxn, a cdc^{2-}, a bound water; five water molecule and two methanol as a solvent of crystallization. The Ni(II) is octahedrally surrounded by N3O3 coordiantion environment. Three N-atoms are comes from one end of the ligand and two carboxylates, cdc^{2-} provides two O-atoms, coordinated in

monodentate fashion and one coordinated water gives the other O-atom. The bond distances are Ni-N_{pyr} 2.086(4) Å, 2.071(3) Å; Ni-N_{CH2} 2.121(4) Å, Ni-O 2.060(3) Å, 2.043(3) Å and Ni-O_{aq}2.076(3) Å. Selected bond length, bond angles are included in Table A38, and A64, respectively. The semirigid bis(tridentate) ligand binds with two Ni(II) and forms a Ni_2 unit which further extends through two cdc^{2-} carboxylates forming a 2D net. The two carboxylate ends of the cdc^{2-} bind from the axial and equatorial site, respectively.

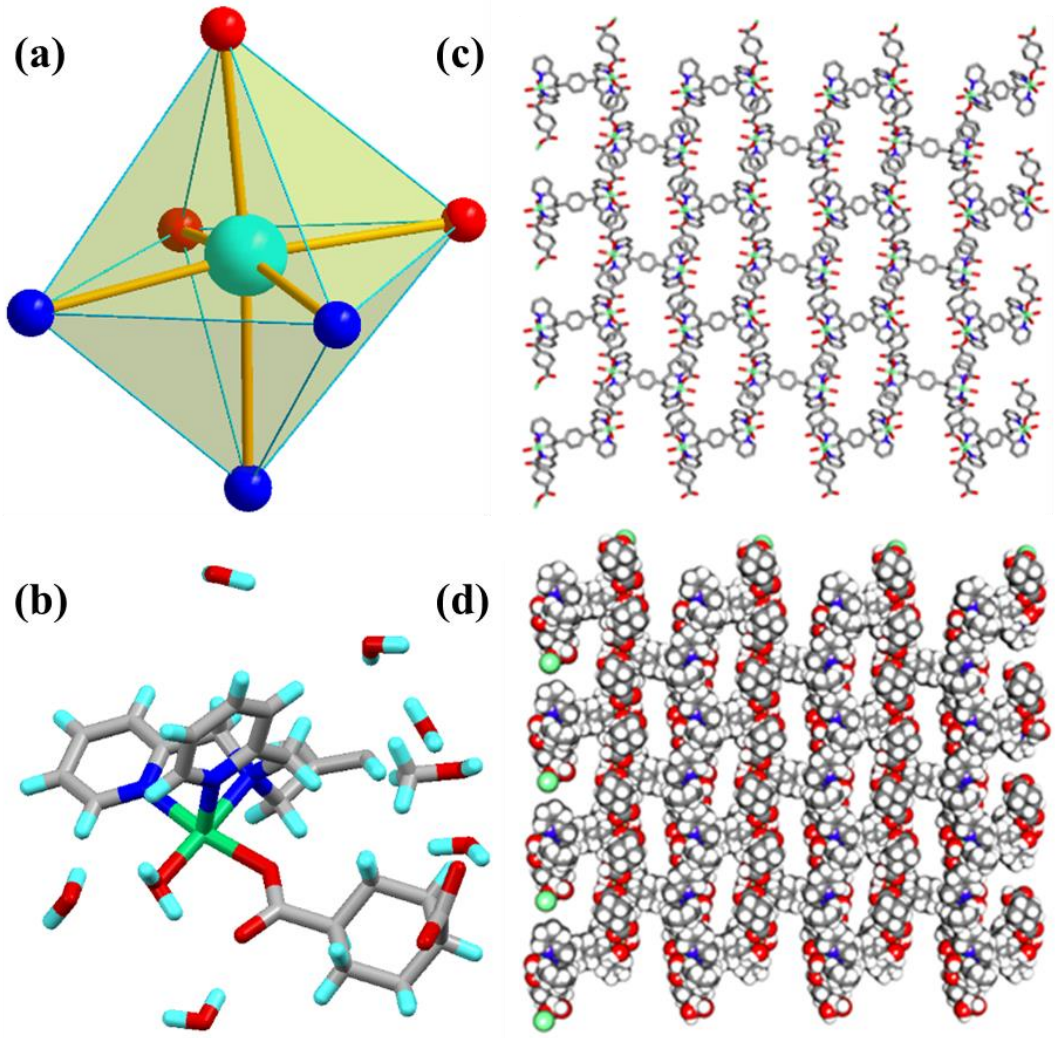

Figure 3.66. X-ray Single Crystal Structure of **66**. (a) the coordination environment around the metal center, (b) the asymmetric unit, (c) 2D coordination polymer, (d) spacefill representation (color code used for different atoms are like, light purple: Co; red: O, blue: N, grey: C, cyano: H).

Comparison of Structures. Both **64** and **66** form a 2D network. Their isostructural nature stems from the fact that the dicarboxylate cdc^{2-} binds to the metal center Co(II) or Ni(II) in a similar monodentate fashion and the coordination environment around the metal center is also same. Obviously, identical pores are also evident in them.

3.2.5. Rigid Carboxylates and Semirigid Spanning Ligands

Synthesis. The compound was synthesized via one pot self-assembly method as shown in Scheme 3.9. A 6:4:3 ratio of Co(II):tricarboxylate:ligand was taken and stirred for 24 h at room temperature in methanol solvent. The solid formed was filtered and air dried. The single crystal suitable for X-ray diffraction analysis was obtained by the direct layering of the components in methanol and water solvent.

$$Co(OAc)_2 \cdot 4H_2O + H_3btc + tpxn \xrightarrow[RT,\ 24\ h]{CH_3OH} \{[Co_3(btc)_2(tpxn)_{1.5}(H_2O)_4]\}_n \quad (67)$$

Scheme 3.9. Synthesis of **67**.

FTIR Analysis. FTIR spectroscopy is very helpful tool to prove the binding mode of carboxylates in the compounds. From the difference of the asymmetric and symmetric stretching frequency of carboxylates ($\Delta\nu = \nu_{asym}-\nu_{sym}$) gives an idea of binding of carboxylates. The presence of solvent molecules can also be proved by FTIR spectrum of the individual compounds. Here the presence of peak at 3225 cm^{-1} (Figure 3.67) indicates the presence of coordinated water molecule whereas the peak at 1700 cm^{-1} shows that the H_3btc is not completely deprotonated, which again confirmed from the structural study of this compound. From the $\Delta\nu$ values (174 and 200 cm^{-1}), it is concluded that carboxylate binds in a chelating bidentate as well as monodentate fashion.

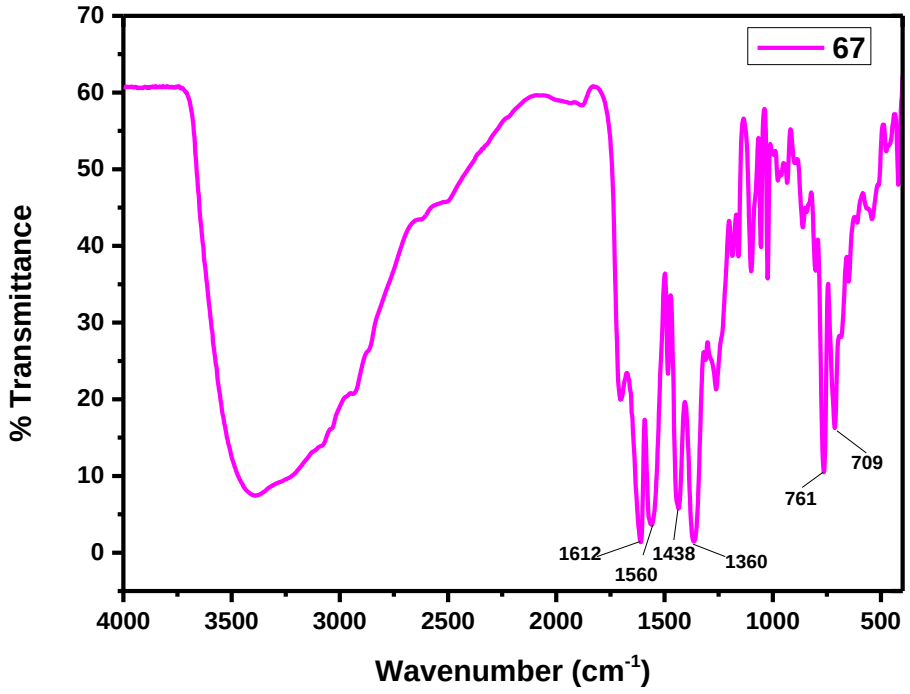

Figure 3.67. FTIR spectrum of **67**.

Thermogravimetric Analysis. As shown in Figure 3.68, the compound follows a two-step decomposition process. The initial loss of 5.25% (ca. 4.85%) corresponds to the loss of four lattice water molecules up to 60 °C, whereas the second weight loss is because of loss of two coordinated water molecules and the ligand, which is corresponding to 38.54% weight loss (ca. 38.75%) up to 388 °C after this the compound undergoes decomposition.

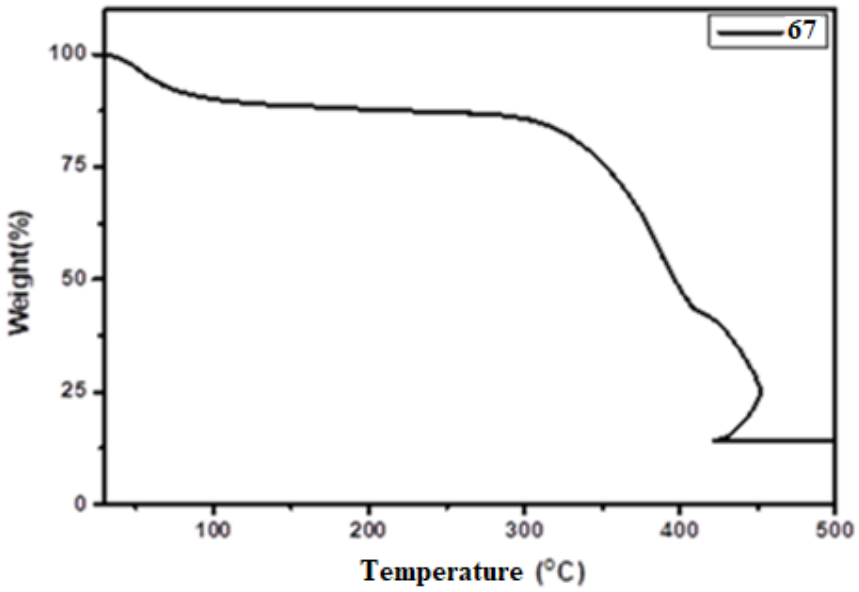

Figure 3.68. TGA scan of **67**.

Table 3.23. TGA calculations for **67**.

Compounds	Weight Loss											
	Step I				Step II				Step III			
	Ca.	Obs.	Loss	^{O}C	Ca.	Obs.	Loss	^{O}C	Ca.	Obs.	Loss	^{O}C
67	4.85	5.25	4H2O	60	38.54	38.75	2H2O+ tpxn	388	---	---	---	---

Structural Description of 67·2CH$_3$OH·11H$_2$O. It crystallizes in the triclinic *P*-1 space group. The crystallographic informations pertaining to data collection and structure refinement are included in Table A13. The asymmetric unit consists of three Co(II), two btc^{3-}, one and half unit of ligand tpxn, eleven lattice water molecules, and two methanol molecules. The linker btc^{3-} acts as a dicarboxylate ligand. There are two kinds of Co(II); each is in distorted octahedral geometry surrounded by a N3O3 coordination enviornment. In one case, the N and O-atoms are bound to the metal center in meridonial and in other case it is in facial fashion. The N3O3 coordiantion environment is formed by one end of bis(tridentate) ligand, one carboxylate end of btc^{3-} and two water molecules; and in other, one end of bis(tridentate) ligand and two carboxylates (chelating bidentate and monodentate), respectively. The overall structure of the molecule is a 1D coordination polymer formed by the connectivity of a Co_4 and Co_2 unit, alternatively (see Figure 3.69).

The Co_4 unit is made up of alternative connection of btc^{3-} (act as dicarboxylate) and the bis(tridentate) ligand tpxn. The unsaturated coordination number of two of these Co(II) centers within this Co_4 unit is saturated by another two water molecules. In case of the other two Co(II), these are bound to the carboxylate end of btc^{3-} in chelating bidentate fashion and the other end of the carboxylate bound in monodentate fashion to a Co(II) atom of the Co_2 unit, which is formed by the connection of the bis(tridentate) ligand with two metals. The selected bond lengths are Co-N_{pyr} 2.118(5) Å, 2.115(5) Å; Co-N_{CH2} 2.176(4) Å, Co-O 2.109(3) Å, and Co-O_{aq} 2.005(3) Å and 2.217(3) Å for the cobalt where the atoms are bound in meridonial fashion. For the other cobalt, where atoms are bound in facial fashion, Co-N_{pyr} 2.096(3) Å, 2.087(4) Å; Co-N_{CH2} 2.265(4) Å, Co-O 2.020(3) Å, 2.096(3) Å and 2.268(3) Å. For the third cobalt, Co-N_{pyr} 2.149(4) Å, 2.131(6) Å; Co-N_{CH2} 2.195(4) Å, Co-O 2.160(3) Å, 2.097(4) Å and 2.057(3) Å. Selected bond length, bond angles are included in Table A39, and A65, respectively.

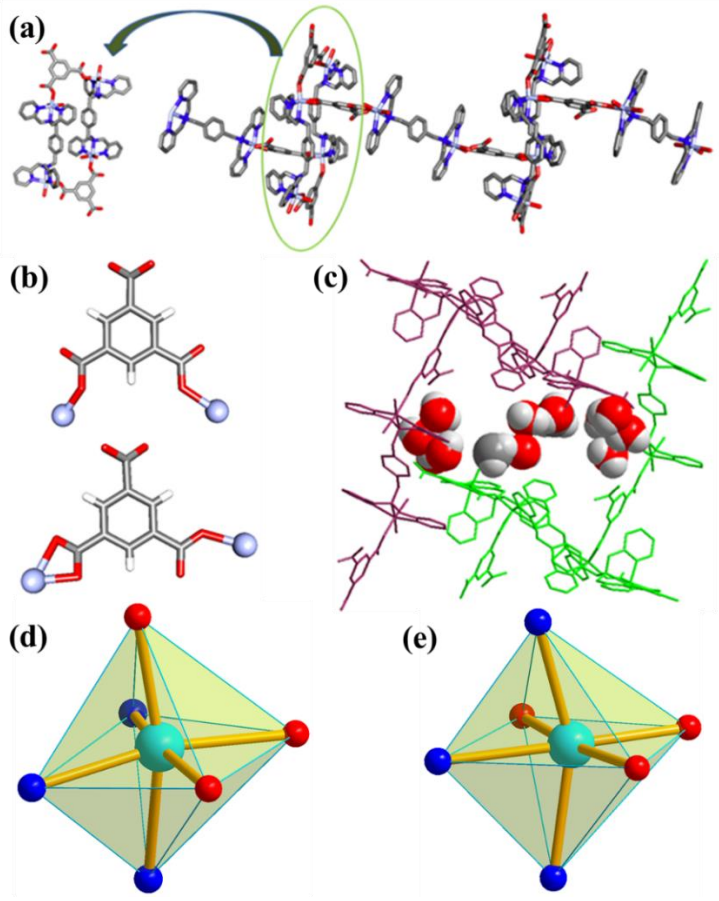

Figure 3.69. Crystal structure of 67. (a) 1D coordination polymer, (b) binding modes of H_3btc, (c) encapsulation of the solvent molecule, (d) and (e) coordination environments around the metal center (color code used for different atoms are like, light purple: Co; red: O, blue: N, grey: C, cyano: H).

CHAPTER IV

Conclusions

(1) One of the main components of Metal Organic Material (MOMs) is an organic ligand. The selection or the design of these ligands has a huge impact on the structural and physical properties of the resultant material. We have designed various organic neutral ligands by modifying or following the reported procedure in the literature. Some of these ligands are already known and few are new or not explore much in this field of MOMs. The spacer within the ligands were chosen judicially to get maximum variation in the flexibility and spacer lengths. Six bis(tridentate) polypyridyl ancillary ligands have been synthesized in good yields with high purity. Along with these ligands, commercially available dicarboxylate were used to get different MOCs with a variation in nuclearity and CPs with different dimensionality.

(2) The metal organic cages were made, targeting the application in the field of magnetism. So, cores which are used is already known for their interesting magnetic behaviour. Three magnetically active cores, $\{Mn_2(\mu\text{-}O)(\mu\text{-}O_2CR)_2\}^{2+}$, $\{Fe_2(\mu\text{-}O)(\mu\text{-}O_2CR)_2\}^{2+}$ and $\{Mn_2(\mu\text{-}O)_2(\mu\text{-}O_2CR)\}^{2+}$ have been used for the synthesis of various tetranuclear and octanuclear MOCs to obtain interesting magnetic materials.

(3) It is found that a combination of tphn ligand with succinate and fumarate dicarboxylate linker gives unprecedented octanuclear molecular cages while all other combinations produce either tetranuclear or polymeric compounds. Both flexibility and methylene chain length of bis(tridentate) polypyridyl ligands and dicarboxylate play a huge role in the structural diversity of these compounds.

(4) Some of these were structurally characterized by single crystal X-ray diffraction study. The structural parameters i.e. bond angles and bond lengths resembles with already published compound with these cores.

(5) All these cores have a signature spectroscopic feature in FTIR and UV-vis spectroscopy. So, a comparison of their spectroscopic properties was very helpful in establishing the formation of similar compounds of those for which no single crystal structure could be obtained.

(6) The nuclearity of the metal organic cages largely dependent on the combination of the ligand and dicarboxylates, hence the Mn···Mn distances between and within the cores. So, their magnetic properties are strongly dependent on the nuclearity of the molecular cages as well as the flexible chain lengths of bis(tridentate) polypyridyl ligands and dicarboxylate. Their magnetic behavior was according to expected ferro- and antiferro interactions within as well as between the cages.

(7) The combination of same ligand and dicarboxylate, either with manganese or with iron, produces compounds with similar structures and nuclearity. This result helps to conclude that Manganese and Iron chemistry showed similar results with respect to the nuclearity.

(8) A series of Coordination Polymers (CPs) with various M(II) centers, anionic carboxylate linkers, and bis(tridentate) polypyridyl ligands have been prepared and structurally characterized. Having the same ratio of the three components, various cationic and neutral CPs with varied dimensionality are obtained due to the variation of flexibility of the ligands and linkers.

(9) The semirigid bis(tridentate) ligands, tpchn and tpxn, have been employed with Mn(II), Co(II) and Ni(II) keeping the dicarboxylate linker fixed as rigid fumarate. In all these cases, a cationic coordination polymer is obtained and one of the fumarate acts as counter anion. While these two ligands with suc^{2-}, glu^{2-}, and adi^{2-} form ladder like 1D coordination polymer or dineuclear compounds with Co(II) and Ni(II). Summing up these results, it is proved that the rigidity of the dicarboxylate is the predominant factor to form the 1D CPs in case of fum^{2-}. While in case of suc^{2-}, glu^{2-}, and adi^{2-} the flexibility of the dicarboxylate allows to bind with more ease and to form diverse structure.

(10) The rigid 2,5-thiophenedicarboxylate was used with Co(II) and Ni(II) metal centers and a series of bis(tridentate) ligands (those are tpbn, tphn, tpchn, tpxn). In case of tpbn and tphn, both the metal center gives similar result as 2D coordination polymers and 1D ladder shaped coordination polymer. The ligands, tpchn and tpxn shown different trend with these two metal centers, Co(II) formed a 2D coordination polymer while Ni(II) formed a dinuclear compound with the same ligand and exactly opposite results were obtained with ligand tpxn.

(11) For the change of ligand from tpbn to tphn to tpchn to tpxn in case of Co(II)-based CPs, structures with different dimensionality ranging from 2D to 1D to a dinuclear unit were obtained.

(12) Spectroscopic properties and thermal behavior of all the synthesized compounds were established.

REFERENCES

(1) Whitesides, G. M. Self-Assembly at All Scales. *Science* **2002**, *295*, 2418–2422.

(2) Yoshizawa, M.; Klosterman, J. K.; Fujita, M. Functional Molecular Flasks: New Properties and Reactions within Discrete, Self-Assembled Hosts. *Angew. Chem., Int. Ed*. **2009**, *48*, 3418-3438.

(3) Severin, K. Supramolecular chemistry with organometallic half-sandwich complexes. *Chem. Commun*. **2006**, 3859-3867.

(4) Han, Y.-F.; Li, H.; Jin, G.-X. Host–guest chemistry with bi- and tetra-nuclear macrocyclic metallasupramolecules. *Chem. Commun*. **2010**, *46*, 6879-6890.

(5) Li, S.; Huang, J.; Cook, T. R.; Pollock, J. B.; Kim, H.; Chi, K.-W.; Stang, P. J. Formation of [3] Catenanes from 10 Precursors via Multicomponent Coordination-Driven Self-Assembly of Metallarectangles. *J. Am. Chem. Soc*. **2013**, *135*, 2084-2087.

(6) Therrien, B. Arene Ruthenium Cages: Boxes Full of Surprises. *Eur. J. Inorg. Chem*. **2009**, 2445-2453.

(7) Holliday, B. J.; Mirkin, C. A. Strategies for the Construction of Supramolecular Compounds through Coordination Chemistry. *Angew. Chemie Int. Ed*. **2001**, *40*, 2022–2043.

(8) Leininger, S.; Olenyuk, B.; Stang, P. J. Self-Assembly of Discrete Cyclic Nanostructures Mediated by Transition Metals. *Chem. Rev*. **2000**, *100*, 853–908.

(9) Guillerm, V.; Kim, D.; Eubank, J. F.; Luebke, R.; Liu, X.; Adil, K.; Lah, M. S.; Eddaoudi, M. A Supermolecular Building Approach for the Design and Construction of Metal-Organic Frameworks. *Chem. Soc. Rev*. **2014**, *43*, 6141–6172.

(10) Perry VI, J. J.; Perman, J. A.; Zaworotko, M. J. Design and Synthesis of Metal-Organic Frameworks Using Metal-Organic Polyhedra as Supermolecular Building Blocks. *Chem. Soc. Rev*. **2009**, *38*, 1400–1417.

(11) Gupta, V.; Mandal, S. K. A Robust and Water-Stable Two-Fold Interpenetrated Metal Organic Framework Containing Both Rigid Tetrapodal Carboxylate and Rigid Bifunctional Nitrogen Linkers Exhibiting Selective CO_2 Capture. *Dalt. Trans*. **2019**, 48, 415-425.

(12) Cui, Y.; Li, B.; He, H.; Zhou, W.; Chen, B.; Qian, G. Metal-Organic Frameworks as Platforms for Functional Materials. *Acc. Chem. Res*. **2016**, *49*, 483–493.

(13) Decoste, J. B.; Peterson, G. W. Metal-Organic Frameworks for Air Purification of Toxic Chemicals. *Chem. Rev*. **2014**, *114*, 5695–5727.

(14) Zhao, X.; Wang, Y.; Li, D. S.; Bu, X.; Feng, P. Metal–Organic Frameworks for Separation. *Adv. Mater*. **2018**, *30*, 869–932.

(15) K. Sumida, D. L. Rogow, J. A. Mason, T. M. McDonald, E. D. Bloch, Z. R. Herm, T.-H. Bae and J. R. Long, *Chem. Rev.*, **2012**, *112*, 724–781.

(16) Wu, Y. L.; Qian, J.; Yang, G. P.; Yang, F.; Liang, Y. T.; Zhang, W. Y.; Wang, Y. Y. High CO2uptake Capacity and Selectivity in a Fascinating Nanotube-Based Metal-Organic Framework. *Inorg. Chem*. **2017**, *56*, 908–913.

(17) Kim, H. R.; Yoon, T. U.; Kim, S. I.; An, J.; Bae, Y. S.; Lee, C. Y. Beyond Pristine MOFs: Carbon Dioxide Capture by Metal-Organic Frameworks (MOFs)-Derived Porous Carbon Materials. *RSC Adv*. **2017**, *7*, 1266–1270.

(18) Batten, S. R.; Murray, K. S. Structure and Magnetism of Coordination Polymers Containing Dicyanamide and Tricyanomethanide. *Coord. Chem. Rev.* **2003**, *246*, 103–130.

(19) Maspoch, D.; Ruiz-Molina, D.; Veciana, J. Magnetic Nanoporous Coordination Polymers. *J. Mater. Chem.* **2004**, *14*, 2713–2723.

(20) Maspoch, D.; Ruiz-Molina, D.; Wurst, K.; Domingo, N.; Cavallini, M.; Biscarini, F.; Tejada, J.; Rovira, C.; Veciana, J. A Nanoporous Molecular Magnet with Reversible Solvent-Induced Mechanical and Magnetic Properties. *Nat. Mater.* **2003**, *2*, 190–195.

(21) Ferey, G. Nanoporous Materials: A Selective Magnetic Sponge. *Nat. Mater.* **2003**, *2*, 136–137.

(22) Kitagawa, S.; Uemura, K. Dynamic Porous Properties of Coordination Polymers Inspired by Hydrogen Bonds. *Chem. Soc. Rev.* **2005**, *34*, 109–119.

(23) Kurmoo, M. Magnetic Metal-Organic Frameworks. *Chem. Soc. Rev.* **2009**, *38*, 1353–1379.

(24) Zheng, Y. R.; Suntharalingam, K.; Johnstone, T. C.; Lippard, S. J. Encapsulation of Pt(IV) Prodrugs within a Pt(II) Cage for Drug Delivery. *Chem. Sci.* **2015**, *6*, 1189–1193.

(25) Horcajada, P.; Serre, C.; Vallet-Regí, M.; Sebban, M.; Taulelle, F.; Férey, G. Metal-Organic Frameworks as Efficient Materials for Drug Delivery. *Angew. Chemie. Int. Ed.* **2006**, *45*, 5974–5978.

(26) Rocca, J. Della; Liu, D.; Lin, W. Nanoscale MetalÀOrganic Frameworks for Biomedical Imaging and Drug Delivery. *Acc. Chem. Res.* **2011**, *44*, 957–968.

(27) Barry, N. P. E.; Zava, O.; Dyson, P. J.; Therrien, B. Excellent Correlation between Drug Release and Portal Size in Metalla-Cage Drug-Delivery Systems. *Chem. Eur. J.* **2011**, *17*, 9669–9677.

(28) Therrien, B. Transporting and Shielding Photosensitisers by Using Water-Soluble Organometallic Cages: A New Strategy in Drug Delivery and Photodynamic Therapy. *Chem. Eur. J.* **2013**, *19*, 8378–8386.

(29) Ma, Z.; Moulton, B. Recent Advances of Discrete Coordination Complexes and Coordination Polymers in Drug Delivery. *Coord. Chem. Rev.* **2011**, *255*, 1623–1641.

(30) Rojas, S.; Colinet, I.; Cunha, D.; Hidalgo, T.; Salles, F.; Serre, C.; Guillou, N.; Horcajada, P. Toward Understanding Drug Incorporation and Delivery from Biocompatible Metal-Organic Frameworks in View of Cutaneous Administration. *ACS Omega* **2018**, *3*, 2994–3003.

(31) Freye, S.; Michel, R.; Stalke, D.; Pawliczek, M.; Frauendorf, H.; Clever, G. H. Template Control over Dimerization and Guest Selectivity of Interpenetrated Coordination Cages. *J. Am. Chem. Soc.* **2013**, *135*, 8476–8479.

(32) Zheng, H.; Xing, L.; Cao, Y.; Che, S. Coordination Bonding Based PH-Responsive Drug Delivery Systems. *Coord. Chem. Rev.* **2013**, *257*, 1933–1944.

(33) Novio, F.; Simmchen, J.; Vázquez-Mera, N.; Amorín-Ferré, L.; Ruiz-Molina, D. Coordination Polymer Nanoparticles in Medicine. *Coord. Chem. Rev.* **2013**, *257*, 2839–2847.

(34) Liu, Y.; Li, G.; Li, X.; Cui, Y. Cation-Dependent Nonlinear Optical Behavior in an Octupolar 3D Anionic Metal-Organic Open Framework. *Angew. Chemie. Int. Ed.* **2007**, *46*, 6301–6304.

(35) Evans, O. R.; Lin, W. Crystal Engineering of NLO Materials Based on Metal-Organic Coordination Networks. *Acc. Chem. Res.* **2002**, *35*, 511–522.

(36) Allendorf, M. D.; Bauer, C. A.; Bhakta, R. K.; Houk, R. J. T. Luminescent Metal-Organic Frameworks. *Chem. Soc. Rev.* **2009**, *38*, 1330–1352.

(37) Cahill, C. L.; De Lill, D. T.; Frisch, M. Homo- and Heterometallic Coordination Polymers from the f Elements. *CrystEngComm* **2007**, *9*, 15–26.

(38) Janiak, C. Engineering Coordination Polymers Toward Applications. *Dalt. Trans.* **2003**, 2781–2804.

(39) Maspoch, D.; Ruiz-Molina, D.; Veciana, J. Old Materials with New Tricks: Multifunctional Open-Framework Materials. *Chem. Soc. Rev.* **2007**, *36*, 770–818.

(40) Suh, M. P.; Cheon, Y. E.; Lee, E. Y. Syntheses and Functions of Porous Metallosupramolecular Networks. *Coord. Chem. Rev.* **2008**, *252*, 1007–1026.

(41) Chakraborty, G.; Mandal, S. K. Neutral Luminescent Metal-Organic Frameworks: Structural Diversification, Photophysical Properties, and Sensing Applications. *Inorg. Chem.* **2017**, *56*, 14556–14566.

(42) Chakraborty, G.; Mandal, S. K. Design and Development of Fluorescent Sensors with Mixed Aromatic Bicyclic Fused Rings and Pyridyl Groups: Solid Mediated Selective Detection of 2,4,6-Trinitrophenol in Water. *ACS Omega* **2018**, *3*, 3248–3256.

(43) Kumar, N.; Mandal, S. K. Design and Application of a Fluorogenic Receptor for Selective Sensing of Cations, Small Neutral Molecules, and Anions. *New J. Chem.* **2018**, *42*, 18278–18287.

(44) Kreno, L. E.; Leong, K.; Farha, O. K.; Allendorf, M.; Van Duyne, R. P.; Hupp, J. T. Metal-Organic Framework Materials as Chemical Sensors. *Chem. Rev.* **2012**, *112*, 1105–1125.

(45) Collins, D. J.; Zhou, H.-C. Hydrogen Storage in Metal–organic Frameworks. *J. Mater. Chem.* **2007**, *17*, 3154.

(46) Forster, P. M.; Cheetham, A. K. Hybrid Inorganic–Organic Solids: An Emerging Class of Nanoporous Catalysts. *Top. Catal.* **2003**, *24*, 79–86.

(47) Eddaoudi, M.; Li, H.; Yaghi, O. M. Highly Porous and Stable Metal-Organic Frameworks: Structure Design and Sorption Properties. *J. Am. Chem. Soc.* **2000**, *122*, 1391–1397.

(48) Seo, J. S.; Whang, D.; Lee, H.; Jun, S. I.; Oh, J.; Jeon, Y. J.; Kim, K. A Homoquiral Metal-Organic Porous Meterial for Enentioselective Seperation Ans Catalysis. *Nature* **2000**, *404*, 982–986.

(49) Wu, C. De; Hu, A.; Zhang, L.; Lin, W. A Homochiral Porous Metal-Organic Framework for Highly Enantioselective Heterogeneous Asymmetric Catalysis. *J. Am. Chem. Soc.* **2005**, *127*, 8940–8941.

(50) Cho, S. H.; Ma, B.; Nguyen, S. B. T.; Hupp, J. T.; Albrecht-Schmitt, T. E. A Metal-Organic Framework Material That Functions as an Enantioselective Catalyst for Olefin Epoxidation. *Chem. Commun.* **2006**, 2563–2565.

(51) Markad, D.; Mandal, S. K. Synthesis and Structural Characterization of a Novel Dinuclear Cu(II) Complex: An Efficient and Recyclable Bifunctional Heterogeneous Catalyst for the Diastereoselective Henry Reaction. *Dalt. Trans.* **2018**, *47*, 5928–5932.

(52) Maji, T. K.; Kitagawa, S. Chemistry of Porous Coordination Polymers. *Pure Appl. Chem.* **2007**, *79*, 2155–2177.

(53) Markad, D.; Khullar, S.; Mandal, S. K. Engineering a Nanoscale Primary Amide-Functionalized 2D Coordination Polymer as an Efficient and Recyclable Heterogeneous Catalyst for the Knoevenagel Condensation Reaction. ACS Appl. Nano Mater. **2018**, *1*, 5226−5236.

(54) Lee, J.; Farha, O. K.; Roberts, J.; Scheidt, K. A.; Nguyen, S. T.; Hupp, J. T. Metal-Organic Framework Materials as Catalysts. *Chem. Soc. Rev.* **2009**, *38*, 1450–1459.

(55) Férey, G.; Mellot-Draznieks, C.; Serre, C.; Millange, F.; Dutour, J.; SurblÃ©, S.; Margiolaki, I. A Chromium Terephthalate-Based Solid with Unusually Large Pore Volumes and Surface Area. *Sci.* **2005**, *309*, 2040–2042.

(56) Hee K. Chae, Diana Y. Siberio-Pe´rez1, Jaheon Kim, YongBok Go, Mohamed Eddaoudi, Adam J. Matzger, Michael O'Keeffe, O. M. Y. A Route to High Surface Area, Porosity and Inclusion of Large Molecules in Crystals. *Nature* **2004**, *427*, 523–527.

(57) Organic cage compounds – from shape-persistency to function. Zhang, G.; Mastalerz, M. *Chem. Soc. Rev.*, **2014**, *43*, 1934-1947.

(58) Chandrasekhar, V.; Palani Sasikumar, P.; Thilagar, P. Formation of a Double-Bicapped Hexatin Phosphate Cage by a De-arylation Reaction. Synthesis and Structure of $[(PhSn)_6(\mu\text{-}OH)_2(\mu_3\text{-}O)_2(\mu\text{-}OEt)_4\{(ArO)PO_3\}_4](Ar)$ 2,6-i-$Pr_2C_6H_3$). *Organometallics*, **2007**, *26*, 4387-4388.

(59) Tidmarsh, I. S.; Faust, T. B. Adams, H.; Harding, L. P.; Russo, L.; Clegg, W.; Ward, M. D. Octanuclear Cubic Coordination Cages. *J. Am. Chem. Soc.*, **2008**, *130*, 15167-15175.

(60) Liu, Y.; Kravtsov, V. C.; Larsen, R.; Eddaoudi, M. Molecular Building Blocks Approach to the Assembly of Zeolite-like Metal-Organic Frameworks (ZMOFs) with Extra-Large Cavities. *Chem. Commun.* **2006**, 1488–1490.

(61) Schmidt, G. M. J. Photodimerization in the Solid State. *Pure Appl. Chem.* **1971**, *27*, 647–678.

(62) Inokuma, Y.; Kawano, M.; Fujita, M. Crystalline Molecular Flasks. *Nat. Chem.* **2011**, *3*, 349–358.

(63) Mal, P.; Breiner, B.; Rissanen, K.; Nitschke, J. R. White Phosphorus Is Air-Stable Within a Self-Assembled Tetrahedral Capsule. *Science.* **2009**, *324*, 1697–1700.

(64) Inokuma, Y.; Yoshioka, S.; Ariyoshi, J.; Arai, T.; Hitora, Y.; Takada, K.; Matsunaga, S.; Rissanen, K.; Fujita, M. X-Ray Analysis on the Nanogram to Microgram Scale Using Porous Complexes. *Nature* **2013**, *495*, 461–466.

(65) Kang, J.; Hilmersson, G.; Santamaría, J.; Rebek, J. Diels - Alder Reactions through Reversible Encapsulation. *J. Am. Chem. Soc.* **1998**, *120*, 3650–3656.

(66) Wageningen, A. M. A. Van; Timmerman, P.; Duynhoven, J. P. M. Van; Verboom, W.; Veggel, F. C. J. M. Van; Reinhoudt, D. N. Calix[4]Arene-Based (Hemi)Carcerands and Carceplexes: Synthesis, Functionalization, and Molecular Modeling Study. *Chem. Eur. J.* **1997**, *3*, 639–654.

(67) Fujita, M.; Takeda, N.; Umemoto, K.; Yamaguchi, K. A Nanometre-Sized Hexahedral Coordination Capsule Assembled from 24 Components . *Nature* **1999**, *398*, 794–796.

(68) Hong, M.; Zhao, Y.; Su, W.; Cao, R.; Fujita, M.; Zhou, Z.; Chan, A. S. C. A Nanometer-Sized Metallosupramolecular Cube with O(h) Symmetry. *J. Am. Chem. Soc.* **2000**, *122*, 4819–4820.

(69) Umemoto, K.; Tsukui, H.; Kusukawa, T.; Biradha, K.; Fujita, M. Molecular Paneling by Coordination: An M15L6 Hexahedral Molecular Capsule Having Clefts for Reversible Guest Inclusion. *Angew. Chemie. Int. Ed*. **2001**, *40*, 2620–2622.

(70) Chand, D. K.; Biradha, K.; Fujita, M.; Sakamoto, S.; Yamaguchi, K. A Molecular Sphere of Octahedral Symmetry. *Chem. Commun.* **2002**, *8*, 2486–2487.

(71) Tominaga, M.; Suzuki, K.; Kawano, M.; Kusukawa, T.; Ozeki, T.; Sakamoto, S.; Yamaguchi, K.; Fujita, M. Finite, Spherical Coordination Networks That Self-Organize from 36 Small Components. *Angew. Chemie. Int. Ed*. **2004**, *43*, 5621–5625.

(72) Suzuki, K.; Kawano, M.; Fujita, M. Solvato-Controlled Assembly of Pd_3L_6 and Pd_4L_8 Coordination "Boxes." *Angew. Chemie. Int. Ed*. **2007**, *46*, 2819–2822.

(73) Yoshizawa, M.; Tamura, M.; Fujita, M. Chirality Enrichment through the Heterorecognition of Enantiomers in an Achiral Coordination Host. *Angew. Chemie. Int. Ed*. **2007**, *46*, 3874–3876.

(74) Fochi, F.; Jacopozzi, P.; Wegelius, E.; Rissanen, K.; Cozzini, P.; Marastoni, E.; Fisicaro, E.; Manini, P.; Fokkens, R.; Dalcanale, E. Self-Assembly and Anion Encapsulation Properties of Cavitand-Based Coordination Cages. *J. Am. Chem. Soc.* **2001**, *123*, 7539–7552.

(75) Bar, A. K.; Chakrabarty, R.; Mukherjee, P. S. Self-Assembly of a Pd6-Molecular Double-Square and a Cu_3-trigonalbipyramidal Cage via a New Tripodal Flexible Ligand. *Inorg. Chem.* **2009**, *48*, 10880–10882.

(76) Wang, S.; Gao, X.; Hang, X.; Zhu, X.; Han, H.; Liao, W.; Chen, W. Ultrafine Pt Nanoclusters Confined in a Calixarene-Based $\{Ni_{24}\}$ Coordination Cage for High-Efficient Hydrogen Evolution Reaction. *J. Am. Chem. Soc.* **2016**, *138*, 16236–16239.

(77) Röder, J. C.; Meyer, F.; Pritzkow, H. An Unusual Hexanickel Cage Complex with μ- and μ_3-Chloro Bridges and an Interstitial μ_6-Chloride. *Chem. Commun.* **2001**, *1*, 2176–2177.

(78) Paul, R. L.; Couchman, S. M.; Jeffery, J. C.; McClevcrty, J. A.; Reeves, Z. R.; Ward, M. D. Effects of Metal Co-Ordination Geometry on Self-Assembly: A Dinuclear Double Belicate Complex and a Tetranuclear Cage Complex of a New Bis-Bidentate Bridging Ligand. *J. Chem. Soc. Dalt. Trans.* **2000**, 845–851.

(79) Fujita, M.;, Tominga, M.; Hori; A.;, Therrien, B. Coordination Assemblies from a Pd(II)-Cornered Square Complex. *Acc. Chem. Res.* **2005**, *38*, 371-380.

(80) Sun, Q.-F.; Iwasa, J.; Ogawa, D.; Ishido, Y.; Sato, S.; Ozeki, T.; Sei, Y.; Yamaguchi, K.; Fujita, M. Self-Assembled $M_{24}L_{48}$ Polyhedra and Their Sharp Structural Switch upon Subtle Ligand Variation. *Science.* **2010**, *328*, 1144 -1147.

(81) García-Simón, C.; Costas, M.; Ribas, X. Metallosupramolecular Receptors for Fullerene Binding and Release. *Chem. Soc. Rev.* **2016**, *45*, 40–62.

(82) Novak, M. A.; Sessoli, R.; Gatteschi, D.; Caneschi, A. Magnetic Bistability in a Metal-Ion Cluster. *Nature* **1993**, *365*, 141–143.

(83) Lin, P. H.; Burchell, T. J.; Ungur, L.; Chibotaru, L. F.; Wernsdorfer, W.; Murugesu, M. A Polinuclear Lanthanide Single-Molecule Magnet with a Record Anisotropic Barrier. *Angew. Chemie. Int. Ed*. **2009**, *48*, 9489–9492.

(84) Woodruff, D. N.; Winpenny, R. E. P.; Layfield, R. A. Lanthanide Single-Molecule Magnets. *Chem. Rev.* **2013**, *113*, 5110–5148.

(85) Yang, E. C.; Hendrickson, D. N.; Wernsdorfer, W.; Nakano, M.; Zakharov, L. N.; Sommer, R. D.; Rheingold, A. L.; Ledezma-Gairaud, M.; Christou, G. Cobalt Single-Molecule Magnet. *J. Appl. Phys.* **2002**, *91*, 7382–7384.

(86) Mereacre, V. M.; Ako, A. M.; Clérac, R.; Wernsdorfer, W.; Filoti, G.; Bartolomé, J.; Anson, C. E.; Powell, A. K. A Bell-Shaped $Mn_{11}Gd_2$ Single-Molecule Magnet. *J. Am. Chem. Soc.* **2007**, *129*, 9248–9249.

(87) Milios, C. J.; Vinslava, A.; Whittaker, A. G.; Parsons, S.; Wernsdorfer, W.; Christou, G.; Perlepes, S. P.; Brechin, E. K. Microwave-Assisted Synthesis of a Hexanuclear MnIII Single-Molecule Magnet. *Inorg. Chem.* **2006**, *45*, 5272–5274.

(88) Mossin, S.; Tran, B. L.; Adhikari, D.; Pink, M.; Heinemann, F. W.; Sutter, J.; Szilagyi, R. K.;

Meyer, K.; Mindiola, D. J. A Mononuclear Fe(III) Single Molecule Magnet with a 3/2↔5/2 Spin Crossover. *J. Am. Chem. Soc.* **2012**, *134*, 13651–13661.

(89) Koizum, S.; Nihei, M.; Nakano, M.; Oshio, H. Antiferromagnetic Fe^{III}_6 Ring and Single-Molecule Magnet $Mn^{III}_3Mn^{III}_4$ Wheel. *Inorg. Chem.* **2005**, *44*, 1208–1210.

(90) Novikov, V. V.; Pavlov, A. A.; Nelyubina, Y. V.; Boulon, M. E.; Varzatskii, O. A.; Voloshin, Y. Z.; Winpenny, R. E. P. A Trigonal Prismatic Mononuclear Cobalt(II) Complex Showing Single-Molecule Magnet Behavior. *J. Am. Chem. Soc.* **2015**, *137*, 9792–9795.

(91) Del Barco, E.; Kent, A. D.; Yang, E. C.; Hendrickson, D. N. Quantum Superposition of High Spin States in the Single Molecule Magnet Ni_4. *Phys. Rev. Lett.* **2004**, *93*, 1–4.

(92) M. Evangelisti,a F. Luis, L. J. de Jonghc, M. Affronte. Magnetothermal properties of molecule-based materials. *J. Mater. Chem.*, 2006, 16, 2534–2549.

(93) Liu, J. L.; Chen, Y. C.; Guo, F. S.; Tong, M. L. Recent Advances in the Design of Magnetic Molecules for Use as Cryogenic Magnetic Coolants. *Coord. Chem. Rev.* **2014**, *281*, 26–49.

(94) Zheng, Y. Z.; Evangelisti, M.; Tuna, F.; Winpenny, R. E. P. Co-Ln Mixed-Metal Phosphonate Grids and Cages as Molecular Magnetic Refrigerants. *J. Am. Chem. Soc.* **2012**, *134*, 1057–1065.

(95) Lorusso, G.; Sharples, J. W.; Palacios, E.; Roubeau, O.; Brechin, E. K.; Sessoli, R.; Rossin, A.; Tuna, F.; McInnes, E. J. L.; Collison, D.; et al. A Dense Metal-Organic Framework for Enhanced Magnetic Refrigeration. *Adv. Mater.* **2013**, *25*, 4653–4656.

(96) Peng, J. B.; Zhang, Q. C.; Kong, X. J.; Zheng, Y. Z.; Ren, Y. P.; Long, L. S.; Huang, R. Bin; Zheng, L. S.; Zheng, Z. High-Nuclearity 3d-4f Clusters as Enhanced Magnetic Coolers and Molecular Magnets. *J. Am. Chem. Soc.* **2012**, *134*, 3314–3317.

(97) Guo, F. S.; Chen, Y. C.; Liu, J. L.; Leng, J. D.; Meng, Z. S.; Vrábel, P.; Orendáč, M.; Tong, M. L. A Large Cryogenic Magnetocaloric Effect Exhibited at Low Field by a 3D Ferromagnetically Coupled Mn(Ii)-Gd(Iii) Framework Material. *Chem. Commun.* **2012**, 12219–12221.

(98) Biswas, S.; Mondal, A. K.; Konar, S. Densely Packed Lanthanide Cubane Based 3D Metal-Organic Frameworks for Efficient Magnetic Refrigeration and Slow Magnetic Relaxation. *Inorg. Chem.* **2016**, *55*, 2085–2090.

(99) Carretta, S.; Santini, P.; Amoretti, G.; Affronte, M.; Candini, A.; Ghirri, A.; Tidmarsh, I. S.; Laye, R. H.; Shaw, R.; McInnes, E. J. L. High-Temperature Slow Relaxation of the Magnetization in Ni_{10} Magnetic Molecules. *Phys. Rev. Lett.* **2006**, *97*, 1–4.

(100) Comstock, R. L. Modern Magnetic Materials in Data Storage. *J. Mater. Sci. Mater. Electron.* **2002**, *13*, 509–523.

(101) Berman, G. P.; Doolen, G. D.; Holm, D. D.; Tsifrinovich, V. I. Quantum computer on a class of one-dimensional Ising systems. *Phys. Lett. A* 1994, 193, 444.

(102) Garanin, D. A.; Chudnovsky, E. M. Thermally Activated Resonant Magnetization Tunneling in Molecular Magnets: $Mn_{12}Ac$ and Others. *Phys. Rev. B* **1997**, *56*, 102–118.

(103) Leuenberger, M. N.; Loss, D. Quantum Computing in Molecular Magnets. *Nature* **2001**, *410*, 789–793.

(104) Aromí, G.; Aguilà, D.; Gamez, P.; Luis, F.; Roubeau, O. Design of Magnetic Coordination Complexes for Quantum Computing. *Chem. Soc. Rev.* **2012**, *41*, 537–546.

(105) Clemente-Juan, J. M.; Coronado, E.; Gaita-Ariño, A. Magnetic Polyoxometalates: From Molecular Magnetism to Molecular Spintronics and Quantum Computing. *Chem. Soc. Rev.* **2012**, *41*, 7464–7478.

(106) Mitrikas, G.; Sanakis, Y.; Raptopoulou, C. P.; Kordas, G.; Papavassiliou, G. Electron Spin-Lattice and Spin-Spin Relaxation Study of a Trinuclear Iron(III) Complex and Its Relevance in Quantum Computing. *Phys. Chem. Chem. Phys.* **2008**, *10*, 743–748.

(107) Bleaney, B.; Bowers, K. D. Anomalous paramagnetism of copper acetate. *Proc. R. Soc. London* **1952**, *A214*, 451

(108) Kambe, K. On the Paramagnetic Susceptibilities of Some Polynuclear Complex Salts. *J. Phys. Soc. Jpn.* **1950**, *5*, 48.

(109) van Niekerk, J. N.; Schoening, F. R. L. A New Type of Copper Complex as Found in the Crystal Structure of Cupric Acetate, $Cu_2(CH_3COO)_4 \cdot 2H_2O$. *Acta Crystallogr.* **1953**, *6*, 227–232.

(110) B. N. Figgis, G. B. R. Crystal-Molecular Structure and Magnetic Properties of $Cr_3(CH_3COO)_6OCl \cdot 5H_2O$. *Nature* **1965**, *205*, 694–695.

(111) *Magneto-Structural Correlations in Exchange Coupled Systems*; Gatteschi, D., Kahn, O., Willett, R. D., Eds.; D. Reidel Publishing Co.: Dordrecht, 1985; 497-522.

(112) Hatfield, W. E. Effect of Bridge Geometry on Exchange Coupling in Ligand- Bridged Copper(II) Dimers and Chains. *Comments Inorg. Chem.* **1981**, *1*, 105–121.

(113) Jorgen Glerup, Derek J Hodgson, E. P. A Novel Correlation between Magnetism and Structural Parameters in Superexchange Coupled Chromium(III) Dimers. *Acta Chem Scand* **1983**, *A37*, 161–164.

(114) Charlot, M. F.; Kahn, O.; Drillon, M. Correlation Structure-Magnetic Properties in $(Cr_2O_{10})^{14-}$ Dimeric Units: A Theoretical Approach. *Chem. Phys.* **1982**, *70*, 177–187.

(115) Van Crawford, H.; Richardson, H. W.; Wasson, J. R.; Hodgson, D. J.; Hatfield, W. E. Relation Between the Singlet-Triplet Splitting and the Cu-O-Cu Bridge Angle in Hydroxo-Bridged Copper Dimers. *Inorg. Chem.* **1976**, *15*, 2107–2110.

(116) Weihe, H.; Güdel, H. U. Angular and Distance Dependence of the Magnetic Properties of Oxo-Bridged Iron(III) Dimers. *J. Am. Chem. Soc.* **1997**, *119*, 6539–6543.

(117) Gorun, S. M.; Lippard, S. J. Magnetostructural Correlations in Magnetically Coupled (μ-Oxo)Diiron(III) Complexes. *Inorg. Chem.* **1991**, *30*, 1625–1630.

(118) Sessoli, R.; Gatteschi, D.; Tsai, H. L.; Hendrickson, D. N.; Schake, A. R.; Wang, S.; Vincent, J. B.; Christou, G.; Folting, K. High-Spin Molecules: $[Mn_{12}O_{12}(O_2CR)_{16}(H_2O)_4]$. *J. Am. Chem. Soc.* **1993**, *115*, 1804–1816.

(119) Haryono M.; Kalisz, M.; Sibille, R.; Lescouezec, R.; Fave, C.; Trippe, A. G.; Li, Y.; Seuleiman, M.; Rousseli ere, H.; Balkhy, A. M.; Lacroixb, J-C.; Journaux, Y.; One dimensional assembly of Mn_6 single molecule magnets linked by oligothiophene bridges. *Dalton Trans.*, **2010**, *39*, 4751–4756.

(120) Moro, F.; Corradini, V.; Evangelisti, M.; De Renzi, V.; Biagi, R.; Del Pennino, U.; Milios, C. J.; Jones, L. F.; Brechin, E. K. Grafting Derivatives of Mn6 Single-Molecule Magnets with High Anisotropy Energy Barrier on Au(111) Surface. *J. Phys. Chem. B* **2008**, *112*, 9729–9735.

(121) Brechin, E. K.; Sañudo, E. C.; Wernsdorfer, W.; Boskovic, C.; Yoo, J.; Hendrickson, D. N.; Yamaguchi, A.; Ishimoto, H.; Concolino, T. E.; Rheingold, A. E.; et al. Single-Molecule Magnets: Structure and Properties of $[Mn_{18}O_{14}(O_2CMe)_{18}(Hep)_4(HepH)_2(H_2O)_2](ClO_4)_2$ with Spin S = 1/3. *Inorg. Chem.* **2005**, *44*, 502–511.

(122) Sañudo, E. C.; Wernsdorfer, W.; Abboud, K. A.; Christou, G. Synthesis, Structure, and Magnetic Properties of a Mn_{21} Single-Molecule Magnet. *Inorg. Chem.* **2004**, *43*, 4137–4144.

(123) Murugesu, M.; Raftery, J.; Wernsdorfer, W.; Christou, G.; Euan K. Brechin, E. K.. Synthesis, Structure, and Magnetic Properties of a [Mn_{22}] Wheel-like Single-Molecule Magnet. *Inorg. Chem.* **2004**, *43*, 4203−4209.

(124) Soler, M.; Wernsdorfer, W.; Folting, K.; Pink, M.; Christou, G. Single-Molecule Magnets: A Large Mn_{30} Molecular Nanomagnet Exhibiting Quantum Tunneling of Magnetization. *J. Am. Chem. Soc.* **2004**, *126*, 2156–2165.

(125) Tasiopoulos, A. J.; Vinslava, A.; Wernsdorfer, W.; Abboud, K. A.; Christou, G. Giant Single-Molecule Magnets: A {Mn_{84}} Torus and Its Supramolecular Nanotubes. *Angew. Chem. Int. Ed.* **2004**, *43*, 2117–2121.

(126) Wernsdorfer, W.; Caneschi, A.; Sessoli, R.; Gatteschi, D.; Cornia, A.; Villar, V.; Paulsen, C. Effects of Nuclear Spins on the Quantum Relaxation of the Magnetization for the Molecular Nanomagnet Fe8. *Phys. Rev. Lett.* **2000**, *84*, 2965–2968.

(127) E. del Barco, N. Vernier, J. M. Hernandez, J. Tejada, E. M. Chudnovsky, E. Molins, G. B. Quantum Coherence in Fe_8 Molecular Nanomagnets. *Europhys. Lett.* **1999**, *47*, 722–728.

(128) Bell, A.; Aromí, G.; Teat, S. J.; Wernsdorfer, W.; Winpenny, R. E. P. Synthesis and Characterisation of a {Ni_8} Single Molecule Magnet and Another Octanuclear Nickel Cage. *Chem. Commun.* **2005**, 2808–2810.

(129) Mukhopadhyay, S.; Mandal, S. K.; Bhaduri, S.; Armstrong, W. H. Manganese Clusters with Relevance to Photosystem II. *Chem. Rev.* **2004**, *104*, 3981–4026.

(130) Mok, H. J.; Davis, J. A.; Pal, S.; Mandal, S. K.; Armstrong, W. H. Sterically Crowded Manganese-Oxo Complexes of N,N-Bis(2- Pyridylmethyl)-Tert-Butylamine with Bridged Binuclear Core Types {$Mn_2(\mu\text{-}O)(\mu\text{-}OAc)_2$} and {$Mn^{IV}{}_2(\mu\text{-}O)_2$(m-OAc)}. *Inorganica Chim. Acta.* **1997**, *263*, 385–394.

(131) Gunay, A.; Theopold, K. H. C–H Activation by Metal Oxo Compounds. *Chem. Rev.* **2010**, *110*, 1060–1081.

(132) Larsen, A. S.; Wang, K.; Lockwood, M. A.; Rice, G. L.; Won, T. J.; Lovell, S.; Sadílek, M.; Tureček, F.; Mayer, J. M. Hydrocarbon Oxidation by Bis-μ-Oxo Manganese Dimers: Electron Transfer, Hydride Transfer, and Hydrogen Atom Transfer Mechanisms. *J. Am. Chem. Soc.* **2002**, *124*, 10112–10123.

(133) Pardo, E.; Lloret, F.; Carrasco, R.; Carmen, M. M.; Temporal-Sanchez, T.; Ruiz-Garcıa, R. Chemistry and reactivity of dinuclear iron oxamate complexes: alkane oxidation with hydrogen peroxide catalysed by an oxo-bridged diiron (III) complex with amide and carboxylate ligation. *Inorg. Chim. Act.* **2004**, *357*, 2713–2720.

(134) Dave, B. C.; Czernuszewicz, R. S. Structural and Spectroscopic Models of the Manganese Catalase Active Site . Isolation and Structures of the Asymmetric [$(H_2O)Mn^{III}(\mu\text{-}O)(\mu\text{-}O_2CR)_2Mn^{III}(L)$] (L= $Cr_2O_7^{2-}$, CH_3OH) Cores: Analogs of a Substrate-Bound Catalase Active Site Intermediate. *Inorganica Chim. Act* **1998**, *281*, 25–35.

(135) Sheats, J. E.; Czernuszewicz, R. S.; Dismukes, G. C.; Lippard, S. J.; Beer, R. H.; Rheingold, A. L.; Petrouleas, V.; Stubbe, J.; Armstrong, W. H. Binuclear Manganese(III) Complexes of Potential Biological Significance. *J. Am. Chem. Soc.* **1987**, *109*, 1435–1444.

(136) Mok, H. J.; Davis, J. A.; Pal, S.; Mandal, S. K.; Armstrong, W. H. Sterically crowded manganese-oxo complexes of N,N-bis(2-pyridylmethyl)-tert-butylamine with bridged binuclear core types {$Mn^{III}{}_2(\mu\text{-}O)(\mu\text{-}OAc)_2$} and {$Mn^{IV}{}_2(\mu\text{-}O)_2(\mu\text{-}OAc)$ }. *Inorg. Chim. Acta* **1997**, *263*, 385-394.

(137) Bossek, U.; Hummel, H.; Weyhermüller, T.; Wieghardt, K.; Russell, S.; van der Wolf, L.; Kolb,

U. The$[Mn_2^{IV}(\mu\text{-}O)(\mu\text{-}PhBO_2)_2]^{2+}$ Unit: A New Structural Model for Manganese-Containing Metalloproteins. *Angew. Chem. Int. Ed. Engl.* **1996**, *35*, 1552–1554.

(138) Characterization, S. Complexes of Manganese (III). Analogues of the Di-Iron (III) Centre in Hemerythrin. ***J. Chem. Soc., Chem. Commun.***, **1985**, 347-349.

(139) Ménage, S.; Girerd, J.-J.; Gleizes, A. A $[Mn^{III}_2(\mu\text{-}O)(\mu\text{-}MeCO_2)_2(H_2O)_2(Bipy)_2]^{2+}$(Bipy = 2,2'-Bipyridine) Unit with Accessible Co-Ordination Sites. Contribution to the Modelling of the Photosynthetic Oxygen Evolving Centre. *J. Chem. Soc., Chem. Commun.* **1988**, *20*, 431.

(140) Nishida, Y.; Oshino, N.; Tokii, T. Preparation and ESR Spectra of Manganese(III) Complexes with 2-[bis(benzimidazol-2-ylmethyl)-amino] Ethanol. *Z. Naturforsch.* **1988**, *43b*, 637–638.

(141) Vincent, J. B.; Folting, K.; Huffman, J. C.; Christou, G. Dinuclear Manganese-Oxide Complexes as Models for Manganese Catalase. *Biochem. Soc. Trans.* **1988**, *16*, 822–823.

(142) Bossek, U.; K. W. Bioinorganic Model Complexes for the Active Site in Manganese Containing Catalases. The Crystal Structures of $[L_2Mn_2(\mu\text{-}OH)(\mu\text{-}O_2CCH_3)_2](PF_6).CH_3OH$ and $[L'_2Mn^{III}_2(\mu\text{-}O)(\mu\text{-}O_2CCH_3)_2]$ $(I_3)I{\cdot}H_2O$. *Inorg. Chim. Acta.***1989**, *165*, 123–129.

(143) Toftlund, H.; Markiewicz, A.; Murray, K. S. Synthesis and Magnetic Properties of a μ-oxo-di(μ-acetato)manganese(III) Complex of a Strapped Tripodal Pyridylamine Ligand N,N,N',N'-Tetrakis(2-Pyridylmethyl)-1,3-Propanediamine. A Model for the Mn_2 Site of Mn-Catalase Enzymes. *Acta Chem. Scand.* **1990**, *44*, 443–446.

(144) Wu, F. J.; Kurtz, D. M.; Vankai, V. A.; Hagen, K. S.; Nyman, P. D.; Debrunner, P. G. (μ-oxo/hydroxo)bis(μ-carboxylato)diiron(III) and -dimanganese(III) Complexes with Capping Tris(imidazol-2-yl)phosphine Ligands. *Inorg. Chem.* **1990**, *29*, 5174–5183.

(145) Blackman, A. G.; Huffman, J. C.; Lobkovsky, E. B.; Christou, G. Towards Functional Models of the Photosynthetic Water Oxidation Centre: Synthesis and Structure of the Asymmetric Complex $[Mn_2O(O_2CMe)_2(bpy)_2(H_2O)(S_2O_8)]{\cdot}H_2O$ (bpy = 2,2'-bipyridine), containing Coordinated H_2O and $S_2O_8^{2-}$. *J. Chem. Soc., Chem. Commun.* **1991**, 989–991.

(146) Hotzelmann, R.; Wieghardt, K.; Ensling, J.; Romstedt, H.; Gütlich, P.; Bill, E.; Flörke, U.; Haupt, H. J. Synthesis, Crystal Structures, Mössbauer, Susceptibility, and EPR Studies of a Series of Spin Exchange Coupled Complexes Containing the (μ-Oxo)Bis(μ-Acetato)Ruthenium metal Core and Its Hydroxo-Bridged Analogue (Metal = V, Cr, Mn, Fe, Co). *J. Am. Chem. Soc.* **1992**, *114*, 9470–9483.

(147) Vincent, J. B.; Blackman, A. G.; Wang, S.; Christou, G.; Tsai, H. L.; Hendrickson, D. N.; Boyd, P. D. W.; Folting, K.; Huffman, J. C.; Lobkovsky, E. B. Models of the Manganese Catalase Enzymes. Dinuclear Manganese(III) Complexes with the $[Mn_2(\mu\text{-}O)(\mu\text{-}O_2CF)_2]2+$ Core and Terminal Monodentate Ligands: Preparation and Properties of $[Mn_2O(O_2CR)_2X_2(bpy)_2]$ (X = Cl^-, N^{3-}, H_2O). *J. Am. Chem. Soc.* **1993**, *115*, 12353–12361.

(148) Mahapatra, S.; Lal, T. K.; Mukherjee, R. Synthesis, Characterization, and Novel Redox Properties of a New Triply Bridged Dimanganese(III) Complex with a $\{Mn^{III}_2(\mu\text{-}O)(\mu\text{-}O_2CCH_3)_2\}^{2+}$ Core. *Inorg. Chem.* **1994**, *33*, 1579–1580.

(149) Gultneh, Y.; Ahvazi, B.; Raza Khan, A.; Butcher, R. J.; Tuchagues, J. P. Modeling the Multinuclear Redox-Active Manganese Enzymes. Synthesis, Structure, and Properties of a Bis(Dinuclear Mn(III)-μ-Oxo-Bis(μ-Acetato)) Complex. *Inorg. Chem.* **1995**, *34*, 3633–3645.

(150) Mandal, S. K.; Armstrong, W. H. A Novel Triply Bridged Dinuclear Manganese(III) Complex Containing the $[Mn_2O(OAc)_2]^{2+}$ Core: Synthesis, Crystal Structure and Properties of $[Mn_2(\mu\text{-}O)(\mu\text{-}OAc)_z(bpea)_2](C1O_4)_2$. *Inorg. Chim. Acta.***1995**, *229*, 261–270.

(151) Tanase, T.; Lippard, S. J. Dinuclear Manganese(II) Complexes with the $\{Mn_2(\mu\text{-}Carboxylato)_2\}^{2+}$ Core and Their Transformation to (μ-oxo)bis(μ-carboxylato)dimanganese(III)

Complexes. *Inorg. Chem.* **1995**, *34*, 4682–4690.

(152) Corbella, M.; Costa, R.; Ribas, J.; Fries, P. H.; Latour, J.-M.; Öhrström, L.; Solans, X.; Rodríguez, V. Structural and Magnetization Studies of a New (μ-Oxo)Bis(μ-Carboxylato)Dimanganese(III) Complex with a Terminal Hydroxo Ligand. *Inorg. Chem.* **1996**, *35*, 1857–1865.

(153) M. V. Rajasekharan, K. Rajender Reddy, S. S. Synthesis and Structural Characterization of an Unsymmetrical (μ-oxo)-di-(μ-acetato)manganese(III, III) Complex ($[Mn_2O(OAc)_2(H_2O)(NO_3)(bpy)_2](ClO_4)\cdot CH_3COOH$). *Polyhedron* **1996**, *15*, 4161–4168.

(154) Hage, R.; Gunnewegh, E. A.; Niël, J.; Tjan, F. S. B.; Weyhermüller, T.; Wieghardt, K. NMR Spectra of Dinuclear Manganese and Iron Compounds Containing 1,4,7-Triazacyclononane and 1,4,7-Trimethyl-1,4,7-Triazacyclononane. *Inorg. Chim. Acta.* **1998**, *268*, 43–48.

(155) Bolm, C.; Meyer, N.; Raabe, G.; Weyhermuller, T.; Bothe, E. A Novel Enantiopure Proline-Derived Triazacyclononane: Synthesis, Structure and Application of Its Manganese Complex. *Chem. Commun.* **2000**, 2435–2436.

(156) Ruiz, R.; Sangregorio, C.; Caneschi, A.; Rossi, P.; Gaspar, A. B.; Real, J. A.; Muñoz, M. C. A Novel Dimer of Oxo-di(acetato)-bridged Manganese(III) Dimers Complex of Potential Biological Significance. *Inorg. Chem. Commun.* **2000**, *3*, 361–367.

(157) Caada-Vilalta, C.; Huffman, J. C.; Streib, W. E.; Davidson, E. R.; Christou, G. Use of the Dicarboxylate Ligand M-Phenylenedipropionate for the Synthesis of New Mn/O Clusters. Synthesis, Characterization and Magnetic Properties. *Polyhedron* **2001**, *20*, 1375–1380.

(158) Chen, C.; Zhu, H.; Huang, D.; Wen, T.; Liu, Q.; Liao, D.; Cui, J. Syntheses, Structures and Magnetic Properties of Mono- and Di-Manganese Inclusion Compounds. *Inorg. Chim. Acta.* **2001**, *320*, 159–166.

(159) Brunold, T. C.; Gamelin, D. R.; Stemmler, T. L.; Mandal, S. K.; Armstrong, W. H.; Penner-Hahn, J. E.; Solomon, E. I. Spectroscopic Studies of Oxidized Manganese Catalase and μ-Oxo-Bridged Dimanganese(III) Model Complexes: Electronic Structure of the Active Site and Its Relation to Catalysis. *J. Am. Chem. Soc.* **1998**, *120*, 8724–8738.

(160) Arulsamy, N.; Glerup, J.; Hodgson, D. J. Mononuclear Iron(II), Manganese(II), and Nickel(II) and Tetranuclear Iron(III) Complexes of a New Hexadentate Ligand. *Inorg. Chem.* **1994**, *33*, 3043–3050.

(161) Fernández, G.; Corbella, M.; Aullón, G.; Maestro, M. A.; Mahía, J. New Dinuclear MnIII compounds with 2-MeC_6H_4COO and 2-FC_6H_4COO Bridges - Effect of Terminal Monodentate Ligands (H_2O, $ClO_4^-$and NO_3^-) on the Magnetic Properties. *Eur. J. Inorg. Chem.* **2007**, *3*, 1285–1296.

(162) Wieghardt, K.; Tolksdorf, I.; Herrmann, W. Coordination Chemistry of the Bimacrocyclic, Potentially Binucleating Ligand 1, 2-bis(1, 4, 7-triaza-1-cyclononyl)ethane (dtne). Electrochemistry of its First Transition Series Metal(II, III) Complexes. Characterization of the New Hemerythrin Model Comple. *Inorg. Chem.* **1985**, *24*, 1230–1235.

(163) Hedman, B.; Armstrong, W. H.; Lippard, S. J.; Co, M. S.; Hodgson, K. O. EXAFS Studies of Binuclear Iron Complexes as Models for Hemerythrin and Related Proteins. *Inorg. Chem.* **1986**, *25*, 3708–3711.

(164) Sessler, J. L.; Sibert, J. W.; Lynch, V.; Markert, J. T.; Wooten, C. L. Structure and Properties of a Tetranuclear Iron(III) Cage Complex. A Model for Hemerythrin. *Inorg. Chem.* **1993**, *32*, 621–626.

(165) Mimmi, M. C.; Miccichè, F.; Kooijman, H.; Spek, A. L.; Warzeska, S. T.; Bouwman, E. Dinuclear Iron Complexes of the Tridentate Ligand N,N-bis(2-ethyl-5-methyl-imidazol-4-

ylmethyl)aminopropane (biap). *Inorg. Chim. Acta.* **2002**, *340*, 197–200.

(166) Qian, J.; Wang, Q. L.; Gu, W.; Tian, J. L.; Xie, M. J.; Yan, S. P.; Liao, D. Z.; Cheng, P. Two Novel Dinuclear Iron(III) Complexes Containing μ-Oxo-Di-μ- Carboxylato Motif. Transition Metal Chemistry **2007**, *32*, 847–850.

(167) Qian, J.; Tian, J. L.; Feng, L.; Gu, W.; Zhao, X. J.; Yan, S. P. Synthesis, Crystal Structure, Magnetic Property, and Nuclease Activity of a Binuclear Iron(III) Complex. *J. Coord. Chem.* **2009**, *62*, 1260–1270.

(168) Visvaganesan, K.; Suresh, E.; Palaniandavar, M. Highly Selective Hydroxylation of Alkanes Catalyzed by (μ-Oxo)Bis(μ-Carboxylato)-Bridged Diiron(Iii) Complexes: Involvement of Mononuclear Iron(Iii) Species in Catalysis. *J. Chem. Soc. Dalt. Trans.* **2009**, *2* (19), 3814–3823.

(169) Marlin, D. S.; Olmstead, M. M.; Mascharak, P. K. Reaction of (μ-Oxo)Diiron(III) Core with Co2 in N-Methylimidazole: Formation of Mono(μ-Carboxylato)(μ-Oxo)Diiron(III) Complexes with N-Methylimidazole as Ligands. *Inorg. Chem.* **2003**, *42* (5), 1681–1687.

(170) Norman, R. E.; Yan, S.; Que, L.; Backes, G.; Ling, J.; Sanders-Loehr, J.; Zhang, J. H.; O'Connor, C. J. (μ-Oxo)(μ-Carboxylato)Diiron(III) Complexes with Distinct Iron Sites. Consequences of the Inequivalence and Its Relevance to Dinuclear Iron-Oxo Proteins. *J. Am. Chem. Soc.* **1990**, *112*, 1554–1562.

(171) Marlin, D. S.; Bill, E.; Rentschler, E.; Wieghardt, K. Long-Distance Magnetic Interaction between a $Mn^{III}Mn^{IV}$ (S=1/2) Core and an Organic Radical: A Spectroscopic Model for the S2Yz·State of Photosystem II. Angew. Chem. Int. Ed. **2002**, *1*, 4775–4779.

(172) Pal, S.; Chan, M. K.; Armstrong, W. H. Ground Spin State Variability in Manganese Oxo Aggregates. Demonstration of an S = 3/2 Ground State for $[Mn_3O_4(OH)(bpea)_3](ClO_4)_3$. *J. Am. Chem. Soc.* **1992**, *114*, 6398–6406.

(173) Karl Wieghardt, Ursula Bossek, Laszlo Zsolnai, Gottfried Huttner, Genevieve Blondin, Jean-Jacques Girerd, F. B. A Novel Mixed-Valent $Mn^{III}Mn^{IV}$-Dimer, $[L_2Mn_2(\mu\text{-}O)_2(\mu\text{-}MeCO_2)][BPh_4]_2$·MeCN: Crystal Structure, Magnetic Properties, and E.S.R. Spectrum (L = 1,4,7-Triazacyclononane). *J Chem. Soc., Chem. Commun.* **1987**, *2*, 651–653.

(174) Pal, S.; Gohdes, J. W.; Wilisch, W. C. A.; Armstrong, W. H. Synthesis, Structure, and Properties of a [Manganese] Complex That Consists of an $\{Mn_2O_2(O_2CCH_3)\}^{2+}$ Core and a Spanning Hexadentate Ligand. *Inorg. Chem.* **1992**, *31*, 713–716.

(175) Lal, T. K.; Mukherjee, R. Modeling the Oxygen-Evolving Complex of Photosystem II. Synthesis, Redox Properties, and Core Interconversion Studies of Dimanganese Complexes Having $\{Mn^{III}{}_2(\mu\text{-}O)(\mu\text{-}OAc)_2\}^{2+}$, $\{Mn^{III}Mn^{IV}(\mu\text{-}O)_2(\mu\text{-}OAc)\}^{2+}$, and $\{Mn^{IV}{}_2(\mu\text{-}O)_2(\mu\text{-}OAc)\}^{3+}$ Cores with MeL as a Terminal Ligand: A New Asymmetric Mixed-Valence Core. *Inorg. Chem.* **1998**, *37*, 2373–2382.

(176) Schäfer, K. O.; Bittl, R.; Zweygart, W.; Lendzian, F.; Haselhorst, G.; Weyhermüller, T.; Wieghardt, K.; Lubitz, W. Electronic Structure of Antiferromagnetically Coupled Dinuclear Manganese (Mn(III)Mn(IV)) Complexes Studied by Magnetic Resonance Techniques. *J. Am. Chem. Soc.* **1998**, *120* (50), 13104–13120.

(177) Christou, G.; Hendrickson, D. N. Mixed Valence Manganese-(Ii,Iii) and-(III, IV) Dinuclear Complexes: Preparation, Structure, Magnetochemistry, and E.S.R. Spectra of $Mn_2(biphen)_2(biphenH)(Bpy)_2$ and $Mn_2O_2Cl_2(OAc)(Bpy)_2$ ($BiphenH_2$ = 2,2'-Biphenol, Bpy = 2,2'-Bipyridine). *J. Chem. Soc., Chem. Commun.* **1988**, *81*, 700–702.

(178) Abdolahzadeh, S.; Boyle, N. M.; Hoogendijk, M. L.; Hage, R.; De Boer, J. W.; Browne, W. R. The Role of Carboxylato Ligand Dissociation in the Oxidation of Chrysin with H_2O_2 catalysed by $[Mn_2^{III,\,IV}(\mu\text{-}CH_3COO)(\mu\text{-}O)_2(Me_4dtne)](PF_6)_2$. *Dalt. Trans.* **2014**, *43*, 6322–6332.

(179) Wieghardt, B. K.; Bossek, U.; Bonvoisin, J.; Girerd, P. B. J.; Nuber, B. Dinuclear

Manganese(II,III,IV) Model Complexes for the Active Center of the Metalloprotein Photosystem II: Synthesis, Magnetism, and Crystal Structure of $[LMn^{III}(\mu\text{-}O)(\mu\text{-}CH_3CO_2)_2Mn^{IV}L][C1O_4]_3$ (L = N, N',N"-trimethyl-l,4,7-triazacyclononane). *Angew. Chem. Int. Ed. Engl.* **1986**, *25*, 1030–1031.

(180) Wieghardt, B. K.; Bossek, U.; Bonvoisin, J.; Girerd, P. B. J.; Nuber, B. Dinuclear Manganese(II,III,IV) Model Complexes for the Active Center of the Metalloprotein Photosystem II: Synthesis, Magnetism, and Crystal Structure of $[LMn^{III}(\mu\text{-}O)(\mu\text{-}CH_3CO_2)_2Mn^{IV}L][C1O_4]_3$ (L = N, N',N"-trimethyl-l,4,7-triazacyclononane). *Angew. Chem. Int. Ed. Engl.* **1986**, *25*, 1030–1031.

(181) Sessler, J. L.; Sibert, J. W.; Lynch, V. Model Studies Related to Hemerythrin. Synthesis and Characterization of a Bridged Tetranuclear Iron(III) Complex. *Inorg. Chem.* **1990**, *29*, 4143–4146.

(182) Toftlund, H.; Murray, K. S.; Zwack, P. R.; Taylor, L. F.; Anderson, O. P. Structural and Electronic Properties of Tetranuclear Iron(III) Pyridylamine Complexes Containing Cofacial Pairs of μ-Oxo-Bis(μ-Acetato)Iron(III) Moieties. Models for Met Hemerythrins. *J. Chem. Soc., Chem. Commun.* **1986**, 191–193.

(183) Gómez, V.; Corbella, M.; Fernández, G.; Roubeau, O.; Teat, S. J.; Maestro, M. A. Aliphatic Dicarboxylate Ligands Assemble Weakly Coupled Molecular Pairs of $[Mn^{III}]_2$ Units. *Eur. J. Inorg. Chem.* **2012**, 2359–2367.

(184) Batten, S. R.; Chen, B.; Vittal, J. J. Coordination Polymers/MOFs: Structures, Properties and Applications. *Chempluschem* **2016**, *81*, 669–670.

17

(185) Tian, A. X.; Ying, J.; Peng, J.; Sha, J. Q.; Pang, H. J.; Zhang, P. P.; Chen, Y.; Zhu, M.; Su, Z. M. Tuning the Dimensionality of the Coordination Polymer Based on Polyoxometalate by Changing the Spacer Length of Ligands. *Cryst. Growth Des.* **2008**, *8*, 3717–3724.

(186) Pan, L.; Frydel, T.; Sander, M. B.; Huang, X.; Li, J. The Effect of PH on the Dimensionality of Coordination Polymers. *Inorg. Chem.* **2001**, *40*, 1271–1283.

(187) Wang, Y. T.; Tang, G. M.; Wu, Y.; Qin, X. Y.; Qin, D. W. Metal-Controlled Assembly Tuning the Topology and Dimensionality of Coordination Polymers of Ag(I), Cd(II) and Zn(II) with the Flexible 2-(1H-imidazole-1-yl)Acetic acid (Hima). *J. Mol. Struct.* **2007**, *831*, 61–68.

(188) Yamada, T.; Otsubo, K.; Makiura, R.; Kitagawa, H. Designer Coordination Polymers: Dimensional Crossover Architectures and Proton Conduction. *Chem. Soc. Rev.* **2013**, *42*, 6655–6669.

(189) Amoore, J. J. M.; Black, C. A.; Hanton, L. R.; Spicer, M. D. Increasing Structural Dimensionality in Ag (I) Multimodal Thioether Pyrazine Ligand. Crystal Growth & Design, 2005, *5*, 1255-1261.

(190) Ghosh, S. K.; Azhakar, R.; Kitagawa, S. Control of Structure Dimensionality and Functional Studies of Flexible CuII Coordination Polymers. *Chem. - An Asian J.* **2009**, *4*, 870–875.

(191) Dybtsev, D. N.; Chun, H.; Kim, K. Rigid and Flexible: A Highly Porous Metal-Organic Framework with Unusual Guest-Dependent Dynamic Behavior. *Angew. Chemie. Int. Ed.* **2004**, *116*, 5143–5146.

(192) Bradshaw, D.; Claridge, J. B.; Cussen, E. J.; Prior, T. J.; Rosseinsky, M. J. Design, Chirality, and Flexibility in Nanoporous Molecule-Based Materials. *Acc. Chem. Res.* **2005**, *38*, 273–282.

(193) Khullar, S.; Mandal, S. K. Effect of Spacer Atoms in the Dicarboxylate Linkers on the Formation of Coordination Architectures-Molecular Rectangles vs 1D Coordination Polymers: Synthesis, Crystal Structures, Vapor/Gas Adsorption Studies, and Magnetic Properties. *Cryst. Growth Des.* **2014**, *14*, 6433–6444.

(194) Batten, S. R.; Neville, S. M.; Turner, D. R. Coordination Polymers: Design, Analysis and Application; Royal Society of Chemistry: Cambridge, U.K., **2009**.

(195) Zhang, C.; Li, Y.; Xu, H.; Ma, J.; Zheng, H. The Mutation in the Single-Crystal Structural Transformation Process, Induced by the Combined Stimuli of Temperature and Solvent. *Chem. Eur. J.* **2018**, *24*, 327–331.

(196) He, Y. C.; Yang, J.; Liu, Y. Y.; Ma, J. F. Series of Solvent-Induced Single-Crystal to Single-Crystal Transformations with Different Sizes of Solvent Molecules. *Inorg. Chem.* **2014**, *53*, 7527–7533.

(197) Du Plessis, M.; Smith, V. J.; Barbour, L. J. Single-Crystal to Single-Crystal Guest Exchange and Phase Transformations in a Porous Metallocycle. *CrystEngComm* **2014**, *16*, 4126–4132.

(198) *APEX2, SADABS and SAINT*; Bruker AXS Inc, Madison, WI, USA, 2008.

(199) Dolomanov, O. V.; Bourhis, L. J.; Gildea, R. J.; Howard, J. A. K.; Puschmann, H. OLEX2 : A Complete Structure Solution, Refinement and Analysis Program. *J. Appl. Crystallogr.***2009**, *42*, 339–341.

(200) Sheldrick, G. M. SHELXT – Integrated Space-Group and Crystal-Structure Determination. *Acta Crystallogr. Sect. A Found. Adv.***2015**, *71*, 3–8.

(201) Sheldrick, G. M. Crystal Structure Refinement with SHELXL. *Acta Crystallogr. Sect. C Struct. Chem.***2015**, *71*, 3–8.

(202) Macrae, C. F.; Bruno, I. J.; Chisholm, J. A.; Edgington, P. R.; McCabe, P.; Pidcock, E.; Rodriguez-Monge, L.; Taylor, R.; van de Streek, J.; Wood, P. A. Mercury CSD 2.0 – New Features for the Visualization and Investigation of Crystal Structures. *J. Appl. Crystallogr.***2008**, *41*, 466–470.

(203) Spek, A. L. *PLATON, Version 1.62*; University of Utrecht, 1999.

(204) Spek, A. L. Single-Crystal Structure Validation with the Program PLATON. *J. Appl. Crystallogr.***2003**, *36*, 7–13.

(205) Khullar, S.; Mandal, S. K. Structural Diversity of Mn(II) Complexes with Acetylene Dicarboxylate and Hexadentate Ancillary Ligands under Ambient Conditions: Effect of Methylene Chain Length on Coordination Architectures. *Cryst. Growth Des.* **2013**, *13*, 3116−3125.

APPENDIX

Table A1. Crystal data and structure refinement parameters for **5**, and **6·CH$_3$CN.**

Identification code	**5**	**6·CH$_3$CN**
Empirical formula	$C_{72}H_{100}Cl_{3.5}Mn_4N_{12}O_{34}$	$C_{80}H_{98}Cl_4Mn_4N_{14}O_{26}$
Formula weight	2021.47	2033.28
Temperature/K	296.15	296.0
Crystal system	monoclinic	triclinic
Space group	*C*2/*m*	*P*-1
a/Å	21.1281(15)	9.040(6)
b/Å	29.320(2)	14.536(10)
c/Å	15.840(2)	17.500(12)
α/°	90	94.017(17)
β/°	112.255(4)	98.289(16)
γ/°	90	103.91(2)
Volume/Å^3	9081.2(16)	2196(3)
Z	4	1
ρ_{calc}(g/cm^3)	1.479	1.538
μ/mm^{-1}	0.735	0.769
F(000)	4190.0	1052.0
Radiation	MoKα (λ = 0.71073)	MoKα (λ = 0.71073)
2Θ range for data collection/°	2.504 to 50.252	3.54 to 50.504
Index ranges	-25 ≤ h ≤ 25, -35 ≤ k ≤ 33, -18 ≤ l ≤ 18	-10 ≤ h ≤ 7, -17 ≤ k ≤ 16, -20 ≤ l ≤ 20
Reflections collected	41806	25292
Independent reflections	8236 [R_{int} = 0.2111, R_{sigma} = 0.2211]	7739 [R_{int} = 0.1352, R_{sigma} = 0.1852]
Data/restraints/parameters	8236/3/603	7739/0/578
Goodness-of-fit on F^2	1.139	0.951
Final R indexes [I>=2σ (I)]	R_1 = 0.1215, wR_2 = 0.3259	R_1 = 0.0672, wR_2 = 0.1290
Final R indexes [all data]	R_1 = 0.2620, wR_2 = 0.4086	R_1 = 0.1842, wR_2 = 0.1688
Largest diff. peak/hole / e Å^{-3}	2.56/-1.93	0.47/-0.43

Table A2. Crystal data and structure refinement parameters for **13·2CH$_3$CN** and **15·2CH$_3$CN**.

Identification code	**13·2CH$_3$CN**	**15·2CH$_3$CN**
Empirical formula	$C_{68}H_{92}N_{12}O_{26}Cl_4Mn_4$	$C_{152}H_{168}Cl_8Mn_8N_{24}O_{55}$
Formula weight	1855.10	3934.21
Temperature/K	296.0	296.0
Crystal system	triclinic	triclinic
Space group	*P*-1	*P*-1
a/Å	9.511(3)	14.121(10)
b/Å	14.913(6)	19.427(5)
c/Å	15.434(5)	19.500(6)
α/°	92.102(5)	119.277(15)
β/°	92.933(11)	94.54(2)
γ/°	108.443(9)	96.66(2)
Volume/Å^3	2070.7(12)	4577(4)
Z	1	1
ρ_{calc}(g/cm^3)	1.488	1.427
μ/mm^{-1}	0.807	0.736
F(000)	960.0	2024.0
Radiation	MoKα (λ = 0.71073)	MoKα (λ = 0.71073)
2Θ range for data collection/°	2.64 to 50.12	2.424 to 49.97
Index ranges	$-11 \le h \le 11$, $-17 \le k \le 17$, $-18 \le l \le 18$	$-15 \le h \le 16$, $-23 \le k \le 21$, $-23 \le l \le 23$
Reflections collected	20834	26797
Independent reflections	7267 [R_{int} = 0.0703, R_{sigma} = 0.1118]	14661 [R_{int} = 0.0490, R_{sigma} = 0.1247]
Data/restraints/parameters	7267/0/552	14661/0/1095
Goodness-of-fit on F^2	0.955	1.353
Final R indexes [I>=2σ (I)]	R_1 = 0.0558, wR_2 = 0.1295	R_1 = 0.1356, wR_2 = 0.3670
Final R indexes [all data]	R_1 = 0.1186, wR_2 = 0.1765	R_1 = 0.2208, wR_2 = 0.4192
Largest diff. peak/hole / e Å^{-3}	0.58/-0.79	1.51/-0.67

Table A3. Crystal data and structure refinement parameters for **19·2CH$_3$CN** and **27·2CH$_3$CN·H$_2$O**.

Identification code	**19·2CH$_3$CN**	**27·2CH$_3$CN·H$_2$O**
Empirical formula	$C_{70}H_{85}Cl_5Fe_4N_{13}O_{30}$	$C_{72}HN_{12}O_{24}Cl_4Mn_4$
Formula weight	1885.73	1779.41
Temperature/K	273.15	296.15
Crystal system	monoclinic	triclinic
Space group	$P2_1/c$	P-1
a/Å	19.1762(5)	15.003(3)
b/Å	14.3836(4)	17.441(4)
c/Å	33.8531(8)	17.507(4)
α/°	90	72.322(12)
β/°	92.502(2)	69.181(12)
γ/°	90	83.188(12)
Volume/Å^3	9328.6(4)	4079.5(16)
Z	4	2
ρ_{calc}(g/cm^3)	1.343	1.449
μ/mm^{-1}	0.829	0.816
F(000)	3725.0	1754.0
Radiation	MoKα (λ = 0.71073)	MoKα (λ = 0.71073)
2Θ range for data collection/°	2.126 to 42.826	2.45 to 50.512
Index ranges	-19 ≤ h ≤ 19, -14 ≤ k ≤ 13, -34 ≤ l ≤ 34	-17 ≤ h ≤ 17, -20 ≤ k ≤ 20, -20 ≤ l ≤ 18
Reflections collected	39589	36044
Independent reflections	10568 [R_{int} = 0.0639, R_{sigma} = 0.0631]	14428 [R_{int} = 0.0431, R_{sigma} = 0.0720]
Data/restraints/parameters	10568/6/1064	14428/12/1045
Goodness-of-fit on F^2	1.397	1.035
Final R indexes [I>=2σ (I)]	R_1 = 0.1140, wR_2 = 0.3217	R_1 = 0.0618, wR_2 = 0.1629
Final R indexes [all data]	R_1 = 0.1537, wR_2 = 0.3591	R_1 = 0.1079, wR_2 = 0.1909
Largest diff. peak/hole / e Å^{-3}	1.71/-1.47	1.02/-0.66

Table A4. Crystal data and structure refinement parameters for **29·2CH$_3$CN** and **34·H$_2$O**.

Identification code	**29·2CH$_3$CN**	**34·H$_2$O**
Empirical formula	$C_{70}H_{84}Cl_4Mn_4N_{16}O_{24}$	$C_{66}H_{82}Cl_4Mn_4N_{12}O_{25}$
Formula weight	1895.09	1804.99
Temperature/K	296.15	296.0
Crystal system	monoclinic	triclinic
Space group	*C*2/c	*P*-1
a/Å	25.145(3)	15.025(5)
b/Å	16.928(2)	17.455(7)
c/Å	20.217(2)	18.551(10)
α/°	90	117.062(19)
β/°	106.267(7)	98.88(3)
γ/°	90	102.77(2)
Volume/Å^3	8260.8(18)	4039(3)
Z	4	2
ρ_{calc}(g/cm^3)	1.524	1.484
μ/mm^{-1}	0.811	0.824
F(000)	3904.0	1860.0
Radiation	MoKα (λ = 0.71073)	MoKα (λ = 0.71073)
2Θ range for data collection/°	2.938 to 50.33	2.578 to 41.744
Index ranges	-29 ≤ h ≤ 30, -19 ≤ k ≤ 19, -23 ≤ l ≤ 23	-14 ≤ h ≤ 15, -17 ≤ k ≤ 17, -18 ≤ l ≤ 18
Reflections collected	41623	22811
Independent reflections	7328 [R_{int} = 0.1068, R_{sigma} = 0.1170]	8116 [R_{int} = 0.3176, R_{sigma} = 0.4643]
Data/restraints/parameters	7328/0/535	8116/9/1013
Goodness-of-fit on F^2	0.974	0.910
Final R indexes [I>=2σ (I)]	R_1 = 0.0639, wR_2 = 0.1610	R_1 = 0.1191, wR_2 = 0.2767
Final R indexes [all data]	R_1 = 0.1269, wR_2 = 0.1838	R_1 = 0.3073, wR_2 = 0.3988
Largest diff. peak/hole / e Å^{-3}	0.76/-1.01	1.05/-0.98

Table A5. Crystal data and structure refinement parameters for **35·2H$_2$O** and **38·2CH$_3$OH**.

Identification code	**35·2H$_2$O**	**38·2CH$_3$OH**
Empirical formula	$C_{20}H_{26}MnN_3O_8$	$C_{22}H_{33}N_3NiO_8$
Formula weight	491.38	526.22
Temperature/K	290	100
Crystal system	triclinic	triclinic
Space group	*P*-1	*P*-1
a/Å	8.2893(10)	8.0774(7)
b/Å	9.4799(12)	11.5857(11)
c/Å	14.7934(18)	13.0373(12)
α/°	71.973(3)	81.520(3)
β/°	87.748(3)	85.540(2)
γ/°	88.463(3)	87.130(3)
Volume/Å^3	1104.4(2)	1202.15(19)
Z	2	2
ρ_{calc}(g/cm^3)	1.478	1.454
μ/mm^{-1}	0.649	0.859
F(000)	512.0	556.0
Radiation	MoKα (λ = 0.71073)	MoKα (λ = 0.71073)
2Θ range for data collection/°	2.896 to 50.1	3.166 to 50.01
Index ranges	-9 ≤ h ≤ 9, -11 ≤ k ≤ 11, -17 ≤ l ≤ 17	-7 ≤ h ≤ 9, -13 ≤ k ≤ 13, -15 ≤ l ≤ 15
Reflections collected	16104	15572
Independent reflections	3887 [R_{int} = 0.0570, R_{sigma} = 0.0492]	4238 [R_{int} = 0.0374, R_{sigma} = 0.0399]
Data/restraints/parameters	3887/0/297	4238/0/317
Goodness-of-fit on F^2	0.891	1.051
Final R indexes [I>=2σ (I)]	R_1 = 0.0444, wR_2 = 0.1223	R_1 = 0.0417, wR_2= 0.1019
Final R indexes [all data]	R_1 = 0.0543, wR_2 = 0.1318	R_1 = 0.0543, wR_2 = 0.1123
Largest diff. peak/hole / e Å^{-3}	0.58/-0.43	0.84/-0.38

Table A6. Crystal data and structure refinement parameters for **39·2CH$_3$OH·H$_2$O** and **46**.

Identification code	**39·2CH$_3$OH·H$_2$O**	**46**
Empirical formula	$C_{86}H_{112}N_{12}Ni_4O_{31}$	$C_{21}H_{27.5}N_3NiO_{7.5}$
Formula weight	2044.64	479.15
Temperature/K	296 K	296.15
Crystal system	monoclinic	triclinic
Space group	$P2_1/c$	P-1
a/Å	14.767(7)	7.3425(12)
b/Å	18.571(8)	11.6619(18)
c/Å	17.019(8)	14.148(2)
α/°	90	68.781(5)
β/°	98.973(12)	82.223(5)
γ/°	90	84.723(5)
Volume/Å^3	4610(4)	1117.7(3)
Z	4	2
ρ_{calc}(g/cm^3)	1.473	1.424
μ/mm^{-1}	0.893	0.913
F(000)	2144.0	502.0
Radiation	MoKα (λ = 0.71073)	MoKα (λ = 0.71073)
2Θ range for data collection/°	2.792 to 50.122	3.106 to 50.104
Index ranges	-16 ≤ h ≤ 16, -21 ≤ k ≤ 7, -19 ≤ l ≤ 9	-8 ≤ h ≤ 8, -13 ≤ k ≤ 12, -16 ≤ l ≤ 16
Reflections collected	8879	17809
Independent reflections	7123 [R_{int} = 0.0591, R_{sigma} = 0.1687]	3944 [R_{int} = 0.0758, R_{sigma} = 0.0784]
Data/restraints/parameters	7123/3/621	3944/0/313
Goodness-of-fit on F^2	0.942	1.032
Final R indexes [I>=2σ (I)]	R_1 = 0.0906, wR_2= 0.2039	R_1 = 0.0572, wR_2 = 0.1333
Final R indexes [all data]	R_1 = 0.1674, wR_2 = 0.2563	R_1 = 0.0874, wR_2 = 0.1486
Largest diff. peak/hole / e Å^{-3}	0.75/-0.47	1.30/-0.70

Table A7. Crystal data and structure refinement parameters for **52** and **53·$CH_3OH·2H_2O$**.

Identification code	**52**	**53·$CH_3OH·2H_2O$**
Empirical formula	$C_{21}H_{23.5}CoN_3O_{6.5}S$	$C_{21.5}H_{24}CoN_3O_{5.5}S$
Formula weight	512.92	609.34
Temperature/K	100	100
Crystal system	monoclinic	triclinic
Space group	$P2_1/c$	$P\text{-}1$
a/Å	8.0678(7)	9.904(13)
b/Å	15.1333(11)	15.833(14)
c/Å	18.8104(16)	16.956(13)
α/°	90	117.167(15)
β/°	94.034(3)	90.330(14)
γ/°	90	105.937(15)
Volume/$Å^3$	2290.9(3)	2248(4)
Z	4	4
$\rho_{calc}(g/cm^3)$	1.487	1.801
μ/mm^{-1}	0.885	1.735
F(000)	1062.0	1257.0
Radiation	MoKα (λ = 0.71073)	MoKα (λ = 0.71073)
2Θ range for data collection/°	3.458 to 50.102	4.328 to 50.204
Index ranges	$-9 \le h \le 9$, $-10 \le k \le 17$, $-22 \le l \le 18$	$-11 \le h \le 11$, $-14 \le k \le 18$, $-20 \le l \le 20$
Reflections collected	7838	10631
Independent reflections	4013 [R_{int} = 0.0366, R_{sigma} = 0.0715]	7158 [R_{int} = 0.0821, R_{sigma} = 0.1567]
Data/restraints/parameters	4013/0/272	7158/0/585
Goodness-of-fit on F^2	1.118	1.039
Final R indexes [I>=2σ (I)]	R_1 = 0.0599, wR_2 = 0.1511	R_1 = 0.0900, wR_2 = 0.1975
Final R indexes [all data]	R_1 = 0.0826, wR_2 = 0.1688	R_1 = 0.1620, wR_2 = 0.2333
Largest diff. peak/hole / e $Å^{-3}$	1.26/-1.06	1.83/-0.53

Table A8. Crystal data and structure refinement parameters for **54·H_2O** and **55·8H_2O.**

Identification code	**54·H_2O**	**55·8H_2O**
Empirical formula	$C_{22}H_{25}CoN_3O_6S$	$C_{23}H_{36.5}CoN_2O_{13}S$
Formula weight	518.44	653.55
Temperature/K	100	100
Crystal system	monoclinic	monoclinic
Space group	$P2_1/c$	$P2_1/n$
a/Å	9.1292(10)	8.8159(3)
b/Å	16.1980(18)	22.6884(9)
c/Å	17.632(2)	16.8728(7)
α/°	90	90
β/°	92.436(7)	103.007(2)
γ/°	90	90
Volume/Å^3	2605.0(5)	3288.3(2)
Z	4	4
ρ_{calc}(g/cm^3)	1.322	1.320
μ/mm^{-1}	0.778	0.645
F(000)	1076.0	1372.0
Radiation	MoKα (λ = 0.71073)	MoKα (λ = 0.71073)
2Θ range for data collection/°	3.416 to 50.026	3.06 to 49.908
Index ranges	$-10 \le h \le 10$, $-19 \le k \le 19$, $-20 \le l \le 15$	$-10 \le h \le 10$, $-26 \le k \le 26$, $-11 \le l \le 20$
Reflections collected	19880	24513
Independent reflections	4589 [R_{int} = 0.0702, R_{sigma} = 0.0668]	5764 [R_{int} = 0.0584, R_{sigma} = 0.0510]
Data/restraints/parameters	4589/1/307	5764/0/417
Goodness-of-fit on F^2	1.049	1.061
Final R indexes [I>=2σ (I)]	R_1 = 0.0508, wR_2 = 0.1178	R_1 = 0.0722, wR_2 = 0.2121
Final R indexes [all data]	R_1 = 0.0830, wR_2 = 0.1314	R_1 = 0.0892, wR_2 = 0.2276
Largest diff. peak/hole / e Å^{-3}	0.66/-0.47	1.71/-0.66

Table A9. Crystal data and structure refinement parameters for **56** and **57**.

Identification code	**56**	**57**
Empirical formula	$C_{20}H_{27}N_3NiO_{8.5}S$	$C_{44}H_{52}N_6Ni_2O_{12}S_2$
Formula weight	536.21	986.54
Temperature/K	100	296.15
Crystal system	triclinic	triclinic
Space group	*P*-1	P-1
a/Å	13.756(3)	9.797(5)
b/Å	14.520(3)	15.859(8)
c/Å	15.620(3)	16.889(9)
α/°	90.171(5)	116.604(9)
β/°	112.414(5)	90.075(11)
γ/°	117.746(5)	107.060(12)
Volume/Å^3	2489.7(8)	2216(2)
Z	4	2
ρ_{calc}(g/cm^3)	1.431	1.479
μ/mm^{-1}	0.913	1.012
F(000)	1120.0	981.0
Radiation	MoKα (λ = 0.71073)	MoKα (λ = 0.71073)
2Θ range for data collection/°	2.892 to 50.442	2.73 to 50.588
Index ranges	-16 ≤ h ≤ 16, -16 ≤ k ≤ 17, -18 ≤ l ≤ 18	-10 ≤ h ≤ 11, -18 ≤ k ≤ 18, -20 ≤ l ≤ 20
Reflections collected	41670	22617
Independent reflections	8901 [R_{int} = 0.0855, R_{sigma} = 0.0790]	7823 [R_{int} = 0.1378, R_{sigma} = 0.2220]
Data/restraints/parameters	8901/0/627	7823/0/605
Goodness-of-fit on F^2	2.099	0.959
Final R indexes [I>=2σ (I)]	R_1 = 0.1161, wR_2 = 0.3025	R_1 = 0.1308, wR_2 = 0.3202
Final R indexes [all data]	R_1 = 0.1391, wR_2 = 0.3192	R_1 = 0.2137, wR_2 = 0.3770
Largest diff. peak/hole / e Å^{-3}	1.13/-0.82	2.64/-1.45

Table A10. Crystal data and structure refinement parameters for **58·CH$_3$OH·2H$_2$O** and **59·2CH$_3$OH·5H$_2$O**.

Identification code	**58·CH$_3$OH·2H$_2$O**	**59·2CH$_3$OH·5H$_2$O**
Empirical formula	$C_{23}H_{33}N_3NiO_9S$	$C_{22}H_{18}N_3NiO_4S$
Formula weight	586.29	479.28
Temperature/K	296.15	296.15
Crystal system	monoclinic	monoclinic
Space group	$P2_1/n$	$P2_1/n$
a/Å	8.844(3)	9.686(3)
b/Å	21.452(7)	14.721(6)
c/Å	16.562(5)	14.221(5)
α/°	90	90
β/°	103.297(5)	93.285(19)
γ/°	90	90
Volume/Å^3	3058.1(17)	2024.4(12)
Z	4	4
ρ_{calc}(g/cm^3)	1.273	1.573
μ/mm^{-1}	0.751	1.103
F(000)	1232.0	953.0
Radiation	MoKα (λ = 0.71073)	MoKα (λ = 0.71073)
2Θ range for data collection/°	3.16 to 50.156	3.986 to 50.482
Index ranges	$-10 \le h \le 10$, $-21 \le k \le 25$, $-19 \le l \le 19$	$-11 \le h \le 11$, $-17 \le k \le 17$, $-16 \le l \le 16$
Reflections collected	21543	14417
Independent reflections	5418 [R_{int} = 0.0308, R_{sigma} = 0.0256]	3608 [R_{int} = 0.1684, R_{sigma} = 0.1812]
Data/restraints/parameters	5418/0/344	3608/0/280
Goodness-of-fit on F^2	1.137	0.941
Final R indexes [I>=2σ (I)]	R_1 = 0.0504, wR_2 = 0.1423	R_1 = 0.0680, wR_2 = 0.1562
Final R indexes [all data]	R_1 = 0.0542, wR_2 = 0.1489	R_1 = 0.1193, wR_2 = 0.1820
Largest diff. peak/hole / e Å^{-3}	1.15/-0.80	0.48/-0.82

Table A11. Crystal data and structure refinement parameters for **60·CH$_3$OH·2H$_2$O** and **61·CH$_3$OH**.

Identification code	**60·CH$_3$OH·2H$_2$O**	**61·CH$_3$OH**
Empirical formula	$C_{86}H_{98}Cd_4N_{12}O_{23}S_4$	$C_{23}H_2CdN_3O_5S$
Formula weight	2245.65	827.52
Temperature/K	100 (K)	100
Crystal system	Monoclinic	monoclinic
Space group	$P2_1/c$	$P2_1$
a/Å	17.1442 (15)	9.774(2)
b/Å	14.4858 (12)	17.421(4)
c/Å	19.3003 (17)	14.549(3)
α/°	90	90
β/°	112.614 (4)	91.459(13)
γ/°	90	90
Volume/Å^3	4424.7 (7)	2476.6(9)
Z	2	4
ρ_{calc}(g/cm^3)	1.686	2.219
μ/mm^{-1}	1.125	1.944
F(000)	2276.0	1648.0
Radiation	0.71073	MoKα (λ = 0.71073)
2Θ range for data collection/°	3.624 to 25.145	3.648 to 50.224
Index ranges		$-11 \leq h \leq 11$, $-20 \leq k \leq 18$, $-17 \leq l \leq 9$
Reflections collected	36160	13706
Independent reflections	7877	7611 [R_{int} = 0.0578, R_{sigma}= 0.1052]
Data/restraints/parameters	585	7611/1/597
Goodness-of-fit on F^2	1.024	0.991
Final R indexes [I>=2σ (I)]	0.0308/0.0631	R_1 = 0.0789, wR_2 = 0.2041
Final R indexes [all data]	0.0465/0.01685	R_1 = 0.1114, wR_2 = 0.2305
Largest diff. peak/hole / e Å^{-3}	0.76/-0.73	2.29/-1.11
Flack parameter	-	0.01(3)

Table A12. Crystal data and structure refinement parameters for **62** and **64**.

Identification code	**62**	**64**
Empirical formula	$C_{88}H_{72}Cd_4N_{12}O_{16}S_4$	$C_{26}H_{37.5}CoN_3O_{10.25}$
Formula weight	2131.41	615.02
Temperature/K	100	100
Crystal system	triclinic	monoclinic
Space group	*P*-1	$P2_1/n$
a/Å	9.148(10)	11.1046(10)
b/Å	21.06(3)	21.6879(17)
c/Å	27.46(3)	13.2068(10)
α/°	88.98(2)	90
β/°	90	94.484(4)
γ/°	90	90
Volume/Å^3	5290(11)	3170.9(4)
Z	2	4
ρ_{calc}(g/cm^3)	1.338	1.288
μ/mm^{-1}	0.932	0.596
F(000)	2136.0	1294.0
Radiation	MoKα (λ = 0.71073)	MoKα (λ = 0.71073)
2Θ range for data collection/°	1.484 to 50.052	3.618 to 50.14
Index ranges	$-10 \leq h \leq 8$, $-24 \leq k \leq 24$, $-32 \leq l \leq 32$	$-13 \leq h \leq 7$, $-25 \leq k \leq 23$, $-15 \leq l \leq 15$
Reflections collected	34034	24518
Independent reflections	16123 [R_{int} = 0.2117, R_{sigma} = 0.5753]	5587 [R_{int} = 0.0478, R_{sigma} = 0.0422]
Data/restraints/parameters	16123/1/1108	5587/0/407
Goodness-of-fit on F^2	0.870	1.093
Final R indexes [I>=2σ (I)]	R_1 = 0.1386, wR_2 = 0.3571	R_1 = 0.0683, wR_2 = 0.2156
Final R indexes [all data]	R_1 = 0.3000, wR_2 = 0.4256	R_1 = 0.0868, wR_2 = 0.2321
Largest diff. peak/hole / e Å^{-3}	3.69/-0.89	2.18/-0.77

Table A13. Crystal data and structure refinement parameters for **66·CH$_3$OH·5H$_2$O** and **67·2CH$_3$OH·11H$_2$O**.

Identification code	**66·CH$_3$OH·5H$_2$O**	**67·2CH$_3$OH·11H$_2$O**
Empirical formula	$C_{26}H_{43}N_2NiO_{11.5}$	$C_{68}H_{89}Co_3N_9O_{27.5}$
Formula weight	626.33	1649.27
Temperature/K	100	100
Crystal system	monoclinic	triclinic
Space group	$P2_1/n$	P-1
a/Å	11.2169(4)	11.0181(6)
b/Å	21.4229(6)	16.7681(10)
c/Å	13.0703(4)	22.4974(12)
α/°	90	75.716(2)
β/°	94.151(2)	77.141(2)
γ/°	90	77.842(2)
Volume/Å^3	3132.53(17)	3873.2(4)
Z	4	2
ρ_{calc}(g/cm^3)	1.328	1.414
μ/mm^{-1}	0.678	0.720
F(000)	1332.0	1722.0
Radiation	MoKα (λ = 0.71073)	MoKα (λ = 0.71073)
2Θ range for data collection/°	3.658 to 50.126	1.898 to 50.026
Index ranges	-9 ≤ h ≤ 13, -25 ≤ k ≤ 25, -15 ≤ l ≤ 15	-13 ≤ h ≤ 13, -19 ≤ k ≤ 19, -26 ≤ l ≤ 26
Reflections collected	25863	55281
Independent reflections	5553 [R_{int} = 0.0238, R_{sigma} = 0.0193]	13603 [R_{int} = 0.0570, R_{sigma} = 0.0601]
Data/restraints/parameters	5553/0/404	13603/3/1023
Goodness-of-fit on F^2	1.103	1.047
Final R indexes [I>=2σ (I)]	R_1 = 0.0746, wR_2 = 0.2251	R_1 = 0.0691, wR_2 = 0.1818
Final R indexes [all data]	R_1 = 0.0801, wR_2 = 0.2307	R_1 = 0.0953, wR_2 = 0.2024
Largest diff. peak/hole / e Å^{-3}	1.94/-0.75	1.56/-0.71

Table A14. Selected Bond lengths (Å) for **5.**

Mn1-O1	1.963(3)	Mn2-O3	2.177(3)
Mn1-O2	2.224(3)	Mn2-O7	1.990(3)
Mn1-O8	1.799(3)	Mn2-O8	1.791(3)
Mn1-N5	2.154(4)	Mn2-N1	2.126(4)
Mn1-N22	2.272(4)	Mn2-N2	2.201(4)
Mn1-N23	2.058(4)	Mn2-N21	2.079(4)

Table A15. Selected Bond lengths (Å) for **6·CH_3CN.**

Mn1-O1	2.014(5)	Mn2-O2	1.777(4)
Mn1-O2	1.785(4)	Mn2-O4	2.026(6)
Mn1-O3	2.120(5)	Mn2-O5	2.073(5)
Mn1-N1	2.091(6)	Mn2-N3	2.144(7)
Mn1-N2	2.181(6)	Mn2-$N5^1$	2.109(6)
Mn1-N4	2.120(5)	Mn2-N6	2.189(6)

Table A16. Selected Bond lengths (Å) for **13·2CH_3CN.**

Mn1-O1	1.962(4)	Mn2-O3	2.176(4)
Mn1-O2	2.224(3)	Mn2-O7	1.990(3)
Mn1-O8	1.799(3)	Mn2-O8	1.791(3)
Mn1-N5	2.155(4)	Mn2-N1	2.125(4)
Mn1-N22	2.274(4)	Mn2-N2	2.203(4)
Mn1-N23	2.059(5)	Mn2-N21	2.079(4)

Table A17. Selected Bond lengths (Å) for **15·2CH_3CN.**

Mn1-$O6^1$	2.109(9)	Mn1-O4	1.804(9)
Mn1-N2	2.169(11)	Mn1-O7	2.009(8)
Mn1-N11	2.179(7)	Mn1-N5	2.111(6)
Mn2-O4	1.792(9)	Mn2-$O1^1$	2.032(9)
Mn2-$N3^1$	2.141(11)	Mn2-O5	2.116(8)
Mn2-$N10^1$	2.12(8)	Mn2-$N9^1$	2.18(3)
Mn3-O2	2.016(7)	Mn3-O3	2.145(9)
Mn3-O8	1.787(9)	Mn3-N1	2.066(6)
Mn3-N4	2.157(11)	Mn3-N6	2.232(8)
Mn4-O8	1.834(8)	Mn4-O9	2.093(8)
Mn4-O11	2.026(12)	Mn4-N7	2.155(12)
Mn4-N8	2.198(6)	Mn4-N12	2.078(10)

Table A18. Selected Bond lengths (Å) for **19·2CH$_3$CN.**

Fe1-O2^1	2.051(7)	Fe1-O3	2.057(7)
Fe1-O9	1.797(7)	Fe1-N4	2.131(9)
Fe1-N6	2.152(9)	Fe1-N7	2.262(9)
Fe2-O1	2.037(8)	Fe2-O4^1	2.023(7)
Fe2-O9	1.801(6)	Fe2-N2	2.299(8)
Fe2-N3	2.117(5)	Fe2-N5	2.128(9)
Fe3-O5	2.016(7)	Fe3-O7	2.018(8)
Fe3-O11	1.799(7)	Fe3-N1	2.283(9)
Fe3-N8	2.133(10)	Fe3-N9	2.143(10)
Fe4-O6	2.040(7)	Fe4-O10	2.033(8)
Fe4-O11	1.790(8)	Fe4-N10	2.126(10)
Fe4-N12	2.311(14)	Fe4-N15	2.110(8)

Table A19. Selected Bond lengths (Å) for **27·2CH$_3$CN·H$_2$O.**

Mn1-O1	1.769(3)	Mn3-O7	1.848(3)
Mn1-O2	1.921(3)	Mn3-O19	2.231(4)
Mn1-O18	1.777(4)	Mn3-O24	1.819(3)
Mn1-N1	2.026(4)	Mn3-N2	2.262(4)
Mn1-N4	2.031(5)	Mn3-N7	2.036(4)
Mn1-N10	2.125(4)	Mn3-N12	2.142(4)
Mn2-O3	1.923(3)	Mn4-O1	1.836(4)
Mn2-O7	1.769(3)	Mn4-O9	2.248(3)
Mn2-O24	1.769(3)	Mn4-O18	1.816(3)
Mn2-N3	2.051(4)	Mn4-N5	2.114(4)
Mn2-N6	2.132(4)	Mn4-N8	2.046(4)
Mn2-N14	2.009(4)	Mn4-N13	2.287(4)

Table A20. Selected Bond lengths (Å) for **29·2CH$_3$CN.**

Mn1-O1	1.942(4)	Mn2-O2	1.847(4)
Mn1-O2	1.776(4)	Mn2-O3	2.213(4)
Mn1-O4	1.776(4)	Mn2-O4	1.821(4)
Mn1-N1	2.136(4)	Mn2-N3^1	2.045(5)
Mn1-N2	2.051(5)	Mn2-N5^1	2.152(5)
Mn1-N4	2.021(5)	Mn2-N6^1	2.239(6)

Table A21. Selected Bond lengths (Å) for **34·H_2O.**

Mn1-N7	2.09(2)	Mn2-O10	1.775(16)
Mn1-O13	2.216(18)	Mn2-N5	2.01(2)
Mn1-O11	1.804(18)	Mn3-O2	1.779(16)
Mn1-O10	1.844(12)	Mn3-N11	1.99(3)
Mn1-N9	2.24(2)	Mn3-O1	1.812(14)
Mn1-N15	2.05(3)	Mn3-N1	2.006(18)
Mn2-O11	1.809(14)	Mn3-N12	2.147(17)
Mn2-N8	2.126(16)	Mn4-N13	2.30(2)
Mn2-N10	2.01(2)	Mn4-N2	2.119(19)
Mn2-O12	1.948(16)	Mn4-O2	1.831(13)
Mn2-O10	1.775(16)	Mn4-O1	1.878(15)
Mn2-N5	2.01(2)	Mn4-O17	2.23(2)
Mn3-O18	1.858(18)	Mn4-N14	2.107(19)
Mn2-O12	1.948(16)		

Table A22. Selected Bond lengths (Å) for **35·H_2O.**

Mn1-O2	2.2381(19)	Mn1-N1	2.376(2)
Mn1-O4	2.1207(18)	Mn1-N2	2.302(2)
Mn1-O7	2.1902(19)	Mn1-N3	2.337(2)

Table A23. Selected Bond lengths (Å) for **38·2CH_3OH.**

Ni1-O1	2.099(2)	Ni1-N1	2.074(2)
Ni1-O2	2.035(2)	Ni1-N2	2.159(2)
Ni1-O6	2.091(2)	Ni1-N3	2.052 (2)

Table A24. Selected Bond lengths (Å) for **39·2CH_3OH·H_2O.**

Ni1-O5	2.043(6)	Ni2-O2	2.078(6)
Ni1-O8	2.068(6)	Ni2-O3	2.066(5)
Ni1-O9	2.081(6)	Ni2-O4	2.052(6)
Ni1-N1	2.051(7)	Ni2-N4	2.176(7)
Ni1-N2	2.156(7)	Ni2-N5	2.061(7)
Ni1-N3	2.081(7)	Ni2-N6	2.118(7)

Table A25. Selected Bond lengths (Å) for **46.**

Ni2-N1	2.048(4)	Ni2-O1	2.083(3)
Ni2-N2	2.075(4)	Ni2-O2	2.055(3)
Ni2-N3	2.172(4)	Ni2-O3	2.053(3)

Table A26. Selected Bond lengths (Å) for **52.**

Co1-O1	2.092(3)	Co1-N1	2.106(4)
Co1-O3	2.160(3)	Co1-N2	2.213(4)
Co1-O4	2.050(3)	Co1-N3	2.114(4)

Table A27. Selected Bond lengths (Å) for **53·CH_3OH·$2H_2O$.**

Co1-O2	2.052(6)	Co2-O1	2.117(6)
Co1-O7	2.239(6)	Co2-O3	2.053(6)
Co1-O8	2.121(6)	Co2-O4	2.228(7)
Co1-N2	2.208(7)	Co2-N1	2.191(7)
Co1-N5	2.102(8)	Co2-N3	2.075(8)
Co1-N6	2.110(8)	Co2-N4	2.095(8)

Table A28. Selected Bond lengths (Å) for **54·H_2O.**

Co1-O1	2.133(3)	Co1-N1	2.226(3)
Co1-$O2^1$	2.065(3)	Co1-N2	2.092(3)
Co1-O5	2.089(3)	Co1-N3	2.092(3)

Table A29. Selected Bond lengths (Å) for **55·$8H_2O$.**

Co1-O1	2.047(3)	Co1-N1	2.072(4)
Co1-O2	2.081(4)	Co1-N2	2.144(4)
Co1-O3	2.100(4)	Co1-N3	2.075(4)

Table A30. Selected Bond lengths (Å) for **56.**

Ni1-O1	2.047(4)	Ni2-$O2^1$	2.052(4)
Ni1-O3	2.125(4)	Ni2-O4	2.038(4)
Ni1-O10	2.048(4)	Ni2-O5	2.096(4)
Ni1-N2	2.057(5)	Ni2-N1	2.077(5)
Ni1-N3	2.142(5)	Ni2-N5	2.143(5)
Ni1-N4	2.033(5)	Ni2-N6	2.054(6)

Table A31. Selected Bond lengths (Å) for **57.**

Ni1-O2[1]	2.190(8)	Ni2-O5[1]	2.170(8)
Ni1-O3[1]	2.091(8)	Ni2-O7[1]	2.095(8)
Ni1-O4	2.031(9)	Ni2-O8	2.035(8)
Ni1-N1	2.108(9)	Ni2-N4	2.123(9)
Ni1-N2	2.060(11)	Ni2-N5	2.047(11)
Ni1-N3	2.033(11)	Ni2-N6	2.043(11)

Table A32. Selected Bond lengths (Å) for **58·CH_3OH·$2H_2O$.**

Ni1-O1	2.092(2)	Ni1-N1	2.050(3)
Ni1-O2	2.036(2)	Ni1-N2	2.157(3)
Ni1-O3	2.075(2)	Ni1-N3	2.070(3)

Table A33. Selected Bond lengths (Å) for **59·$2CH_3OH$·$5H_2O$.**

Ni1-O1	1.978(4)	Ni1-N10	2.296(5)
Ni1-N1	2.089(5)	Ni1-O10	1.991(4)
Ni1-N2	2.058(5)		

Table A34. Selected Bond lengths (Å) for **60·CH_3OH·$2H_2O$.**

Cd1-O1	2.390(3)	Cd2-O3	2.387(3)
Cd1-O2	2.412(3)	Cd2-O4	2.451(3)
Cd1-O5	2.458(3)	Cd2-O7	2.370(3)
Cd1-O6	2.385(3)	Cd2-O8	2.447(3)
Cd1-N1	2.328(4)	Cd2-N4	2.329(4)
Cd1-N2	2.455(4)	Cd2-N5	2.535(4)
Cd1-N3	2.362(4)	Cd2-N6	2.330(4)

Table A35. Selected Bond lengths (Å) for **61·CH_3OH.**

Cd1-O1[1]	2.284(14)	Cd2-N1	2.514(15)
Cd1-O5[1]	2.571(17)	Cd2-O2[2]	2.318(13)
Cd1-O6	2.237(16)	Cd2-O3	2.30(2)
Cd1-N2	2.336(18)	Cd2-O4[2]	2.453(14)
Cd1-N3	2.478(19)	Cd2-N4	2.362(15)
Cd1-N6	2.297(19)	Cd2-N5	2.35(2)

Table A36. Selected Bond lengths (Å) for **62.**

Cd1-O4	2.218(7)	Cd2-O2[2]	2.327(9)
Cd1-O6	2.260(7)	Cd2-O8	2.258(8)
Cd1-N4[1]	2.317(9)	Cd2-N1	2.282(10)
Cd1-N5[1]	2.516(9)	Cd2-N2	2.416(9)
Cd1-N6[1]	2.292(9)	Cd2-N3	2.311(9)
Cd2-O1[2]	2.487(7)		

Table A37. Selected Bond lengths (Å) for **64.**

Co1-O1[1]	2.093(3)	Co1-N1	2.127(4)
Co1-O2	2.057(3)	Co1-N2	2.171(4)
Co1-O3	2.125(3)	Co1-N3	2.156(4)

Table A38. Selected Bond lengths (Å) for **66·CH_3OH·$5H_2O$.**

Ni1-O4	2.060(3)	Ni1-N1	2.086(4)
Ni1-O6	2.043(3)	Ni1-N2	2.071(3)
Ni1-O7	2.076(3)	Ni1-N14	2.121(4)

Table A39. Selected Bond lengths (Å) for **67·$2CH_3OH$·$11H_2O$.**

Co1-O2	2.020(3)	Co2-N7	2.118(5)
Co1-O7	2.096(3)	Co2-N8	2.176(4)
Co1-O8	2.268(3)	Co2-N9	2.115(5)
Co1-N1	2.087(4)	Co3-O3[1]	2.160(3)
Co1-N2	2.097(4)	Co3-O15	2.097(4)
Co1-N3	2.265(4)	Co3-O16	2.057(3)
Co2-O12	2.109(3)	Co3-N4	2.149(4)
Co2-O13	2.005(3)	Co3-N5	2.195(4)
Co2-O14	2.217(3)	Co3-N6	2.131(6)

Table A40. Selected Bond angles (°) for **5.**

O1-Mn1-O2	91.06(13)	O7-Mn2-O3	85.13(13)
O1-Mn1-N5	87.75(13)	O7-Mn2-N1	91.27(12)
O1-Mn1-N22	96.05(14)	O7-Mn2-N2	90.50(13)
O1-Mn1-N23	167.87(13)	O7-Mn2-N21	166.86(15)
O2-Mn1-N22	172.75(13)	O8-Mn2-O3	96.78(13)
O8-Mn1-O1	99.26(13)	O8-Mn2-O7	97.39(12)
O8-Mn1-O2	90.39(12)	O8-Mn2-N1	167.13(14)
O8-Mn1-N5	165.56(14)	O8-Mn2-N2	94.33(15)
O8-Mn1-N22	89.90(13)	O8-Mn2-N21	92.40(14)
O8-Mn1-N23	92.83(15)	N1-Mn2-O3	93.40(13)
N5-Mn1-O2	102.16(12)	N1-Mn2-N2	76.03(14)
N5-Mn1-N22	76.74(14)	N21-Mn2-O3	85.04(14)
N23-Mn1-O2	87.95(13)	N21-Mn2-N1	80.64(14)
N23-Mn1-N5	80.65(14)	N21-Mn2-N2	97.50(14)
N23-Mn1-N22	84.80(14)	Mn2-O8-Mn1	124.93(18)
O3-Mn2-N2	168.50(13)		

Table A41. Selected Bond angles (°) for **6·CH_3CN.**

O1-Mn1-O3	86.1(2)	O2-Mn2-O5	95.51(19)
O1-Mn1-N1	165.7(2)	O2-Mn2-N3	92.7(2)
O1-Mn1-N2	89.3(2)	O2-Mn2-$N5^1$	171.2(2)
O1-Mn1-N4	90.15(19)	O2-Mn2-N6	94.3(2)
O2-Mn1-O1	98.30(18)	O4-Mn2-O5	90.9(2)
O2-Mn1-O3	96.91(19)	O4-Mn2-N3	166.3(2)
O2-Mn1-N1	93.8(2)	O4-Mn2-$N5^1$	87.2(2)
O2-Mn1-N2	94.4(2)	O4-Mn2-N6	91.0(2)
O2-Mn1-N4	166.7(2)	O5-Mn2-N3	95.6(2)
O3-Mn1-N2	168.29(19)	O5-Mn2-$N5^1$	90.9(2)
N1-Mn1-O3	84.9(2)	O5-Mn2-N6	169.59(19)
N1-Mn1-N2	97.5(2)	N3-Mn2-N6	80.6(2)
N1-Mn1-N4	79.4(2)	$N5^1$-Mn2-N3	80.7(3)
N4-Mn1-O3	93.8(2)	$N5^1$-Mn2-N6	79.0(2)
N4-Mn1-N2	75.4(2)	Mn2-O2-Mn1	123.0(2)
O2-Mn2-O4	98.7(2)		

Table A42. Selected Bond angles (°) for **13·2CH$_3$CN.**

O1-Mn1-Mn2	79.62(10)	O3-Mn2-N2	168.50(15)
O1-Mn1-O2	91.09(14)	O7-Mn2-Mn1	82.44(10)
O1-Mn1-N5	87.80(15)	O7-Mn2-O3	85.17(14)
O1-Mn1-N22	96.05(15)	O7-Mn2-N1	91.29(14)
O1-Mn1-N23	167.89(15)	O7-Mn2-N2	90.48(15)
O2-Mn1-Mn2	71.79(9)	O7-Mn2-N21	166.91(17)
O2-Mn1-N22	172.71(15)	O8-Mn2-Mn1	27.63(11)
O8-Mn1-Mn2	27.49(11)	O8-Mn2-O3	96.79(15)
O8-Mn1-O1	99.25(15)	O8-Mn2-O7	97.43(14)
O8-Mn1-O2	90.43(14)	O8-Mn2-N1	167.10(15)
O8-Mn1-N5	165.48(16)	O8-Mn2-N2	94.32(16)
O8-Mn1-N22	89.86(15)	O8-Mn2-N21	92.36(16)
O8-Mn1-N23	92.84(16)	N1-Mn2-Mn1	164.94(12)
N5-Mn1-Mn2	165.82(12)	N1-Mn2-O3	93.39(15)
N5-Mn1-O2	102.19(14)	N1-Mn2-N2	76.03(16)
N5-Mn1-N22	76.71(15)	N2-Mn2-Mn1	117.51(12)
N22-Mn1-Mn2	110.89(11)	N21-Mn2-Mn1	102.84(12)
N23-Mn1-Mn2	111.44(12)	N21-Mn2-O3	85.05(15)
N23-Mn1-O2	87.94(15)	N21-Mn2-N1	80.63(15)
N23-Mn1-N5	80.61(16)	N21-Mn2-N2	97.46(16)
N23-Mn1-N22	84.77(16)	Mn2-O8-Mn1	124.9(2)
O3-Mn2-Mn1	72.51(9)		

Table A43. Selected Bond angles (°) for **15·2CH$_3$CN.**

O4-Mn1-Mn2	28.4(3)	O4-Mn1-O6^{1}	94.5(4)
O4-Mn1-N2	175.0(4)	O4-Mn1-N5	95.1(3)
O4-Mn1-N11	97.4(4)	O6^{1}-Mn1-Mn2	73.5(2)
O6^{1-}Mn1-N2	88.8(4)	O6^{1-}Mn1-N5	91.1(3)
O6^{1-}Mn1-N11	168.0(3)	O7-Mn1-Mn2	80.3(2)
O7Mn1-O6^{1}	95.5(4)	O7-Mn1-N2	86.4(3)
O7-Mn1-N5	165.6(3)	O7-Mn1-N11	84.9(3)
N2-Mn1-Mn2	156.6(3)	N2-Mn1-N11	79.2(4)
N5-Mn1-Mn2	113.9(2)	N5-Mn1-N2	81.0(3)
N5-Mn1-N11	86.1(3)	N11-Mn1-Mn2	118.3(2)
O1^{1-}Mn2-Mn1	80.1(2)	O1^{1-}Mn2-O5	86.7(3)
O1^{1-}Mn2-N3^{1}	87.5(4)	O1^{1-}Mn2-N9^{1}	88(3)

$O1^{1-}$Mn2-$N10^{1}$	164(2)	O4-Mn2-Mn1	28.6(3)
O4-Mn2-$O1^{1}$	97.5(4)	O4-Mn2-O5	94.4(3)
O4-Mn2-$N3^{1}$	173.1(4)	O4-Mn2-$N9^{1}$	99(2)
O4-Mn2-$N10^{1}$	96(3)	O5-Mn2-Mn1	71.0(2)
O5-Mn2-$N3^{1}$	90.5(3)	O5-Mn2-$N9^{1}$	166(2)
O5-Mn2-$N10^{1}$	83.2(14)	$N3^{1-}$Mn2-Mn1	158.2(3)
$N3^{1-}$Mn2-$N9^{1}$	76(2)	$N9^{1-}$Mn2-Mn1	121(2)
$N10^{1-}$Mn2-Mn1	108(3)	$N10^{1-}$Mn2-$N3^{1}$	80(3)
$N10^{1-}$Mn2-$N9^{1}$	98(3)	O2-Mn3-Mn4	74.2(2)
O2-Mn3-O3	89.8(3)	O2-Mn3-N1	168.9(4)
O2-Mn3-N4	90.4(3)	O2-Mn3-N6	82.2(4)
O3-Mn3-Mn4	76.8(2)	O3-Mn3-N4	85.9(4)
O3-Mn3-N6	161.9(3)	O8-Mn3-Mn4	29.6(3)
O8-Mn3-O2	96.5(3)	O8-Mn3-O3	96.0(4)
O8-Mn3-N1	94.6(3)	O8-Mn3-N4	172.9(4)
O8-Mn3-N6	101.0(4)	N1-Mn3-Mn4	115.8(2)
N1-Mn3-O3	88.0(3)	N1-Mn3-N4	78.5(3)
N1-Mn3-N6	96.7(3)	N4-Mn3-Mn4	156.6(3)
N4-Mn3-N6	78.0(4)	N6-Mn3-Mn4	116.0(2)
O8-Mn4-Mn3	28.8(3)	O8-Mn4-O9	94.3(4)
O8-Mn4-O11	97.7(4)	O8-Mn4-N7	173.7(5)
O8-Mn4-N8	99.5(3)	O8-Mn4-N12	94.2(4)
O9-Mn4-Mn3	77.4(3)	O9-Mn4-N7	88.4(4)
O9-Mn4-N8	164.4(3)	O11-Mn4-Mn3	76.2(3)
O11-Mn4-O9	95.1(4)	O11-Mn4-N7	87.8(5)
O11-Mn4-N8	90.6(4)	O11-Mn4-N12	168.1(4)
N7-Mn4-Mn3	157.4(3)	N7-Mn4-N8	77.3(4)
N8-Mn4-Mn3	118.2(2)	N12-Mn4-Mn3	115.4(3)
N12-Mn4-O9	85.5(4)	N12-Mn4-N7	80.3(5)
N12-Mn4-N8	86.0(3)		

Table A44. Selected Bond angles (°) for **19·2CH$_3$CN.**

O2^{1-}Fe1-O3	87.2(3)	O2^{1-}Fe1-N4	82.4(3)
O2^{1-}Fe1-N6	167.8(3)	O2^{1-}Fe1-N7	93.2(3)
O3-Fe1-N4	157.4(3)	O3-Fe1-N6	88.2(3)
O3-Fe1-N7	84.2(3)	O9-Fe1-O2^{1}	97.8(3)
O9-Fe1-O3	101.4(3)	O9-Fe1-N4	99.8(3)
O9-Fe1-N6	94.1(3)	O9-Fe1-N7	167.8(3)
N4-Fe1-N6	97.8(3)	N4-Fe1-N7	76.4(3)
N6-Fe1-N7	75.1(3)	O1-Fe2-N2	81.0(3)
O1-Fe2-N3	158.6(3)	O1-Fe2-N5	86.4(3)
O4^{1-}Fe2-O1	90.2(3)	O4^{1-}Fe2-N2	88.8(3)
O4^{1-}Fe2-N3	86.7(3)	O4^{1-}Fe2-N5	164.1(3)
O9-Fe2-O1	100.0(3)	O9-Fe2-O4^{1}	95.5(3)
O9-Fe2-N2	175.5(3)	O9-Fe2-N3	101.3(3)
O9-Fe2-N5	100.4(3)	N3-Fe2-N2	77.8(3)
N3-Fe2-N5	90.8(3)	N5-Fe2-N2	75.3(3)
O5-Fe3-O7	93.4(3)	O5-Fe3-N1	85.8(3)
O5-Fe3-N8	162.9(3)	O5-Fe3-N9	89.4(3)
O7-Fe3-N1	82.7(3)	O7-Fe3-N8	89.3(3)
O7-Fe3-N9	160.0(3)	O11-Fe3-O5	97.7(3)
O11-Fe3-O7	99.1(3)	O11-Fe3-N1	175.9(4)
O11-Fe3-N8	98.5(4)	O11-Fe3-N9	100.2(3)
N8-Fe3-N1	77.8(3)	N8-Fe3-N9	82.4(3)
N9-Fe3-N1	77.7(3)	O6-Fe4-N10	162.5(4)
O6-Fe4-N12	84.2(4)	O6-Fe4-N15	93.0(4)
O10-Fe4-O6	89.3(3)	O10-Fe4-N10	87.9(4)
O10-Fe4-N12	85.6(6)	O10-Fe4-N15	164.2(5)
O11-Fe4-O6	100.7(3)	O11-Fe4-O10	97.7(3)
O11-Fe4-N10	96.8(4)	O11-Fe4-N12	174.1(4)
O11-Fe4-N15	97.2(4)	N10-Fe4-N12	78.3(4)
N15-Fe4-N10	85.2(4)	N15-Fe4-N12	79.2(6)

Table A45. Selected Bond angles (°) for **27·2CH$_3$CN·H$_2$O.**

Mn1-O1	1.769(3)	Mn3-O7	1.848(3)
Mn1-O2	1.921(3)	Mn3-O19	2.231(4)
Mn1-O18	1.777(4)	Mn3-O24	1.819(3)
Mn1-N1	2.026(4)	Mn3-N2	2.262(4)
Mn1-N4	2.031(5)	Mn3-N7	2.036(4)
Mn1-N10	2.125(4)	Mn3-N12	2.142(4)
Mn2-O3	1.923(3)	Mn4-O1	1.836(4)
Mn2-O7	1.769(3)	Mn4-O9	2.248(3)
Mn2-O24	1.769(3)	Mn4-O18	1.816(3)
Mn2-N3	2.051(4)	Mn4-N5	2.114(4)
Mn2-N6	2.132(4)	Mn4-N8	2.046(4)
Mn2-N14	2.009(4)	Mn4-N13	2.287(4)

Table A46. Selected Bond angles (°) for **29·2CH$_3$CN.**

O1-Mn1-N1	91.32(17)	O2-Mn2-N3^1	97.06(19)
O1-Mn1-N2	86.39(17)	O2-Mn2-N5^1	176.55(19)
O1-Mn1-N4	167.74(17)	O2-Mn2-N6^1	103.2(2)
O2-Mn1-O1	95.48(17)	O3-Mn2-N6^1	168.85(18)
O2-Mn1-N1	172.92(19)	O4-Mn2-O2	84.30(17)
O2-Mn1-N2	97.17(18)	O4-Mn2-O3	90.37(16)
O2-Mn1-N4	92.66(19)	O4-Mn2-N3^1	176.6(2)
O4-Mn1-O1	94.22(18)	O4-Mn2-N5^1	97.87(18)
O4-Mn1-O2	87.77(18)	O4-Mn2-N6^1	91.22(19)
O4-Mn1-N1	93.74(17)	N3^1-Mn2-O3	86.52(18)
O4-Mn1-N2	174.95(18)	N3^1-Mn2-N5^1	80.9(2)
O4-Mn1-N4	95.25(19)	N3^1-Mn2-N6^1	91.5(2)
N2-Mn1-N1	81.24(18)	N5^1-Mn2-O3	94.69(19)
N4-Mn1-N1	80.32(19)	N5^1-Mn2-N6^1	74.2(2)
N4-Mn1-N2	83.50(19)	Mn1-O2-Mn2	92.38(18)
O2-Mn2-O3	87.96(17)	Mn1-O4-Mn2	93.28(18)

Table A47. Selected Bond angles (°) for **34·H_2O.**

O1-Mn1-O2	95.12(16)	O7-Mn3-N7	97.80(17)
O1-Mn1-O18	88.10(18)	O7-Mn3-N12	178.23(17)
O1-Mn1-N1	94.05(18)	O19-Mn3-N2	167.97(16)
O1-Mn1-N4	94.17(19)	O24-Mn3-O7	84.39(16)
O1-Mn1-N10	171.93(18)	O24-Mn3-O19	89.30(15)
O2-Mn1-N1	168.14(18)	O24-Mn3-N2	92.14(17)
O2-Mn1-N4	87.41(17)	O24-Mn3-N7	177.69(17)
O2-Mn1-N10	91.99(17)	O24-Mn3-N12	96.31(16)
O18-Mn1-O2	96.54(16)	N7-Mn3-O19	90.04(16)
O18-Mn1-N1	91.26(18)	N7-Mn3-N2	88.05(18)
O18-Mn1-N4	175.26(18)	N7-Mn3-N12	81.52(17)
O18-Mn1-N10	94.87(19)	N12-Mn3-O19	93.35(15)
N1-Mn1-N10	78.41(18)	N12-Mn3-N2	74.62(17)
N4-Mn1-N1	84.44(19)	O1-Mn4-O9	88.63(15)
N4-Mn1-N10	82.3(2)	O1-Mn4-N5	172.45(16)
O3-Mn2-N3	86.58(17)	O1-Mn4-N8	100.57(19)
O3-Mn2-N6	91.78(16)	O1-Mn4-N13	96.96(17)
O3-Mn2-N14	169.54(18)	O9-Mn4-N13	173.13(16)
O7-Mn2-O3	95.74(16)	O18-Mn4-O1	84.45(17)
O7-Mn2-N3	97.90(17)	O18-Mn4-O9	88.14(15)
O7-Mn2-N6	172.37(17)	O18-Mn4-N5	94.86(18)
O7-Mn2-N14	92.23(18)	O18-Mn4-N8	170.09(17)
O24-Mn2-O3	94.37(17)	O18-Mn4-N13	96.36(17)
O24-Mn2-O7	88.63(17)	N5-Mn4-O9	98.87(15)
O24-Mn2-N3	173.29(18)	N5-Mn4-N13	75.62(17)
O24-Mn2-N6	92.12(17)	N8-Mn4-O9	83.47(16)
O24-Mn2-N14	92.58(17)	N8-Mn4-N5	81.29(19)
N3-Mn2-N6	81.21(18)	N8-Mn4-N13	91.54(17)
N14-Mn2-N3	85.62(18)	Mn1-O1-Mn4	92.24(17)
N14-Mn2-N6	80.15(18)	Mn2-O7-Mn3	91.82(15)
O7-Mn3-O19	88.28(15)	Mn1-O18-Mn4	92.79(17)
O7-Mn3-N2	103.75(17)	Mn2-O24-Mn3	93.01(16)

Table A48. Selected Bond angles (°) for **35·H_2O.**

O2-Mn1-N1	86.19(7)	O7-Mn1-O2	80.92(8)
O2-Mn1-N2	150.98(8)	O7-Mn1-N1	103.11(8)
O2-Mn1-N3	87.80(8)	O7-Mn1-N2	85.06(8)
O4-Mn1-O2	97.17(8)	O7-Mn1-N3	167.60(8)
O4-Mn1-O7	201.06(8)	N2-Mn1-N1	72.39(8)
O4-Mn1-N1	154.82(8)	N2-Mn1-N3	102.75(8)
O4-Mn1-N2	110.59(8)	N3-Mn1-N1	70.79(7)
O4-Mn1-N3	84.37(8)		

Table A49. Selected Bond angles (°) for **38·2CH_3OH.**

O1-Ni1-N2	92.15(9)	N1-Ni1-O1	87.62(9)
O2-Ni1-O1	93.66(9)	N1-Ni1-O6	175.56(9)
O2-Ni1-N6	91.80(8)	N1-Ni1-N2	78.03(9)
O2-Ni1-N1	90.62(9)	N3-Ni1-O1	170.84(9)
O2-Ni1-N2	167.02(9)	N3-Ni1-O6	86.59(9)
O2-Ni1-N3	94.22(9)	N3-Ni1-N1	96.95(10)
O6-Ni1-O1	88.51(8)	N3-Ni1-N2	81.10(9)
O6-Ni1-N2	99.95(9)		

Table A50. Selected Bond angles (°) for **39·2CH_3OH·H_2O.**

O5-Ni1-O8	92.5(2)	O2-Ni2-N4	92.7(3)
O5-Ni1-O9	91.9(3)	O2-Ni2-N6	172.9(3)
O5-Ni1-N1	93.0(3)	O3-Ni2-O2	91.5(2)
O5-Ni1-N2	173.8(3)	O3-Ni2-N4	93.2(3)
O5-Ni1-N3	94.8(3)	O3-Ni2-N6	90.5(3)
O8-Ni1-O9	90.1(3)	O4-Ni2-O2	90.7(3)
O8-Ni1-N2	93.0(3)	O4-Ni2-O3	93.8(3)
O8-Ni1-N3	91.2(3)	O4-Ni2-N4	172.2(3)
O9-Ni1-N2	91.1(3)	O4-Ni2-N5	89.3(3)
N1-Ni1-O8	174.4(3)	O4-Ni2-N6	95.9(3)
N1-Ni1-O9	90.5(3)	N5-Ni2-O2	92.6(3)
N1-Ni1-N2	81.5(3)	N5-Ni2-O3	174.8(3)
N1-Ni1-N3	87.6(3)	N5-Ni2-N4	83.5(3)
N3-Ni1-O9	173.1(3)	N5-Ni2-N6	85.0(3)
N3-Ni1-N2	82.1(3)	N6-Ni2-N4	80.4(3)

Table A51. Selected Bond angles (°) for **46**.

N1-Ni2-N2	91.71(15)	O2-Ni2-N2	172.78(15)
N1-Ni2-N3	82.23(15)	O2-Ni2-N3	95.73(13)
N1-Ni2-O1	174.07(15)	O2-Ni2-O1	87.32(13)
N1-Ni2-O2	91.39(14)	O3-Ni2-N2	93.52(14)
N1-Ni2-O3	94.66(14)	O3-Ni2-N3	171.04(13)
N2-Ni2-N3	78.23(14)	O3-Ni2-O1	91.18(13)
N2-Ni2-O1	88.93(14)	O3-Ni2-O2	92.73(13)
O1-Ni2-N3	92.13(13)		

Table A52. Selected Bond angles (°) for **52**.

O1-Co1-O3	89.67(12)	O4-Co1-N3	89.70(14)
O1-Co1-N1	166.24(14)	N1-Co1-O3	86.92(13)
O1-Co1-N2	89.24(14)	N1-Co1-N2	78.58(15)
O1-Co1-N3	86.60(13)	N1-Co1-N3	96.80(14)
O3-Co1-N2	103.03(14)	O8-Cd2-O2[2]	86.7(3)
O4-Co1- O1	95.79(13)	O8-Cd2-N1	107.5(3)
O4-Co1- O3	90.34(13)	O8-Cd2-N2	127.8(3)
O4-Co1-N1	97.55(14)	N3-Co1-O3	176.25(13)
O4-Co1-N2	165.76(14)	N3-Co1-N2	77.28(15)

Table A53. Selected Bond angles (°) for **53·CH_3OH·$2H_2O$.**

O2-Co1-N2	86.8(2)	O1-Co2-N1	166.4(2)
O2-Co1-O7	167.1(2)	O1-Co2-O4	60.5(2)
O2-Co1-O8	106.5(2)	O3-Co2-O1	107.5(2)
O2-Co1-N5	92.0(3)	O3-Co2-N1	86.0(2)
O2-Co1-N6	93.0(3)	O3-Co2-N3	90.9(3)
N2-Co1-O7	106.0(2)	O3-Co2-O4	167.6(2)
O8-Co1-N2	166.5(2)	O3-Co2-N4	92.1(3)
O8-Co1-O7	60.8(2)	N1-Co2-O4	106.1(2)
N5-Co1-N2	79.0(3)	N3-Co2-O1	97.8(3)
N5-Co1-O7	92.5(3)	N3-Co2-N1	80.3(3)
N5-Co1-O8	98.0(3)	N3-Co2-O4	93.8(3)
N5-Co1-N6	156.3(3)	N3-Co2-N4	157.6(3)
N6-Co1-N2	78.2(3)	N4-Co2-O1	102.4(3)
N6-Co1-O7	87.8(3)	N4-Co2-N1	77.7(3)
N6-Co1-O8	102.8(3)	N4-Co2-O4	87.9(3)

Table A54. Selected Bond angles (°) for **54·H_2O.**

O1-Co1-N1	93.94(12)	O5-Co1-N2	86.48(11)
$O2^1$-Co1-O1	95.84(11)	O5-Co1-N3	171.77(12)
$O2^1$-Co1-O5	91.86(11)	N2-Co1-O1	169.20(11)
$O2^1$-Co1-N1	164.64(11)	N2-Co1-N1	78.47(11)
$O2^1$-Co1-N2	93.23(11)	N2-Co1-N3	99.73(12)
$O2^1$-Co1-N3	93.16(11)	N3-Co1-O1	85.64(11)
O5-Co1-O1	87.38(11)	N3-Co1-N1	75.79(12)
O5-Co1-N1	100.40(12)		

Table A55. Selected Bond angles (°) for **55·8H_2O.**

O1-Co1-O2	93.41(14)	N1-Co1-O2	172.24(15)
O1-Co1-O3	92.07(14)	N1-Co1-O3	85.10(16)
O1-Co1-N1	91.39(15)	N1-Co1-N2	79.69(17)
O1-Co1-N2	168.55(15)	N1-Co1-N3	100.35(17)
O1-Co1-N3	94.04(15)	N3-Co1-O2	85.41(16)
O2-Co1-O3	88.62(14)	N3-Co1-O3	171.70(16)
O2-Co1-N2	96.26 (15)	N3-Co1-N2	80.66(16)
O3-Co1-N2	94.29(16)		

Table A56. Selected Bond angles (°) for **56.**

O1-Ni1-O3	91.59(16)	$O2^1$-Ni2-O5	89.86(17)
O1-Ni1-O10	88.64(17)	$O2^1$-Ni2-N1	176.94(19)
O1-Ni1-N2	94.36(18)	$O2^1$-Ni2-N5	99.27(18)
O1-Ni1-N3	170.04(18)	$O2^1$-Ni2-N6	83.59(19)
O3-Ni1-N3	95.00(17)	O4-Ni2-$O2^1$	87.81(17)
O10-Ni1-O3	88.74(16)	O4-Ni2-O5	92.80(18)
O10-Ni1-N2	176.26(18)	O4-Ni2-N1	94.72(19)
O10-Ni1-N3	98.95(18)	O4-Ni2-N5	170.08(19)
N2-Ni1-O3	88.95(18)	O4-Ni2-N6	92.8(2)
N2-Ni1-N3	78.33(19)	O5-Ni2-N5	94.15(19)
N4-Ni1-O1	93.21(18)	N1-Ni2-O5	88.30(19)
N4-Ni1-O3	171.06(19)	N1-Ni2-N5	78.43(19)
N4-Ni1-O10	83.85(18)	N6-Ni2-O5	171.2(2)
N4-Ni1-N2	98.19(19)	N6-Ni2-N1	98.0(2)
N4-Ni1-N3	81.3(2)	N6-Ni2-N5	81.1(2)

Table A57. Selected Bond angles (°) for **57.**

$O3^1$-Ni1-$O2^1$	61.7(3)	$O7^1$-Ni2-$O5^1$	62.9(3)
$O3^1$-Ni1-N1	167.5(4)	$O7^1$-Ni2-N4	167.5(3)
O4-Ni1-$O2^1$	166.2(3)	O8-Ni2-$O5^1$	167.9(3)
O4-Ni1-$O3^1$	104.4(3)	O8-Ni2-$O7^1$	105.4(3)
O4-Ni1-N1	88.0(4)	O8-Ni2-N4	87.1(4)
O4-Ni1-N2	89.4(4)	O8-Ni2-N5	89.9(4)
O4-Ni1-N3	92.7(4)	O8-Ni2-N6	90.6(4)
N1-Ni1-$O2^1$	105.8(4)	N4-Ni2-$O5^1$	104.6(3)
N2-Ni1-$O2^1$	92.2(4)	N5-Ni2-$O5^1$	89.3(4)
N2-Ni1-$O3^1$	96.4(4)	N5-Ni2-$O7^1$	99.4(4)
N2-Ni1-N1	83.1(4)	N5-Ni2-N4	79.8(4)
N3-Ni1-$O2^1$	89.9(3)	N6-Ni2-$O5^1$	93.7(4)
N3-Ni1-$O3^1$	99.5(3)	N6-Ni2-$O7^1$	97.0(4)
N3-Ni1-N1	79.9(3)	N6-Ni2-N4	83.1(4)
N3-Ni1-N2	162.8(4)	N6-Ni2-N5	162.8(4)

Table A58. Selected Bond angles (°) for **58·CH_3OH·$2H_2O$.**

O1-Ni1-N2	92.90(10)	N1-Ni1-O1	175.53(10)
O2-Ni1-O1	93.30(9)	N1-Ni1-O3	88.81(10)
O2-Ni1-O3	90.38(10)	N1-Ni1-N2	83.09(11)
O2-Ni1-N1	90.93(10)	N1-Ni1-N3	90.69(11)
O2-Ni1-N2	170.47(10)	N3-Ni1-O1	90.64(10)
O2-Ni1-N3	91.30(11)	N3-Ni1-O3	178.25(10)
O3-Ni1-O1	89.74(9)	N3-Ni1-N2	81.39(11)
O3-Ni1-N2	96.89(10)		

Table A59. Selected Bond angles (°) for **59·$2CH_3OH$·$2H_2O$.**

O1-Ni1-N1	103.50(19)	N2-Ni1-N1	110.3(2)
O1-Ni1-N2	94.05(19)	N2-Ni1-N10	77.27(18)
O1-Ni1-N10	170.94(18)	O10-Ni1-N1	126.64(17)
O1-Ni1-O10	101.24(18)	O10-Ni1-N2	114.21(19)
N1-Ni1-N10	77.57(18)	O10-Ni1-N10	84.87(17)

Table A60. Selected Bond angles (°) for **60·CH_3OH·$2H_2O$.**

O1-Cd1-O2	54.87(10)	N3-Cd1-N2	70.11(13)
O1-Cd1-O5	96.60(11)	O3-Cd2-O4	54.44(10)
O1-Cd1-N2	107.50(11)	O3-Cd2-O8	104.93(11)
O2-Cd1-O5	129.64(10)	O3-Cd2-N5	132.77(12)
O2-Cd1-N2	82.23(11)	O4-Cd2-N5	155.01
O6-Cd1-O1	88.03(11)	O7-Cd2-O4	83.47(10)
O6-Cd1-O2	81.41(11)	O7-Cd2-O8	54.64(10)
O6-Cd1-O5	54.43(10)	O7-Cd2-N5	90.19(11)
O6-Cd1-N2	144.60(11)	O8-Cd2-N5	11.12(11)
N1-Cd1-O1	93.43(12)	N4-Cd2-O3	81.76(12)
N1-Cd1-O2	130.50(12)	N4-Cd2-O4	131.25(12)
N1-Cd1-O5	86.03(11)	N4-Cd2-O7	128.39(12)
N1-Cd1-O6	140.26(12)	N4-Cd2-O8	87.51(12)
N1-Cd1-N2	71.96(12)	N4-Cd2-N5	70.62(12)
N1-Cd1-N3	95.66(13)	N4-Cd2-N6	132.52(13)
N2-Cd1-O5	147.91(12)	N6-Cd2-O3	104.58(12)
N3-Cd1-O1	169.23(11)	N6-Cd2-O4	83.55(12)
N3-Cd1-O2	114.47(11)	N6-Cd2-O7	78.78(12)
N3-Cd1-O5	89.78(12)	N6-Cd2-O8	132.93(12)
N3-Cd1-O6	88.66(12)	N6-Cd2-N5	71.49(12)

Table A61. Selected Bond angles (°) for **61·CH_3OH.**

$O1^1$-Cd1-$O5^1$	53.8(5)	$O2^2$-Cd2-N1	86.8(5)
$O1^1$-Cd1-N2	108.0(6)	$O2^2$-Cd2-$O4^2$	55.3(4)
$O1^1$-Cd1-N3	102.5(6)	$O2^2$-Cd2-N4	94.4(6)
$O1^1$-Cd1-N6	131.3(7)	$O2^2$-Cd2-N5	138.0(6)
O6-Cd1-$O1^1$	118.7(7)	O3-Cd2-N1	150.9(7)
O6-Cd1-$O5^1$	104.7(6)	O3-Cd2-$O2^2$	109.3(6)
O6-Cd1-N2	92.7(7)	O3-Cd2-$O4^2$	119.7(7)
O6-Cd1-N3	138.8(8)	O3-Cd2-N4	84.8(7)
O6-Cd1-N6	82.7(8)	O3-Cd2-N5	106.4(7)
N2-Cd1-$O5^1$	159.3(6)	$O4^2$-Cd2-N1	89.3(5)
N2-Cd1-N3	71.2(7)	N4-Cd2-N1	69.6(5)
N3-Cd1-$O5^1$	101.2(6)	N4-Cd2-$O4^2$	144.8(6)
N6-Cd1-$O5^1$	79.4(7)	N5-Cd2-N1	71.8(6)
N6-Cd1-N2	114.4(7)	N5-Cd2-$O4^2$	87.9(6)
N6-Cd1-N3	71.0(6)	N5-Cd2-N4	110.3(6)

Table A62. Selected Bond angles (°) for **62.**

O4-Cd1-O6	115.2(3)	O8-Cd2-O2^{2}	86.7(3)
O4-Cd1-N4^{1}	115.8(3)	O8-Cd2-N1	107.5(3)
O4-Cd1-N5^{1}	91.0(3)	O8-Cd2-N2	127.8(3)
O4-Cd1-N6^{1}	128.3(3)	O8-Cd2-N3	94.7(3)
O6-Cd1- N4^{1}	96.3(3)	N1-Cd2-O1^{2}	83.8(3)
O6-Cd1- N5^{1}	153.7(3)	N1-Cd2-O2^{2}	103.9(3)
O6-Cd1- N6^{1}	88.3(3)	N1-Cd2-N2	72.9(3)
N4^{1}-Cd1- N5^{1}	72.6(3)	N1-Cd2-N3	144.5(4)
N6^{1}-Cd1- N4^{1}	105.5(3)	N2-Cd2-O1^{2}	90.9(3)
N6^{1}-Cd1- N5^{1}	72.5(3)	N3-Cd2-O1^{2}	96.2(3)
O2^{2}-Cd2-O1^{2}	54.5(3)	N3-Cd2-O2^{2}	104.7(3)
O2^{2}-Cd2-N2	145.1(3)	N3-Cd2-N2	71.1(3)
O8-Cd2-O1^{2}	141.2(3)		

Table A63. Selected Bond angles (°) for **64.**

O1^{1}-Co1-O3	88.57(12)	O2-Co1-N3	164.27(14)
O1^{1}-Co1-N1	174.12(12)	O3-Co1-N1	97.23(13)
O1^{1}-Co1-N2	97.39(12)	O3-Co1-N2	174.04(13)
O1^{1}-Co1-N3	83.57(12)	O3-Co1-N3	101.91(13)
O2-Co1-O1^{1}	90.12(11)	N1-Co1-N2	76.81(13)
O2-Co1-O3	92.29(12)	N1-Co1-N3	96.13(13)
O2-Co1-N1	88.68(12)	N3-Co1-N2	79.22(13)
O2-Co1-N2	87.36(12)		

Table A64. Selected Bond angles (°) for **66·CH$_3$OH·5H$_2$O.**

O4-Ni1-O7	89.78(12)	O6-Ni1-N14	87.27(12)
O4-Ni1-N1	84.94(12)	O7-Ni1-N1	99.44(14)
O4-Ni1-N2	174.25(13)	O7-Ni1-N14	174.71(12)
O4-Ni1-N14	95.52(12)	N1-Ni1-N14	81.23(15)
O6-Ni1-O4	89.75(11)	N2-Ni1-O7	95.97(13)
O6-Ni1-O7	92.61(12)	N2-Ni1-N1	93.83(13)
O6-Ni1-N1	166.79(14)	N2-Ni1-N14	78.74(14)
O6-Ni1-N2	90.24(12)		

Table A65. Selected Bond angles (°) for **67·2CH$_3$OH·11H$_2$O.**

O2-Co1-O7	101.20(13)	O13-Co2-N9	102.64(18)
O2-Co1-O8	88.25(13)	N7-Co2-O14	88.39(14)
O2-Co1-N1	103.17(15)	N7-Co2-N8	77.79(15)
O2-Co1-N2	93.14(15)	N8-Co2-O14	101.88(13)
O2-Co1-N3	169.71(13)	N9-Co2-O14	88.64(14)
O7-Co1-O8	60.35(11)	N9-Co2-N7	153.62(16)
O7-Co1-N3	88.98(13)	N9-Co2-N8	77.20(15)
N1-Co1-O7	96.81(13)	O3^1-Co3-N5	99.06(14)
N1-Co1-O8	156.38(13)	O15-Co3-O3^1	84.90(14)
N1-Co1-N2	108.81(15)	O15-Co3-N4	86.19(15)
N1-Co1-N3	76.84(14)	O15-Co3-N5	93.27(15)
N2-Co1-O7	146.92(14)	O15-Co3-N6	166.75(15)
N2-Co1-O8	90.84(13)	O16-Co3-O3^1	93.97(13)
N2-Co1-N3	77.28(15)	O16-Co3-O15	97.72(15)
N3-Co1-O8	95.57(13)	O16-Co3-N4	91.29(15)
O12-Co2-O14	173.18(12)	O16-Co3-N5	163.64(16)
O12-Co2-N7	91.32(15)	O16-Co3-N6	91.61(17)
O12-Co2-N8	84.71(13)	N4-Co3-O3^1	170.19(15)
O12-Co2-N9	94.60(15)	N4-Co3-N5	77.34(16)
O13-Co2-O12	87.96(13)	N6-Co3-O3^1	170.19(15)
O13-Co2-O14	85.47(13)	N6-Co3-N4	103.05(17)
O13-Co2-N7	103.24(18)	N6-Co3-N5	79.76(17)
O13-Co2-N8	172.62(14)		

Vita

The author, Biswajit Laha, was born on 27th of April, 1986 in India. He earned his B.Sc. (Chemistry Hons.) and M.Sc. (Chemistry) from Saldiha College, The University of Burdwan and National Institute of Technology, Rourkela in 2008 and 2010, respectively. He joined Indian Institute of Science Education and Research Mohali (IISERM) with a fellowship from MHRD, Govt. of India, to pursue his Ph.D. degree in Chemistry under the supervision of Professor Sanjay K. Mandal in January, 2013.